UNIVERSITA' DEGLI STUDI DI VERONA

DEPARTMENT OF Cardiosurgery

GRADUATE SCHOOL OF Life and Health Science

DOCTORAL PROGRAM IN Cardiovascular Science

University of Verona

Cycle XXVII

Microdomain–specific localization of functional L-type calcium channels in atrial cardiomyocytes: novel concept of local regulation and remodelling in disease

S.S.D. MED/46

Coordinatore:
Prof. Giovanni Battista Luciani

Tutori:
Prof. Giuseppe Faggian
Prof. Julia Gorelik
Dr. Andrew Shevchuk

Dottorando:

Dott.ssa Marina Balycheva

Abstract

Recently, novel concept of microdomain-specific regulation in cardiac cells have greatly extended our understanding of how specific subcellular localization impacts on channel function and regulation.
Microdomain is a small region of cell membrane, which has a distinct structure, composition and function. It has been recognized that discrete clusters of different ion channels exist in the sarcolemma in different microdomains such as T-tubules, caveolae.

This study addresses the hypothesis that distinct spatial compartmentalization of functional calcium channels in different intercellular microdomains are coupled with structural proteins and receptors and play an important role in unique Ca^{2+} signaling in atrial cardiomyocytes in health and pathology.

Using several technical approaches (super-resolution scanning and whole-cell patch-clamp, confocal and electron microscopy), this study aims to investigate characteristics of subcellular micrdomains such as T-tubules and caveolae in atrial cardiomyocytes; and to answer the question whether in atrial cardiomyocytes functional L-type calcium channels (LTCCs) are specifically distributed within different microdomains and forming signalling complexes with receptors, that potentially causes a unique atrial cardiomyocyte Ca^{2+} signaling process.

First, it was found that atrial cells could be characterised by heterogeneous T-tubule system the structure of which influenced by the cell size and atrial chamber localization. This study provides the first direct evidence for two distinct subpopulations of functional LTCCs in rat and human healthy atrial cardiomyocytes, with a micro-domain-specific regulation of their biophysical properties. In atrial cells, L-type calcium channels are equally distributed inside and outside of T-tubules, in contrast to ventricular cardiomyocytes where LTCCs are clustered in T-tubules (Bhargava, Lin et al. 2013). The population of LTCCs observed outside of T-tubules was associated with caveolae. LTCCs located in

caveolae contribute essentially to atrial Ca^{2+} signaling, particularly in cardiomyocytes lacking the organized T-tubule network.

Second, β_1-adreneric stimulation, which increases single LTCC activity and antiadrenergic effect of adenosine on functional LTCCs were investigated in both microdomains in rat atrial cariomyocytes.

Third, using animal model, heart failure was found to be associated with loss of T-tubule structure and decrease in single amplitude of T-tubular LTCCs localized in atrial cardiomyocytes.

Fourth, human studies revealed, that chronic atrial fibrillation is associated with the loss of T-tubule structure and downregulation of the L-type calcium current with increased activity of single LTCCs localized in T-tubule microdomains and the loss channels outside of T-tubules. Decrease of calcium current was associated with the downregulation of gene expression.

These results support the notion that functional L-type calcium channels are linked with structural components of cardiac membrane and undergo remodelling in association with loss of structures during pathology.

Declaration: This thesis represents my own work. Where I have also used materials from other investigators, this is clearly stated. This thesis has not been submitted for a degree to any other academic institution.

Marina Balycheva, Verona, April 2015.

WITH THE FINANCIAL CONTRIBUTION OF

University of Verona,

Cooperint 2013 and Cooperint 2014 programs

Table of contents

To my mother, the bravest person I will ever know

“Practice, practice and practice, and ALL is coming”

Sri K. Pattabhi Jois (*Guruji)*

Acknowledgement

I thank Prof Giuseppe Faggian who supervised this work closely and for his mentorship and friendship. His commitment on excellence is a colossal inspiration to me.

I thank Prof Julia Gorelik who also supervised this work and offered great support throughout my doctoral work and I am grateful to her for meticulous attention.

I thank Dr Andrew Shevchuk who was co-supervisor in this work and offered great technical support for Scanning Ion Conductance Microscopy.

I thank Prof Giovanni Battista Luciani who co-ordinated this doctoral work and supported me.

I also thank my colleagues for their direct and indirect contribution to the work described here, including Dr Ivan Diakonov, Ms Sophie Schobesberger, Ms Francisca Schultz, Dr Jose L. Sanchez Alonso-Mardones, Dr Anita Alvarez Laviada, Mr Zeki Ilkan, Ms Navneet Bhorgal and I am grateful for their efforts. I will remember fondly the time I spent with all my collegues in Gorelik's group for a lot of «scientific fun».

I also thank all surgeons and administrative stuff in Cardiosurgery Department, Ospedale Maggiore (Verona, Italy) and in Hammersmith Hospital (London, UK) for their contribution to human project including Prof Aldo Milano, Prof. Alessandro Mazzuco, Dr Prakash Punjabi, Dr Maddalena Tessari, Dr Francesco Onorati, Dr Alessio Rungatscher.

I also thank Dr Laura Marcazzan for her administrative support within all these years. I am very grateful to her.

I am eternally grateful to my friends who have given moral support to me and without whom I would not have started this PhD.

I must especially thank Dr Anamika Bhargava who explained me basic principles of single channel biophysic and inspired me so much during this work.

Dr Alexey Glukhov has been my companion since I was first introduced to the “Microdomain conception” of the heart. I am blessed beyond measure to be still learning by his side and for his direct contribution in this work. He has encouraged, comforted and inspired me. I thank him for the outstanding job he did in discussion of this thesis and for a better understanding of the cellular mechanism of the heart.

Lastly, I thank my mother so much. She supports me in all my projects and this work has not been done without her in my life.

1 CHAPTER 1. General introduction

1.1 THE HEART

The heart is a muscular organ pumping oxygenated and deoxygenated blood to whole body and lungs, respectively (Bettex, Pretre et al. 2014) The heart perfectly drives blood flow through circulatory system separating cardiovascular system to pulmonary and systemic circulation by coordinated contraction of heart chambers: two atria and two ventricles. Four chambers of heart detached by valves are continually contracting

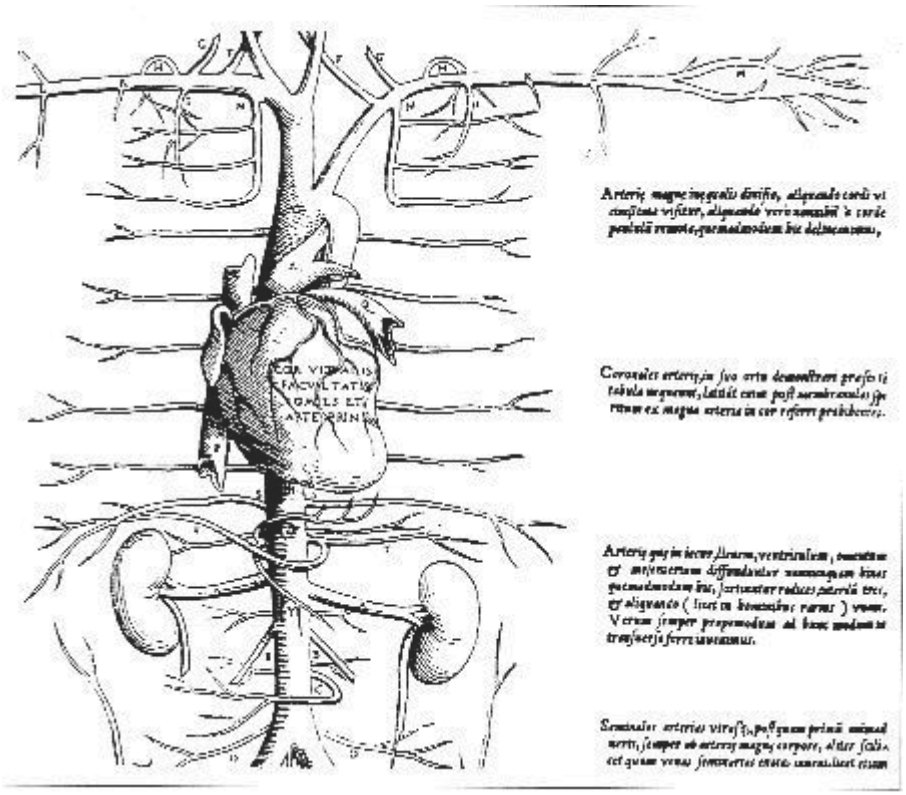

Figure 1.1. The heart at the center of the circulation. (Vesalius, A. and Kalkar, J.S. (1538). Tabulae Anatomica, P.D. Bernardi, Venice).

and relaxing in a sequence known as the cardiac cycle (Bettex, Pretre et al. 2014). Thus, heart is not only one, but also two separated pumps, one on the right side that supplies the pulmonary circulation and one on the left that supplies the systemic circulation (Bettex, Pretre et al. 2014).

1.2 CARDIAC CYCLE

The heart undergoes a cycle of events that cause blood to be pushed to all organs of the body with each heartbeat. There are two basic phases of the cardiac cycle: systole and diastole (Saks, Dzeja et al. 2006). In the diastole phase, the heart ventricles are relaxed and the heart fills with blood. In the systole phase, the ventricles contract and pump blood to the arteries. One cardiac cycle is completed when the heart fills with blood and the blood is pumped out of the heart. The cardiac cycle is initiated by the sinoatrial node a group of specialized non-contractile cardiomyocytes positioned in the wall of the right atrium and spread through whole heart from atria to ventricle.

The atrial chambers contract and relax before the ventricular systole, and their activation is evident as separate electrical activity in an electrocardiogram. The time course of contraction is marginally shorter in atria compared to ventricles. Both cell types reach peak contraction within a few tens of milliseconds (Luss, Boknik et al. 1999). The ventricles contract more forcefully than the atrial chambers and are predominantly responsible for forcing blood out of the heart. However, atria can play a significant role in altering the amount of blood that loads into the ventricles before to systole.

To simplify cardiac cycle, the events of the cardiac cycle trace the path of the blood as it enters the heart, is pumped to the lungs, travels back to the heart and is pumped out to the rest of the body.

Diastole represents the period of time when the ventricles are relaxed and blood is passively flowing from the left atrium (LA) and right atrium (RA) into the left ventricle (LV) and right ventricle (RV), respectively through atrioventricular valves (mitral and tricuspid) that detach the atria from the ventricles. Deoxygenated

venous blood from the body is derived into the RA via superior vena cava (SVC) and inferior vena cava (IVC). The LA receives oxygenated arterial blood from lungs through pulmonary veins that enter the LA. At the end of diastole, both atria contract, that moves an additional amount of blood into the ventricles. Because there are no valves between the atria and the veins, much of the atrial blood is actually forced back into the veins. Nevertheless, some additional blood is also pushed forward into the ventricles, causing further increases in ventricular pressure and volume. Although the benefit of atrial contraction at normal heart rates may be negligible, it can substantially increase ventricular filling at high heart rates when diastolic filling time is curtailed.

During systole, LV and RV contract and push blood into the aorta and pulmonary artery, respectively. At this time, the aortic and pulmonic valves are opened and the atrioventricular valves are closed, therefore no blood is entering the ventricles. The systole is followed by period of ventricular relaxation and cardiac cycle repeats itself.

1.2.1 Abnormalities in the cardiac cycle

Cardiac cycle dysfunction results in blood flow abnormalities and structural and functional changes in heart chambers. Accordingly, valve pathology such as mitral or aortic valve insufficiencies can lead to volume overload of the left ventricle and left atrium with often-progressive enlargement and remodeling associated with worse clinical outcomes (Matsumura, Ohtaki et al. 2003; Tribouilloy, Grigioni et al. 2009). Valve impairment gives rise to blood leakage (regurgitation) back to ventricle as a systolic retrograde flow because of the lack of jointing of the valve's leaflets and this impairs pressure gradient between two chambers (Pierard and Carabello 2010). Furthermore, mitral valve regurgitation may enhance left ventricular dilatation (Judge, Kennedy et al. 1971) which may accelerate dilated cardiomyopathy which is associated with the subsequent contractility defect and development of heart failure.

This kind of cardiac cycle dysfunction can also cause enlargement and dilatation of left atrium, which in accordance to Framingham Heart Study, increases the development of AF by 39% by each 5-mm increase in LA diameter (Andersen, Egeblad et al. 1991; Vaziri, Larson et al. 1994; Psaty, Manolio et al. 1997). However, not only systolic but also diastolic dysfunction can accelerate development of heart failure or atrial fibrillation (Kass, Bronzwaer et al. 2004; Rosenberg and Manning 2012).

1.3 Cardiac tissue

Cardiac tissue is a striated muscle structurally similar to skeletal one. However, the electrophysiology of the two muscles differs dramatically. Whereas in skeletal muscle an action potential causing contraction is very short (2-5 ms) and generated by central nervous stimulation, cardiac action potential is not initiated by neural activity. Instead, specialized cardiac muscle tissue in the heart itself initiates the action potential, which then spreads directly from cell to cell. Neural stimulation can only modulate effect on the heart rate. Moreover, the duration of the cardiac action potential is quite long (200-400 ms). As a result, the full force of cardiac contraction results from a single action potential, but not from a sequence of stimulations, which force skeletal contraction. The force of contraction is not the same for every beat of the heart and can be modulated by the cardiac nerves.

Despite on difference in neural regulation of contraction the main mechanism of contraction appears to be the same (not to be confused with excitation-contraction coupling, which is different in both types of muscle). These two types of muscle have similar tissue structure. Two main proteins, actin and myosin, form striated filament network moving along each other. Myofilaments form the main muscle unit named as sarcomere incased between z-disk. Unlike skeletal muscle, cardiac tissue is built by separated cells, which communicate through intercalated disks. That allows the cardiac cells in the heart contract together as a unit with every beat.

Two types of muscle cells are found within the heart:

1. contractile cells
2. conductive cells.

Contractile cells are the working cardiomyocytes and constitute the bulk of the muscle cells that make up the atria and the ventricles. An action potential in any one of these cells leads to a mechanical contraction of that cell. Furthermore, an action potential in one cardiac muscle cell will stimulate neighboring cells to undergo an action potential. Thus, propagation of action potential appears in whole heart.

Conductive cells are specialized muscle cells that are involved with the initiation or propagation of action potentials but have little mechanical capability.
Conductive cells concentrated in specific areas of myocardium in the right atrium near the vena cava form structure known as sinoatrial node (SAN); in the interatrial septum between the ostium of the coronary sinus and the septal leaflet of the tricuspid valve - the atrioventricular (AVN) node and spread in inner ventricular wall as Purkinje fibers. Paramount conductive structure is a SAN, which generates spontaneous action potential and triggers normal pacemaker activity in the heart.
Because of SAN is localized in atrium, action potentials firstly propagates over the atria, spreads across the atria and reaches AVN. The AV node serves two important functions: to transfer depolarization from the atria to the ventricles and to delay the spread of excitation from the atria to the ventricles. Conduction through the AV is very slow, that allows the atria to eject blood to fill ventricles before contraction of the latest starts.

1.4 Action potential in heart

Action potential (AP) is a short event, which is characterized by rapid rise and fall of membrane electrical potential in excitable cells. In muscle cells AP triggers events underling contraction. AP differs in type of cells by duration and shape.

Cardiac AP can be characterized by plateau, what assign specific shape of AP and long duration up to 400 ms in comparison to other type of cells such as neurons or skeletal muscle cells where AP duration is 1 ms and 2-5 ms, respectively. **Figure 1.2** describes phases of cardiac AP. Phase 4, or the resting potential, is stable at - 90 mV in normal working myocardial cells. Phase 0 is the phase of rapid depolarization, resulting from the activation of voltage-gated Na^+ (Na_v) channels (Fozzard 2002). The membrane potential shifts into positive voltage range. This phase is central to rapid propagation of the cardiac impulse (conduction velocity, 1 m/s). Phase 0 of the action potential in atrial and ventricular cardiomyocytes is followed by a rapid transient repolarization (phase 1), reflecting Na_v channel inactivation and the activation of the fast transient voltage-gated outward K^+ current ($I_{to,f}$). This phase sets the potential for the next phase of the action potential and influences the height and duration of the action potential plateau (phase 2). Phase 2, a plateau phase, is the longest phase. It is unique and derived by calcium entry through voltage-dependent calcium (Ca_v) channels into the cell. The plateau phase is the main trigger for excitation-contraction coupling in the working myocardium (Fabiato and Fabiato 1979; Bers and Perez-Reyes 1999).

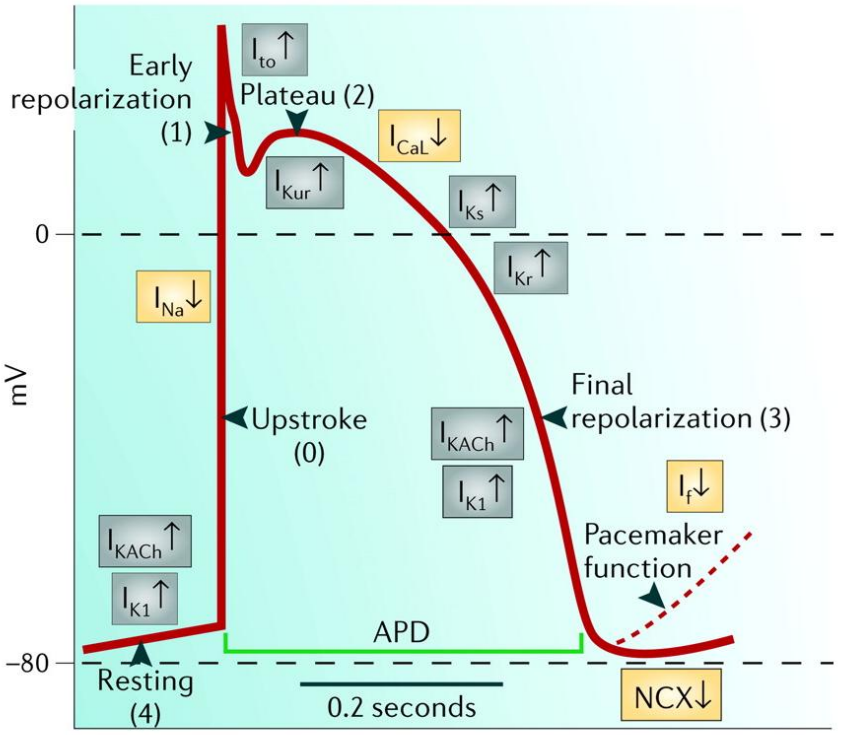

Figure 1.2. Membrane currents that generate the normal action potential.

Resting (4), upstroke (0), early repolarization (1), plateau (2), and final repolarization are the 5 phases of the action potential. A decline of potential at the end of phase 3 in pacemaker cells, such as the sinus node, is shown as a broken line. The inward currents, I_{Na}, I_{Ca}, and I_f, are shown in yellow boxes; the sodium-calcium exchanger (NCX) is also shown in yellow. It is electrogenic and may generate inward or outward current. I_{KAch}, I_{K1}, I_{to}, I_{Kur}, I_{Kr}, and I_{Ks} are shown in gray boxes. The action potential duration (APD) is approximately 200 ms. (Reproduced with permission from Stanley and Carlsson (Nattel, Andrade et al. 2014).

The driving force for K^+ efflux is high during the plateau phase of the action potential in ventricular and atrial myocardium and, as the Ca_v channels inactivate, the outward K^+ currents predominate, resulting in phase 3 of rapid repolarization, bringing the membrane voltage back to the resting potential (Hoffman BF 1960).

The action potentials of pacemaker cells in SAN and AVN are significantly different from those in working myocardium. The membrane potential at the onset of phase 4 is more depolarized (50 to 65 mV), undergoes slow diastolic depolarization, and gradually merges into phase 0. The rate of depolarization in phase 0 is much slower than that in the working myocardial cells and results in slow propagation of the cardiac impulse in the nodal regions (0.1 to 0.2 m/s). Phase 0 is markedly slower in SAN and AVN cells, than in atria/ventricles, suggesting that Na_v channels do not play a prominent role in depolarization.

1.4.1 Action potential: difference between cardiomyocytes

The heterogeneity in action potentials waveforms in terms of shape, amplitude and duration was observed in different cell types. Significant differences in ionic currents are responsible for the different action potential configurations (Gossop and Connell 1975; Anumonwo, Tallini et al. 2001) as well as have impact refractoriness and rhythmicity (Luo and Rudy 1994; Clancy, Tateyama et al. 2002).

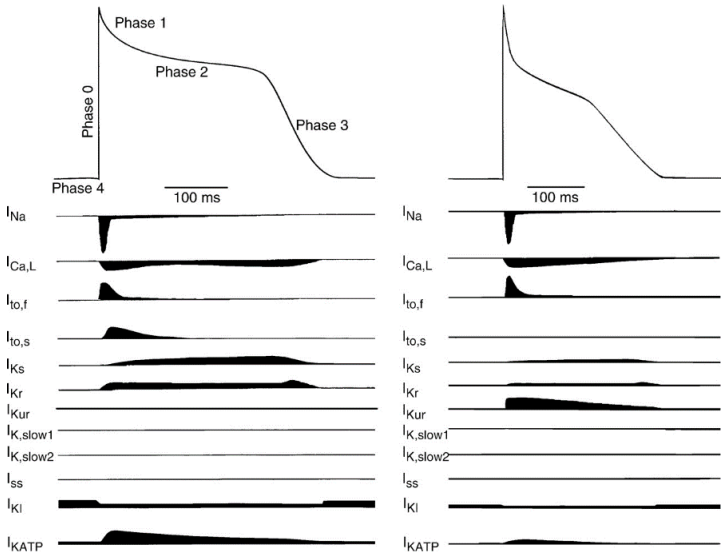

Figure 1.3. Action potential waveforms and underlying ionic currents in adult human and ventricular (*left*) and atrial (*right*) cardiomyocytes.

The time- and voltage-dependent properties of the voltage-gated inward Na+ (Na_v) and Ca2+ (Cav) currents expressed in human atrial and ventricular cardiomyocytes are similar. In contrast, there are multiple types of K+ currents, particularly K_v currents, contributing to atrial and ventricular action potential repolarization. The properties of the various K_v currents are distinct, and in contrast to the inward currents, there are multiple K_v currents expressed in individual cardiomyocytes throughout the myocardium (Nerbonne and Kass 2005).

	Atrial cells	Ventricular cells
Resting membrane potential (mV)	**-73-4+5-1 (36)**	**-74-1 +3-3 (35)**
Action potential overshoot (mV)	**35-8+9-2 (34)**	**41-7 +5-9 (26)**
Vmax (V/s)	**83-9±21-4 (23)**	**80-8±17-7 (18)**
Action potential duration 90% (ms)	**140-5 +54-5 (34)**	**496-5+115-5 (26)**

TABLE 1. Electrical properties of isolated cardiomyocytes.

Values are means+ S.D. Number of cells in parentheses (Wong and Smith 1975).

Compared with the ventricular action potential, the atrial AP has a less negative resting potential, an abbreviated plateau phase, smaller overshoot, and slower terminal repolarization. These differences are predominantly due to increased I_{to} and I_{Kur} currents, as well as decreased I_{K1} current. Differences in I_{K1} are believed to be important in contributing to characteristic differences between atrial and ventricular action potentials, particularly the less negative resting potential and slower terminal repolarization typical of atrial cells (Wang, Yue et al. 1998). Due to a smaller calcium influx, atrial cells demonstrate narrow phase plateau. In contrast to ventricular cardiomyocytes, atrial cells express not only $Ca_v1.2$ L-type calcium channels but also $Ca_v1.3$ isoform, which is also expressed in pacemaker cells. T-type calcium channel, which presence in ventricular cells only in neonatal mammalians, have been recorded in adult atrial cardiomyocytes. It has been

suggested, that T-type calcium channels play a role in automaticity (Bers and Perez-Reyes 1999; Perez-Reyes 2003).

1.4.2 Electrocardiography displays action potential

Electrocardiography (ECG) traces cardiac cycle and represents action potential in different areas of heart. Thus, P wave is responsible to atrial depolarization. Period between P wave and R wave (PR interval) represent atrial contraction. Interestingly, PR interval is responsible to time electrical impulse travels from atria to ventricles (AVN delay time). QRS complex displays different ventricular parts depolarization. The average duration of the ventricular action potential duration is reflected in the QT interval on the ECG. Factors that prolong the action potential duration (eg, a decrease in outward K currents or an increase in inward late Na current) prolong the action potential duration and the QT interval on the ECG.

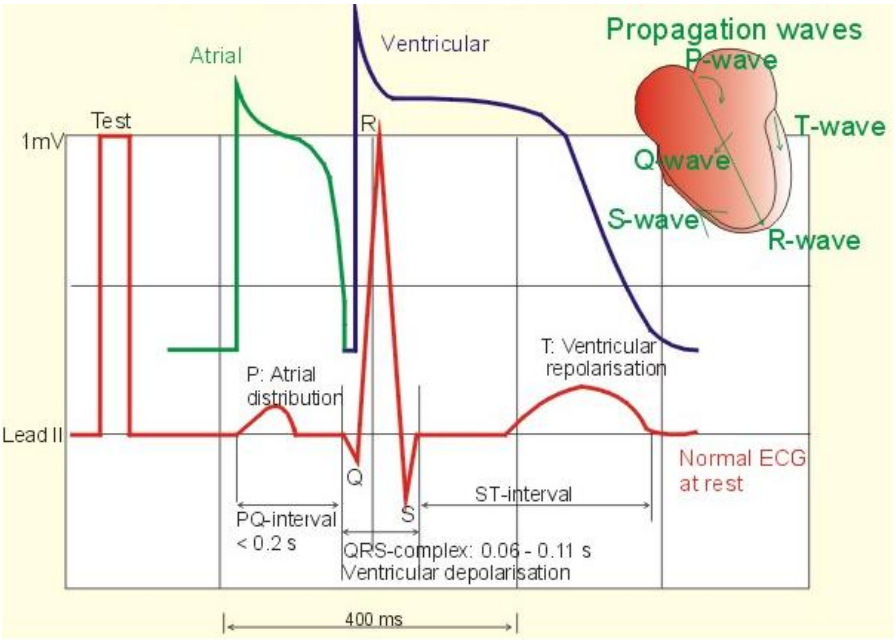

Figure 1.4. Normal ECG (II. lead).

The action potentials from an atrial (green curve) and a ventricular fibre (blue curve) are shown above. To the right is shown the direction of propagating waves in the frontal plane and their relation to the ECG waves. (New Human Physiology. Poul-Erik Paulev. Copenhagen Medical Publishers 2000)

Ventricular contraction happens during ST interval between S and T waves, which represents ventricular repolarisation. Time between T wave and next P wave relates to ventricular relaxation and filling by blood. Sequence of all waves and complexes of waves described before repeats itself with each heartbeat or cardiac cycle with constant regularity and rate about 60-90 beats per minute (bpm) is typical for normal ECG and also named as sinus rhythm of heart. Sinus rhythm is driven by SAN activity and associated with upright P wave in ECG, which is present in every cardiac cycle and followed by QRS complex in ratio 1:1.

1.5 Role of atria

Atrial function appears to be in a close relationship with ventricular function, and it plays a key role in maintaining an optimal cardiac performance. Atria modulate ventricle filling through its systolic pump function, whereas ventricle function influences atrial function throughout the cardiac cycle (Rosca, Lancellotti et al. 2011).

During cardiac cycle, blood continually flows from the venous system into the atria; about 70-80 per cent of the blood passes directly through the atria into the ventricles before atrial contraction. Thus, atrial contraction usually causes only an additional 20-30 per cent filling of the ventricles. Both atria serve as a reservoir during systole, a conduit during early diastole and a pump during late ventricular diastole. Hence, the atria work as primer pumps that increase the ventricular pumping productivity as much as 20-30 per cent. Actually, heart can operate even without this extra 20-30 per cent performance. However, atrial failure is unlikely to be noticed unless a patient exercises, at the time of those acute sighs of heart failure may develop, for example, shortness of breath. Therefore, pulmonary artery hypertension, which can enlarge risk of mortality, is associated with left atrial dysfunction (Saraiva, Matsumura et al. 2010).

In pathological case, atrial dysfunction is associated with 'impaired relaxation' stage of diastolic dysfunction of ventricles, the reservoir and pump function of the atria are enhanced. Atrium acts as a volume reservoir and pressure sensor during diastolic dysfunction for ventricle. Volume overload is communicated to the rest of the body by secreting natriuretic peptides and activating renin-angiotensin-aldosterone system. While diastolic dysfunction progresses to the next stage of compensation, blood begins to assemble during early systole and correspondingly increases the atrial pressure. Adaptively, in order to increased pressures, the left atrium increases in size. Thus, the atrial enlargement is a sensitive marker of ventricular dysfunction. The assessment of LA size and volume is being used as a marker for diastolic dysfunction (Phillip, Pastor et al. 2003). Considerably most of the parameters used for the assessment of diastolic dysfunction are affected by

changes in the loading conditions, rate, rhythm, and position of the patient in the perioperative period.

Respiratory disorders, including chronic obstructive pulmonary disease, idiopathic pulmonary fibrosis, sarcoidosis, neuromuscular or chest wall disorders, and disorders of ventilator control including sleep apnea syndromes and obesity hypoventilation syndrome result in pulmonary hypertension. Later it and may lead to left atrial dysfunction, which in couple with pulmonary venous hypertension forms pulmonary arterial hypertension and later reach to increased right ventricular loading and dysfunction (Han, McLaughlin et al. 2007; Saraiva, Matsumura et al. 2010). Left atrial dysfunction also occurs in significant mitral valve diseases, long standing systematic hypertension (Matsuda, Toma et al. 1983).

Despite on right atrial ejection force had never been studied for long time Cioffi et al. investigated role of pulmonary hypertension in subsequent RA dysfunction. They found patients suffering from chronic pulmonary hypertension demonstrated echocardiographic feature of a marked enlarged right atrium, RA end-diastolic stress and RA systolic function, which usually parallels RV dilatation and systolic dysfunction, and leads to chronic atrial fibrillation. In the same time, that these changes have been shown in patients with normal RV dimension and RV systolic function (Cioffi, de Simone et al. 2007).

1.6 From organ to cell

Cardiac tissues is generally made up by cardiomyocytes and fibroblast. Mammalian cardiomyocytes are highly organized cells with normally one or two nucleus and mass of mitochondria. The well-developed and complicatedly organized membrane architecture of cardiomyocyte is a distinguishing feature directly reflecting its specific function. There are two unique membrane formation, such as transverse -tubules and intercalated disk, which are response for electrical-mechanical coupling of single cell and transduction of electrical stimulation of contraction from cell to cell, respectively. Thus, transverse-tubules allow cell synchronically contracts, whereas intercalated disks transmit precisely timed and homogeneous depolarizing waves within amount of cells and ensure the

rapid and coordinated propagation of the action potential throughout the heart. In the recent years, one more membrane domain in cardiac cell became as object of interest. While T-tubules mirror the main site triggers excitation-contraction coupling, another membrane structure, which is of key importance in the spatial control of signaling in the cardiac myocytes, is represented by the caveolae. These microdomains house several proteins involved in mass of signaling process regulating huge spectrum of cardiomyocyte function (Razani, Woodman et al. 2002; Cohen, Hnasko et al. 2004; Gratton, Bernatchez et al. 2004; Harvey and Calaghan 2012).

Based on their critical roles in structure, signaling, and electric inter- and intracellular communication, it is not surprising that dysfunction in these membrane structures is associated with anomalous pathophysiology, resulting in potentially lethal congenital and acquired disease.

This chapter reviews the fundamental components of cardiomyocyte transverse-tubule and caveolar membranes with a focus on calcium channels function in these membranes as an important primal contraction trigger in normal and pathological cases.

1.7 Excitation-contraction coupling in cardiomyocyte. Role of Ca^{2+}

All cardiomyocytes are able to generate action potentials (electrical impulses) what promote contraction. Shortly in mammalian cardiomyocytes the action potential induces contraction of the cell by a process known as excitation-contraction (E-C) coupling. (Bers 2002). With each heart beat action potential of cardiomyocyte induces activation of voltage-dependant calcium channels also named as L-type calcium channels (LTCCs) located in the sarcolemma and allows the trigger Ca^{2+} flows through LTCC to closely approach the sarcoplasmic reticulum (SR) Ca^{2+} release channel, the ryanodine receptors (RyRs) (Bers 2008). This amplifying process, termed Ca^{2+}-induced Ca^{2+} release (CICR) (Fabiato and Fabiato 1979), causes a rapid increase in intracellular Ca^{2+} concentration ($[Ca^{2+}]_i$) (from ~100 nM to ~1 μM) to a level required for optimal binding of Ca^{2+} to troponin C, what

promotes troponin C and subsequent myofilament proteins activation, producing contraction in cardiomyocytes (Carafoli, Santella et al. 2001). It is clear that Ca^{2+} is the link in excitation-contraction (EC) coupling. Unlike skeletal muscles, Ca^{2+} influx is required for contraction in cardiac muscle with each beat. There is a close correlation between activation of the L-type Ca^{2+} current ($I_{Ca,L}$) and cardiac contraction. Contraction is followed by Ca^{2+} disconnect from troponin C and its reuptake by the SR via activation of the SR Ca^{2+}-ATPase 2a (SERCA2a) Ca^{2+} pump in addition to extrusion across the sarcolemma via the Na^{+}/Ca^{2+} exchanger (NCX). In the human heart under resting conditions, the time required for cardiac myocyte depolarization, Ca^{2+}-induced Ca^{2+} release, contraction, relaxation, and recovery is 600 ms. This process occurs approximately 70 times a minute or over 2 billion times in the average lifespan. This paragraph shows importance of few central proteins contraction appears to be impossible without their dysfunction. LTCCs play an important role in Ca^{2+} signaling and consequently in cardiac function, because connect the electrical depolarization of cardiomyocytes with contraction (excitation-contraction coupling). Along with protein function, localization of the molecular trigger is an important key in spatial and timed homogenous Ca^{2+} increase during EC coupling. This is promoted by the specific membrane microdomain localization of functional LTCCs pass calcium ions and trigger calcium release. Synchronized Ca^{2+} release during each membrane excitation allows coordinated contraction among the many contractile units within each working ventricular cardiomyocyte in each heartbeat. Ultimately, synchronized myofilament contraction within among millions of working cardiomyocytes permit the heart muscle to generate the maximal contractile force. Synchronous and spatial homogenous whole-cell Ca2+ increase during cardiac Ca^{2+} signaling was observed by many investigators in cardiomyocytes isolated from the ventricles during depolarization (Cannell, Cheng et al. 1995; Guatimosim, Dilly et al. 2002; Brette, Despa et al. 2005). In addition, this coordinated calcium release is due to well-organized transverse-tubule membrane structure, what is critical for normal excitation-contraction coupling and cardiac function (Brette and Orchard 2003).

1.8 Ca^{2+} signals particularity during EC coupling in atrial cardiomyocyte

Whereas Ca^{2+} signaling in ventricular cardiomyocytes is well described, much less is known regarding the Ca^{2+} signals within atrial cells. In contrast to ventricular cardiomyocytes, atrial cells possess two populations of RyRs. One minor group (junctional RyRs) sit just beneath the sarcolemma. The other channels (non-junctional RyRs) are deeper inside the cell and constitute the mass of the RyR population. Although the junctional RyRs represent a small fraction of the total number of RyRs, they are crucially important in atrial EC-coupling, as they are responsible for initiating CICR. Due to the lack of T-tubules, the sarcolemma does not regularly invaginate into atrial cells. Therefore, based on immunostaining studies the localization of LTCCs is entirely different in ventricular and atrial cardiomyocytes. Thus, LTCCs are expressed around the periphery of atrial cardiomyocytes (Bootman, Smyrnias et al. 2011). As it was noticed before, ventricular cardiomyocytes display homogenous responses, which arise from the simultaneous recruitment of Ca^{2+} sparks throughout a cell. However, in atrial cardiomyocytes, EC coupling is initiated around the periphery of the cells, because this is the only place where the LTCCs and junctional RyRs come together to form dyads. Rapid imaging of Ca^{2+} responses in atrial cardiomyocytes has demonstrated that Ca^{2+} sparks are rapidly triggered around the periphery of the cell (Kockskamper, Sheehan et al. 2001; Mackenzie, Bootman et al. 2001). Subsequently, the Ca^{2+} signal emanating from the spark sites appears to spread laterally, eventually providing a contiguous Ca^{2+} signal that is solely located around the edge of the cells (Bootman, Smyrnias et al. 2011).

1.9 T-tubule system

The critical ultrastructure detail of mammalian ventricular cardiomyocytes that promotes homogenous global Ca^{2+} transients is the presence of an extensive transverse tubule system (T-tubules) (Song, Pi et al. 2005). These narrow (average diameter ~200 nm) inwardly directed invaginations of the sarcolemma

occur at each Z-disk and form both transverse and longitudinal elements throughout the cardiomyocyte have a regular spacing (~1.8 μm) (Brette and Orchard 2003). The highly organized system of T-tubules forms a three-dimensional network allowing synchronising myofilament contraction within the whole cell. The extensive T-tubule system forms tight couplings with the sarcoplasmic reticulum (SR) membrane, termed dyads, and conducts an electrical impulse (the action potential) deep into the cell, bringing the plasma membrane in close to junctional SR through the width of the cell. That triggers Ca^{2+} dependent Ca^{2+} release from the SR and allows synchronous Ca^{2+} release occurs throughout the cell with each depolarization (Kaftan, Marks et al. 1996; Soeller and Cannell 1999). It has been shown that the clusters of LTCCs and RyRs or dyadic couplings have strongly spatial distributions and form connection opposite each other (Scriven, Klimek et al. 2002) and occur predominantly within the transverse T-tubule network (Mackenzie, Roderick et al. 2004; Chen-Izu, McCulle et al. 2006). Also recently it was demonstrated that functional LTCCs are predominantly clustered in the T-tubules of adult ventricular cardiomyocytes (Bhargava, Lin et al. 2013).

Unlike ventricular cardiomyocytes, atrial cells do not possess an extensive T-tubule system, although some atrial cells possess a more rudimentary T-tubule network and differential coupling of atrial LTCCs to the ryanodine receptors (RyRs) of the SR has been proposed to underlie a unique atrial cardiomyocytes Ca^{2+} s (Brette and Orchard 2003; Trafford, Clarke et al. 2013).

In atrial cardiomyocytes, Ca^{2+} transients is initiated around the periphery of the cells (Kockskamper, Sheehan et al. 2001; Mackenzie, Bootman et al. 2001) and spread within a next tens of millisecond deeper inside. Similar results have been obtained using atrial cells from different mammalian species, including rat (Mackenzie, Bootman et al. 2001; Woo, Cleemann et al. 2002), guinea pig (Lipp, Pott et al. 1990; Berlin 1995) cat (Huser, Lipsius et al. 1996; Kockskamper, Sheehan et al. 2001; Sheehan and Blatter 2003) and human (Hatem, Benardeau et al. 1997).

The dogma that T-tubules are present only in ventricular cardiomyocytes, and are either absent or less developed in atrial, pacemakers or conducting tissue (Ayettey

and Navaratnam 1978; Huser, Lipsius et al. 1996; Cordeiro, Spitzer et al. 2001) has largely been disputed. Some studies have shown that the T-tubule network is present in atrial tissue of both small (Kirk, Izu et al. 2003) and large mammalians and humans (Richards, Clarke et al. 2011). Recently, it has been shown, that approximately third part of rat atrial cardiomyocytes have a T-tubular network (Frisk, Koivumaki et al. 2014). Amongst atrial cardiomyocytes with T-tubules, membrane network was distinguished with organized T-tubules similar to that in ventricular cardiomyocytes, and with disorganized T-tubules.

Despite on such important funcion as a domain synchronising cardiac contraction, T-tubules were also shown to accumulate a number of molecules that are important in Ca^{2+} signaling such as mentioned before L-type calcium channels, Na^{+}/Ca^{2+} exchanger (NCX), β_1 and β_2 adrenergic receptors, protein kinase A (PKA), and other regulatory proteins, many of them are localised in a signalosome with the LTCCs (Davare, Avdonin et al. 2001). All together, they form macromolecular signaling complexes targeted to specific membrane domains (Best and Kamp 2012). Clustering of these macromolecular complexes is essential for the proper timing of molecular events that couple electric activation with the contraction of the cardiaomyocyte, and for autonomic regulation of excitation-contraction coupling.

Thus, microdomain localization of functional proteins is being very important in normal cardiac contraction.

1.9.1 T-tubules loss in cardiac disease

Numerous heart diseases are associated with a progressive loss of the T-tubular structure. This study focuses on cardiac remodeling caused by heart failure and atrial fibrillation, as major causes of morbidity and mortality. The most common “stressors” of both heart failure and atrial fibrillation remodeling include tachycardia and volume or pressure overload. Specific stressors, such as diastolic dysfunction, ischemia, and valves insufficiency increase pressure and/or volume load on the chambers. These specific factors trigger intracellular changes such as cardiac

myocyte growth, hypertrophy, necrosis, and apoptosis, as well as changes in metabolism and in the expression of cellular ionic channels and hormones. Such changes create a substrate for remodeling with structural, functional, electrical, metabolic, and neurohormonal consequences.

Heart failure is characterized by a weakened myocardial contractile force, partially due to abnormal excitation-contraction coupling resulting in reduced SR Ca^{2+} release (Bito, Heinzel et al. 2008; Lyon, MacLeod et al. 2009; Lyon, Bannister et al. 2011). Cardiomyocyte micro-architecture is critically important to the efficacy of Ca^{2+}-induced Ca^{2+} release and the stability of the amplification mechanism. Chronic heart failure is characterized by a reduction of T-tubule density in rodent failing hearts (Louch, Mork et al. 2006; Song, Sobie et al. 2006). Cardiomyocytes isolated from failing spontaneous hypertensive rats demonstrated temporal delay in excitation-contraction coupling related to increased spatial separation of the junctional SR from the T-tubule membrane (Song, Sobie et al. 2006; Heinzel, Bito et al. 2008), with an associated increase in spontaneous Ca^{2+}-release events (Ca^{2+} sparks) (Song, Sobie et al. 2006). Experimental disruption of T-tubule structures by either prolonged culturing or osmotic shock produces changes similar to those observed in heart failure, with dyssynchronous release of Ca^{2+} leading to a slow Ca^{2+} transient as well as diminished contractile amplitude and prolonged contraction cycle (Lipp, Huser et al. 1996; Brette, Salle et al. 2004; Brette, Despa et al. 2005).

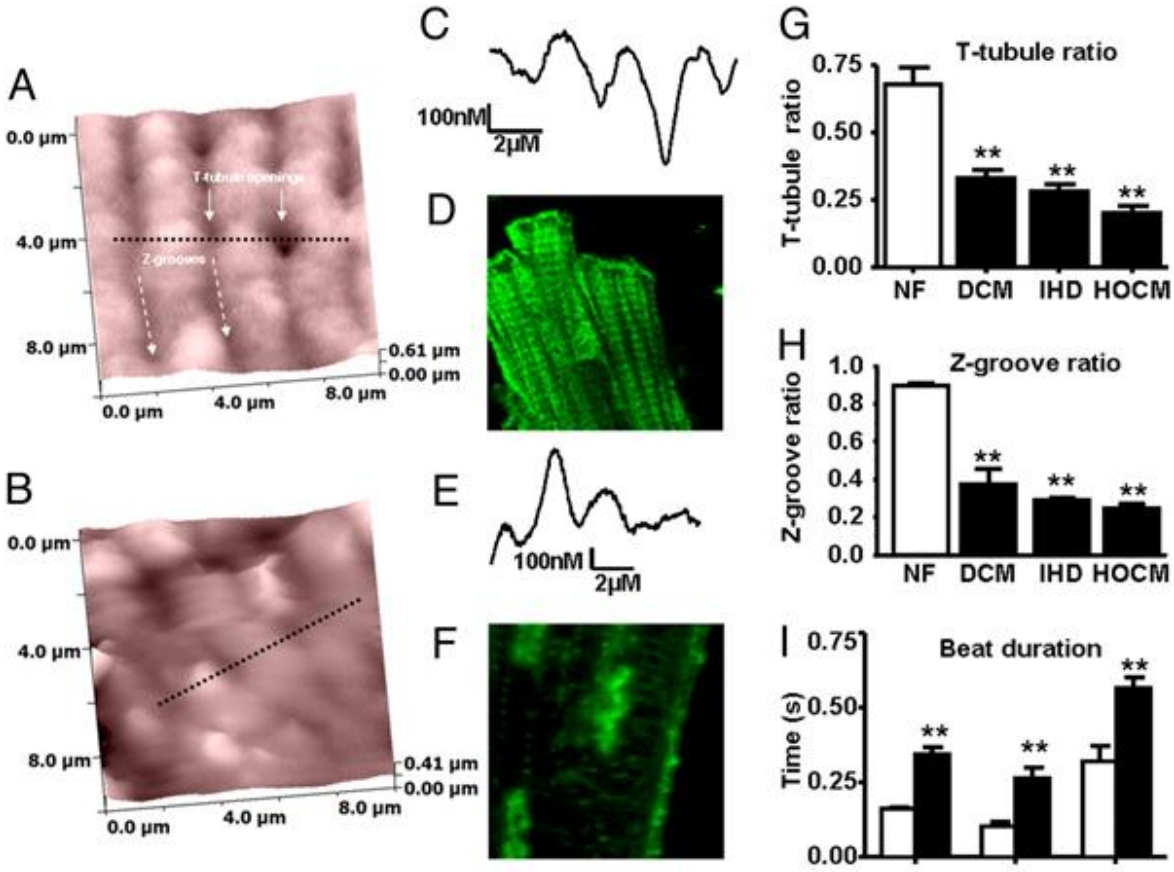

Figure 1.5. Loss of transverse tubules (T-tubules) and surface topography changes in ventricular cardiomyocytes from the failing human heart.

Scanning ion conductance microscopy (SICM) images from the surface of cardiomyocytes isolated from nonfailing (A) and failing (B) human hearts. Black dotted line represents the linear selection presented as a 1-dimensional (1D) surface contour map from nonfailing (c) and failing (e) human cardiomyocytes. d, f Confocal images after staining with di-8-ANNEPPS in human nonfailing (D) and failing cardiomyocytes (F). (G, H) T-tubule (G) and Z-groove (H) ratios in cardiomyocytes isolated from patients with dilated cardiomyopathy (DCM), heart failure (HF) secondary to ischaemic heart disease (IHD) or hypertrophic obstructive cardiomyopathy (HOCM); NF nonfailing. (I) Prolonged contraction time to peak (TTP) and relaxation times (R50 and R90) in failing human cardiomyocytes (solid bars, n=12) compared with nonfailing human cardiomyocytes (open bars, n=6). **P<0.01 vs. nonfailing. From (Lyon, MacLeod et al. 2009)

Previous studies confirmed the loss of T-tubule structures in ventricular cardiomyocytes from patients with heart disease (**Figure 1.5**), in a cell population that was typical of cardiomyocytes isolated from failing human ventricle as evidenced by contractile properties (Lyon, MacLeod et al. 2009). Interestingly, T-tubule changes were seen not only in ischemic and dilated cardiomyopathy but also in cardiomyocytes isolated from sections taken during septal reduction of hearts with hypertrophic obstructive cardiomyopathy. It was also found that T-tubule loss couldn't be considered as an isolated phenomenon in failing human heart; rather, it occurs as part of a general disruption of the sarcolemma. Significant changes to the remaining sarcolemmal architecture included loss of Z-grooves and reduced depth of the remaining Z-grooves interconnecting the T-tubule openings in failing ventricular cardiomyocytes (**Figure 1.5**). It appears that the observed pathological changes in surface structure were independent of the underlying etiology. Similar changes were observed in the ventricular cardiomyocytes from the infarcted failing rat hearts, with Z-groove structures markedly disrupted. The parallels between the human and rat cardiomyocytes suggest that the surface structure alterations are an integral part of the remodeling process that occurs during cardiac failure.

Reduction of the T-tubular network in ventricular cardiomyocytes leads to spatial heterogenesity of Ca^{2+} transient (Lipp, Huser et al. 1996) underlining the importance of this system for excitation-contraction coupling. Thus, T-tubules were shown as the key component of electrophysiological coupling required for dyads formation. However, it remains unknown how this loss of structural organization affects the spatial location and activity of LTCCs. Alteration of single channel activity and regulation of macroscopic LTCC current have been reported in heart failure, although data is divergent (Benitah, Alvarez et al. 2010). Though some studies have reported a decrease in LTCC current density (Santos, Barcellos et al. 1995; Aimond, Alvarez et al. 1999), others report no change in macroscopic LTCC current (Song, Pi et al. 2005). At present LTCC regulation in atrial cardiomyocytes generally remains undiscovered as does structural change during pathology; however few existing reports on patients with atrial fibrillation showed a marked

reduction of LTCC current density (Bosch, Zeng et al. 1999) and increased activity of single LTCCs (Klein, Schroder et al. 2003). Klein et al. (2003) suggested one possible mechanism of the increased single channel open probability during atrial fibrillation might involve a reduced activity of phosphatase 2A which is responsible for the channel dephosphorylation (Klein, Schroder et al. 2003).

A 45% decrease in T-tubule density in the sheep model of persistent atrial fibrillation has been associated with fewer LTCCs-RyR couplings and reduced efficiency of the excitation-contraction coupling (Lenaerts, Bito et al. 2009). In a sheep model of heart failure, T-tubules were disrupted more dramatically in atrial rather than in ventricular cardiomyocytes (Louch, Bito et al. 2004; Louch, Mork et al. 2006; Dibb, Clarke et al. 2009). This effect occurs because of T-tubule structural degradation and cellular hypertrophy. Naturally, this loss of T-tubules and disruption in dyad coupling are accompanied by dramatic changes in the spatial profile of the systolic Ca^{2+} transient.

1.10 L-type calcium channels

1.10.1 Classification of all voltage-gated calcium channels

Voltage-gated calcium channels (VGCCs) react to membrane potential changing by selectively allowing ions to flow by their electrochemical gradient. All VGCCs expressed in mammalians can be divided accordingly with current-voltage characteristics of current passing through into high voltage-activated (HVA) and low voltage-activated (LVA) channels, defined by the membrane potential at which the channels open. Physiological and pharmacological distinctions between VGCCs are represented by variation of α1subunits. Phylogenetic analysis divides α1 subunits into three clusters known as Ca_v1 ($Ca_v1.1$, $Ca_v1.2$, $Ca_v1.3$ and $Ca_v1.4$), Ca_v2 and Ca_v3, which correspond to L-type, non-L-type (HVA) and LVA or T-type channels, respectively (Catterall, Perez-Reyes et al. 2005). A further source of variation in LTCC currents is the influence of auxiliary subunits, of which

the β subunit has been most extensively studied (Birnbaumer, Qin et al. 1998; Walker and De Waard 1998; Hanlon and Wallace 2002; Dolphin 2003).
LTCC of the $Ca_V1.3$ type prevail in pacemaker cells and embryonic cardiomyocytes.

1.10.2 Structure of LTCC

LTCCs are composed with a pore-forming α subunit and smaller auxiliary subunits β, α2δ (Best and Kamp 2012) and in some channels γ (Perez-Reyes and Schneider 1995; Catterall 2000; Kamada, Yamada et al. 2004).

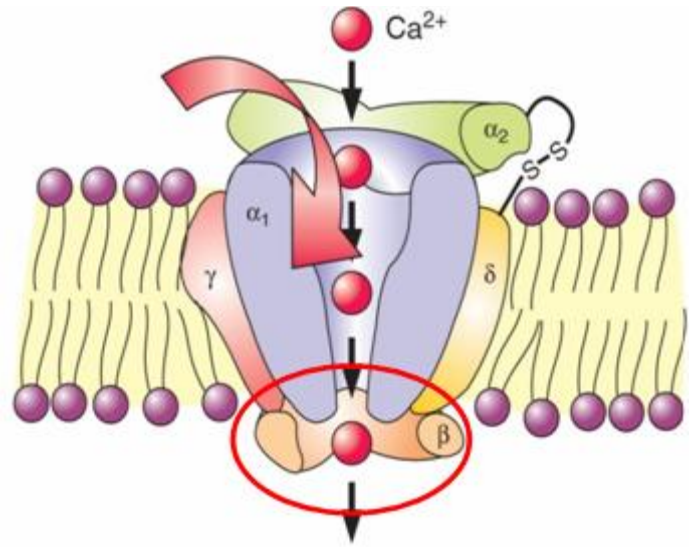

Figure 1.6. L-type calcium channel structure. The main pore-forming α_1 and auxiliary β, $\alpha_2\delta$ and γ subunits integrated in membrane phospholipid bilayers.

1.10.3 Ca_vα1C

All α_1 subunits of LTCCs contain four transmembrane homologous domains (I–IV) connected by intracellular loops that form the sides of the membrane pore (Doyle and Stubbs 1998). Each domain consists of six segments (S1–S6) with S4 segment including positively charged residues that act as a voltage sensor and the extracellular P-loop between S5 and S6 determining the ion selectivity of the channel. $Ca_v1.2$ (α1C, encoded by the CACNA1C gene) is the predominant α1 subunit in ventricular cardiomyocytes, but both $Ca_v1.2$ and $Ca_v1.3$ (α1D, encoded by CACNA1D) are expressed in atrial tissue as well as nodal cells, where $I_{Ca,L}$ contributes to automaticity (Mikami, Imoto et al. 1989; Takimoto, Li et al. 1997; Platzer, Engel et al. 2000; Mangoni, Couette et al. 2003; Zhang, Timofeyev et al. 2011).

The α_1 subunit plays the main functional role in the channel complex as pore-forming structure containing specific sites that interact with auxiliary subunits, binding sites for activators and blockers, and second messengers (G-proteins, PKA) (Hell, Yokoyama et al. 1993; Hell, Yokoyama et al. 1995).

1.10.4 Role of auxiliary β subunits

Although the α_1 subunit largely determines the current gating, the auxiliary subunits affect the voltage-dependence, the rate of activation and the kinetics of current inactivation of the channel (Lacerda, Kim et al. 1991; Birnbaumer, Qin et al. 1998).

Four main categories of modulating effects are observed (Foell, Balijepalli et al. 2004):

1 changes in channel gating;
2 alterations in membrane trafficking and localization of channels;
3 regulation of channels by second messenger systems; and
4 alterations in drug block properties.

The auxiliary subunits determine the increase in current density (Singer, Biel et al. 1991; Hermosilla, Moreno et al. 2011) well as the open probability and the duration of the current (Singer, Biel et al. 1991; Kamp, Perez-Garcia et al. 1996) and enhances ligand binding to the α_1 subunit (Chien, Zhao et al. 1995). For example, both functional and radio-ligand binding studies have provided the evidence that Ca^{2+} channel inhibition is affected by the interaction between $Ca_v\alpha_1$ and $Ca_v\beta$ subunits of the channel (Mitterdorfer, Froschmayr et al. 1994). It has been observed that the apparent sensitivity of $Ca_v1.2$ channels to verapamil is almost 14-fold higher if the $Ca_v\alpha_1$ subunit of the $Ca_v1.2$ channel is co-expressed with the $Ca_v\beta_3$ as compared with single $Ca_v\alpha_1$ expression (Lacinova, Ludwig et al. 1995). In addition, $Ca_v\beta$ subunits promote trafficking of the channel complex to the plasma membrane and modulate gating properties of the channel (Rickert and Fischer 1975; Singer, Biel et al. 1991; Chien, Zhao et al. 1995; Kamp, Perez-Garcia et al. 1996; Bichet, Cornet et al. 2000). Another potential important difference between $Ca_v\beta$ subunits exists for the regulation of Cav1.2 channels by protein kinase A (PKA) that, in part, involves the specific phosphorylation of residues uniquely found in the carboxyl terminus of the $Ca_v\beta2$ subunit and not the other $Ca_v\beta$ subunits (Gerhardstein, Puri et al. 1999). Many studies have described multiple functional effects of co-expression of $Ca_v\beta$ subunits with pore-forming $Ca_v\beta$ subunits. Co-expression of human $Ca_v\beta_{1b}$ and $Ca_v\beta_{1d}$ subunits increases single-channel activity of rabbit LTCC α_{1c}-subunit in HEK-293 cells (Cohen, Foell et al. 2005). An increased activity of the α_{1c}-subunit co-expressed with $Ca_v\beta_{2a}$ is also demonstrated in COS-7 cells (Kamada, Yamada et al. 2004). Until recently, the β_{2a} subunit was the only β_2 the single-channel property of Ca^{2+} channels reconstituted with β_{2a} subunits splice variant described in the rat heart (Perez-Reyes, Castellano et al. 1992). It was found that current characteristics of α_{1c} subunit co-expressed with β_{2a} are different from native channels (Birnbaumer, Qin et al. 1998; Yamada, Nagashima et al. 2001; Kamada, Yamada et al. 2004). Later, it was shown that β_{2c} subunit is also expressed in rat ventricular cardiomyocytes. Whole-cell patch clamp recordings demonstrated that the inactivation kinetics of recombinant channels co-expressed with β_{2c} subunits were different from those with β_{2a}

subunits but comparable with those of the native cells (Yamada, Nagashima et al. 2001).

1.10.5 β subunits in different mammalian

So far, four β subunit isoforms (β1–β4), encoded by distinct genes (CACNB1–4) each of which undergoes alternative splicing to generate a total of 18 or more unique β subunit isoforms in human myocardium (Foell, Balijepalli et al. 2004).
The human heart expresses a number of $Ca_v\beta_1$ (Collin, Wang et al. 1993), $Ca_v\beta_{2a}$ (Perez-Reyes, Castellano et al. 1992), and $Ca_v\beta_3$ isoforms (Hullin, Khan et al. 2003), while rabbit and rat hearts show only $Ca_v\beta_2$ (Hullin, Singer-Lahat et al. 1992; Haase, Pfitzmaier et al. 2000). Differences between species may contribute to the confusion (Perez-Reyes, Castellano et al. 1992; Gao, Puri et al. 1997). Immunolabelling analysis of canine ventricular membrane fractions demonstrated that all four $Ca_v\beta$ subunits are expressed at the protein level, and the $Ca_v\beta$ subunits show differential subcellular localization (Foell, Balijepalli et al. 2004).

1.10.6 Spatial distribution of β subunits in cardiomyocyte

In the ventricles, $Ca_v\beta_{1b}$, $Ca_v\beta_2$, and $Ca_v\beta_3$ are predominantly localized to the T-tubule, whereas $Ca_v\beta_{1a}$ and $Ca_v\beta_4$ are more prevalent on the surface of the cell (Foell, Balijepalli et al. 2004). Earlier investigations have shown $Ca_v\beta_2$ and α_{1C} subunits to co-localize on T-tubule membranes in rabbit ventricular cardiomyocytes (Gao, Puri et al. 1997). Interestingly, atrial and ventricular cardiomyocytes demonstrate different levels of mRNA of β_2 subunits. For example, expression of β_2 subunits is significantly higher in ventricle than in atria, while β_4 is highly expressed in atria than in ventricles (Chu, Larsen et al. 2004).

1.10.7 Spatial localization of LTCCs in cardiomyocytes

Immunostaining studies of ventricular cells (Scriven, Dan et al. 2000; Brette and Orchard 2003; Brette, Salle et al. 2006) demonstrated that approximately 80% of all LTCCs are located in T-tubules in close proximity to the calcium sensing and release units, the ryanodine receptors (RyRs) at the sarcoplasmic reticulum (Smyrnias, Mair et al. 2010). Such T-tubule organization allows the electrical impulse to be conducted effectively into the cell interior, where Ca^{2+} influx triggers the opening of RyRs and subsequent release of Ca^{2+} from SR stores which brings about cell contraction (Kaftan, Marks et al. 1996). Detailed description of the microarchitecture of the dyads and LTCC-RyR interaction has been reviewed elsewhere (Winslow and Greenstein 2011; Scriven, Asghari et al. 2013).

Until recently, spatial distribution of LTCCs on the cellular membrane was assessed by immunolabelling or electron microscopy techniques, which lacked information on the functionality of visualized proteins. As a result, the observed images likely represent mixed populations of both functional and silent channels, as well as those in reserve pools waiting to be recruited under changing physiological or pathological conditions (Gu, Gorelik et al. 2002). However, recent methodological approaches made it possible to study the clustering of functional ion channels within specific microdomains (Bhargava, Lin et al. 2013; Novak, Gorelik et al. 2013). To study the distribution of functional ion channels on a cellular membrane, a combination of SICM and conventional patch clamp was used. Using this new method, Bhargava et al (2013) have recently assessed the likelihood of detecting LTCCs in discrete regions of the sarcolemma (Bhargava, Lin et al. 2013). **Figure 1.7B** shows the distribution of functional LTCCs recorded in dyadic (T-tubules) and extradyadic (crest of the sarcolemma) microdomains in rat adult ventricular cardiomyocytes. Of 30 patches formed with a clipped pipette (Rp=30-35 MΩ) in the crest region, only 2 showed channel activity (6.6%) as opposed to a higher LTCC activity observed in 23 of 80 patches in T-tubules (28.75%; $P<0.02$) (**Figure 1.7C**). The low occurrence of channels at the crest, their sensitivity to isoproterenol, and their biophysical properties are all consistent with

the notion that the obtained recordings are from LTCCs, with nanoscale spatial resolution (Chen-Izu, Xiao et al. 2000; Gu, Gorelik et al. 2002).

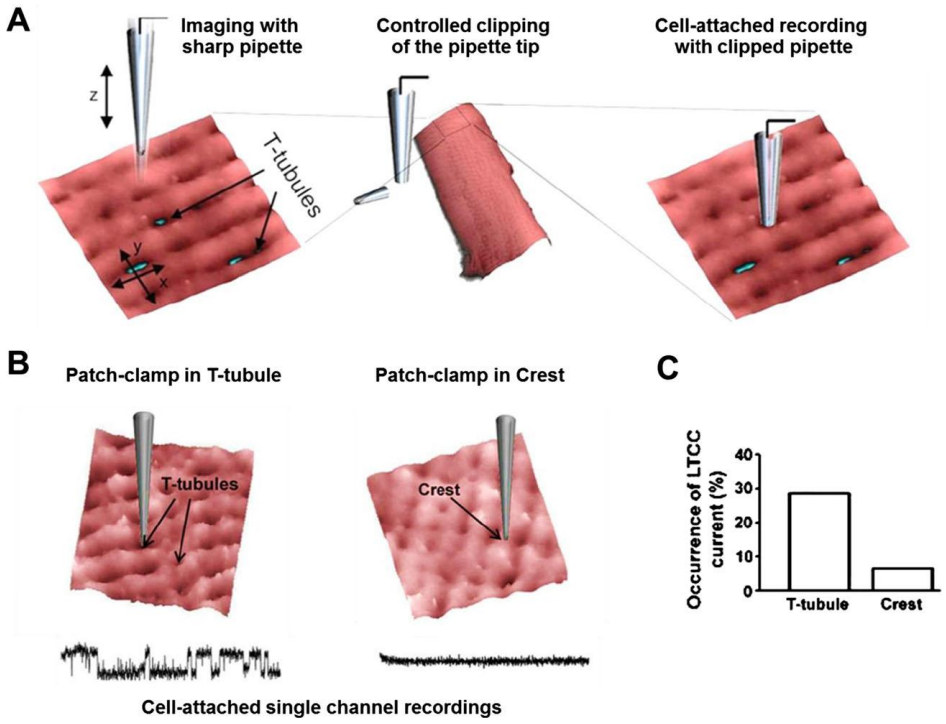

Figure 1.7. Super-resolution scanning patch-clamp reveals distribution of functional L-type calcium (Ca2+) channels in ventricular cardiomyocytes.

(A) A sharp high resistance pipette used to resolve the topographical structure of the cardiomyocytes. The pipette is moved to a cell-free area on the dish and the fall rate is increased to clip the pipette tip. The pipette is then returned to the surface of choice, and patch clamp can be performed with a wider pipette tip. (B) Functional L-type Ca2+ channels recorded in the T-tubule (left panel) and crest (right panel). (C) Occurrence of functional L-type Ca2+ channels (LTCC) recorded in T-tubules and crest in rat adult ventricular cardiomyocytes. From (Bhargava, Lin et al. 2013).

Of note, the probability of recording LTCCs on the surface of neonatal rat ventricular cardiomyocytes, which lack T-tubular structures (Haddock, Coetzee et

al. 1999) was 30.8% (LTCC activity observed in 4 of 13 separate recordings (Bhargava, Lin et al. 2013), suggesting that the structural organization of the T-tubule coincides with increased clustering of functional LTCCs at that specific location. Lack of a regular T-tubular system in atrial cardiomyocytes has been thought to underlie their unique Ca^{2+} signaling (Dobrev, Teos et al. 2009).

Thus, differential subcellular distribution of LTCCs and their coupling to RyRs of the SR has been proposed in atrial cardiomyocytes (Trafford, Clarke et al. 2013).

1.11 Ca efflux

Besides Ca^{2+} influx prior to contraction, T-tubular network is also an important site for Ca^{2+} extrusion during diastole. It has been shown that T-tubules are responsible for ~71% of trans-sarcolemmal Ca^{2+} extrusion (Chase and Orchard 2011). Ca^{2+} efflux occurs by three main routes: re-sequestration of Ca^{2+} into SR via a Ca-ATPase (SERCA), Ca^{2+} removal from the cell by NCX and plasmalemmal Ca-ATPase (PMCA). By using pharmacological separation as well as detubulation procedure, Chase and Orchard (2011) had shown in rat ventricular cardiomyocytes, that SR is responsible for 86% of cytoplasmic calcium removal while NCX contributes 8%, and Ca ATPase 6%, to calcium removal (Chase and Orchard 2011). The authors also demonstrated that calcium extrusion via the sarcolemmal Ca-ATPase occurs only at the T-tubules, and is not regulated by basal PKA activity, while calcium extrusion via NCX occurs across both the surface (34%) and T-tubule membranes (66%), but predominantly across the T-tubule membrane due, in part, to localized stimulation of NCX by PKA at the T-tubules. These results agree with previous estimates obtained by co-immunolocalization analysis (Scriven, Dan et al. 2000; Thomas, Sjaastad et al. 2003). In addition to local positive control of SR Ca^{2+} release by LTCC, NCX that is located closely to the junctional SR has been proposed to negate local Ca^{2+} induced Ca^{2+} release by suppressing SR Ca^{2+} leak and Ca^{2+} sparks during rest (Bovo, de Tombe et al. 2014). It should be noticed that the fraction of calcium that

is re-uptaken into the SR by SERCA or extruded from the cell by NCX and PMCA might vary significantly depending on the animal species. In rats and mice, Ca^{2+} removal mechanisms predominantly rely on SERCA activity, whereas in larger species (e.g., rabbit, human), there is a significant contribution of NCX to $[Ca^{2+}]_i$ regulation. As shown by Bassani et al. (1994) the fractions of Ca^{2+} transported during a twitch by the SR, NCX and slow systems are 70, 28 and 2% respectively in rabbit cardiomyocytes and 92, 7 and 1% respectively in rat cardiomyocytes (Bassani, Bassani et al. 1994). It could be thus proposed that spatial organization of the Ca^{2+} extrusion mechanisms may vary from species to species similar to Ca^{2+} influx mechanisms. Detailed review of recent and ongoing discoveries that focus on the dyad structure and function can be found elsewhere (Cannell and Kong 2012; Scriven, Asghari et al. 2013; Sipido, Acsai et al. 2013; Sipido and Cheng 2013).

1.12 EC coupling gain

Ca^{2+} entry via LTCC is the major trigger for SR Ca^{2+} release (Ca^{2+} sparks) by RyR_2 and summation of the Ca^{2+} sparks during depolarization of the cell underlie the basis for Ca^{2+} homeostasis.

It was demonstrated several times that cardiomyocytes isolated from failing mammalian heart display smaller Ca^{2+} transient and contractility in parallel with unchanged calcium current I_{Ca} (Gomez, Valdivia et al. 1997). (Beuckelmann, Nabauer et al. 1992).

Reduction in Ca^{2+} transient might be explained by decrease in I_{Ca} or by reduction in the sensitivity of RyR_2 to the Ca^{2+} trigger. Any changes in properties of the SR Ca^{2+} release are the characteristics of a defective EC coupling observed in failing heart.

The relationship between calcium current and the probability of triggering Ca^{2+} release from the SR has been termed EC coupling gain (Beuckelmann and Wier 1988; Wier, Egan et al. 1994). The authors (Gomez, Valdivia et al. 1997) indicated that EC coupling gain was decreased in their heart failure rat model. This

decreased EC gain appears to be a sign of a defect in the coupling between the LTCCs and RyR2s. In many cases, the reduced gain is due to a reduced SR Ca^{2+} load observed in some types of heart failure (Hobai and O'Rourke 2001; Pogwizd, Schlotthauer et al. 2001).

Lindner et al. investigated Ca^{2+} sparks in cardiomyocytes from terminally failing human hearts. Failing cardiomyocytes showed significant differences in specific spontaneously Ca^{2+} spark properties compared with non-failing hearts (decreased spark frequency and increased time to peak and half-time decay) (Lindner, Brandt et al. 2002). The authors suggest that besides the decreased SR Ca^{2+} load (Lindner, Erdmann et al. 1998), other mechanisms in the Ca^{2+} release mechanism should be considered (Sjaastad, Wasserstrom et al. 2003). In contrast to the results of Gomez et al.(Gomez, Valdivia et al. 1997), Shorofsky et al., using cardiomyocytes from hypertrophied spontaneously hypertensive rats, found an increase in contractility, Ca^{2+} transients, and the average Ca^{2+} spark amplitude (big sparks) with unchanged calcium current density and SR Ca^{2+} load. (Shorofsky, Aggarwal et al. 1999)

Thus, Ca^{2+} influx via LTCCs coupled with RyRs provides raised Ca^{2+} release from SR without big calcium sparks and finally increases EC coupling gain (Wier, Egan et al. 1994). Other possibility of EC coupling gain include T-tubule system altering and, or increased phosphorylation of RyR_2, LTCCs. (Marx, Reiken et al. 2000; Ibrahim, Gorelik et al. 2011). Moreover, reduction in phosphorylation of LTCCs and SERCA, or reduced Ca^{2+}-sensitivity of SERCA2a must be also considered (Schwinger, Munch et al. 1999).

NCX when overexpressed behaves like a sponge and provides compensatory help by reducing the amount of Ca^{2+} entering through the LTCCs before the trigger-induced Ca^{2+} release from SR; this mechanism represents a new vision of altered EC coupling during heart failure. However, Henderson et al. reported a cardiac-specific NCX KO mouse model with normal cardiac function (Henderson, Goldhaber et al. 2004).

1.13 EC coupling changes in atrial cardiomyocytes

Maisel et al. demonstrated that patients with heart failure frequently develop atrial fibrillation (AF) (Maisel and Stevenson 2003). In parallel with conductive and structural changes such as atrial dilatation, atrial cardiomyocytes represent alterations in Ca^{2+} handling (Yeh, Wakili et al. 2008; Greiser, Neuberger et al. 2009).

Slower Ca^{2+} transient decay in AF vs sinus rhythm might be caused by increased Ca^{2+} leak via RyR, whose activity is enhanced in AF (Neef, Dybkova et al. 2010). Moreover, the heterogeneous subcellular Ca^{2+} dynamics of human atrial cells and slow propagation of Ca^{2+} transients from peripheral to central sarcoplasmic reticulum (SR), occurring in AF can be expected because of lack of T-tubules (Koivumaki, Korhonen et al. 2011). Disrupted Ca^{2+} may be explained also by changed activity of SERCA2a. Unfortunately, this part is not clear as there are many controversial studies of atrial cardiomyocytes in AF which reported either no changes (Schotten, Greiser et al. 2002; Lenaerts, Bito et al. 2009), or reduced (Greiser, Neuberger et al. 2009), or increased (El-Armouche, Boknik et al. 2006) function of SERCA2a (based on protein expression and phosphorylation levels). Recent work in rats has shown that the PLB/ SERCA2a ratio is lower in atria compared with ventricles (Walden, Dibb et al. 2009) compatible with increased SERCA2a function in atria.

1.14 CAVEOLAE

Caveolae are specialized lipid rafts, invagination of the plasma membrane which are enriched in cholesterol, glycophospholipids and lipid-anchored proteins (Razani, Woodman et al. 2002; Cohen, Hnasko et al. 2004; Gratton, Bernatchez et al. 2004; Harvey and Calaghan 2012). Caveolin, the main protein component of caveolae, are the most well studied and are 18-22 kDa membrane proteins, which serve to produce a bend of the membrane and the shape of the caveolae. Caveolin recruits components of various signaling pathways, including G_i proteins,

endothelial (Lisanti, Scherer et al. 1994) nitric oxide synthase (Barouch, Harrison et al. 2002; Feron and Balligand 2006) and several protein kinases. Accordingly, caveolae are implicated in endocytosis, transcytosis and as being signalosomes (Kurzchalia and Parton 1999; Harvey and Calaghan 2012).

Three genes (CAV1–3) encode six known caveolin subtypes (caveolin-1α and -1β; caveolin-2α,-2β, and -2γ; and caveolin-3) that have varying tissue distribution (Razani, Woodman et al. 2002). Caveolin Cav 1 and Cav2 are expressed in most cell types, whereas expression of Cav3 is restricted to cardiac, skeletal, and smooth muscle types, as well as some types of neurons (Song, Scherer et al. 1996; Razani, Woodman et al. 2002; Boulware, Kordasiewicz et al. 2007). The lack of morphologically distinct caveolae in skeletal muscle from Cav3 knockout mice highlights the importance of caveolin in caveolae formation (Galbiati, Engelman et al. 2001). Neonatal ventricular cardiomyocytes lack T-tubules, but have an increased caveolae density. It has been shown that T-tubular development in striated muscle depends on cholesterol and Cav3 (Parton, Way et al. 1997; Razani, Woodman et al. 2002), thus caveolae may be a developmental precursor of T-tubules and share some of their functions.

Cav3 is crucial for the function of caveolae in cardiomyocyte, and it has been shown to be present in cell within T-tubular and outside of T-tubular domains. There are series of controversial studies demonstrated caveolae connected with T-tubule system. For example, Levin et al. showed that true caveolae did not appear to be present in the domains of T-tubules directly opposing junctional SR (Levin and Page 1980). However, at the same time Cav3 was found to be co-localized with T-tubular membrane as a messenger of EC coupling supporting interaction between T-tubule with RyR (Calaghan and White 2006). Recent super-resolution microscopy studies suggested that Cav3 is present in T-tubules but it can form caveolae structures only at the T-tubule openings in front of extracellular matrix (Wong, Baddeley et al. 2013).

Caveolae are shown to house G-proteins and members of G-protein signaling pathways (Head, Patel et al. 2005), suggesting important role of caveolae membrane structure in the spatial control of signaling in the cardiomyocytes, while

dyad represents a prime site of signaling cascades leading to excitation-contraction coupling. Along with the essential scaffolding protein Cav3, a number of different ion channels and transporters have been found to localize to caveolae in ventricular cardiomyocytes including Ca^{2+} and Na^{+} channels, pacemaker channels (HCN4), Na^{+}/Ca^{2+} exchanger and others (Balijepalli and Kamp 2008). Closely associated with these channels are specific macromolecular signaling complexes that provide highly localized regulation of the channels. In addition to critical subpopulation of LTCCs localized to dyadic junctions, extradyadic LTCCs associated with district regions of surface membrane have been distinguished (Balijepalli, Foell et al. 2006; Makarewich, Correll et al. 2012). Several methods, including co-immunoprecipitation (Balijepalli, Foell et al. 2006; Shibata, Brown et al. 2006), immunofluorescence (Balijepalli, Foell et al. 2006; Cavalli, Eghbali et al. 2007) and caveolae-specific inhibition of LTCCs (Makarewich, Correll et al. 2012) have been used to demonstrate the presence of LTCCs within caveolae in ventricular cardiomyocytes. The presence of Cav3 has been used as a marker of the localization of proteins to caveolae versus non-caveolar lipid rafts.

The function of LTCCs localized in caveolar structures remain open to question. It has been proposed that some LTCCs housed in Cav3–rich signaling microdomains, could play an important role in modulation of Ca^{2+} signaling, particularly in cells lacking T-tubules such as atrial (Schulson, Scriven et al. 2011) and neonatal ventricular (Lohn, Furstenau et al. 2000) cardiomyocytes. Probably, caveolae targeted LTCCs might be responsible for an abundant peripheral (non-junctional) focal Ca^{2+} release (Ca^{2+} sparks) in atrial cardiomyocytes, via inositol 1,4,5-trisphosphate (IP_3) dependent activation of non-junctional RyRs (Woo, Cleemann et al. 2003; Wang, Dedkova et al. 2005). Recently, using a caveolae targeted LTCCs antagonist, Makarewich et al. (2012) demonstrated that in ventricular cardiomyocytes the Ca^{2+} influx through LTCCs within caveolae signaling domains could activate pathological cardiac hypertrophic signaling. Notably, the authors demonstrated that this Ca^{2+} influx could be selectively blocked without reducing cardiac contractility (Makarewich, Correll et al. 2012).

Since a variety of different ion channels is localized to caveolae microdomains, it has been proposed that caveolae-specific ion channel remodeling can be critical to

the pathological remodeling and the genesis of arrhythmias. The extent to which caveolar ion channels contribute to these conditions is only emerging. Given that ion channels co-localize with Cav3 in caveolae, their pathological modifications may underlie arrhythmia mechanisms in conditions like hypertension, diabetes, ischemic heart disease, and heart failure. Structural remodeling of caveolae was observed during certain cardiac pathologies. The distribution of Cav3 protein is dramatically altered in heart failure, with an increased proportion of Cav3 in the detergent-soluble fraction (Ratajczak, Damy et al. 2003). Mutations in CAV3 have been linked to the LQT syndrome phenotype associated with a 2- to 3-fold increase in late sodium current compared with wild-type Cav3 (Vatta, Ackerman et al. 2006). Subsequently, Vaidyanathan et al (2013) have shown $K_{ir}2.1$ loss of function is additive to the increase described previously in late I_{Na}, prolonging repolarization and leading to arrhythmia generation in Cav3-mediated LQT9 (Vaidyanathan, Vega et al. 2013). Similar increases in late I_{Na} as well as reduced $I_{Ca,L}$ and I_{to}, however no changes in I_{K1}, have been observed in $Cav3^{-/-}$ mice (Markandeya, Feng et al. 2013). Interestingly, pharmacological drugs widely used for the prevention of cardiovascular disease such as statins and atorvastatin, which directly act on the cholesterol synthesis pathway and lipids rafts, affect caveolar turnover by limiting their endocytosis (Goebel, Logan et al. 2005; Peivandi, Huhn et al. 2005).

1.15 Beta-adrenergic regulation of heart

Contraction and relaxation of the heart are regulated by its electric activity. Heartbeat is tightly regulated by autonomic and hormonal control. Activation of the sympathetic nervous system increases the heartbeat rate, contractility, and relaxation rate (positive chronotropic, inotropic, and lusitropic effects, respectively). This is caused by catecholamine epinephrine and, or norepinephrine (as also known as adrenalin and noradrenalin, respectively) binding to adrenergic receptors (AR).

The catecholamines are ordinary secreted by the sympathetic nerve endings and by the adrenal medulla, and bind to the ARs in huge spectrum of organs and tissue such as myocardium, smooth muscle cells of arteries and bronchopulmonary segment, skeletal muscle, iris, pancreatic cells, adipocytes. That provokes increase in heart rate in respiratory rate, muscle contraction, inhibition of insulin secretion, enhance lipolysis, and provide the fight-or-flight response.

Mammalian heart express nine AR subtypes, which mediate a variety of cellular functions. Distinct genes encode them. The most abundant types are the β-ARs. There are three subtypes: β_1, β_2 and β_3, primarily in ventricle the β_1-AR and substantially β_2-AR in ratio 70-80%: 30-20%, respectively (Brodde 1991; Post, Hammond et al. 1999). In the human atrium the ratio is 60–70%: 40–30% (Brodde 1991).

Adrenergic receptors (ARs) are G protein-coupled receptors, which contain seven hydrophobic membrane-spanning α-helical domains. Highest amino acid conservation is present in the transmembrane regions, which determine the specificity of ligand binding. The cytoplasmic regions, which interact with other cellular proteins to mediate various signalling events, have more variability (Lefkowitz, Rockman et al. 2000).

β_1-AR is coupled exclusively to $G\alpha_S$, whereas β_2-AR is coupled to both G_s and the inhibitory $G_{i/o}$ (Xiao, Zhu et al. 2004). Activity of β_1-AR, located at the plasma membrane, produces elevation in cAMP throughout the cell, whereas β_2-AR produces spatially restricted cAMP increase, probably close to the T-tubules.(Xiao, Cheng et al. 1999; Nikolaev, Moshkov et al. 2010; Best and Kamp 2012). β_1-AR plays a dominant role in increasing chronotropy and ionotropy in cardiac cardiomyocytes, whereas β_2-AR produces only modest chronotropic effects (Xiang and Kobilka 2003; Xiao, Zhu et al. 2006). In addition, a minor β_3AR subtype is also expressed in myocardium and modulates cardiomyocytes function (Rasmussen, Figtree et al. 2009).

1.16 Control of cardiac-excitation-contraction coupling

Mechanism of β-adrenergic receptor action involves activation of G-protein subunit. Activated $G\alpha_s$-GTP separates from Gβγ and activates adenylyl cyclase (AC), resulting in elevated cyclic AMP (cAMP) levels and activation of the cAMP-dependent protein kinase (protein kinase A [PKA]), which can phosphorylates multiple target protein, among them LTCCs, troponin I, and PLB. The β_1-AR and β_2-AR couple to G_s proteins to activate adenylate cyclase (AC), which mediates the conversion of adenosine triphosphate (ATP) into cyclic adenosine monophosphate (cAMP). This leads to the activation of PKA, which in turn phosphorylates several substrates, including L-type Ca^{2+} channels. The β_2-ARs also couple to G_i proteins, which counteract the G_s coupled activation of AC, resulting in a reduction of cAMP levels (Brodde and Michel 1999; Chen-Izu, Xiao et al. 2000; Lefkowitz, Rockman et al. 2000; Xiao 2000). The physiological impact as well as the mechanism of action of β_3-ARs is less clear, although a more prominent role in heart failure has been suggested. Because β_3-ARs have been reported to produce negative inotropy in human ventricle, a future therapeutic modality might be their blockade in the setting of heart failure (Conrath and Opthof 2002).

Catecholamines produces their effect by exerting both of the sarcolemmal and SR Ca^{2+} fluxes. PKA phosphorylates the L-type calcium channels, which increases its open probability and causes more Ca^{2+} to enter the cell with each action potential contributing to the increase of contractile force. If more Ca^{2+} enters the cell, more will be available to be pumped into the SR, causing more to be available for release with subsequent action potentials.

The second action of catecholamines is to increase the SERCA activity via phosphorylation of phospholamban on the SR enhancing the efficiency of contraction (positive lusitropy). If the activity of SERCA is increased, a greater portion of the cytosolic Ca^{2+} will be pumped into the SR, making a greater amount

available for release by a subsequent action potential. Thus, catecholamines tend to shorten phase 2 of action potential and thus shorten the duration of systole.

The third action, catecholamines triggers phosphorylation of the myofilament protein Troponin I decreasing its calcium sensitivity and enhancing lusitropic effect as dissociation occurs more rapidly.

Finally, phosphorylation of RyR increases its sensitivity and in consequence increases the amplitude of CICR.

1.17 Beta-adrenergic regulation of L-type calcium channels

Increased Ca^{2+} entry into the cardiomyocytes via the cardiac $Ca_V1.2$, mediated by both β_1- and β_2-AR, (Reuter 1983; Tsien 1983; Trautwein and Hescheler 1990; Benitah, Alvarez et al. 2010) substantially contributes to the positive inotropic effect of β-AR activation. This process is central to normal cardiac physiology and is involved in pathophysiological changes occurring in cardiac hypertrophy and heart failure (Post, Hammond et al. 1999; Marban 2002; Benitah, Alvarez et al. 2010). Detailed characterization of the β-AR–activated, PKA-mediated regulation of LTCC is, therefore, crucial for understanding normal and pathological cardiac physiology.

Two forms (of different size) of the main subunit (α_{1C}) of the L-type Ca^{2+} channel have been detected: a full-length form of ~240–250 kDa and a C-terminally truncated form of ~190–210 kDa. The full-length rabbit α_{1C} subunit is phosphorylated both in vitro and in vivo by PKA in response to elevated cAMP concentrations, but the truncated channel subunit is not (Gao, Puri et al. 1997; Schwencke, Yamamoto et al. 1999; Kamp and Hell 2000; Steinberg and Brunton 2001; Steinberg 2004). In intact cardiomyocytes, the majority of α_{1C} subunits are full-length. The truncated form of the α_{1C} subunit is generated by post-translational proteolytic processing (Liu, Yasui et al. 1999). The C-terminal fragment of 30–50

kDa contains a domain rich in proline, which mediates membrane association. Deletion of either the proline-rich domain or truncation of the C-terminus results in an increase of $I_{Ca\text{-}L}$, which suggests that a region in the C-terminal domain has an inhibitory effect on the function of LTCCs (Gerhardstein, Gao et al. 2000).

According to previous studies, the full-length rabbit cardiac α_1 subunit contains six potential PKA phosphorylation sites: Ser 124 in the N-terminal part, and five others in the C-terminal part at positions 1575, 1627, 1700, 1848, and 1928. Mutation of Ser 1928 to alanine results in complete loss of cAMP-mediated phosphorylation and in reduction of $I_{Ca\text{-}L}$ (Perets, Blumenstein et al. 1996; Kamp and Hell 2000). The C-terminally truncated α_{1C} subunit lacks Ser 1928 and, thereby, is no longer a substrate for PKA, confirming that, despite the presence of six putative sites, Ser 1928 is the only site, which is in fact phosphorylated by PKA in the α_{1C} subunit (De Jongh, Murphy et al. 1996; Kamp and Hell 2000). A previous report on the phosphorylation of the α_{1C} subunit by PKA at Ser 1627 and possibly Ser 1700 (Norman and Leach 1994), has not been confirmed.

Besides the α_{1C} subunit, also the β_2 subunit is a second important target of PKA (Haase, Karczewski et al. 1993). PKA still increases $I_{Ca\text{-}L}$ generated by channels with a truncated α_{1C} subunit, when they are associated with a wild type β_{2a} subunit (Bunemann, Gerhardstein et al. 1999). Although the rat β_{2a} subunit contains two strong consensus sites for PKA-mediated phosphorylation at Thr 164 and Ser 591, the actual sites of PKA-mediated phosphorylation are at other residues, because mutants that lack both of the consensus sites remain good substrates for phosphorylation by PKA (Gerhardstein, Puri et al. 1999). Phosphopeptide mapping and β_{2a} truncation demonstrated that the major sites of PKA-mediated phosphorylation occur at three loose consensus sites for PKA: Ser 459, Ser 478 and Ser 479. Mutation of Ser 459 to alanine results in a reduced rate and degree of phosphorylation of the β_{2a} subunit by PKA (Gerhardstein, Puri et al. 1999), without altering the basic functional properties of the regulatory β_{2a} subunit (Bunemann, Gerhardstein et al. 1999). Mutation of Ser 478 and Ser 479 to alanine, however, completely abolishes the PKA-induced phosphorylation (Gerhardstein, Puri et al. 1999) and prevents PKA-induced $I_{Ca\text{-}L}$ (Bunemann, Gerhardstein et al. 1999; Kamp and Hell 2000). Phosphorylation of the β_{2a} subunit

at Ser 478 and Ser 479 is pivotal for the regulation of the cardiac LTCC in response to PKA. Phosphorylation of the other associated subunit, the $\alpha_2\delta$ complex, which is less tightly associated with the α_1 subunit and consists of an extracellular subunit, has not been detected (Kamp and Hell 2000).

For the regulation of the LTCC by PKA, localization of the enzyme to the Ca^{2+} channel is required. PKA is often anchored to specific subcellular compartments by PKA anchoring proteins (AKAPs). These proteins contain a targeting domain that directs the AKAP to a specific cellular site, and a kinase anchoring domain that binds the regulatory subunits of PKA (Bunemann, Gerhardstein et al. 1999). Targeting PKA in close proximity to the LTCC by an AKAP may facilitate phosphorylation of the channel. Anchoring of PKA to the membrane through association with AKAP79 indeed facilitates PKA-mediated phosphorylation of Ser 1928 in the rabbit α_{1C} subunit. AKAP15 directly interacts with α_{1C} through a leucine zipper motif present in the C-terminal tail of the subunit (Hulme, Lin et al. 2003). Phosphorylation of the β_{2a} subunit however does not require an AKAP (Bunemann, Gerhardstein et al. 1999; Liu, Yasui et al. 1999). Thus, for appropriate PKA-dependent phosphorylation and stimulation of L-type Ca^{2+} channels the enzyme has to be anchored to the membrane by an AKAP. Another important giant sarcolemmal protein (AHNAK) with comparable function has been described as well (Haase, Podzuweit et al. 1999).

Besides co-localization of PKA with LTCC adenylate cyclase was investigated to be close to the LTCCs in the T-tubules (Gao, Puri et al. 1997) and to Cav3 (Schwencke, Yamamoto et al. 1999). That gives a suggestion about specific compartmentalisation of whole signalling system involving kinases, second messengers and adrenergic receptors as a primal transmitters for introcellular signal transduction.

1.18 Compartmentalization of beta-adrenergic receptors

The concept of spatiotemporal regulation of LTCC activities by second messengers provides new insights into understanding how β-ARs signaling is translated into physiological contraction response in highly organized cardiomyocytes (Cooper 2005; Houslay, Baillie et al. 2007; Zaccolo and Movsesian 2007; Zaccolo 2009)
Recent studies have significantly advanced understanding of these structures in the spatial distribution of βAR signaling in cardiomyocytes.

Based on cAMP signaling localization, activation of LTCCs was shown in a local vicinity by β_2-AR at the stimulation site (Xiao and Lakatta 1993; Jurevicius, Skeberdis et al. 2003; Cooper 2005) stimulation and in the distance by β_1-AR stimulation along with far-reaching cAMP diffusion (Xiao and Lakatta 1993; Cooper 2005).
Using real-time imaging in living cardiomyocytes, Nikolaev et al observed that the cAMP induced by β_2AR stimulation is confined in the T-tubules in ventricular cardiomyocytes (Nikolaev, Moshkov et al. 2010). In contrast, the cAMP induced by β_1AR is distributed in both sarcolemma membrane and T-tubules (Nikolaev, Moshkov et al. 2010), while the β_1ARs themselves are distributed throughout both caveolae or, and lipid rafts and non-lipid raft membrane domains (Rybin, Xu et al. 2000).

Together, these studies indicate that activation of β_1AR promotes a broad distribution of intracellular cAMP signal, whereas the β_2AR actions are local. Given that in contrast to β_1-AR, the β_2AR signaling is sensitive to disruption of caveolae (Balijepalli, Foell et al. 2006).
That gives a controversial to previous study suggestion that T-tubules do not have caveolae in their structure.

1.19 Pathological changing of the beta adrenergic receptors

Patients with dilated cardiomyopathy demonstrate reduced β-AR responsiveness of the myocardium. This disturbed β-AR function may be based on an elevated sympathetic tone observed during heart failure. In these patients the tissue concentration of norepinephrine is decreased and the plasma concentration elevated, providing evidence of sympathetic stimulation (Thomas and Marks 1978; Leimbach, Wallin et al. 1986). Such an increase in plasma catecholamines may result in downregulation of the β-AR and in the depression of the β-AR-mediated signal transduction axis (Bristow, Ginsburg et al. 1986; Brodde 1991).

Moreover, prolonged adrenergic stimulation may induce metabolic and electrophysiological disturbances in the myocardium, resulting in tachyarrhythmia and even sudden death (Haft 1974). Such chronic adrenergic stimulation causes alterations of the expression and activity of the components of the β-AR-mediated signal transduction cascade. Human studies investigated impairment of targets of the β_1-AR signal cascade and reduced expression of the β_1-AR on the mRNA and protein levels (Bristow, Minobe et al. 1988; Ungerer, Bohm et al. 1993) accompanied with reduced adrenergic responsiveness of the cardiomyocytes. It has been also found that in heart failure the potentiation of LTCC current by beta-adrenergic regulation is lost, indicating phosphorylation defects (Zhang, Moore et al. 1995; Aimond, Alvarez et al. 1999).
Furthermore, the expression of the G-protein receptor kinase is elevated. This kinase induces the uncoupling of the β-AR. These alterations of the β-AR signal cascade might be induced by an elevated catecholamine release or by agonist-like autoantibodies directed against the β_1-AR found in patients with dilated cardiomyopathy. Both, permanent stimulation with catecholamines and chronic treatment with agonistic β_1-AR autoantibodies cause a reduction of the expression of the β_1-AR on mRNA and protein level in “in vitro” experiments. Moreover, an overexpression of the β_1-AR, the stimulatory G_s protein, and the PKA induce detrimental alterations of the cardiac function and morphology in transgenic animals, which developed heart failure accompanied by an increased mortality

rate. Thus, β_1-AR signal cascade contributes to the progression of cardiac dysfunction and the development of heart failure in animal models and in humans.

Interestingly, in failing cardiomyocytes β_2-ARs redistribute from the T-tubule microdomains and are detected elsewhere across the plasma membrane, which correlates with impaired cAMP signaling through these receptors. Association of β_2-ARs and LTCCs within the Ca^{2+} signaling complex in neurons has been previously shown (Davare, Avdonin et al. 2001). It has been thus hypothesized that the re-localization of β_2-ARs in heart failure may be accompanied by re-localization of LTCCs to the sarcolemma and thus may explain the loss of LTCC communication with RyRs in dyads. Some preliminary results obtained from both the rat model of heart failure (Bhargava, O'Hara et al. 2012) and patients with dilated cardiomyopathy (Sanchez-Alonso, Bhogal et al. 2014) confirm this hypothesis.

To prove this hypothesis, it was demonstrated, that on a molecular level, human ventricular cells have a decrease in expression of auxiliary β subunits; at the same time mRNA level of a_{1c} subunit remained unchanged (Hullin, Asmus et al. 1999), an increased expression of the auxiliary β_2 subunit, what was also shown in human failing ventricular cardiomyocytes (Hullin, Matthes et al. 2007).

1.20 HYPOTHESIS

The evidence presented above suggests that cardiomyocytes express a variety of ion channels and regulatory receptors such as adrenergic, muscarinic, adenosine, prostaglandin, angiotensin pathways, among others, spatially compartmentalized to multiple distinct subcellular microdomains, and this compartmentalization may affect their function and regulation. Importantly, many of these proteins form an interacting network where they work together as a part of a macromolecular signaling complex (Willoughby and Cooper 2007; Best and Kamp 2012; Cerrone and Delmar 2014).

These include complexes located in T-tubules (Kamp and Hell 2000), lipid rafts/caveolae (Balijepalli, Foell et al. 2006), where they are associated with different structural proteins. Such organization allows the specificity, reliability and accuracy of the autonomic modulation of excitation–contraction processes by a variety of neurohormonal pathways, either via direct interaction or by second messengers through different G-protein-coupled receptors.

During pathological remodeling, cell structural integrity and architecture are altered and ion channel redistribution occurs, with loss of the protein–protein interaction (Nattel and Khan 2007). Disruption of normal macromolecular signaling complex involving ion channels and associated signaling proteins caused by loss of intercellular structures may contribute to the pathophysiology of a variety of cardiac diseases, including heart failure and certain arrhythmias (Schaper, Kostin et al. 2002; Dibb, Clarke et al. 2009).

This thesis addresses the hypothesis that distinct spatial compartmentalization of functional calcium channels in different intercellular microdomains are coupled with structural proteins and receptors and play an important role in unique Ca^{2+} signaling in atrial cardiomyocytes.

1. Structural variation of T-tubule system throughout the atria might underlie unique Ca^{2+} signaling process observed in atrial cardiomyocytes. High diversification in the distribution of T-tubule system among cells isolated

from different regions of atria may be explained by heterogeneous expression of LTCCs with regards to their coupling to RyR2s which potentially causes a unique atrial cardiomyocyte Ca^{2+} signaling process. In contrast to ventricular cardiomyocytes, atrial cells have a different unique mechanism behind Ca^{2+} sparks occurrence, which is not coupled with T-tubule-RyR dyads but with non-junctional RyR abundantly present in atria.

2. Microdomain compartmentalization of functional L-type calcium channels in atrial cells might be different from ventricular cardiomyocytes, where LTCCs are exclusively presented in T-tubule system. LTCCs which are clustered outside of T-tubules might be associated with unique Ca^{2+} signaling in atrial cells.

3. The function of LTCCs localized in caveolae remains open to question. It has been proposed that some LTCCs housed in Cav3–rich microdomains, could play an important role in modulation of Ca^{2+} signaling. Atrial cardiomyocytes exhibit a significantly higher occurrence of spontaneous Ca^{2+} release events than ventricular cardiomyocytes. Thus, caveolae may have a key function in controlling the formation of local SR Ca^{2+} release events in the absence of global cytosolic Ca^{2+} elevations in cells lacking organized T-tubules such as atrial. And the extradyadic channels linked with caveolae structures may play important role in the regulation of Ca^{2+} signaling in atrial cardiomyocytes.

4. The functional LTCCs might be associated with several crucial receptors regulated cardiac function such as adrenergic and adenosine receptors. Generated signaling complexes of ion channels with receptors might be associated with distinct microdomains and be responsible for regulation of calcium signaling. Signaling complexes coupled with caveolae structures might play a dominant role during pathology like heart failure, while T-tubule system is degraded. The hypothesis was tested using animal model of heart failure.

5. The molecular mechanism of increased activity of LTCCs during chronic atrial fibrillation is not understood. Here both whole-cell and single-channel recordings were applied to investigate effect of chronic atrial fibrillation on Ca^{2+} influx throughout cellular membrane and in distinct microdomains in different regions of atria.

2 CHAPTER 2. Materials and Methods

2.1 Animals

All animals were treated and maintained under conditions fulfilling the criteria of Animals in Scientific Procedures Act 1986 (UK Home Office, ASPA 1986).

2.1.1 Sprague Dawley Rats

Both male and female Outbred, wild type rats (*rattus norvegicus*) were obtained from Harlan Laboratories (Wyton, UK). This strain is possibly the most widely used Outbred strain used in research. They were fed standard rat chow, which they had access to *ad libitum.* Rats were housed at a density of 4-6 per cage and maintained on a 12-hour light/dark cycle at 21^{o}C. Males were culled for the isolation of adult cardiomyocytes when >250g. Males and Females were used for echocardiographic procedures between the ages of 8 and 10 weeks (Males 250-350g and Females >190g).

2.1.2 Heart failure model (to prove)

The rat was anaesthetized and placed in ventral recumbence; the animal's dorsal mid-lumbar region was shaved and swabbed with antiseptic agents. An incision through the skin was made along the mid-line half way between the caudal edge of the rib cage and towards the base of the tail. Incisions through the musculature were made a third of the distance between the spinal cord and the ventral midline on both right and left sides. The ovary and oviducts were exteriorized, the uterine vasculature was clamped to provide haemostasis and both ovaries and part of the oviducts were removed to give a bilateral oophrectomy. The remaining uterine material is placed back into the animal the musculature is not sutured. Sterile wound clips are used to close the incision in the skin. Harlan provided post-operative relief by maintaining the animals in a clean stable environment with food

and water *ad libitum*. Wound healing was monitored for 72 hours and wound clips were removed after a minimum of one week. These animals were delivered to the Imperial College animal house following complete recovery from the procedure and removal of wound clips. Animals showed no outward signs of having been operated upon save for a slight patchiness to the hair on their backs.

2.2 Human patients

2.2.1 Patients screening

Patients included in the study were scheduled for routine cardiac surgery.
The patient's history including examination, anamnesis data, electrocardiogram and echocardiography data were used to establish main disease, additional pathology, and pharmacological therapy. ECHO provided helpful information, including the size and shape of the heart (internal chamber size quantification), heart contractility, pumping function, and the location and extent of any tissue damage, conditions of valves.
ECG as an interpretation of the electrical activity of the heart over a period of time characterised cardiac rhythm, myocardium and electro conduction system damaging.

2.2.2 Tissue/biopsy storing

Tissue was obtained from human subjects in strict concordance with the Declaration of Helsinki.
Biopsies were collected from the auricles of the right and left atria during cannulation for CABG, mitral, or aortic valves replacement.. Excised tissue was collected in cold St. Thomas Hospital solution and transported to laboratory within 20 min of excision. Obtained tissue was immediately used for cardiomyocyte isolation. Small pieces of tissue were frozen in liquid nitrogen and stored at −80°C.

2.3 Atrial cardiomyocytes

2.3.1 Isolation of mammalian cardiomyocytes

Technological advances have made single fresh isolated and, or cultured cells using as an important tool in many research fields. Adult cardiomyocytes are widely applied as a good model for cardiac cellular normal physiology and pathophysiology, as well as for pharmaceutical intervention on the fundamental biophysical and intracellular signaling processes. Despite on missing cell-to-cell communication and whole heart features isolation of single cardiomyocytes avoids the neural and humoral impacts. Thus, isolation and, or culturing of high quality functional cardiomyocytes allows to dramatically improve cardiovascular research and provide an important tool for cell functional, drug development and cardiac arrhythmia or insufficiency model studying.
Enzymatic digestion was used for isolation of atrial rat and human cardiomyocytes. Both protocols were moderated and improved, which benefit a consistent high quality and quantity of atrial cardiomyocytes. Part of atrial tissue was stored for molecular biological investigations in liquid nitrogen at -80°C.

2.3.2 Rat atrial cardiomyocytes isolation

Cardiomyocyte isolation was done as previously described (Vescovo, Jones et al. 1989). Sprague-Dawley rats (150–250 g) were anesthetized with 5% isoflurane-95% O_2 and then killed by cervical dislocation. Hearts were fast extracted and placed in Tyrode solution containing in (mmol/L): 140 NaCl, 6 KCl, 1 $MgCl_2$, 1 $CaCl_2$, 10 glucose and 10 HEPES, adjusted to pH 7.4 with 2 mmol/L NaOH. Using aortic cannulation with the Langendorff setting, the hearts were perfused with Tyrode solution for 5 min, then with low Ca^{2+} solution containing in (mmol/L): 120 NaCl, 5.4 KCl, 5 $MgSO_4$, 5 sodium pyruvate, 20 glucose, 20 taurine, 10 HEPES, 5 nitrilotriacetic acid, and 0.04 $CaCl_2$, adjusted to pH 6.96 with 2 mmol/L NaOH for 5 min, and finally for 10 min with enzyme solution containing in (mmol/L): 120 NaCl,

5.4 KCl, 5 $MgSO_4$, 5 sodium pyruvate, 20 glucose, 20 taurine, 10 HEPES, and 0.2 $CaCl_2$, pH 7.4 with collagenase (1 mg/ml; Worthington) and hyaluronidase (0.6 mg/ml; Sigma-Aldrich). The both atriums was then removed, cut into small pieces, re-suspended in enzyme solution, but containing only collagenase (1 mg/ml; Worthington) and shaken in a water bath at 37°C for 20 minutes. Then the achieved cells were filtered through a 200-µm nylon mesh and left in buffer solution at room temperature without centrifuge.

Cardiomyocytes were plated on dishes coated with laminin. Laminin was left to stick to the bottom for at least 45 minutes before experiments. Cardiomyocytes were used on the same day of isolation. Cells were washed twice with the external solution and mounted on the microscope stage for recordings.

2.3.3 Human atrial cardiomyocyte isolation and plating

Atrial cardiomyocytes were isolated by enzymatic dissociation and mechanical disaggregation using modification of Harding's isolation protocol (Workman, Kane et al. 2001).

Tissue was cut into chunks of ~1mm^3 and shaken (130 rpm) at 37°C in a Ca2+ free solution containing (mM) NaCl (120), KCl (5.4), MgSO4 (5.0), pyruvate (5.0), glucose (20.0), taurine (20.0), HEPES (10.0), nitriloacetic acid (5.0); pH 6.95. Tissue were washed in this solution 3x4 minutes, then protease (Type XXIV, Sigma, 4U/ml) and CaCl2 (50µM) were added, and tissue were shaken for a further 45 min. Protease was then substituted by collagenase (Type II, Worthington, 350-400 U/ml), for further digestion of tissue. After 15 minutes cardiomyocytes appeared and cell suspension was transferred to centrifuge tubes and tissue chunks transferred 6 to fresh collagenase solution until more cardiomyocytes appeared. This procedure was repeated 3-4 times. The cell suspensions obtained after each incubation of partially digested tissue were centrifuged at 40 g for 3 min. The supernatant was removed and cells were re-suspended in KB medium containing (mmol/L): 10 taurine, 70 glutamic acid, 25 KCl, 10 KH2PO4, 22 glucose, 0.5 EGTA (pH 7.4).

2.3.4 Cardiomyocytes plating

Both, for the same day experiments and cell culturing, MatTek (MatTek Corp) dishes (35 mm) coated with 2µl of 1mg/ml laminin (Sigma-Aldrich, UK) were used.

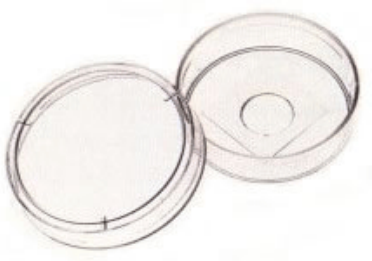

Figure 2.1 MatTek dish.

Laminin as a heterotrimeric protein of glycoproteins with high molecular weight ~400 kDa forms extracellular matrix and the basal membrane in many tissue, including heart, this protein plays an important role in processes of cell differentiation, migration and adhesion.

Cardiomyocytes were plated on MatTek dishes (**Figure 2.1**) coated by laminin and left to stick to bottom for at least 45-60 minutes before experiments. Before plating each dish was uniform covered by 1-2 µl of laminin and left for 30 min until it dries.

Cardiomyocytes were used on the same day of isolation or next 24-48 hours. Cells were washed twice with the external solution and mounted on the microscope stage for recordings or fixed in 4% formaldehyde in PBS solution for immunochemical staining.

2.4 T-tubule network visualizing

The T-tubules were visualized in the following ways:

-Using Di-8-ANEPPS and confocal microscopy: during these experiments, the cell was imaged throughout its depth to enable three-dimensional reconstruction for the T-tubules and assessment of the density of the t-tubule network and also to calculate the cell
width/length parameters. One plane of the cell was selected for high resolution scanning, which allowed assessment of the regularity of the t-tubule network.

-Scanning Ion Conductance Microscopy: performed on single cardiomyocytes to provide an image of the surface of the cell membrane. and also to calculate the cell
width/length parameters

2.4.1 Confocal microscopy of Di-8-ANEPPS labelled t-tubules

2.4.1.1 T-tubule Labeling

T-tubule density was measured after sarcolemmal membrane labeling with Di-8-ANEPPS as described previously (Kawai, Hussain et al. 1999).
Cardiomyocytes incubated with 10mM Di-8-ANEPPS (Molecular Probes, Eugene, OR, USA) solved in DMSO for 1 min and then washed for 3 min before being observed under the confocal microscope.

2.4.1.2 Di-8-ANEPPS

Di-8-ANEPPS (di-8-aminonaphthylethenylpyridinium) (Molecular Probes, Invitrogen, Oregon, USA) is a fluorescent, voltage-sensitive membrane binding dye. The excitation maxima is 465nm and the emission maxima is 635nm. Di-8-ANEPPS is non-fluorescent until bound to membranes.

2.4.1.3 Cardiomyocytes selection

Cells were selected using the following rules:
-was rod-shaped
-was not contracting
-was stuck flat

2.4.1.4 T-tubules density measuring

After Di-8-ANEPPS labeling, MatTek dish with platted cardiomyocytes was mounted on the stage of a conventional inverted microscope (Diaphot 200, Nikon Corporation, Tokyo, Japan). The microscope was then switched to laser scanning mode with excitation at 488 nm and emission detected at 520nm (Louch, Bito et al. 2004), and a digital crop along the longitudinal axis of the cell was made. The focal plane of the cell was manipulated in 2 μm steps until a plane was found which did not show nuclei. An initial scanning stack was used to define the top and bottom of the cell. Then, another scan with 1 μm step was taken.

2.4.1.5 Analysis

The density of T-tubules was quantified by the ratio of T-tubule fluorescence (T-tubule membrane) to total plasma membrane fluorescence (total membrane) in the same confocal slice,

The Di-8-ANEPPS signal was converted to a binary signal, using the auto threshold function of ImageJ software. After exclusion of the surface sarcolemma, the whole z-series was analyzed to provide the percentage stained. This was represented as T-tubule density.

Offline analysis of the t-tubule density and cell volume was performed simultaneously in ImageJ (using a custom-written macro (provided by Dr Mark Stagg) (U.S. National Institutes of Health; http://rsb.info.nih.gov/ij/)) and previously described (Stagg, Carter et al. 2008). The steps of this macro are:

-Conversion to 8-bit images
-Autothresholding of the images to generate binary images. This employs serial divisions of the “top” and “bottom” ends of the range of foreground and background pixel intensities.
-Calculation of the average percentage area of staining at every optical slice. These values were further divided into ten regions along the length of the cell (z1-z10). z1 and z10 were not included as these regions show dense staining, related to the cell edge.
-The mean of these values excluding the cell edge was taken as the average Di-8-ANEPPS staining, a marker of the t-tubule density. Using a second macro, the completely intracellular space of every optical slice was stained and used to generate a three-dimensional reconstruction, where all optical slice volumes were added to provide a total cell volume. Assessment of the t-tubule regularity was performed using a custom-written macro in Matlab software. Initially, images were prepared in ImageJ. This involved rotation of the image to ensure the t-tubules were aligned in the vertical direction. Using the auto threshold function of ImageJ, a binary image was created. A central portion of the cell membrane was selected, always of fixed dimensions (140 pixels in length and 25 pixels wide) to allow comparison between cells and cell groups of differing sizes. A plot profile was then generated from this binary image and exported to Matlab, where a standard Fourier transform was performed. This plotted the underlying frequencies in the image and provided a power-frequency curve. The dominant peak always occurred at the t-tubule frequency, because the images were dominated by the regular t-tubules. The power of that peak, at approximately 0.5 cycles per micron (therefore occurring every 2 microns, approximately the length of a sarcomere) provided a t-tubule regularity index. This methodology was adapted from published reports (Swift, Birkeland et al. 2008).

2.4.2 Scanning ion conductance microscopy (SICM)

Scanning ion conductance microscopy (SICM) is a non-contact scanning microscopy technique, which empowers three-dimensional imaging of surface structures on live cells with resolution of up to ≤ 20 nm (15). (**Figure 2.3**). SICM based on the principle that the flow of ions passing through the glass pipette filled with electrolytes decreases when the pipette approaches the surface of the sample (Hansma, Drake et al. 1989; Korchev, Bashford et al. 1997; Bhargava, Lin et al. 2013).

Technically, a sharp borosilicate glass nanopipette (with I.D. of 100 nm) mounted on a three-axis piezo-actuator (**Figure 2.2**), moves in x-y-z direction along selected area of a sample, controlled by a piezo-acruator (Novak, Li et al. 2009). Pacing along the surface pipette hops in vertical direction in the same time and never touches the sample. The corresponding vertical and lateral displacements are recorded and used to build a three-dimensional image of the sample surface. Non-contact scanning is provided by a distance-modulated feedback control system which keeps the ionic conductance and sample-pipette distance constant. Briefly, ion current through the pipette is measured between the pipette tip and the sample by controller during scanning process. Dropping of current to given % of the initial value makes the pipette to rebounds apart from the surface. After the system moves pipette in X-Y direction to the next line of scanning. Thus, the pipette moves via serpentine path.

Scanning system composes conventional inverted microscope (Diaphot 200, Nikon Corporation, Tokyo, Japan), a high-performance piezo actuator (PI, Germany) and the ICnano sample scan system (Ionscope Ltd, UK), controlled by software (ScanIC 1.9.3.248 version). The scan head of the ICnano system consists of a three axis piezo-translation system (Physik Instrumente, UK) with a 100 x 100 µm x–y piezo-stage for sample positioning and 38 µm z-axis piezo-actuator for the vertical movement of the pipette, mounted on the stage of a microscope. The whole system is placed on an anti-vibration table and shielded by Faraday cage which protects from electro-magnetic fields. To begin scanning, the pipette is filled with solution and fixed in the holder (**Figure 2.2**).

All scanning parameters are manually keyed in the software. Depending on cell type pre-scanning hop amplitude, fall rate, set point and resolution can be selected. First, pipette approaches the sample thus decreasing the pipette-sample distance. It stops at a distance equivalent to the inner radius of the pipette (Novak, Li et al. 2009). To reveal surface structure of atrial cardiomyocytes the pipette with I.D. 100 nm was used (Rheinlaender 2009).

Thus, SICM allowed to reveal a regular structure of lines of T-tubule openings forming Z-grooves and areas between them, termed crests (**Figure 2.3**). The space between Z-grooves was equal 2 μm which corresponds to a Z-line of a sarcomere.

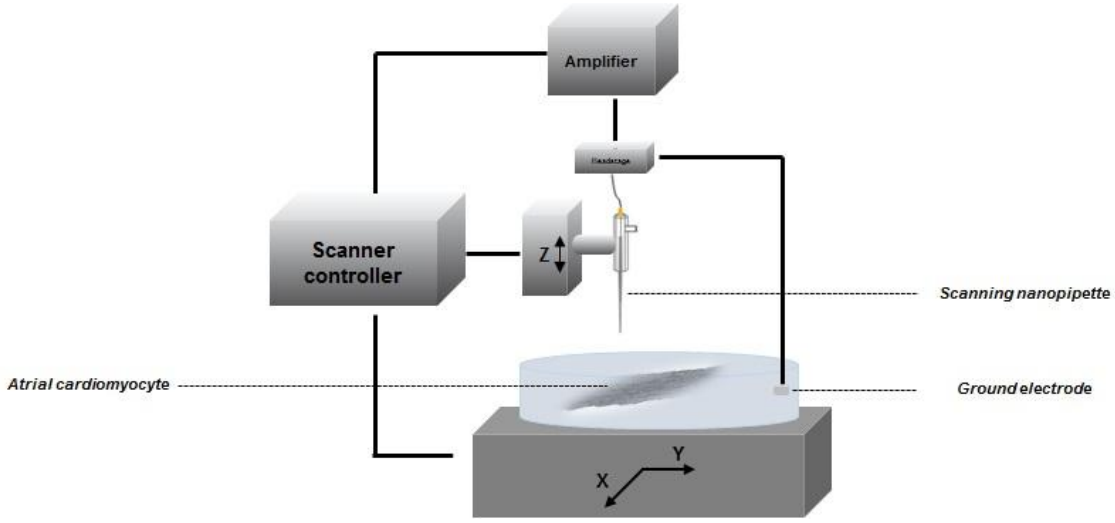

Figure 2.2. SICM scheme.

2.4.2.1 Surface structure analysis. Z-groove index

To quantify surface structure development Z-groove index was used (Gorelik, Yang et al. 2006). Z-groove index is a ratio of the Z-groove length observed on

single scan to size of image (**Figure 2.3**). SICM Image Viewer was applied for Z-groove index calculation. Normally healthy ventricular cardiomyocyte has 85-100% Z-groove index (Gorelik, Yang et al. 2006). Each image obtained during scanning underwent the Z-groove index calculation.

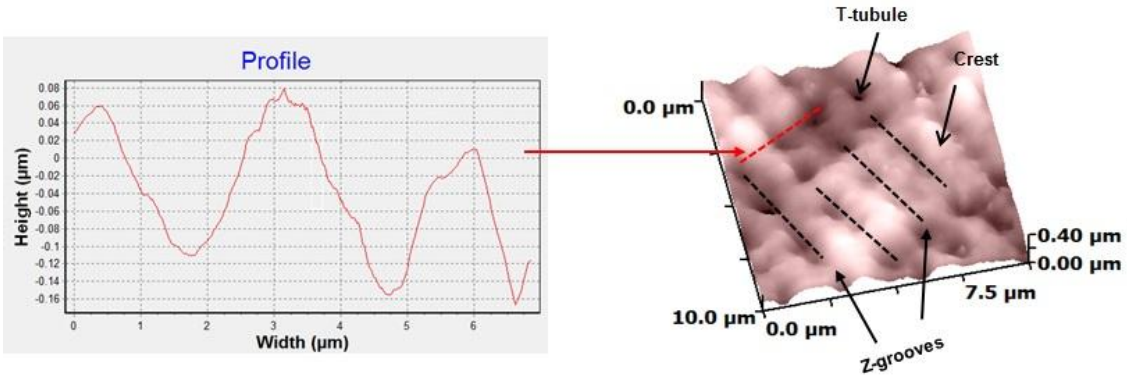

Figure 2.3. Z-groove index calculation.

2.4.2.2 Pipette fabrication

Glass nanopipettes used for scanning mode had a tip diameter ~100 nm, that corresponds to ~ 100 Ohm resistance. Borosilicate capillaries (1.0 mm O.D. 0.5 mm I.D.) were used in nanopipettes preparation.

To fabricate a nanopipette glass capillary was mounted in CO_2 laser-based Micropipette Puller System (**Figure 2.4**).

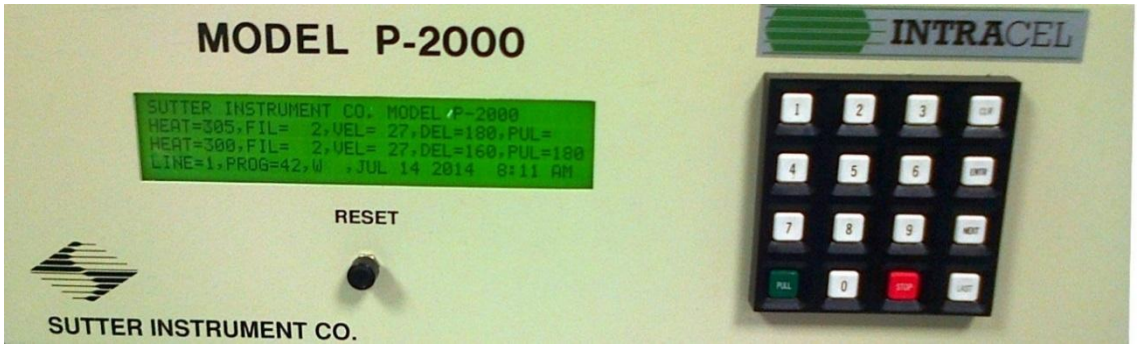

Figure 2.4. Micropipette Puller System

Parameters such as heat (305 and 300), filament (2), velocity (27), delay (180 and 160) and pull (180) were adjusted for first and second steps to obtain pipettes with required resistance.

2.5 Electrophysiological measuring

2.5.1 Patch clamp technique

The patch-clamp recording technique allows to measure single or whole-cell ionic currents though the pipette electrode under voltage-clamp. Under such “voltage-clamped” conditions, current is directly proportional to the conductance of interest. Voltage changes determined at the electrode result in maintaining the voltage signal at a constant level. The resulting current through the electrode is assumed to flow exclusively across the cell membrane proportionally to the membrane conductance (mediated by plasma-membrane ion channels). Patch clamp technique allows studying single ion channel, receptor properties under basic conditions or with drug interaction.

Single-electrode switching amplifier was used for calcium current measuring. Main principle is to apply only single electrode, which serves double duty as voltage and current electrode. For very short periods, the amplifier connects its voltage-sensing input to the electrode, takes a reading, and subsequently connects the current source output to the same electrode to deliver current to the cell. This approach has a limitation in time-resolution by switching between two modes.
Patch-clamp setup is built with several components: amplifier, oscilloscope, stimulator, PC, microscope.

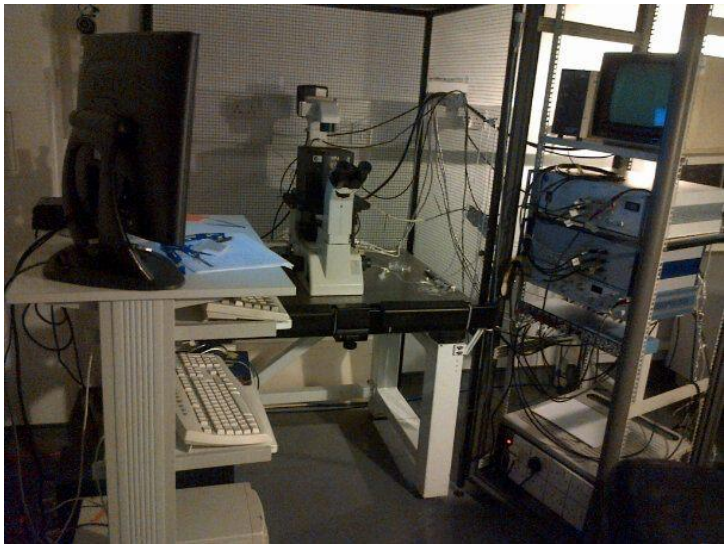

Figure 2.5. SICM system

A recording chamber is mounted on microscope stage, where amplifier's headstage and measuring electrode are also fixed (**Figure 2.5**).

2.5.2 Calcium current measuring

For ionic current measuring borosilicate glass pipette is used with Ag/AgCl electrode inserted in. Diameter of pipette's tip is in direct proportion to its resistance. Pipette electrode was filled with internal pipette solution (**Table 2.2**) and finally was plaves in a petri dish with cells in external recording solution (**Table 2.1**).

Approaching pipette electrode to cell surface by manual or piezo-controlled manipulator is monitored continuously by applying a small voltage pulse (1–5 mV, 2–10 ms) to electrode. Once pipette touches the cell, electrode resistance spontaneously increases by 10-15% and thus the assigned patch-clamp configuration can be performed. A gentle suction applied to pipette results in the formation of a contact between the cell surface and the tip of pipette with high resistance about 1-16 GΩ, named gigaseal. Traditionally mouth or a small syringe makes suction. In this work, another type of suction system was used. Specifically designed water column pressure system with U-shape tube gently applied a negative or positive pressure (**Figure 2.6**).

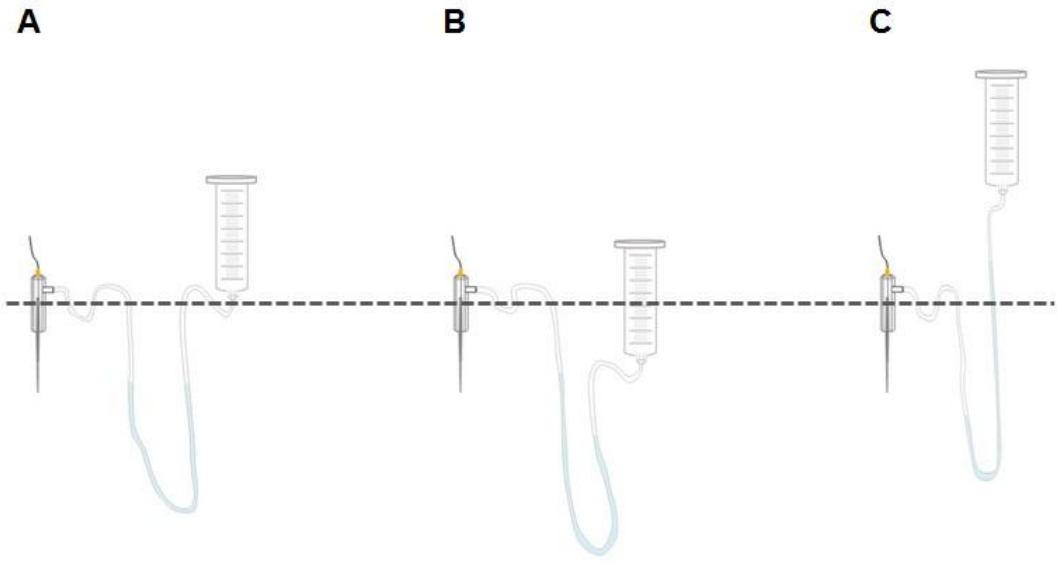

Figure 2.6. Cell-attached patch-clamp configurations forming with water pressure.
A – neutral pressure; B – negative pressure; C – positive pressure.

Briefly, balanced between pipette and tube in zero level pressure was set before pipette approaches external solution (**Figure 2.6A**). In next short moment, as pipette resistance dropped in 10-15% right part of the U-shape tube was lower that results in the negative pressure apply to electrode (**Figure 2.6B)**. In some case, to stabilize gigaseal and relax cell membrane positive pressure used by lifting U-shape up (**Figure2.6C**).

Time required getting gigaseal and gigaseal property depend on cell quality.

At this point, gigaseal grade can be improved by applying a negative holding potential to the electrode, more negative pressure or sometimes positive pressure which helps to relax cell membrane.

This patch-clamp configuration is well known as cell-attached, allows recording single ionic current that flow is very small, just a few picoamperes, or even less than 1pA through ion channels embedded in patch (**Figur 2.7_2**). Cell-attached configuration is applied for single-channel properties, drug target tests and molecule coupling study.

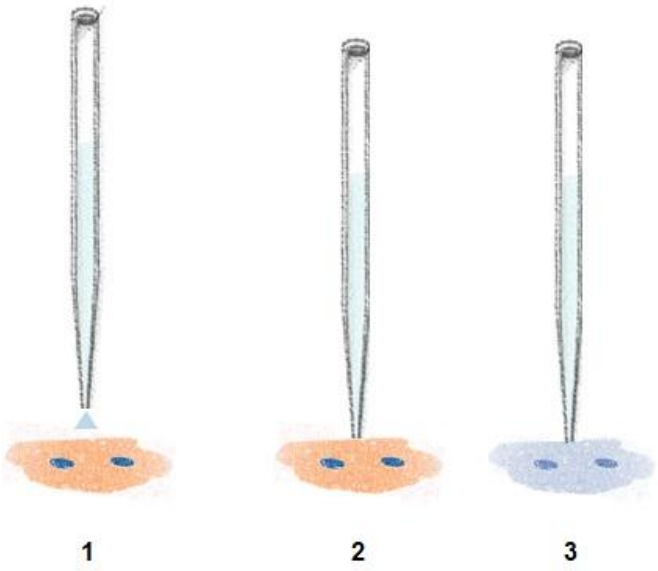

Figure 7. Patch-clamp configurations.

1 - pipette electrode approaches to cell surface; 2 – cell-attached configuration; 3 – whole-cell configuration.

In this cell-attached configuration, pipette capacitance is reduced using the fast compensation adjustment at the amplifier, which is essential for proper series resistance compensation and further channel recordings.

Having reached a gigaseal, by applying a short negative pressure applying to the pipette one can achieve another patch-clamp configuration when internal pipette solution is connected with the intracellular field. This so called whole-cell patch-clamp configuration (**Figure 2.7_3**) is able to measure whole cell current density which summarises the activity of thousands of channels.

2.5.3 Super-resolution scanning patch-clamp technique

Super-resolution scanning patch-clamp is a novel technical advance that allows distinguishing topography of living cell and then recording ion channels from a distinct area with super high resolution up to 20 nm. This new approach is a

combination of Scanning Ion Conductance Microscopy with patch-clamp technique in cell-attached configuration that increases the resolution of an imaging system into nanoscale, it uses the platform of scanning ion conductance microscopy (Korchev, Milovanovic et al. 1997). Using this method, recently, clustering of functional sodium and calcium channels in adult ventricular cardiomyocyte sarcolemma was characterised (Bhargava, Lin et al. 2013). In this work, clipping mode was applied to increase probability of capturing functional ion channels under the patch. Previously, super-resolution scanning patch-clamp had a big limitation by the conflicting a small nano-pipette (~100 nm I.D.) which was applied to resolve nano-structures of cell surface, with ability to find functional ion channels during recordings. The occurrence of every events is in direct proportion to pipette size. However, the pipette with larger diameter, which is able to cover area of membrane embedded ion channels, cannot reveal topography structure with high resolution.

Thus, a new method involving computer-controlled movements of piezo-actuators result in clip of the tip to get enhanced tip diameter (Bhargava, Lin et al. 2013).

2.5.3.1 Super-resolution scanning patch-clamp system

Set up built with components of SICM system and Axopatch 200A patch-clamp amplifier (Molecular Devices, USA) was used to record ion channel activity from specifically distinct microdomains. Cell-attached currents were digitized using Digidata 1200B and a pClamp 10 data acquisition system (Axon Instruments; Molecular devices).

2.5.3.2 Pipette clipping modification

Pipette clipping mode is a tip-breaking procedure taken place directly after generating topography image. The procedure consisted of three steps was used to find functional LTCCs in atrial cardiomyocytes with average occurrence 30%.

Firstly, followed to scanning step the pipette was placed apart from the cell surface to a previously observed zone of the dish bottom free of cells or any stuck fragments.

Then, as a next second step, pipette was chopped using piezo-controlled clipping mode. 10-fold increased fall rate (from normally 50-60 nm/ms to 300-700 nm/ms) was set up to drive the pipette to dish bottom. At these conditions, non-contact mode cannot be provided by the feedback system and finally the pipette results in crashing into the coverslip, damaging its tip and hence increasing its diameter due to the conical shape of the pipette. Pipette tip clipping gives enhanced current through itself according to its resistance fell down (Novak, Gorelik et al. 2013) . After each breaking fall-rate was returned back to baseline. Increasing fall-rate parameter required pipette resistance could be obtained via a several steps. The most important features of this technique is a preserved the overall shape of the pipette tip. That plays a crucial role in a further gigaseal performing.

Depending on subsequent area of patching every pipette size was adjusted individually. For example, to distinguish channels in T-tubule microdomain precisely Rp=30-40 MΩ was applied. Alternatively, LTCCs located outside of T-tubules in Crest of in the non-structured microdomains could be recorded by pipettes with Rp=16-20 MΩ.

As a final step, using piezo-actuator and SICM software pipette was placed back onto the cell in front of area of interest. Each area on the cell surface could be selected by simple click on the scan image. Afterword, non-contact mode of SICM was switched off and pipette could be manually dropped down until it touched cell membrane. Then, gigaseal was obtained (see above).

2.5.3.3 Definition of recording sites

Each area of patching was selected, as it was previously published (Gorelik, Yang et al. 2006). **Figure 2.3** illustrates different optional positions for recordings: T-tubule openings, domed areas named as crest, z-grooves. A depth profile along the xy plane (on **Figure 2.3** marked by the red dotted line is shown on the left

hand side) was used to reveal periodic crests and grooves microdomains of adult cardiomyocytes. As it was shown (Nikolaev, Moshkov et al. 2010) each Z-groove corresponds to the position of the Z-line in the intracellular side and be situated in ~ 2 μm distance from the next z-groove.

2.5.4 Single L-type calcium channels recording

Single-channel recordings were obtained using super-resolution scanning patch-clamp with pipette clipping modification. Cell-attached patch-clamp recordings were performed at room temperature as previously described (Bhargava, Lin et al. 2013). All electrophysiological recordings were performed in the cell-attached patch-clamp configuration with resistance more than 4 GOhm and current leak remained at 0-2 pA maximum. Single LTCCs were characterized and identified by their conductance properties (Rosenberg, Hess et al. 1988). Two main principles were applied to identify LTCCs:

1. The channels are identical and behave independently.
2. The total number of channels remains constant.

To obtain single LTCC recordings nano-pipette with silver electrode was filled by internal/pipette recording solution, while atrial cells were platted in MatTec dish filled by external/bath recording solution (see **Table 2.2**)

2.5.5 Single channel solutions for recording calcium currents

Compound	mM	FW	g/1000 ml	g/500 ml
K-gluconate	120	234.25	28.11	14.055
KCl	25	74.55	1.86375	0.931875
MgCl2	2	203.31	0.40662	0.20331
CaCl2	1	147.00	0.147	0.0735
EGTA	2	380.40	0.7608	0.3804
Glucose	10	180.16	1.8016	0.9008
HEPES	10	238.30	2.383	1.1915

Table 2.1. External solution for single L-type calcium channels recording.
pH=7.4 was adjusted with NaOH, while osmolality was equal without adjusting ~300mosm

Compound	mM	FW	g/1000 ml	g/500 ml	g/50 ml	g/25 ml
BaCl2	90	244.28	21.9852	10.9926	1.09926	0.54963
Sucrose	10	342.3	3.423	1.7115	0.17115	0.085575
HEPES	10	238.30	2.383	1.1915	0.11915	0.059575

Table 2.2. Internal (pipette) solution for single L-type calcium channels recording.
pH=7.4 was adjusted with TEA-OH, while osmolality without adjusting was equal ~300mosm

While external recording solution could be used during couple of months storing at -4°C, pipette solution underwent renewing each 3-4 weeks. Refreshing of internal recording solution provided guarantied high (30-40%) chance to obtain single channel activity in patch.

2.5.6 Data analysis

Single L-type calcium channels (LTCCs) were identified and characterized by their voltage dependent properties. For this purpose depolarizing pulses from a holding potential of -80 mV were elicited to test potentials between -20 and + 20 mV with 10 mV interval (**Figure 2.8**). Applied voltage was corrected for a liquid junction potential of -16.7 mV.

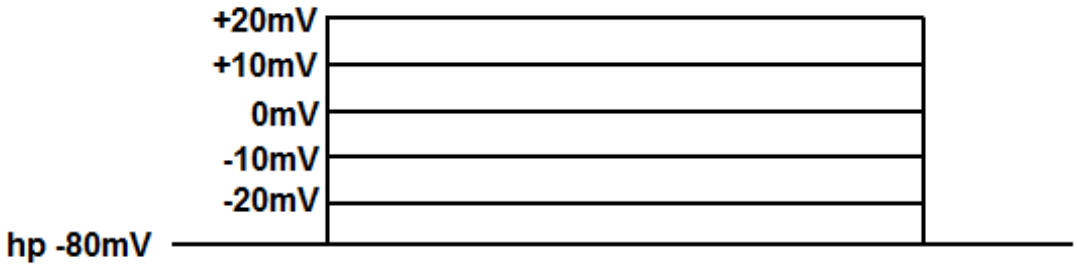

Figure 2.8. Single LTCCs voltage protocol recording.

Analysis was performed as previously described (Klein, Drexler et al. 2000). Single channels were sampled at 10 kHz and filtered at 2 kHz (- 3 dB, 8-pole Bessel).Single channel data were analysed using Clampfit version 10.2. Several parameters such as voltage-current dependence (I-V characteristics), conductance, open probability, availability and occurrence of single LTCCs in each patch were analysed. Recordings with observed current leakage or presence of contamination with another type of channels (chloride channels) were not used for this work. Baseline of each sweep was manually adjusted.

2.5.6.1 Occurrence

This specific parameter describes well the probability to meet channel activity in every patch-clamp recording in cell-attached configuration. Calculated as a ratio of numbers of activities observed in each patch to all cell-attached recordings obtained. Occurrence of a single L-type calcium current characterises the distribution of channels within different microdomains in normal healthy cardiomyocytes versus damaged cells following a disease such as chronic atrial fibrillation or heart failure. In addition, the occurrence can be useful in characterising several chemical, pharmacological or biological agents resulting to channel blocking. Thus, occurrence can show re-distribution of single channels in different conditions that can explain remodelling processes.

2.5.6.2 Voltage-current characteristics

Voltage-current dependence was analysed for each good quality LTCC recording. Several recordings from the same patch of the same cell were analysed. For I-V graphs, only single full voltage protocol with five 2 sec steps (from -20 to +20 mV) was used. Each patch showed 1-4 channel numbers. In multichannel recording single channel amplitude was analysed by applying few levels. The amplitude of the second and any following level was divided by the magnitude of the corresponding level.
The final average amplitude in accordance to used voltage step was plotted in final graph.

2.5.6.3 Conductance

Channel conductance was calculated by plotting the amplitude of fully resolved openings against the test potential for every single experiment. Single channel

conductance is constituted by slope of I-V curve. Normally, conductance of single LTCC is equal 10-30 pS.

2.5.6.4 Open probability

Open probability characterises fast gating between channels “modes” (Cavalie, Pelzer et al. 1986) and how the available channel moves between the closed, open, and inactivated states during depolarization (typically in order of milliseconds, to 10 ms). For this work, open probability was calculated from at least 10-15 consecutive 1 s sweeps of short voltage protocol. In case of double- or triple-channel patches, *n* was derived from the maximum current amplitude divided by the number of channels in the patch. Mean open times were calculated from the total open time of the channel divided by the sum of the number of closures and the number of active sweeps. Event with duration less than 1 ms were not picked up by software.

2.5.6.5 Availability

The single channel availability is a fraction of sweeps containing at least one channel opening and it describes slow gating between “modes” of channel (Hess, Lansman et al. 1984; Cavalie, Pelzer et al. 1986; Klockner and Isenberg 1994).

2.5.6.6 Multiple conductance levels of single channel amplitude

The relationship between single channel conductance and ion binding affinity previously observed (Ellinor, Yang et al. 1995). Ion selectivity can affect channel state. L-type calcium channels are well-known as having several conductance states (Talvenheimo, Worley et al. 1987; Ma and Coronado 1988; Kunze and Ritchie 1990; Church and Stanley 1996; Gondo, Ono et al. 1998) and an analysis

of different subconductance states can be helpful to fully characterise these channels.

Single channel current records were initially examined for the presence of subconductance states using all points histograms. Most patches exhibited three to four conductance levels, which were used for analysis and are named as levels 1 to 4. Each record was analyzed separately for the conductance levels 1-4 using a threshold appropriate to the substate amplitude of openings. Openings that reached the 90% threshold for a given conductance state and events which were smaller than the next subconductance level were included. Single brief events shorter than 1ms were not included in the analysis.

2.6 Statistical analysis

All graphs and statistical analysis were performed using either GraphPad prism 5 or Origin version 6.1. All data are presented as mean ± SEM for the given number of experiments. Statistical significance was calculated by a t- test and significance was. $P<0.05$ means as a significant.

3 CHAPTER 3. Microdomain–specific localization and regulation of functional L-type calcium channels in rat atrial cardiomyocytes

3.1 INTRODUCTION

In the heart, L-type calcium channels (LTCCs) are essential in determining the electrical and mechanical properties of the cardiac muscle (Bers 2008). In adult ventricular cardiomyocytes, LTCCs are predominantly located in the T-tubules (Bhargava, Lin et al. 2013), where they form dyadic complexes with calcium sensing and release units, the ryanodine receptors (RyR2s) on the opposing junctional sarcoplasmic reticulum (SR). A well-developed network of ventricular T-tubules ensures the electrical impulse is conducted into the cell interior, where Ca2+ influx can trigger the opening of RyR_2 and subsequent release of SR Ca2+ stores. Atrial cardiomyocytes are believed to lack an elaborate T-tubule network (Forbes and van Neil 1988; Brette, Komukai et al. 2002; Kirk, Izu et al. 2003; Richards, Clarke et al. 2011) and their Ca2+ signalling is substantially different from that in ventricular cardiomyocytes (Huser, Lipsius et al. 1996; Mackenzie, Bootman et al. 2001; Walden, Dibb et al. 2009). Lack of a regular T-tubular system has been thought to primarily affect distribution of LTCC and the unique Ca2+ signalling in atrial cardiomyocytes (Huser, Lipsius et al. 1996; Dobrev, Teos et al. 2009; Bootman, Smyrnias et al. 2011).

A number of important LTCC subpopulations have been identified in ventricular cardiomyocytes that associate with unique macromolecular signalling complexes and scaffolding proteins, which enables modulation of Ca2+ signalling (Best and Kamp 2012). While the main population of LTCCs is localized to dyadic junctions, extradyadic channels are also associated with the surface membrane (Balijepalli, Foell et al. 2006; Makarewich, Correll et al. 2012). Caveolin-3 (Cav3)-rich signalling microdomains are found to harbour specific LTCCs which may play an important role in modulation of Ca2+ signalling, particularly in cells lacking T-tubules such as atrial (Schulson, Scriven et al. 2011) and neonatal (Lohn, Furstenau et al. 2000) cardiomyocytes. However, until recently, it was difficult to test this hypothesis due to lack of appropriate experimental approaches.

The spatial compartmentation of Ca2+ signalling complexes was first assessed by immunofluorescence microscopy (Grabner, Dirksen et al. 1998), but the imaging results lacked information on the functionality of channel proteins within a subcellular domain. Recent methodological advances have made it possible to routinely image the topography of a live cardiomyocyte and study the clustering of functional ion channels within a specific microdomain (Bhargava, Lin et al. 2013). Here, a super-resolution scanning patch-clamp technique was used to study the distribution of functional LTCCs on the sarcolemma of rat atrial cardiomyocytes. This novel approach allowed to probe functional ion channels in the microdomains in live cells, which is not possible by any other existing methodology. Investigation of spatial distribution of functional LTCCs in distinct compartments might underlie regional heterogeneity of Ca2+ signalling and susceptibility to spontaneous Ca2+ sparks in the atria.

3.2 MATERIALS AND METHODS

3.2.1 Whole mount immunofluorescence labeling

In intact atria tissue, we measured T-tubule organization in a manner similar to those previously reported. For this, whole mount preparation of right and left atria was used as described previously (Glukhov, Kalyanasundaram et al. 2013). Briefly, the heart was cannulated and retrogradely perfused with Tyrode solution. The ventricles were dissected away, and the atria were stretched and then pinned to the bottom of a Sylgard-coated chamber and superfused with Tyrode solution. The medial limb of the crista terminalis was cut to open the right atrium appendage. Tissue sections were fixed in freshly prepared 4% paraformaldehyde (PFA) for 30 min before incubation with wheat germ agglutinin (WGA), Alexa Fluor 488 conjugate prepared in PBS (Invitrogen, Glasgow, UK) at 20 μg/ml for 2 hours to visualize T tubules. Mounted whole mount preparations were analyzed with an Olympus FV 1000 Spectral Confocal microscope under a 10X objective; Z stacks were collected and integrated for final 3D images.

3.2.2 T-tubule Labeling

T-tubule density was measured after sarcolemmal membrane labeling with Di-8-ANEPPS as described previously (Kawai, Hussain et al. 1999). Cardiomyocytes were incubated with 10mM Di-8-ANEPPS (Molecular Probes, Eugene, OR, USA) for 1 min and then washed for 3 min before being observed under the confocal microscope. After Di-8-ANEPPS labeling, the density of T-tubules was quantified by the ratio of T-tubule fluorescence (T-tubule membrane) to total plasma membrane fluorescence (total membrane) in the same confocal slice, with excitation at 488 nm and emission detected at 520nm(Louch, Bito et al. 2004). The T-tubule density was calculated by converting the Di-8-ANEPPS signal to a binary signal, using the autothreshold function of ImageJ. After exclusion of the surface sarcolemma, the whole z-series was analysed to provide the percentage stained.

This was represented as T-tubule density.

3.2.3 3D visualization of T-tubules

Reconstructions of the T-tubular network were performed from confocal stack images. To obtain high-quality visualizations, images were processed with ImageJ (Schindelin, Arganda-Carreras et al. 2012). After contrast enhancement (2% saturated pixels), the T-tubular network was manually traced on each image. A threshold was applied and a 3D view was generated using the 3D plugin. The graphical models were then created using the freely-available software Art of Illusion (http://www.artofillusion.org/).

3.2.4 Scanning ion conductance microscopy (SICM) and confocal microscopy

SICM is a scanning probe microscopy technique in which a nano-pipette was used for non-contact visualization of the surface topography of living cells (Novak, Li et al. 2009). The subcellular T-tubule system was visualized by confocal imaging of atrial cells stained with the lipophilic membrane indicator Di-8-ANEPPS.

3.2.5 Super-resolution scanning patch-clamp with pipette clipping modification

After generating a topographical image of the cell surface by SICM, the tip diameter of the pipette was widened by clipping (Novak, Gorelik et al. 2013) to increase the area of attachment. The pipette was then lowered to a specific location (T-tubule or crest) until it touched the membrane and a high resistance seal was established. Recordings were then performed in a cell-attached mode (Bhargava, Lin et al. 2013). Controlled widening of the scanning nano-pipette tip is

described in details in the Chapter 2. Macroscopic calcium currents were recorded using the whole-cell patch-clamp technique as described previously (Wright, Nikolaev et al. 2013).

3.2.6 Optical mapping and data analysis

The Ca^{2+}-sensitive fluorescent dye Fluo-4 was used to monitor localized changes in cytoplasmic [Ca^{2+}]. Optical mapping of Ca^{2+} transients was performed with modifications as previously described (Lyon, MacLeod et al. 2009). Briefly, aliquots of cells were incubated with Fluo-4 AM (10 μmol/L) for 25-30 min. The cells were then superfused with Hanks balanced salt solution for 10 minutes to allow intracellular de-esterification. Imaging was conducted on an inverted Nikon microscope (Eclipse Ti) equipped with a MiCAM Ultima-L CMOS (SciMedia, USA Ltd., CA) camera and sampled at 1,000-500 frames/sec. The fluorescent signals were amplified, digitized, and visualized during the experiment using specialized software (SciMedia, USA Ltd., CA). A custom-made Matlab-based computer program was used to analyze APs offline (Lou, Fedorov et al. 2011). The signals were filtered using the low-pass Butterworth filter at 64 Hz. Ca^{2+} transient activation maps were constructed from activation times which were determined from the $(dF/dt)_{max}$ of each channel, where F is the Ca^{2+} fluorescent signal. Ca^{2+} transient duration was measured as the time from the upstroke to 80% recovery.

To investigate spontaneous Ca^{2+} transient events, pacing frequency was progressively increased from 0.5 Hz up to 4 Hz. Cells were electrically paced at 4Hz for 1 min to enhance sarcoplasmic reticulum Ca^{2+} loading. Non-propagating Ca^{2+} sparks and propagation throughout the entire cell Ca^{2+} waves were quantified during 8-16sec rest period after cessation of pacing (Voigt, Li et al. 2012; Hohendanner, Walther et al. 2014).

3.2.7 Whole-cell electrophysiological recordings

Macroscopic Ca^{2+} currents were recorded using the whole-cell patch-clamp configuration with the external recording solution of the following composition (in mmol/L): 120 Tetraethylammonium-chloride, 10 CsCl, 10 Glucose, 10 HEPES, 1.5 $MgCl_2$, 1 $CaCl_2$, pH 7.4 with CsOH. An internal pipette solution contained (in mmol/L): 100 Cs-methanesulfonate, 40 CsCl, 10 HEPES 5 EGTA, 2 $MgCl_2$, 5 Mg-ATP, 0.75 $MgCl_2$, pH 7.2 with CsOH. Patch pipettes had mean resistances of 3.5–5 MΩ. Currents were recorded using an Axopatch-1D amplifier connected to a Digidata1322A acquisition system (Axon Instruments, Foster City, CA, USA). The bath was connected to the ground via an Ag–AgCl pellet. Data were low-pass filtered at 2 kHz using the built-in Bessel filter of the amplifier and sampled at 10 kHz. All recordings were performed at room temperature (22-24°C). $I_{Ca,L}$ channel activity was recorded during 200 ms from a holding potential of -40 mV to test potentials ranging from -40 to +60 mV, with pulses applied every 2s in 5 mV increments. Results were analyzed offline using pCLAMP10 (Axon Instruments) and OriginPro8.6 (OriginLab) software packages. Series resistance and whole cell capacitance were electronically compensated between 70 and 80% for each cell. Current amplitude at 10 mV was taken as a peak current for each cell. This value was divided by cells capacitance and was termed Ca^{2+} current density. Mean current values ± SEM were plotted as current-voltage (I-V) relationship. *I–V*'s were fitted with the modified Boltzmann equation, $I = [G_{max} \times (V_m - E_{rev})]/\{1 + \exp[(V_m - V_{0.5a})/K_a]$, where V_m is the test potential, $V_{0.5a}$ is the half-activation potential, E_{rev} is the extrapolated reversal potential, G_{max} is the maximum slope conductance and K_a reflects the slope of the activation curve.

3.2.8 Electron microscopy

To visualize surface structures, electron microscopy was applied as previously described (Wright, Nikolaev et al. 2013). Briefly, isolated cardiomyocytes were fixed with 2.5% glutaraldehyde for 2 to 4 h and then centrifuged at 500 *g* for 5 min

and the pellet was left overnight. The pellet was washed three times in cacodylate buffer and fixed in 1% osmium-tetroxide, followed by a 5-10 min washing with pure water. A small amount (25 to 50 µL) of liquid 2% agar at 45°C was added to the pellet. Drops were left to solidify on polythene, providing agar blocks with evenly distributed cells. The blocks were dehydrated through a series of graded alcohols, propylene oxide, and embedded in araldite. For low power examination by light microscopy before EM examination, 1 µm thick sections were cut and stained with 1% toluidine blue in 1% borax. For transmission electron microscopy, ultra-thin sections were stained with uranyl acetate and lead citrate. The ultrastructural features of cardiac myocytes, especially the membrane area were examined.

3.2.9 Cell culture and adenoviral transduction

Adenovirus constructs co-expressing GFP and Rem^{1-265} were used. In addition, the cytosolic truncation mutant Rem^{1-265} was used (Finlin, Crump et al. 2003; Correll, Pang et al. 2007). Deletion of the conserved, polybasic C-terminus after residue 265 prevented efficient localization of Rem to the plasma membrane and eliminated inhibition of $Ca_V1.2$ activity (Heo, Inoue et al. 2006; Correll, Pang et al. 2007). To specifically target Rem to caveolae, a canonical caveolin binding domain, RNVPPIFNDVYWIAF 4 was fused to Rem^{1-265} and Rem^{1-265}-Cav was created (Makarewich, Correll et al. 2012). As shown previously in rat ventricular myocytes, Rem^{1-265}-Cav localized to plasma membrane specifically within caveolin-containing lipid rafts, rather than lipid rafts in general, and did not displace molecules normally found in caveolae (Makarewich, Correll et al. 2012).

Isolated atrial myocytes were washed (3X) with a serum-free medium (Medium 199, Sigma) supplemented with penicillin, streptomycin and gentamycin and plated on laminin-coated glass cover-slips or culture plates (Makarewich, Correll et al. 2012). Myocytes were then infected with adenovirus expressing Rem^{1-265}/GFP and Rem^{1-265}-Cav for 12 hours at a multiplicity of infection of 100. During the experimental period, culture media was changed once per day. Infection efficiency

was determined 48 hours after infection by GFP fluorescence intensity and was typically assessed to be 60-65%.

3.2.10 Statistical analysis

Quantitative data are shown as mean ± SEM for the given number of experiments. Statistical analysis was carried out using an unpaired student t-test. A value of $P<0.05$ was considered statistically significant.

3.3 RESULTS

3.3.1 Cellular population

To characterize rat atrial cardiomyocytes light microscopy was applied. Rat atrial cells demonstrated three different groups related to their size (**Figure 3.1**).
In contrast to ventricular cardiomyocytes (**Figure 3.1A**), atrial cells have smaller cross sectional dimension, or width, 7-25 μm. 13 % of cardiomyocytes observed in all experiments show width 27±0.6 μm (**Figure 3.1B),** 62 % of all atrial cardiomycotes have width 20±0.6 μm (**Figure 3.1C**), and 25 % of cardiomyocytes demonstrate transvers size 8±0.6 μm (**Figure 3.1D)**

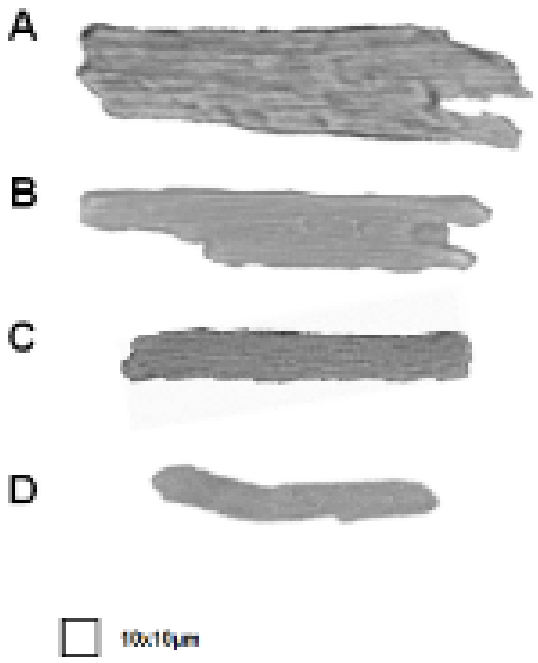

Figure 3.1. Rat control cardiomyocytes.
Optical images of a ventricular cardiomyocytes (**A**) and atrial cardiomyocytes of 20μm (**B**), 12.5μm (**C**), and 7μm (**D**).

Figure 3.2 represents dispersion of atrial cells width in whole cell population.

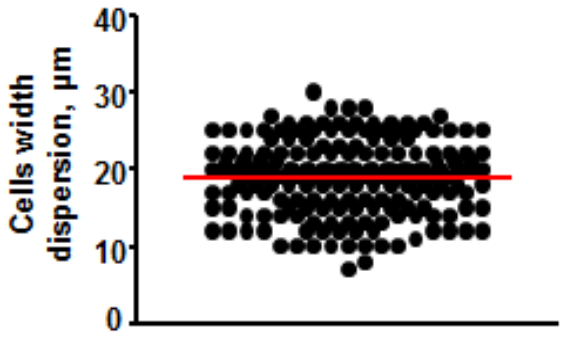

Figure 3.2. Dispersion of transverse size of rat control atrial cardiomyocytes.
Each black dot relates to single atrial cardiomyocyte (N=188).

3.3.2 In situ T-tubule imaging in isolated atria preparations

To characterize the atrial T-tubular network, T-tubule imaging was performed in situ on intact atria preparations using whole mount immunofluorescence labelling with glycophilic lectin WGA. Significant region-dependent heterogeneity in T-tubule structure throughout the atria was found. While the left atrial myocardium predominantly consisted of cardiomyocytes with T-tubules (**Figure 3.3A**, right panel), in the right atrium, three groups of cardiomyocytes were observed: cells (1) with organized T-tubules, (2) with disorganized T-tubules, and (3) with absent T-tubules (**Figure 3.3A**, left panel). Interestingly, in both the right and left atria, the location of cardiomyocytes with well-developed T-tubule structure correlated well with the arrangement of pectinate muscle bundles in atrial appendages (hatched areas on the scheme in **Figure 3.3A**).

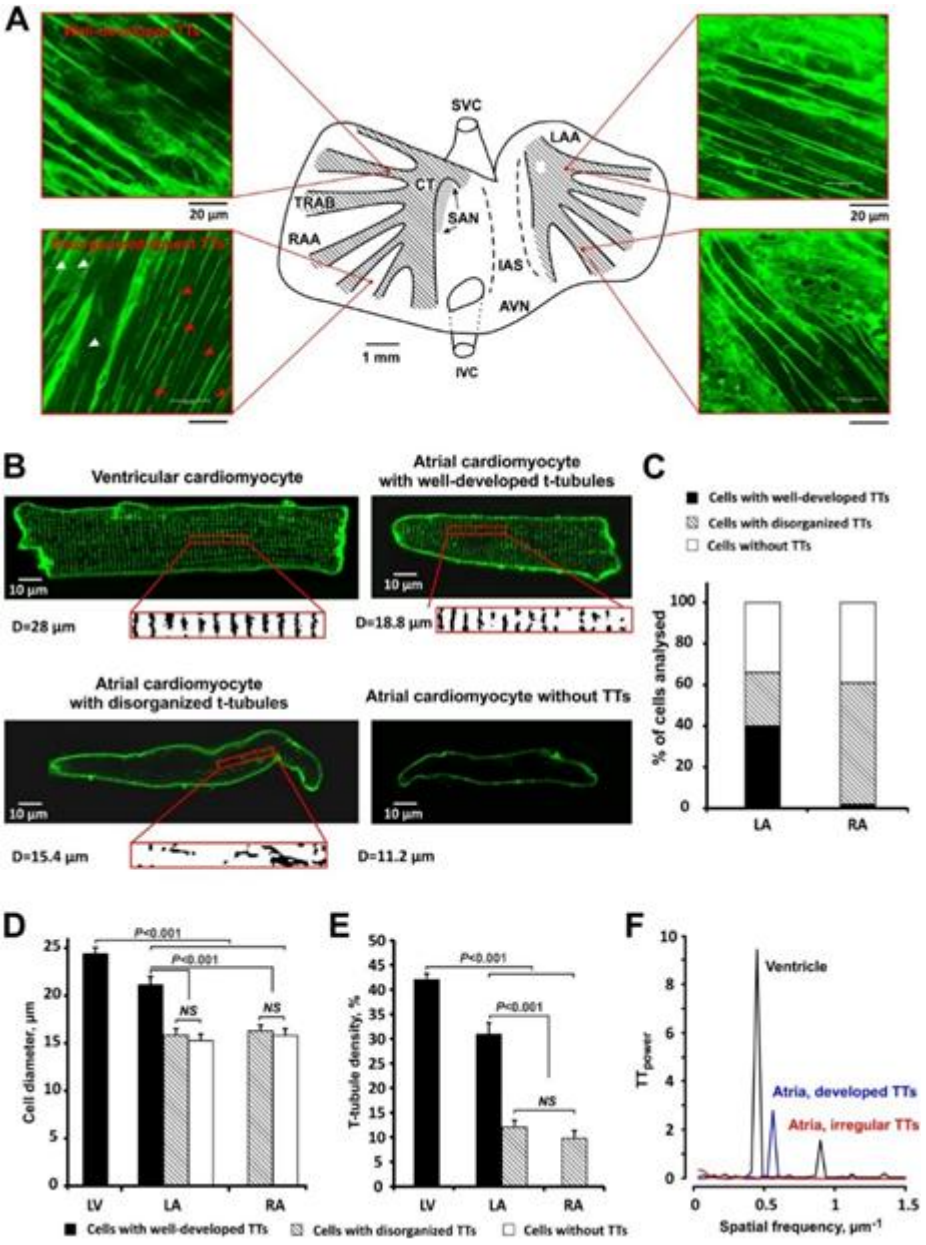
A
SVC
LAA
CT
TRAB
SAN
RAA
IAS
AVN
IVC
20 μm
1 mm
B
Ventricular cardiomyocyte
Atrial cardiomyocyte with well-developed t-tubules
Atrial cardiomyocyte with disorganized t-tubules
Atrial cardiomyocyte without TTs
10 μm
D=28 μm
D=18.8 μm
D=15.4 μm
D=11.2 μm
C
Cells with well-developed TTs
Cells with disorganized TTs
Cells without TTs
% of cells analysed
LA
RA
D
Cell diameter, μm
P<0.001
NS
LV
LA
RA
E
T-tubule density, %
F
Ventricle
Atria, developed TTs
Atria, irregular TTs
Spatial frequency, μm-1

Figure 3.3. Spatial heterogeneity of the atrial T-tubular system: in situ and in vitro measurements.

(A) In situ confocal imaging of T-tubules (TTs) in intact rat atrial preparation stained with WGA. In the middle, the schematic outlines of the isolated rat atria preparation showing main anatomical features including locations of the pectinate muscles in both right and left atria. The enlarged images from the endocardium of the right and left atrial appendages demonstrate typical atrial cardiomyocytes with either organized TTs (white arrows), or disorganized TTs (red arrows), or mixture of both types. SVC and IVC – superior and inferior vena cava, SAN – sinoatrial node, CT – crista terminalis, RAA and LAA – right and left atria appendages, TRAB – trabecle, AVN – atrio-ventricular node, IAS – inter-atrial septum. **(B)** Di-8-ANEPPS membrane staining showing a T-tubule network in ventricular cardiomyocytes and in atrial cardiomyocytes with organized, disorganized, and absent T-tubular systems. Below the confocal images, enlarged areas of 40μmx5μm are shown that were binarized and used in T-tubule density and regularity measurements. **(C)** 3D reconstructions of the T-tubular network obtained from confocal stack images. For organized T-tubules, a 4μmx10μmx10μm area was used, while for disorganized T-tubules, a 15μmx10μmx2μm area was used, as sections of this size best depict the specificities of the T-tubule network in the two cell types. (**D**) Composition (in %) of populations of cardiomyocytes isolated from the left (LA; n=111 cells from four rats) and the right (RA; n=119 cells from six rats) atria made of cardiomyocytes with different T-tubular structures. **(E)** Average cell width in populations of cardiomyocytes with different T-tubule structure isolated from LA and RA. For comparison, average cell width of cardiomyocytes isolated from the left ventricle (LV) is also shown. Bar legend is as in (D). **(F)** T-tubular system density measured in LV, LA and RA cardiomyocytes with organized and disorganized T-tubules. Bar legend is as in (D). **(G)** Power of the predominant frequency retrieved from 2D Fourier transformation of confocal images (panel B insets), a characteristic of the regularity of the T-tubular system (by Mr. Zeki Ilkan).

3.3.3 Subcellular T-tubule system in atrial cardiomyocytes

Cardiomyocytes isolated separately from the left and right atria were also studied. Confocal imaging of Di-8-ANEPPS stained cardiomyocytes revealed that while about a third of cells do not have T-tubules (~39% in the right atrium; 34% in the left atrium); other cardiomyocytes possess a T-tubular network of some sort. It was found that cells with organized T-tubular networks similar to that in ventricular cardiomyocytes, and those with disorganized T-tubules (**Figures 3.3B, C**). The majority of atrial cardiomyocytes with organized T-tubules were located within the left atrium (~40% in the left atrium vs 2% in the right atrium); while in the right atrium cells with less organized T-tubules prevailed (~59% vs 26% in the left atrium) (**Figure 3.3D and Figure 3.4**). Organization of the atrial T-tubular network correlates with the cell width: cells showing organized T-tubular networks were larger than cells with disorganized or no T-tubules (**Figure 3.3E** and **Figure 3.5**).

In ventricular cardiomyocytes, T-tubules are distributed regularly at ~2μm intervals. In contrast, the atrial T-tubular network is less dense and less regular than ventricular system (**Figure 3.3F**). The peak power which characterized T-tubule integrity at the dominant frequency (TTpower) measured by the Fast Fourier transform. **Figure 3.3G** shows representative traces of TTpower obtained from the cells depicted in **Figure 3.3B**. In ventricular cardiomyocytes with well-organized T-tubules, the dominant frequency at ≈0.5μm-1 corresponds to the spatial distance between the T-tubules of ≈2μm (Song, Sobie et al. 2006; Wei, Guo et al. 2010). Atrial cells with disorganized or absent T-tubules (both left and right atria) did not show a dominant peak.

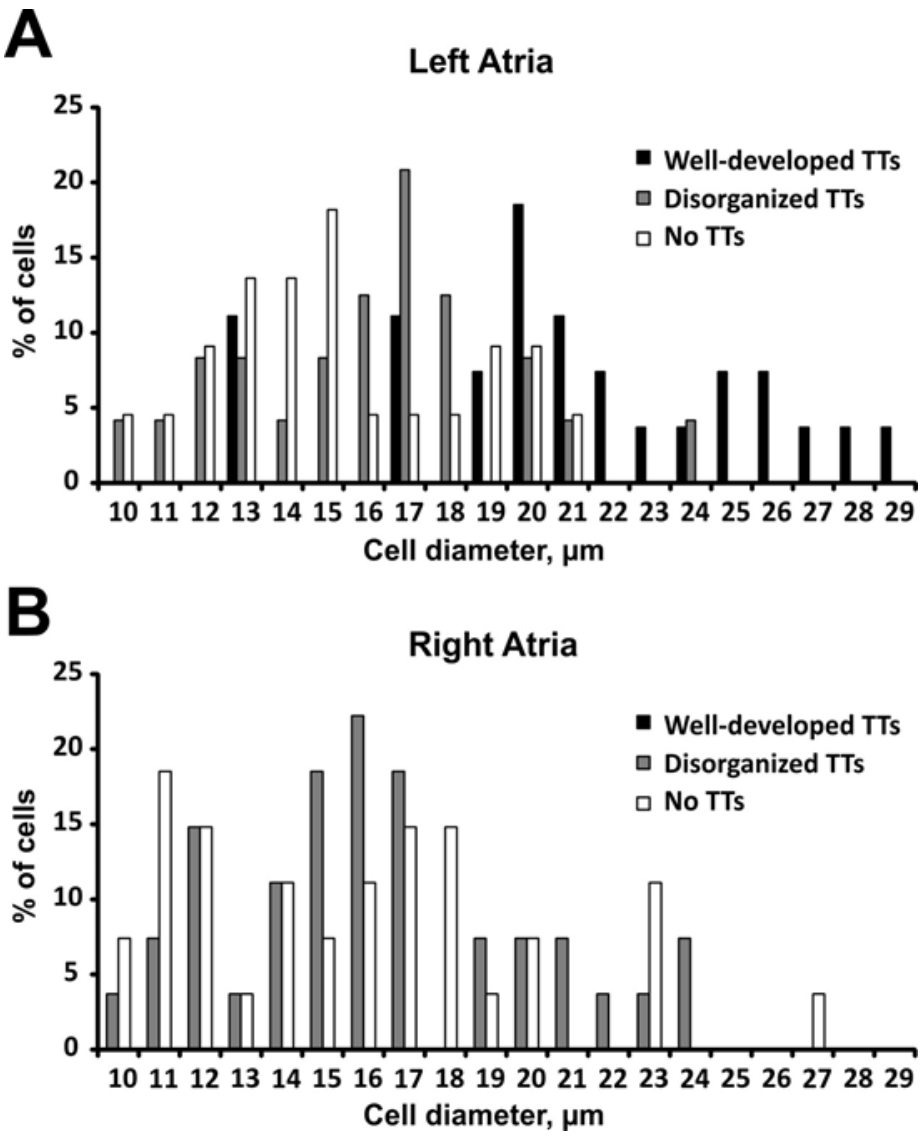

Figure 3.4. Cells with T-tubules are larger and the left atrium has more cells with T-tubules. Histograms of cell widths measured for left **(A)** and right atria **(B)** for three groups of atrial cardiomyocytes with: organized T-tubules **(black columns)**, disorganized T-tubules **(grey columns)**, and absent T-tubules **(empty columns)**.

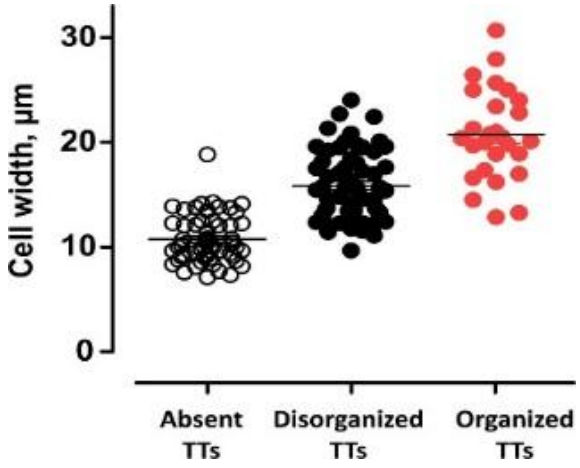

Figure 3.5. Cell width measured in atrial cardiomyocytes with different T-tubule structure. Cell widths for individual cardiomyocytes with organised T-tubules (TTs, red circles), disorganized TTs (black circles), and absent TTs (empty circles) are shown. Horizontal lines for each group show average values (average cell width: 13.0±0.4µm, 15.9±0.4 µm, and 20.7±0.8 µm for cells with absent TTs, disorganized TTs, and organized TTs, respectively). P<0.001 between all groups.

3.3.4 Surface structures in atrial cardiomyocytes

SICM imaging of ventricular cardiomyocytes previously clearly showed the surface topography with evident location of the T-tubule openings and the domed crest between the Z-grooves (Gorelik, Yang et al. 2006). Moreover, to characterize cardiomyocyte topography the Z-groove index (Gorelik, Yang et al. 2006): a ratio of the observed Z-groove length to the total extrapolated Z-groove length (as if they were present throughout the entire surface). In this work, for the first time, this analysis was applied to characterize topography of atrial cardiomyocytes. Bigger the atrial cardiomyocytes demonstrated the more regular its surface topography; a similar correlation was observed for the subcellular T-tubule network. Atrial cardiomyocytes with organized surface structures and apparent T-tubule openings, similar to those seen in ventricular cardiomyocytes (**Figures 3.6A,B**), had a larger mean cell width than the intermediate size cells showing patches of

non-structured areas on their surface (**Figure 3.6C**) and thin atrial cardiomyocytes which entirely lacked surface structures (**Figure 3.6D**).

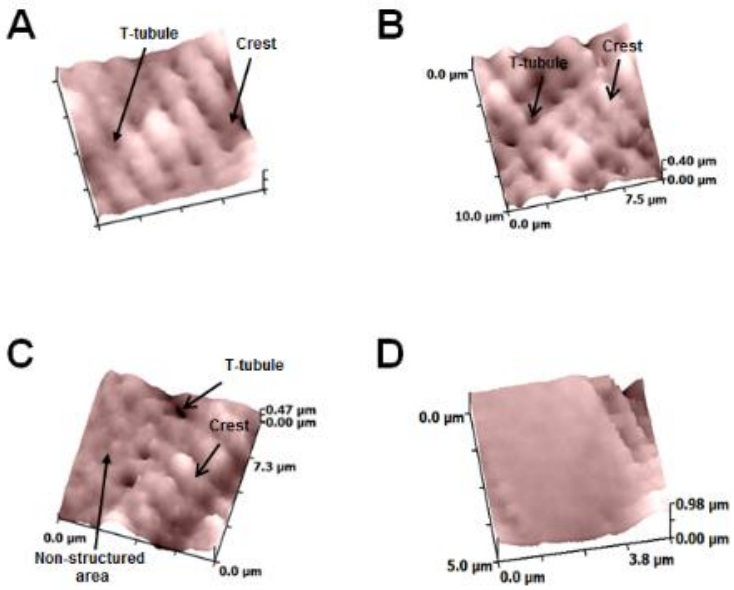

Figure 3.6. Different organization of surface structure in rat control cardiomyocytes.
Surface topography structure of rat control ventricular (A) and atrial cardiomyocyte with organized surface structure (B), non-organized (C) and with no surface structure (D). Arrows indicate T-tubules, crests, and non-structured areas.

The Z-groove index calculated for cells with a mean cell width of >16µm was significantly higher than that calculated for cells <15µm. This difference was clearly demonstrated within the right atrium, while in the left atrium, the difference in surface regularity between small and bigger cells is less pronounced (**Figure 3.7**).

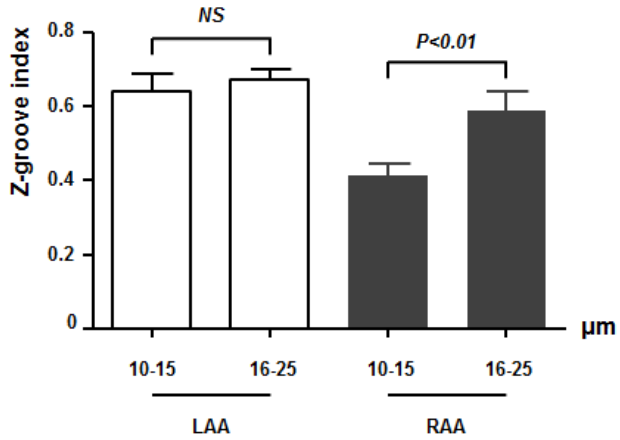

Figure 3.7. Correlation between the surface structure and cell size.

Average Z-groove index measured for thin (<15µm) and thick (>16µm) atrial cells isolated from both left (n=11 of thin cells and n=14 of thick cells) and right (n=12 of thin cells and n=10 of thick cells) atria.

3.3.5 Atrial cardiomyocyte Ca2+ signalling

Optical mapping of spontaneous Ca2+ activity revealed distinct atrial cardiomyocytes Ca2+ cycling when compared with that in ventricular cardiomyocytes. Spontaneous Ca2+ activity was evoked by SR-Ca2+ loading for 1 min at 4Hz pacing. Amongst all spontaneous Ca2+ release events, Ca2+ waves propagating throughout the entire cell (**Figure 3.8A**) were distinguished from non-propagating Ca2+ release events (Ca2+ sparks, **Figure 3.8B**). In comparison with ventricular, atrial cells showed a significantly higher spontaneous Ca2+ release events following cessation of stimulation. Atrial cardiomyocytes exhibited more Ca2+ sparks (P<0.001) than ventricular cells (**Figure 3.8C, D** and **Figure 3.9**).

It was demonstrated, that wider atrial cardiomyocytes exhibited significantly higher number of spontaneous Ca2+ release events (**Figure 3.8E** and **Figure 3.9**). No spontaneous Ca2+ activity was observed in atrial cells that were less than 11.0±0.4µm wide (P=0.002 vs. that with sparks and waves, **Figure 3.8E**). In addition, Ca2+ sparks were observed in atrial cardiomyocytes 13.2±0.6µm wide,

whereas Ca2+ waves were found in cells 14.9±1.1μm wide and above (data not shown). Cardiomyocytes isolated from the left atrium demonstrated a higher number of spontaneous calcium sparks than right atrial cardiomyocytes (**Figure 3.8F, G**). A positive correlation between cell width and number of events per cell was revealed in atrial cardiomyocytes, that exhibit spontaneous Ca2+ release events, as shown in **Figure 3.8H**.

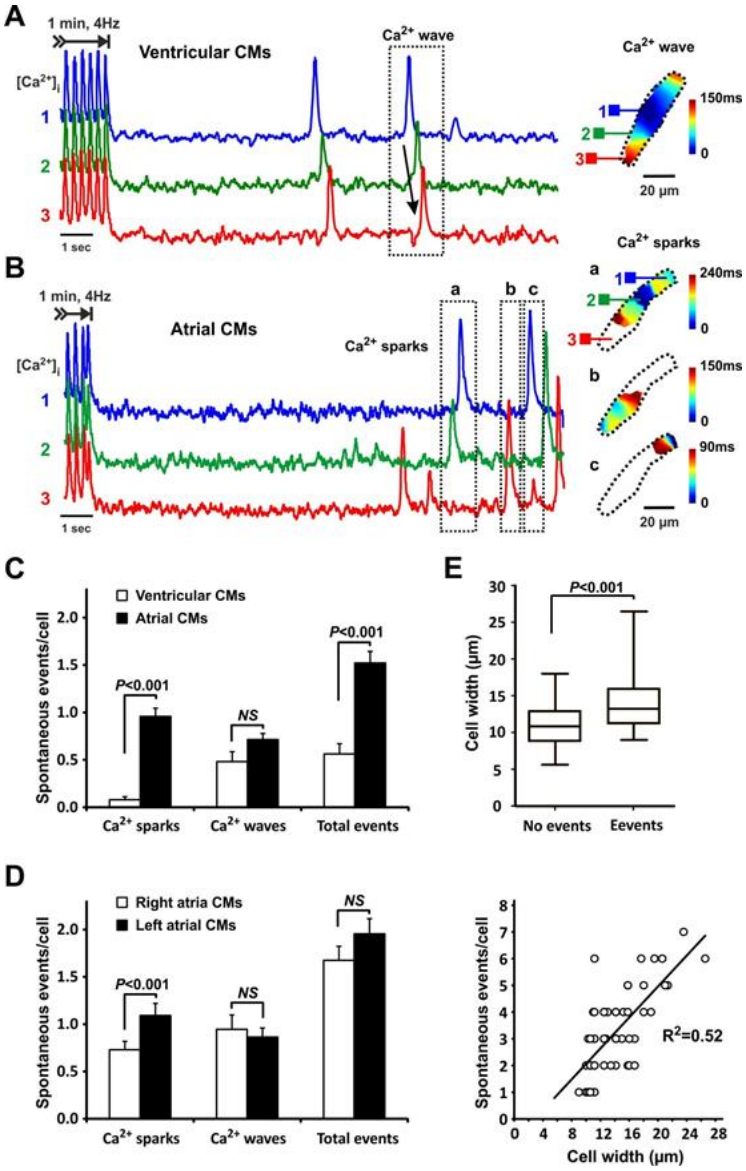

Figure 3.8. Spontaneous Ca2+ release events.

Spontaneous Ca2+ activity was measured in isolated ventricular **(A)** and atrial **(B)** cardiomyocytes (CMs). Cells were electrically paced at 4Hz for 1 min to enhance sarcoplasmic reticulum Ca2+ loading. Ca2+ sparks and waves were quantified during 8-16sec rest period after cessation of pacing. On the left, optical traces indicating changes in [Ca2+]i during measurements are shown from three different areas (1-3) from the selected cardiomyocytes. On the right, Ca2+ transient propagation color contour maps are presented for spontaneous Ca2+ wave recorded from the ventricular myocyte (**A**) and three Ca2+ sparks obtained from the atrial cardiomyocytes **(B)**. Near the maps, the corresponding color time scales for propagation time are shown. **(C)** Average frequency of spontaneous Ca2+ sparks and waves measured in ventricular (n=126 from 8 rats) and atrial (n=357 from 9 rats) cardiomyocytes. **(D)** Percentage of atrial and ventricular cardiomyocytes with spontaneous Ca2+ events. **(E)** Average cell width for atrial cardiomyocytes with and without spontaneous Ca2+ release events (n=117 from 7 rats). **(F)** Average frequency of spontaneous Ca2+ sparks and waves measured separately in the right (RA, n=156 from 4 rats) and left (LA, n=201 from 4 rats) atrial cardiomyocytes. **(G)** Percentage of RA and LA cardiomyocytes with spontaneous Ca2+ events. **(H)** Correlation between cell width and frequency of spontaneous Ca2+ events for atrial cardiomyocytes together with a correlation coefficient (by Dr. Alexey Glukhov).

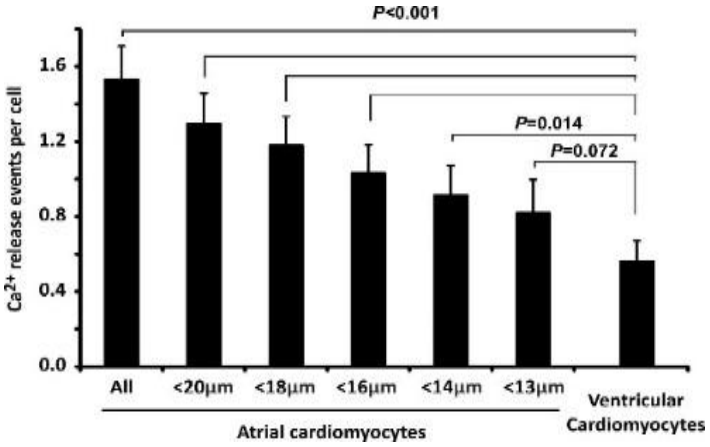

Figure 3.9. Dependence of spontaneous Ca^{2+} release events from cell width. Number of spontaneous Ca^{2+} release events per cell was measured for all atrial cardiomyocytes and for atrial cardiomyocytes of different cell width. Note that number of Ca^{2+} release events significantly decreases with cell width narrowing. For atrial cardiomyocytes thinner than 13µm, number of Ca^{2+} release events did not differ from that measured in ventricular cardiomyocytes (by Dr. Alexey Glukhov).

3.3.6 Spatial localization of functional LTCCs in atrial cells

It was recently demonstrated that in healthy adult ventricular cardiomyocytes, functional LTCCs are predominantly localized in the T-tubules (Bhargava, Lin et al. 2013). Apart from some controversial results which are obtained by immunofluorescence microscopy methods and suggested all LTCCs can be also found outside of T-tubules (Carl, Felix et al. 1995; Schulson, Scriven et al. 2011), no data regarding the spatial distribution of functional atrial LTCCs is available. In order to address this question directly, the super-resolution scanning patch-clamp method (Bhargava, Lin et al. 2013) was applied to record single LTCC activity in atrial cardiomyocytes with different T-tubule system structures (**Figures 3.10-3.12**). Of note, LTCC current in atrial cardiomyocytes was recorded with similar frequency from T-tubules, crests and non-structured areas (28% of 78 successful patches in T-tubules vs. 30.1% of 63 successful patches in the crest and 29% of 26 successful patches in non-structured areas, **Figure 3.13**).

Although no difference in open probability between the channels recorded in different locations were found [p(open) at -6.7mV: 0.06±0.006 in the T-tubule vs. 0.067±0.013 in the crest, NS; and vs. 0.053±0.006 in non-structured area, NS] (**Figure 3.14**) channels located in T-tubules possessed ~40% higher amplitude at negative voltages compared to LTCCs obtained in the crests of sarcolemma and non-structured areas (**Figure 3.15**). No difference in amplitude between LTTCs located in T-tubules or in the crest was observed in rat atrial cardiomyocytes isolated from left and right atria (**Figure 3.16**).

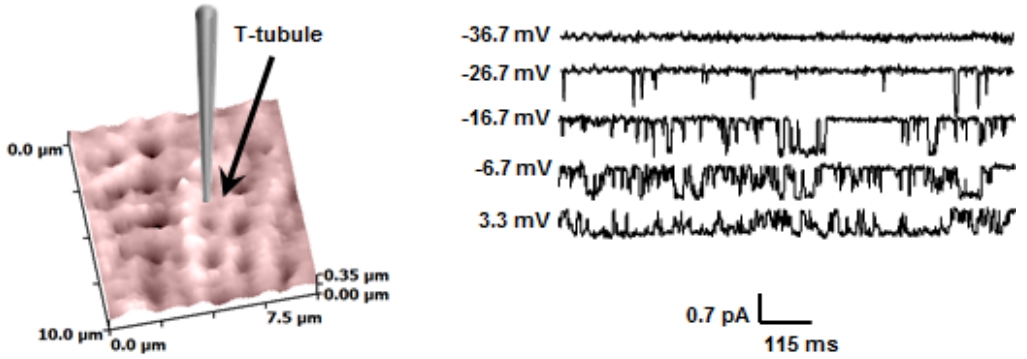

Figure 3.10. Single LTCC activity recorded from T-tubule area in rat atrial cardiomyocytes.
Typical 10µmx10µm topographic scans of cardiomyocytes showing locations where a pipette was placed after clipping and a giga-seal was obtained over a T-tubule area of the sarcolemma. On the right, corresponding representative current traces of single LTCC activity at the given voltages using a pipette of 25MΩ resistance.

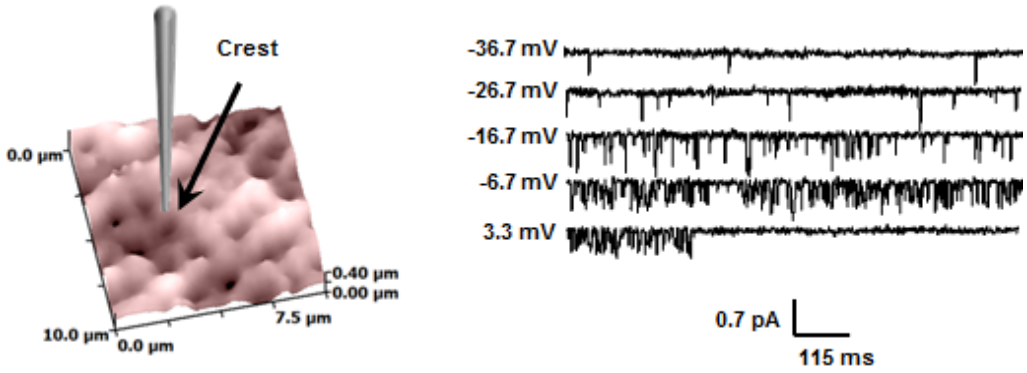

Figure 3.11. Single LTCC activity recorded from the crest area in rat atrial cardiomyocytes.
Typical 10µmx10µm topographic scans of cardiomyocytes showing locations where a pipette was placed after clipping and a giga-seal was obtained over a crest area of the sarcolemma. On the right, corresponding representative current traces of single LTCC activity at the given voltages using a pipette of 25MΩ resistance.

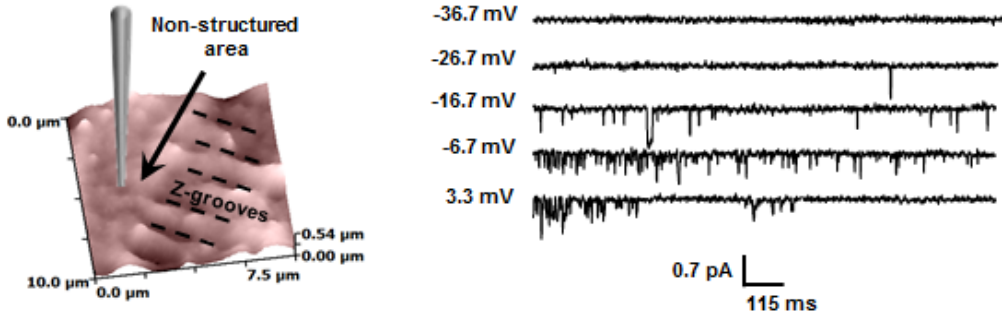

Figure 3.12. Single LTCC activity recorded from a non-structured area in rat atrial cardiomyocytes.
Typical 10µmx10µm topographic scans of cardiomyocytes showing locations where a pipette was placed after clipping and a giga-seal was obtained over a non-structured area of the sarcolemma. On the right, corresponding representative current traces of single LTCC activity at the given voltages using a pipette of 25MΩ resistance.

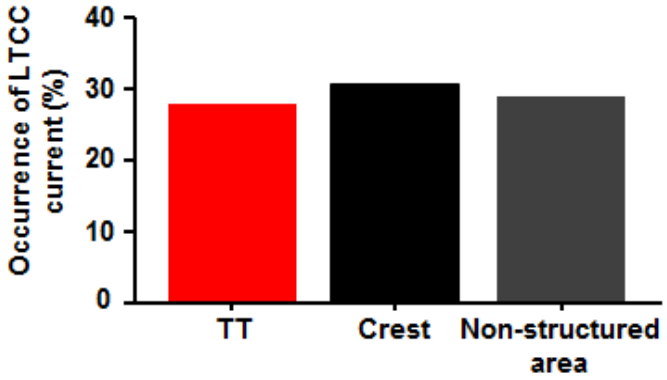

Figure 3.13. Occurrence of L-type calcium current recorded from different areas in rat atrial cardiomyocytes.

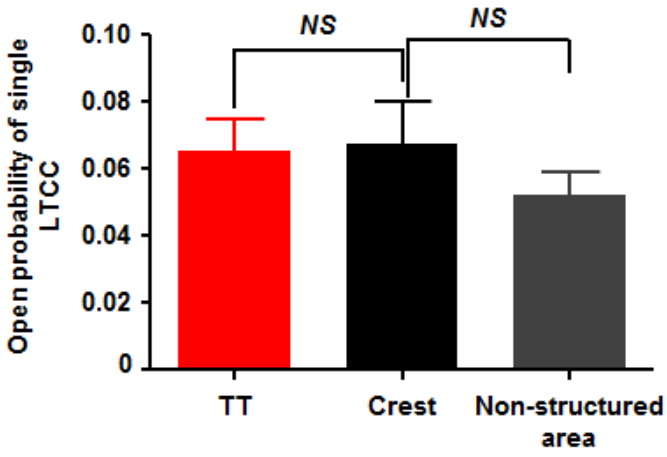

Figure 3.14. Open probability of single LTCC recorded from different areas in rat atrial cardiomyocytes.

P(open) of LTCCs recorded from T-tubules (TT) (N=43), crest (N=25) and non-structured areas (N=13), where N is number of channels.

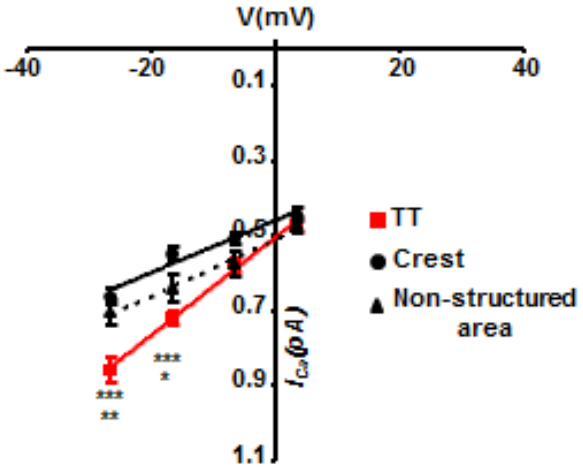

Figure 3.15. Voltage-current characteristic of single LTCCs in rat atrial cardiomyocytes.
I-V of single LTCC activity recorded from the T-tubules (TT), crest, and non-structured areas. n=6-16 for T-tubules, n=8-12 for crests, and n=5 for non-structured areas. * *P*<0.05 and ** *P*<0.001 crest vs. T-tubules.

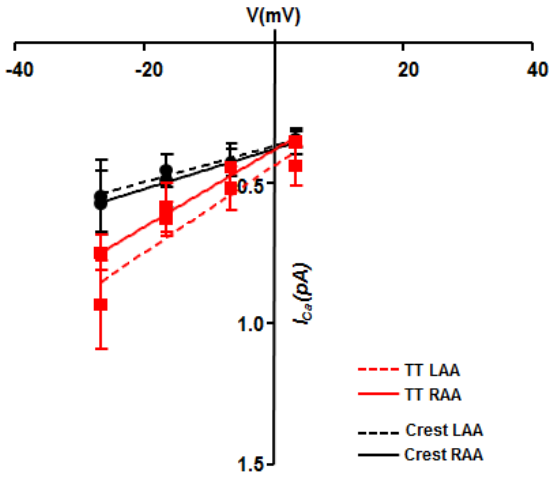

Figure 3.16. Voltage-current characteristic of single LTCCs in rat atrial cardiomyocytes isolated from left and right atrial.
I-V of single LTCC activity recorded from the T-tubules (TT), crest. N=6 for TT in left atrium, n=5 for TT in right atrium; n=4 for crests in left atrium, and n=5 for crests in right atrium. Where N is a number of atrial cells.

Like many other types of channels, LTCCs show multiple sub-conductance levels in addition to the largest and main open state of the channel (Gondo, Ono et al. 1998; Cloues and Sather 2000). Examples of these substates are illustrated in **Figure 3.17**. Clear openings to three-four distinct conductance levels were observed at -26.7mV. The LTCCs substates appear to be true openings to smaller conductance states and did not arise from filtering artefacts. Openings to the substates were well resolved, greatly exceeding the filter rise time (average open time of the small substate = 2.98±0.20ms (n=127), shorted open time = 1.1ms; filter rise time = 100μs), so they were not produced by unresolved transitions of relatively slow interconversions between open and closed conformations. Indeed, the amplitude of all conduction states was voltage-dependent (**Figure 3.19 and 3.20**). As summarized in **Figure 3.18**, channels located in the crest had a more accessible occupancy of low-amplitude sub-conductance states than T-tubule LTCCs: open probability of low-amplitude sub-conductance states was 0.027±0.005 and 0.005±0.002 for crest (n=4) and T-tubule LTCC (n=5), respectively, P<0.01 (**Figure 3.21**). In the same time, at -6.7 mV channels located in T-tubules and in the crest have similar sub-conductance distribution with (**Figure 3.22**).

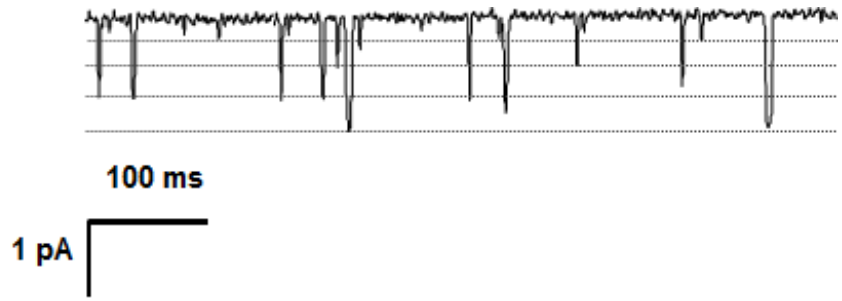

Figure 3.17. Sub-conductance levels of single LTCC amplitude.

Representative LTCC trace with openings evoked by voltage jumps to −26.7 mV and using 90 mM Ba2+ as the charge carrier. The dotted lines indicate substates and fully open levels.

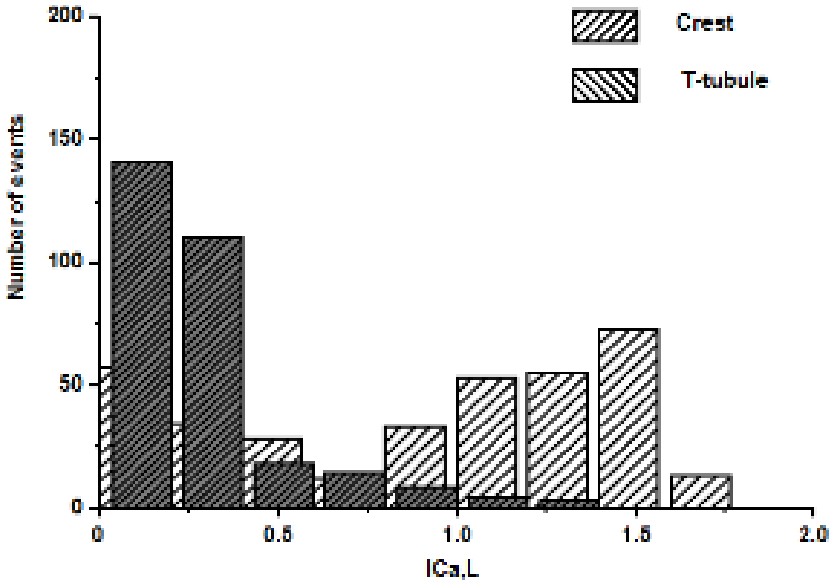

Figure 3.18. The LTCC amplitude histogram of single channel openings to different substate levels at -26.7 mV measured as shown on the panel above.

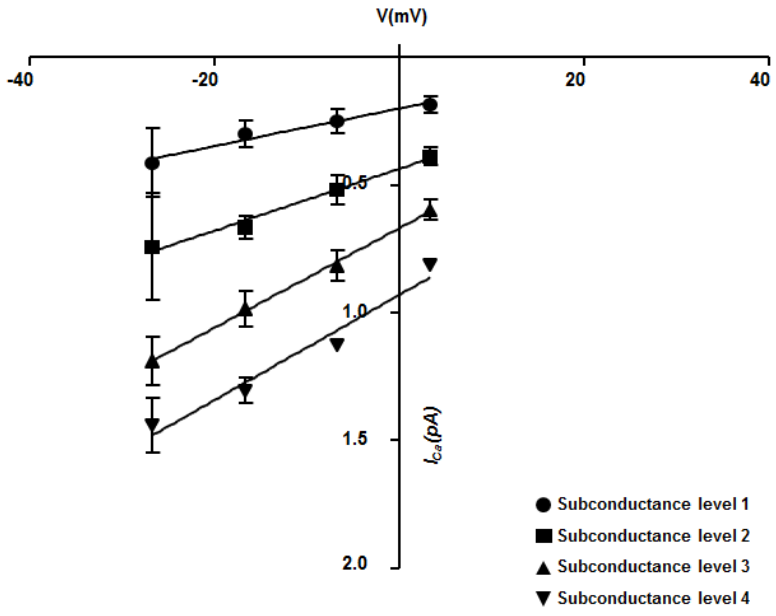

Figure 3.19. Single channel current-voltage (*I*-V) relationships for different conductance levels of LTCCs recorded in T-tubule, with 90 mM Ba^{2+} as the charge carrier.

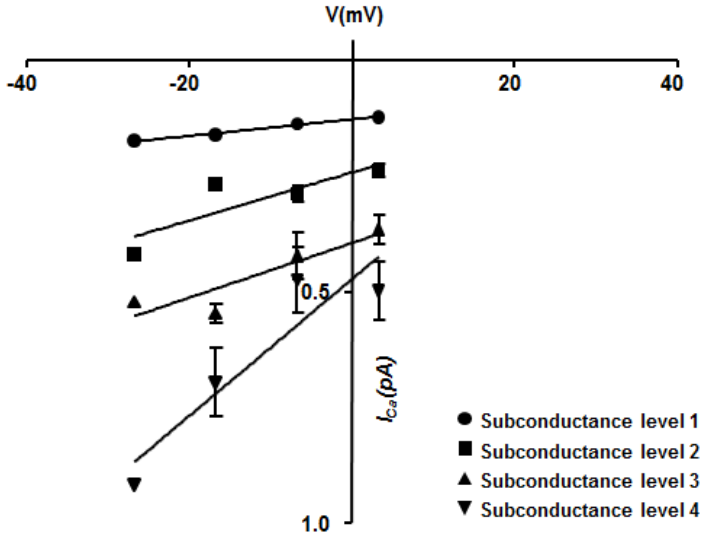

Figure 3.20. Single channel current-voltage (*I*-V) relationships for different conductance levels of LTCCs recorded in T-tubule, with 90 mM Ba^{2+} as the charge carrier.

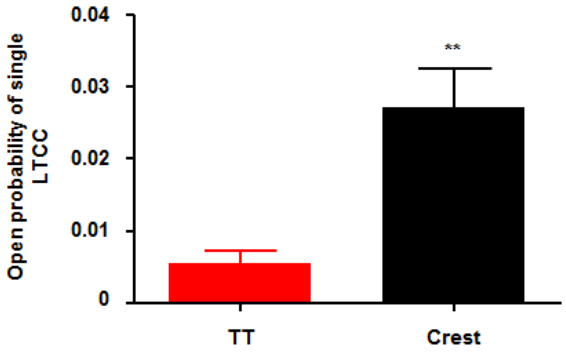

Figure 3.21. Open probability of single LTCC recorded from different areas in rat atrial cardiomyocytes at -6,7 mV.

P(open) of sub-conductance levels with lowest amplitude recorded from T-tubules (TT) (N=5), crest (N=4), where N is number of channels.

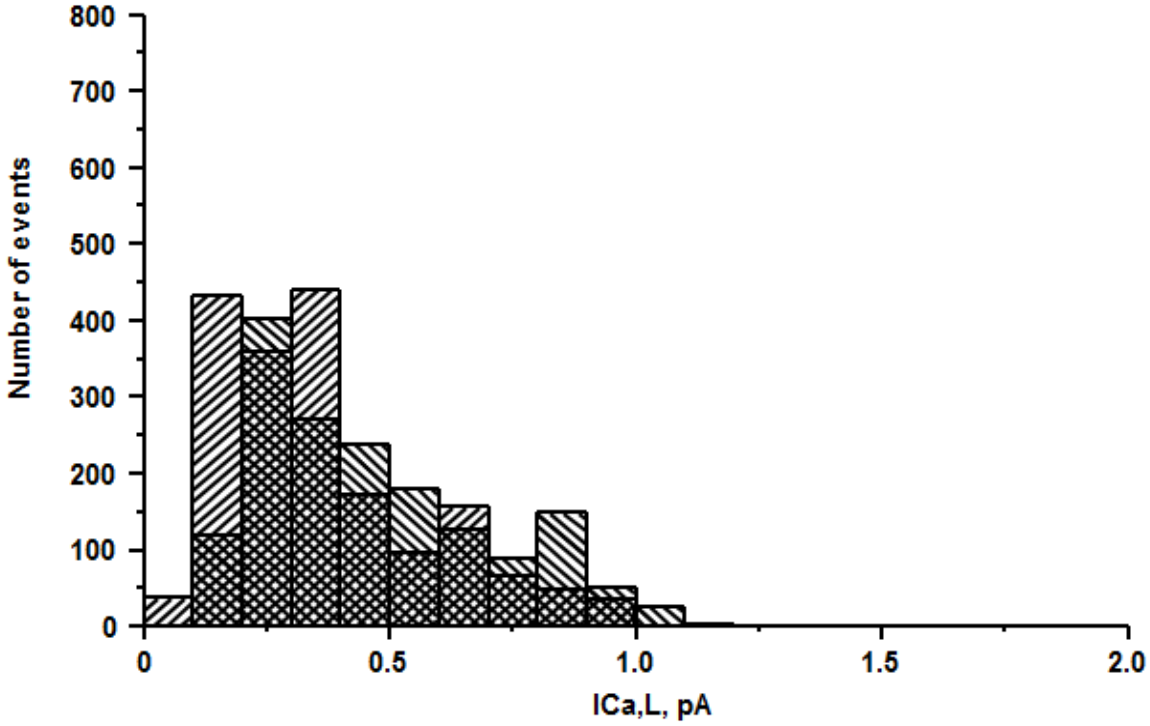

Figure 3.22. The LTCC amplitude histogram of single channel openings to different substate levels at -6.7 mV measured as shown on the panel above.

3.3.7 Caveolae as a source of L-type Ca2+ channels

It has been demonstrated in ventricular cardiomyocytes, that some LTCCs could be housed in caveolae structures (Balijepalli, Foell et al. 2006; Makarewich, Correll et al. 2012). The hypothesis is that atrial extradyadic LTCC recorded from the crests and non-structured areas might be localized to caveolae. To address this hypothesis, two different approaches were used to disrupt caveolae: first, treatment with methyl-β-cyclodextrin (MβCD) and second, direct LTCC inhibition in Cav3-containig membranes using a specific peptide inhibitor.

Figure 3.23 (top) shows the distribution of caveolae in atrial cardiomyocytes**.** Interestingly, the number of caveolae observed in atria is ~5-fold higher than the

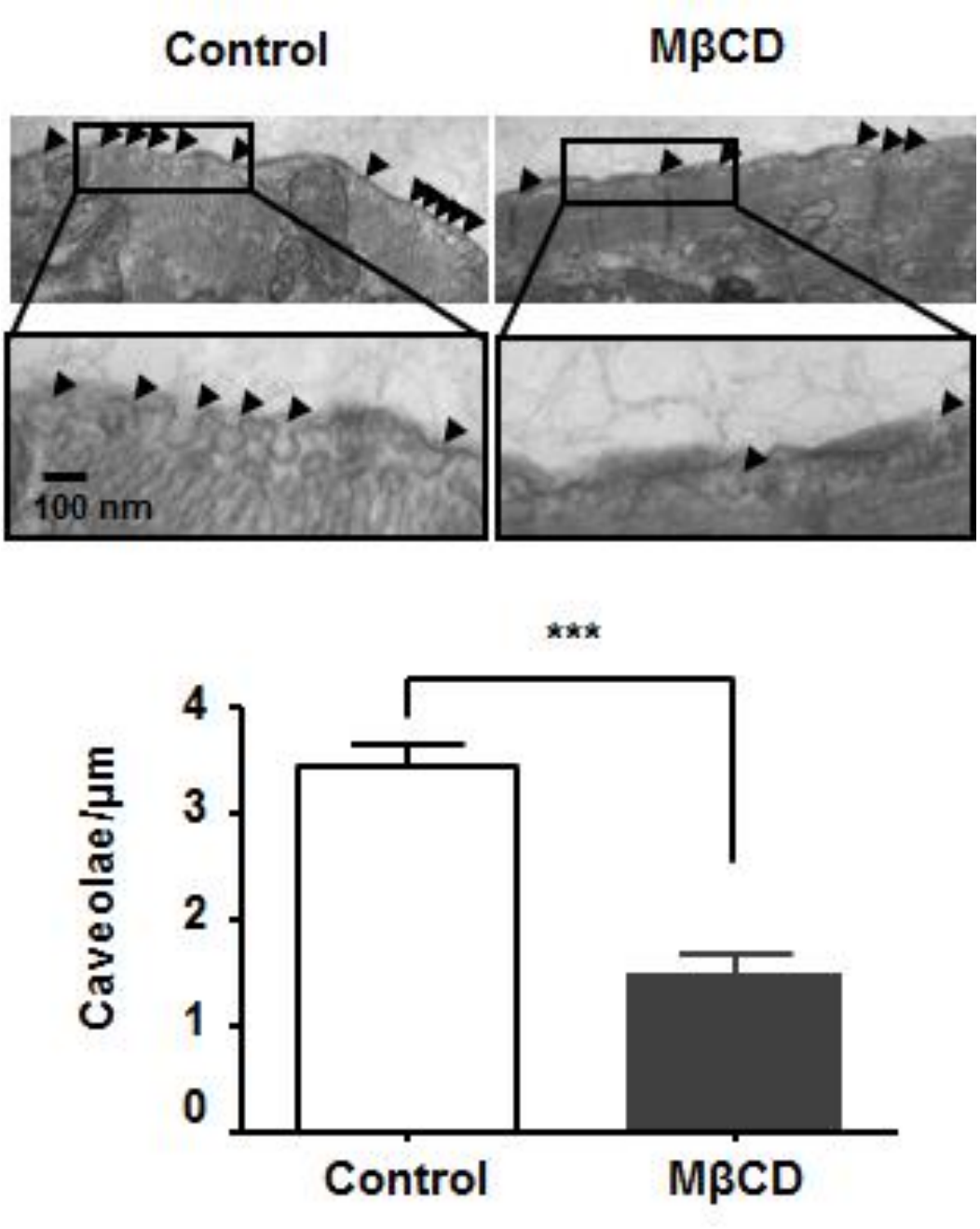

Figure 3.23. Ultrastructural changes in rat atrial cardiomyocytes after methyl-β-cyclodextrin incubation.

Top, electron micrograph of a representative control cell (*left*) and a 10mM methyl-β-cyclodextrin (MßCD) treated cell (**right**) are shown. Caveolae are marked by arrowheads. **Bottom**, caveolae per micron in the cellular membrane before and after MßCD treatment (n=3 rats per group) (by Dr. Ivan Diakonov).

number that was reported recently for ventricular cardiomyocytes (Wright, Nikolaev et al. 2013).

Incubation of atrial cardiomyocytes with 10mM MβCD for 30 min at room temperature resulted in ~60% depletion of caveolae (**Figure 3.23, bottom**).

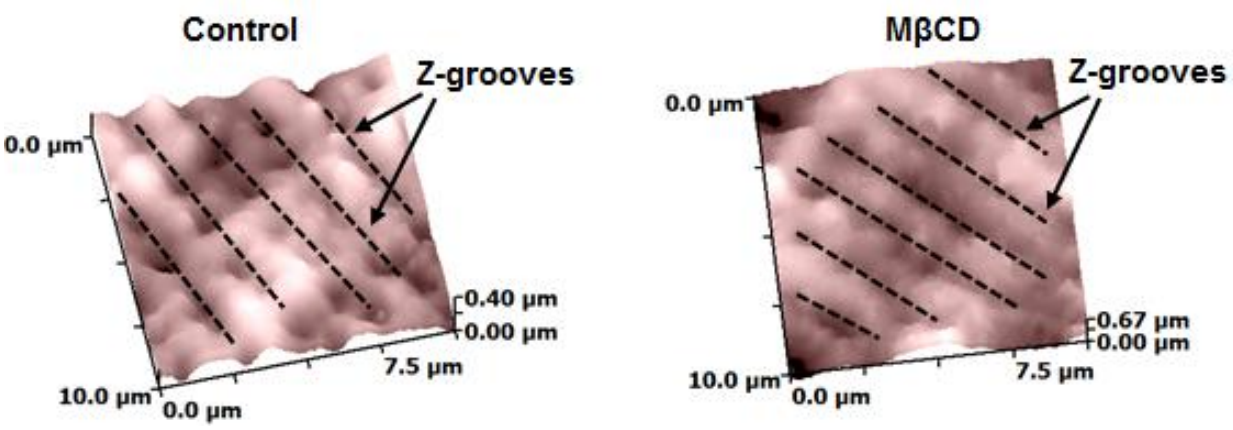

Figure 3.24. Surface structure changes in rat atrial cardiomyocytes after methyl-β-cyclodextrin incubation.

Representative SICM scans of untreated (**left**) and MßCD treated (**right**) atrial cardiomyocytes. Dotted lines on the scans show Z-grooves.

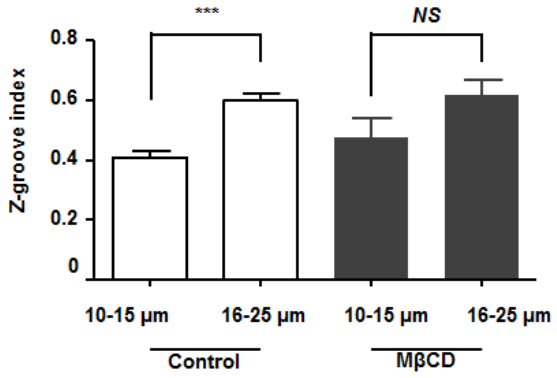

Figure 3.25. Z-groove index in rat atrial cardiomyocytes after methyl-β-cyclodextrin incubation.

Average Z-groove indexes measured for thin (<15µm) and thick (>16µm) atrial cells before (n=29 of thin cells and n=53 of thick cells) and after (n=8 of thin cells and n=9 of thick cells) MßCD treatment.

Then MβCD treatment was applied to deplete cholesterol and disrupt cholesterol- and sphingolipid-enriched membrane structures, including both lipid rafts and caveolae (Lohn, Furstenau et al. 2000; Calaghan and White 2006). To examine the possible effect of MβCD on surface structures of atrial cardiomyocytes, the Z-groove index was calculated for both thin (cell width <15µm) and thick (cell width >16µm) atrial cardiomyocytes before and after treatment with MβCD (**Figure 3.24**). No changes in cell topography and T-tubule density (8.6±1.1% vs 10.3±0.6% for MβCD treated vs control cells, respectively, P=0.192; cell size: 14.8±1.4µm and 14.3±0.6µm in MβCD group vs 15.6±0.6µm and 14.9±0.7µm in control group for cells with disorganized and absent T-tubules, respectively, NS) were observed after MβCD treatment (**Figure 3.25**).

At the same time, atrial cells showed a significant change in LTCCs distribution after treatment with MβCD. Figure 26 shows representative 10x10 µm surface topography scan and L-type calcium channels traces recorded from T-tubules and from the crest microdomains.

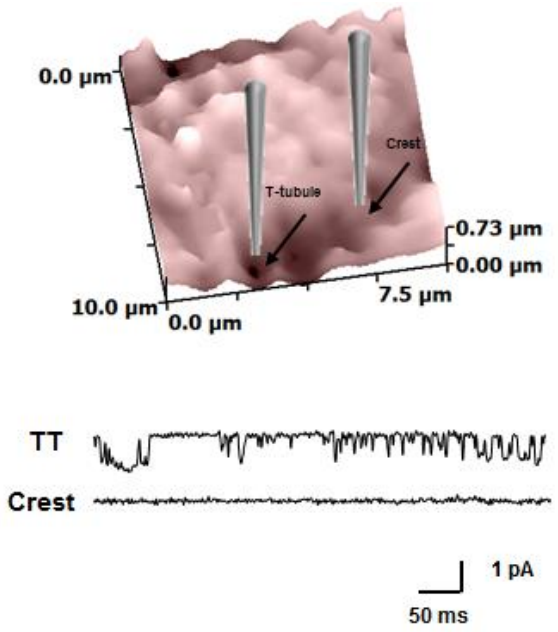

Figure 3.26. L-type calcium channels in rat atrial cardiomyocytes after methyl-β-cyclodextrin incubation.

Typical 10 µm x 10µm topographic scans of methyl-β-cyclodextrin (MßCD) treated rat atrial cardiomyocytes. Below are single channel recordings obtained from the T-tubule (TT) and the crest of sarcolemma (Crest).

While MβCD did not affect LTCCs occurrence in the T-tubules (28% vs. 28%, before and after MβCD treatment, NS), it completely abolished the occurrence of LTCCs on the crest of sarcolemma (30.1% vs. 0% before and after MβCD treatment, respectively, P<0.001) (**Figure 3.27**), suggesting a crucial role of caveolae for spatial compartmentation of LTCCs in atrial cardiomyocytes.

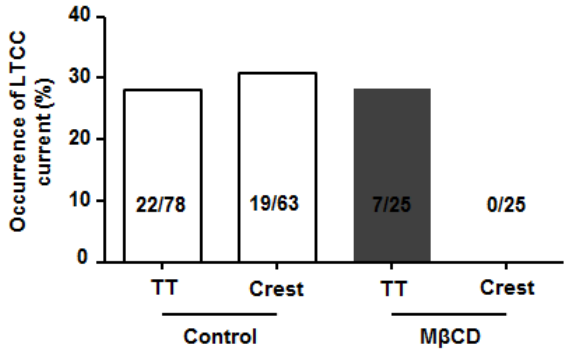

Figure 3.27. Cholesterol depletion abolishes the occurrence of LTCCs in crest of sarcolemma but not in T-tubules and decreases whole cell *I*Ca,L.

Percentage of LTCC current occurrence for LTCCs recorded from the T-tubules and the crests before and after MßCD treatment.

No changes in either LTCC open probability or current-voltage relationship of single LTCCs were observed for channels recorded in T-tubule openings after MβCD treatment (**Figure 3.28, 3.29**).

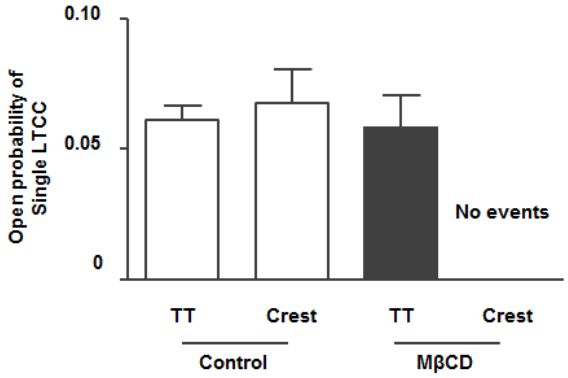

Figure 3.28. Open probability of L-type calcium channels in rat atrial cardiomyocytes after methyl-β-cyclodextrin incubation.

Open probability for LTCCs recorded from the T-tubules and the crests before (control) and after MßCD treatment.

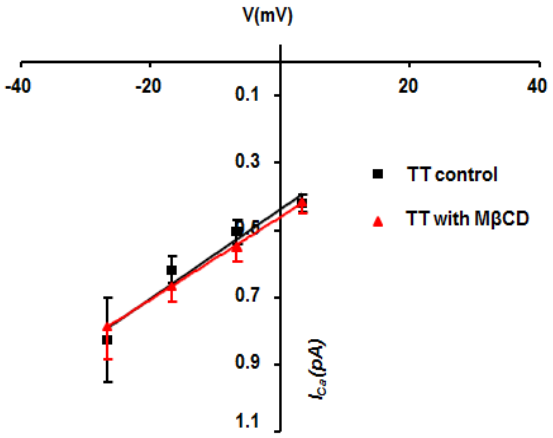

Figure 3.29. Voltage-current relationship of L-type calcium channels recorded in T-tubules in rat atrial cardiomyocytes before (control) after methyl-β-cyclodextrin incubation.

Associated with LTCC removal from the crest, MβCD significantly decreased the whole-cell calcium current ($I_{Ca,L}$) density by approximately 30% without affecting cell capacitance (**Figure 3.30**).

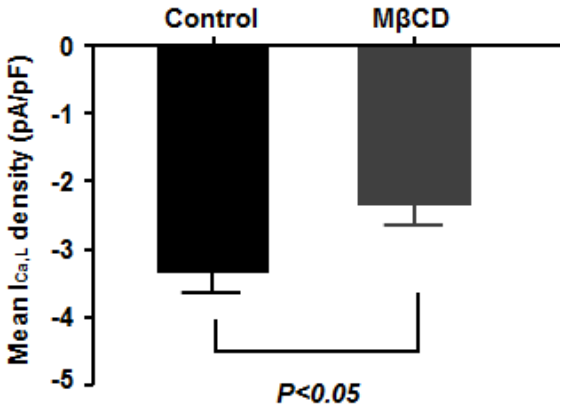

Figure 3.30. Cholesterol depletion decreases whole cell *I*Ca,L.

Mean $I_{Ca,L}$ peak normalized to cell capacitance (pA/pF), n=9 for control and n=12 for MßCD-treated atrial cardiomyocytes.

In contrast, in ventricular cardiomyocytes, no changes in either cell capacitance (136.9±8.1pF and 112.1±9.5pF for control and MβCD groups, n=10/group, P=0.062) or $I_{Ca,L}$ was observed after MβCD treatment (mean $I_{Ca,L}$ current density: -4.924±0.672pA/pF for control, n=10, vs -4.794±0.646pA/pF for MβCD group, n=8, P=0.876; **Figure 3.31**).

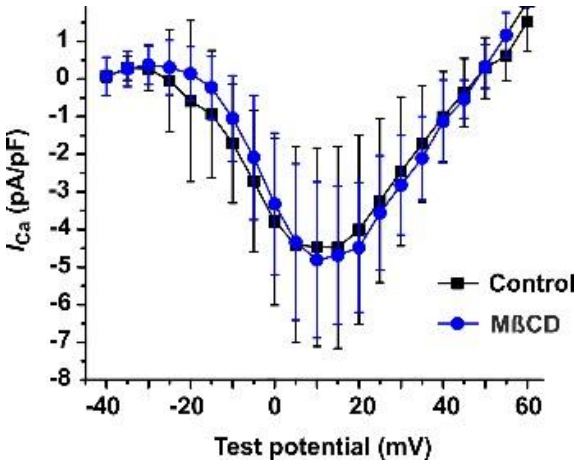

Figure 3.31. Effect of methyl-β-cyclodextrin (MßCD) treatment on ventricular myocytes whole cell current-voltage relationship.

n=10 for untreated (control) ventricular cardiomyocytes; n=8 for 10mM MßCD treated ventricular cardiomyocytes (by Dr. Anita Alvarez-Laviada).

3.3.8 Ignition of Ca2+ sparks through caveolae

Along with changes in LTCC distribution, MβCD significantly suppressed the occurrence of spontaneous calcium events (**Figure 3.32A**). MβCD treatment significantly decreased the number of spontaneous Ca2+ sparks, but not waves (**Figure 3.32B**) and reduced the number of cells featuring spontaneous Ca2+ events (**Figure 3.32C**). Moreover, removing caveolae via MβCD treatment also reduced the spatial size of the Ca2+ sparks in atrial cardiomyocytes (**Figure**

3.32D) as has been previously demonstrated in neonatal ventricular cardiomyocytes and arterial smooth muscle cells (Lohn, Furstenau et al. 2000).

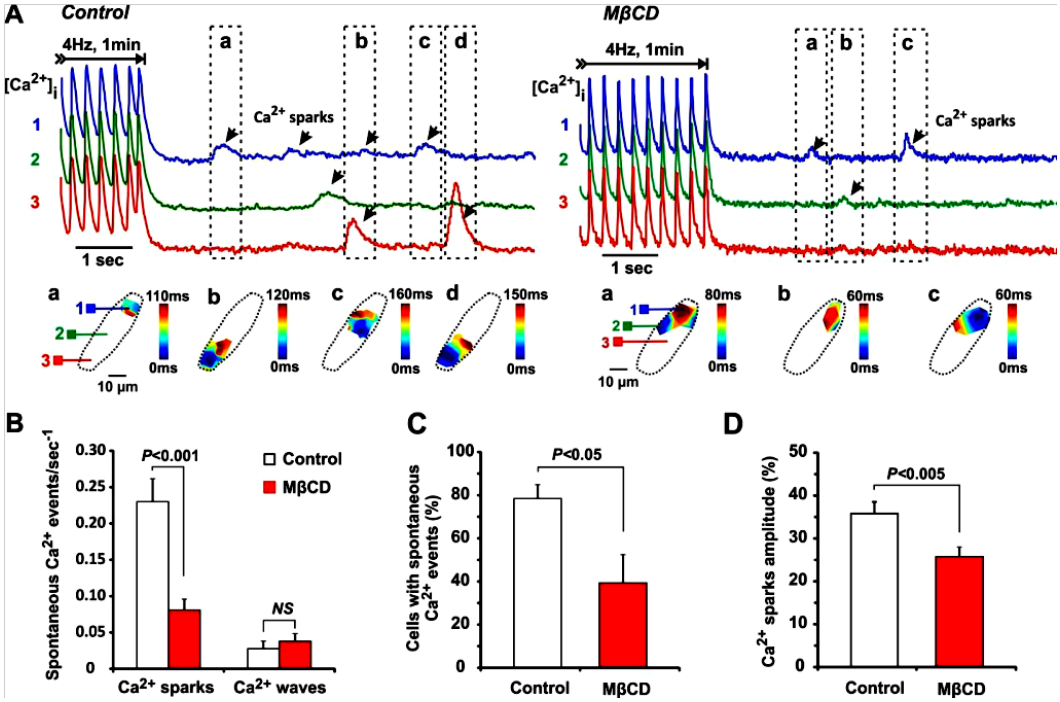

Figure 3.32. Suppression of spontaneous Ca2+ sparks after caveolae disruption by cholesterol depletion.

(**A**) Representative optical mapping recordings of Ca2+ transients during spontaneous Ca2+ sparks evoked by Ca2+ overload induced by pacing at 4Hz for 1 minute. Optical recordings were obtained before (*left*) and after 30min pre-treatment with methyl-β-cyclodextrin, MßCD (*right*). Top, optical traces are shown from three different areas (1-3) from the selected cardiomyocytes. Below the traces, Ca2+ transient propagation color contour maps are presented for spontaneous Ca2+ sparks recorded from the atrial cardiomyocyte before and after MßCD treatment. Note that MßCD significantly suppressed the occurrence of spontaneous Ca2+ sparks (**B**), the amount of cells with spontaneous Ca2+ events in untreated and MßCD treated groups (**C**), and Ca2+ spark amplitude (**D**). Ca2+ spark amplitude was calculated as a percentage from the amplitude of electrically induced Ca2+ transient measured during 4Hz pacing. n=82 from 12 rats and n=99 from 7 rats for control and MßCD groups, respectively (by Dr. Alexey Glukhov).

A caveolae-targeted LTCC antagonist eliminates occurrence of extradyadic LTCC current. To confirm that extradyadic LTCCs are localized to Cav3-associated caveolae structures, rather than lipid rafts, a Cav3-targeted LTCC-blocking agent, Rem peptide, was used (Makarewich, Correll et al. 2012). The caveolae targeted LTCC blocker (Rem1-265-Cav) was generated by molecular modification of Rem, a member of the RGK GTPase family that is known to potently inhibit LTCCs (Xu, Lai et al. 2010). Makarewich et al has demonstrated in rat ventricular cardiomyocytes that Rem1-265-Cav localized to plasma membrane specifically within caveolin-containing lipid rafts, rather than lipid rafts in general, and did not displace molecules normally found in caveolae (Makarewich, Correll et al. 2012).

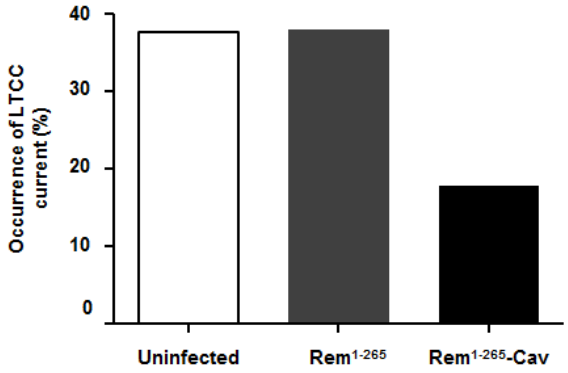

Figure 3.33. A caveolae-targeted LTCC antagonist decreases the occurrence of single LTCC current on the crest area of the sarcolemma.

Percentage of occurrence of the single LTCC current from the crest area of uninfected (48-hours of culturing without a virus), Rem1-265 and Rem1-265-Cav 48-hours after infection atrial cardiomyocytes.

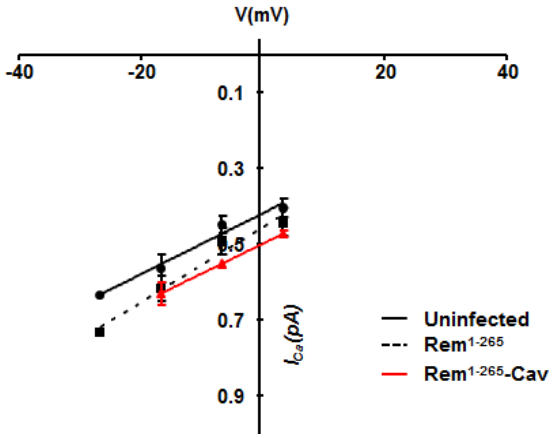

Figure 3.34. A caveolae-targeted LTCC antagonist does not affect single LTCC current in the crest area of the sarcolemma.

Current-voltage relationship of the single LTCC current from the crest area of uninfected (48-hours of culturing without a virus), Rem1-265 and Rem1-265-Cav 48-hours after infection atrial cardiomyocytes.

In these experiments, infection efficiency was determined after 48 hours culturing with a virus by GFP fluorescence intensity and was typically assessed to be 60-65%. Expressing Rem in atrial cardiomyocytes resulted in a significant decrease in the occurrence of the single LTCC on the crest area of sarcolemma (**Figure 3.33**) without affecting LTCC biophysical properties (**Figures 3.34**). Truncation of this membrane-docking domain (Rem1-265) resulted in the inability of Rem to affect the occurrence of the single LTCC current on the crest and to change spontaneous Ca2+ events. No difference in the single channel open probability was observed between the groups.

3.4 CONCLUSION

These results provide the first direct evidence of caveolae specific localization and regulation of functional LTCCs in atrial cardiomyocytes and suggest their possible role in the mechanism of unique atrial calcium cycling in atrial cardioymyocytes, which lack T-tubules.

This study demonstrates for the first time that the rat atrial LTCCs housed in caveolae microdomains show ~40% decrease in amplitude compared with channels located in T-tubules. This difference can be linked to a more accessible occupancy of low-amplitude sub-conductance states of crest channels. It has been shown that the expression of α_1 subunit alone was sufficient to exhibit these subconductance levels, and co-expression of β_{2a} subunit significantly increased the number of openings in all four levels without changing the conductance values (Gondo, Ono et al. 1998). Subconductance states of various LTCC subtype have been reported to be regulated by processes such as phosphorylation (Greif, Lin et al. 1995), G-protein coupled receptor activation (Kuo and Bean 1993) or membrane plasticity-inducing stimulation (i.e. by cholesterol or phospholipids (Bialecki and Tulenko 1989)), all of which are being associated with caveoli. Physiologically, different single channel conductance levels would give rise to heterogeneity of the Ca^{2+} trigger signals (Chen-Izu 2010). Thus, lower amplitude of caveolae-housed LTCCs may give rise to lower amounts of Ca^{2+} entry during a single channel opening and be associated with a distinct Ca^{2+} sensitivity and efficacy of IP_3-associated signaling pathway in caveolae. However, the extent to which caveolae LTCC are involved in non-junctional Ca^{2+} release events, and the mechanism beyond the LTCCs and IP_3 receptors interaction, remain unknown and requires further investigation.

4 CHAPTER 4. Compartmentalization of signaling system in atrial cardiomyocytes. Anti-adrenergic effect of adenosine in regulation of L-type calcium channels

4.1 INTRODUCTION

Compartmentalization of the signalling systems in cardiac cells is an important property. This property allows the regulation of multiple cellular functions, such as electrical activity, Ca^{2+} dynamics, and cellular contraction (Balijepalli and Kamp 2008; Rudy, Ackerman et al. 2008; Harvey and Calaghan 2012; Weiss, Oz et al. 2013). The experimental data demonstrate differential localization of the components of the β-adrenergic signalling systems (Rybin, Xu et al. 2000; Balijepalli, Foell et al. 2006; Best and Kamp 2012). It was investigated that the localization of adenylate cyclase is close to the L-type Ca^{2+} channels in the T-tubules (Gao, Puri et al. 1997). Moreover, there is evidence that the β-AR co-localizes with Cav3, a component of caveolae (Steinberg 2004) and the same has been demonstrated for AC (Schwencke, Yamamoto et al. 1999). Rybin et al demonstrated in cardiac cells, that β_1-adrenergic receptors are mostly localized in membrane compartments that lack caveolin-3, while β_2-adrenergic receptors are mostly found in caveolin-3-rich domains with the majority of the β_1-adrenergic receptors being found outside of the caveolae compartment (Rybin, Xu et al. 2000).

In addition, β_1- and β_2-adrenergic receptors modulate differently cardiac ionic currents and contraction proteins, which are also localized in different cellular compartments (Maguy, Hebert et al. 2006; Balijepalli and Kamp 2008).

There is an enormous literature describing the effects of catecholamines on $I_{Ca\text{-}L}$ in isolated cells through single LTCCs and in multicellular preparations. In summary, data obtained in multicellular preparations (Dukes and Vaughan Williams 1984) and in isolated cells (McDonald, Pelzer et al. 1994) show an increase of $I_{Ca\text{-}L}$ by β_1-adrenergic stimulation. The peak inward current increases primarily by a decrease

of the closed time of the channels (van der Heyden, Wijnhoven et al. 2005). Previous results have shown, that the increase in whole-cell calcium currents in acutely dissociated ventricular cardiomyocytes by Iso (Kuznetsov, Pak et al. 1995; Xiao, Zhang et al. 2003; Balijepalli, Foell et al. 2006); and other nonselective β-adrenergic agonists is predominantly caused by activation of the β_1-adrenergic receptor in rat, mouse, and dog (Xiao and Lakatta 1993; Chen-Izu, Xiao et al. 2000).

Activation of β-ARs results in the activation of $I_{Ca\text{-}L}$ along many pathways (van der Heyden, Wijnhoven et al. 2005). The pathway via PKA, which will ultimately lead to phosphorylation of residues of the channel itself, causes calcium current density increasing. cAMP produced during β-ARs stimulation binds to the regulatory subunits of PKA results in the liberation of the catalytic subunits, which phosphorylate specific serine and threonine residues of the L-type Ca^{2+} channel (Kamp and Hell 2000; Keef, Hume et al. 2001).

The observation of three active gating modes has several important implications for previous work on L-type Ca channels. Multiple modes of gating have been observed at the single channel level: mode 0, 1 and 2. At mode 0, channels do not open or open very rarely in response to depolarization. At mode 1, in which the probability of opening is low with brief open times. At mode 2, in which the probability of opening is much higher and the openings are long-lasting and the closings are brief (Catterall 2000; Davare, Horne et al. 2000).
The increase in Ca^{2+} currents observed after the activation of PKA are due to an increase in the open state probability of the channel, resulting from a shift in gating mode (Striessnig 1999; Kamp and Hell 2000)

The proposal that β-adrenergic stimulation of Ca current proceeds predominantly by an "increase in the number of functional channels" (Bean, Nowycky et al. 1984) overlooks the important contribution of shifts from mode O_a to modes 1 and 2 (Yue, Herzig et al. 1990)

Positive adrenergic effects of catecholamines are described besides of negative inotropic effect of adenosine on myocardium. This effect can occur in the presence of adenosine alone (direct effect) and/or in the presence of additional stimulation (indirect effect). It was previously shown, that adenosine depresses indirectly ventricular pumping under β_1-adrenergic stimulation (Dobson 1983). This antiadrenergic effect of adenosine is associated mainly by an exhaustion of the catecholamine-enhanced L-type Ca^{2+} inward current (Mallet, Lee et al. 1996) via a decrease in cyclic AMP (Dobson 1978). The same action of adenosine was demonstrated also in atrial muscle where it reduces basal calcium current by 35% (Cerbai, Klockner et al. 1988).

As a purine nucleoside a naturally occurring metabolite derived from ATP, adenosine can act on it receptors on the outside of the sarcolemma and appears to be an important regulator within the cardiovascular system, and throughout the body. Released in response to stimuli, local adenosine interacts with four adenosine receptor subtypes, expressed in cardiovascular system: A_1, A_{2A}, A_{2B}, and A_3ARs (Newby, Worku et al. 1985; Headrick and Willis 1989; Shryock and Belardinelli 1997). These G-protein coupled receptors mediate varied responses, from modulation of coronary flow, heart rate and contraction, to cardioprotection, inflammatory regulation, and control of cell growth and tissue remodeling.

The anti-adrenergic effects of adenosine in animal models are mediated via A_1ARs, involve $G_{\alpha i}$ inhibition of PKA activation by β-adrenergic (Dobson 1983; Romano and Dobson 1990), and modulation of β_1-ARs stimulated G_s cycling (Fenton and Dobson 2007). Dobson and colleagues also showed that the A_1AR could exhaust β-adrenergic responses in a PKC-dependent process (Perlini, Khoury et al. 1998; Dobson, Shea et al. 2008) involving $G_{\beta\gamma}$ (Fenton, Shea et al. 2010).

Moreover, adenosine affects via A_1-AR β-adrenoceptor-mediated phosphorylation of phospholamban. A_1-AR stimulation decreases the phosphorylation of PLB stimulated by isoproterenol in ventricular cardiomyocytes from rat and guinea pig (Kroll, Decking et al. 1993), what leads to faster relaxation, as more Ca^{2+} is available for the next heartbeat.

In addition to effects on cardiomyocyte adrenoceptor responses, adenosine and A_1ARs inhibit release of noradrenaline from cardiac nerves (Lorbar, Chung et al. 2004), reducing levels during ischemia and reperfusion (Richardt, Waas et al. 1987; Burgdorf, Richardt et al. 2001). These effects are shown to be protective (Richardt, Waas et al. 1987), and will contribute (with the abovementioned responses) to inhibition of cardiac activation during periods of enhanced adenosine release.

In consideration to β_1-adrenergic signaling system (Best and Kamp 2012) and different subpopulations of L-type Ca^{2+} channels (see Chapter 3) are distributed among the cellular compartments related to caveolin-3, non-caveolae cellular membrane and T-tubular microdomains, that is possible to predict another signaling molecules and receptors are housed in membrane compartments.

Thus, this chapter reveals biophysical reactions that occur during stimulation of β_1-adrenoceptors and A1-adenosine receptors, the dynamics, such as modification of voltage-current characteristic and open probability, of single LTCCs, recorded in different subcellular compartments in atrial cells.

4.2 MATERIAL AND METHODS

4.2.1 Animals

Both male and female Sprague Dawley Rats (8-10 weeks old, weight ~250 g) were used in these experiments (number of animals is 28).

4.2.2 Control atrial cardiomyocytes isolation

Cells were isolated from rats as described in Chapter 2 (General material and methods). Both left and right atrial appendages were placed all together in isolation tube with enzymes (number of cells is 310).

4.2.3 Super-resolution scanning patch-clamp with pipette clipping modification

All calcium channels were recorded in cell-attached mode using super-resolution scanning patch-clamp technique as described in Chapter 2. In experiment with β_1-adrenergic stimulation specific β-ARs agonist isoproterenol with β_2-AR antagonist ICI-11855 were added in basic external recording solution. Adenosine as an agonist to A1-adenosine receptor were added in pipette recording solution to get local stimulation of A1-adenosine receptor.

4.2.4 Protocol of the whole cell β_1-adrenergic receptor agonist application

Whole-cell β_1-adrenergic stimulation was reached by applied synthetic nonselective βAR agonist isoproterenol (2μM) and β_2AR antagonist ICI 11855 (50 nM) in bath solution. 10-15 minutes were required to achieve full effect of adrenergic receptors stimulation (**Figure 4.1**). As β_1-adrenergic stimulation

enhances EC coupling within the heart chronic stimulation and acute overstimulation can provide toxic effect on myocardium and cause damage to cardiac cells. Thus, single L-type calcium channels recording was performed not longer than 90-120 minutes.

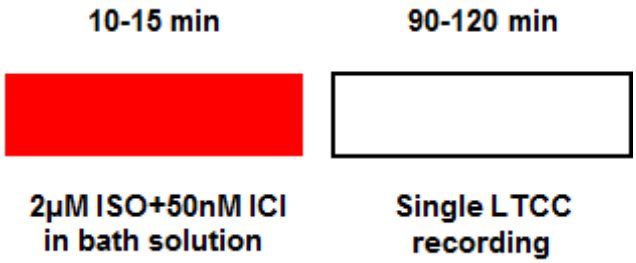

Figure 4.1. Protocol of whole-cell β_1-adrenergic stimulation of rat atrial cardiomyocytes.

4.2.5 Protocol of the local A1-adenosine receptor agonist application

As it was mentioned before, activation of A1-adenosine receptor modulates catecholamine-enhanced L-type Ca^{2+} current indirectly. Thus, to reveal compartmentalization of A1-adenosine receptors and co-localization of those with LTCCs whole cell β_1-adrenergic stimulation and local application of adenosine (20μM) through the recording pipette were used. All channels affected with adenosine were recorded in cell-attached mode only 5-7 minutes after giga-seal was obtained.

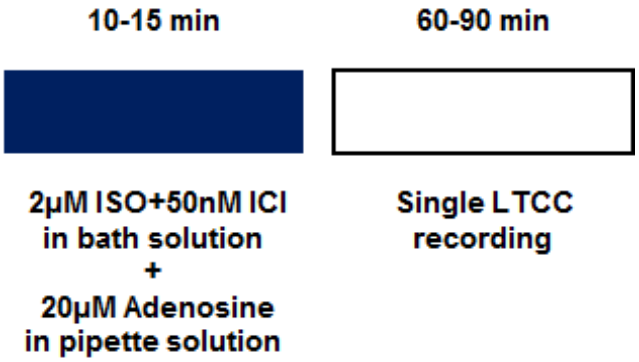

Figure 4.2. Protocol of whole-cell β_1-adrenergic stimulation with local A1- adenosine receptor stimulation of rat atrial cardiomyocytes.

4.2.6 Statistical analysis

Quantitative data are shown as mean ± SEM for the given number of experiments. Statistical analysis was carried out using an unpaired student t-test. A value of $P<0.05$ was considered statistically significant.

The analysis was performed using Prism4 software (GraphPad software Inc., San Diego, CA, USA).

4.3 RESULTS

4.3.1 β_1-adrenergic regulation of single L-type calcium channels in atrial cardiomyocytes

Previous studies confirmed that adenosine could modulate β_1-adrenergic enhanced L-type calcium current, however no evidence has been presented about compartmentalization of single Ca^{2+} current with adrenergic and adenosine receptors in different membrane domains. In order to answer this question directly, the super-resolution scanning patch-clamp method (Bhargava, Lin et al. 2013) was applied to record single LTCC activity in atrial cardiomyocytes before and after β_1-adrenergic stimulation alone and with local adenosine simulation applied through the recording pipette.

As expected, LTCC current in atrial cardiomyocytes was recorded with similar frequency from T-tubules and crests (see Chapter 3). But the occurrence of single LTCCs was higher in presence of 2μM ISO+50nM ICI in bath solution (42% of 47 successful patches in T-tubules and 45% of 51 successful patches in the crest after β_1-adrenergic stimulation vs. 28% of 78 successful patches in T-tubules and 30.1% of 63 successful patches in the crest without β_1-adrenergic stimulation).

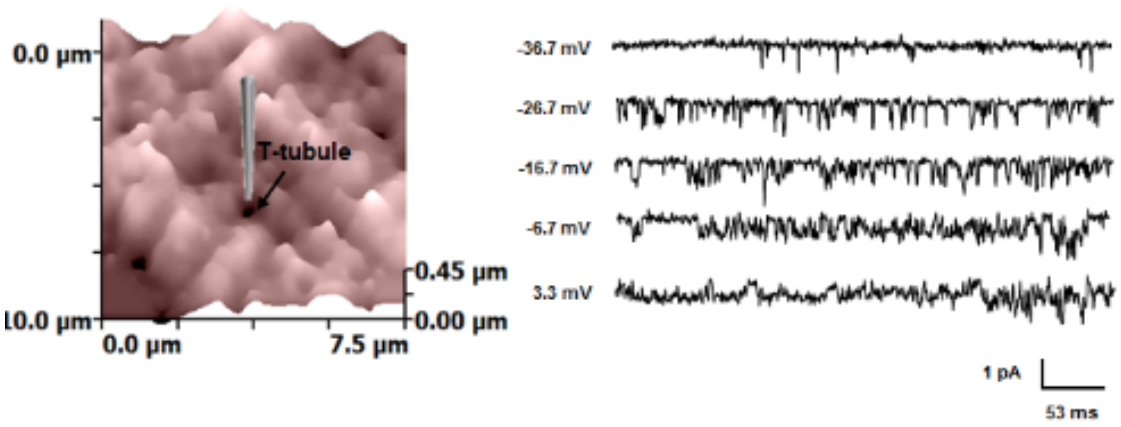

Figure 4.1. Single LTCC activity recorded from the T-tubule area in rat atrial cardiomyocytes after 2µM ISO+50nM ICI incubation.

Left panel: a typical 10µmx10µm topographic scan of cardiomyocytes showing locations where a pipette was placed after clipping and a giga-seal was obtained over a T-tubule area of the sarcolemma. **Right panel**: corresponding representative current traces of single LTCC activity at the given voltages using a pipette of 25MΩ resistance.

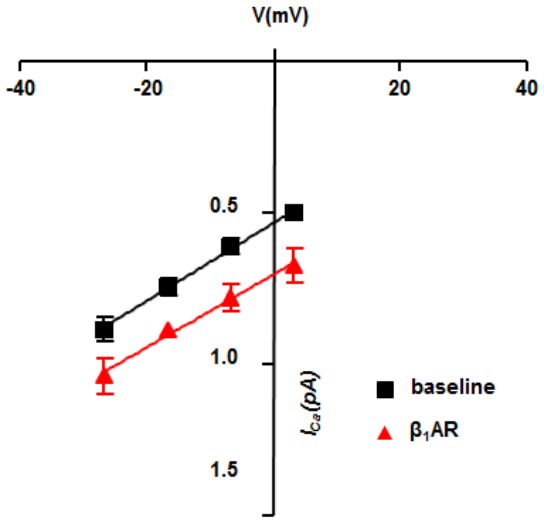

Figure 4.2. Voltage-current characteristic of single LTCCs from the T-tubule in rat atrial cardiomyocytes before and after 2µM ISO+50nM ICI incubation.

I-V of single LTCC activity recorded from the T-tubules before (**baseline**) and after (**β_1AR**) 2µM ISO+50nM ICI incubation. N=11-22 for baseline and n=8-10 for β_1AR.

This finding is not surprising as β_1-adrenergic stimulation increases availability of single LTCCs. In addition, single channel amplitude underwent changes. After β_1-adrenergic stimulation, channels possessed ~30% higher amplitude in the T-tubules and ~15% in the crest microdomains [at -6.7mV:in the T-tubules, Amp=0.78±0.05 pA and in the crest, Amp=0.51±0.04 pA, *P<0.01*] in comparison to baseline [at -6.7mV: in the T-tubules, Amp=0.6±0.03 pA and in the crest, Amp=0.46±0.03 pA] (**Figures 4.2 and 4.4**).

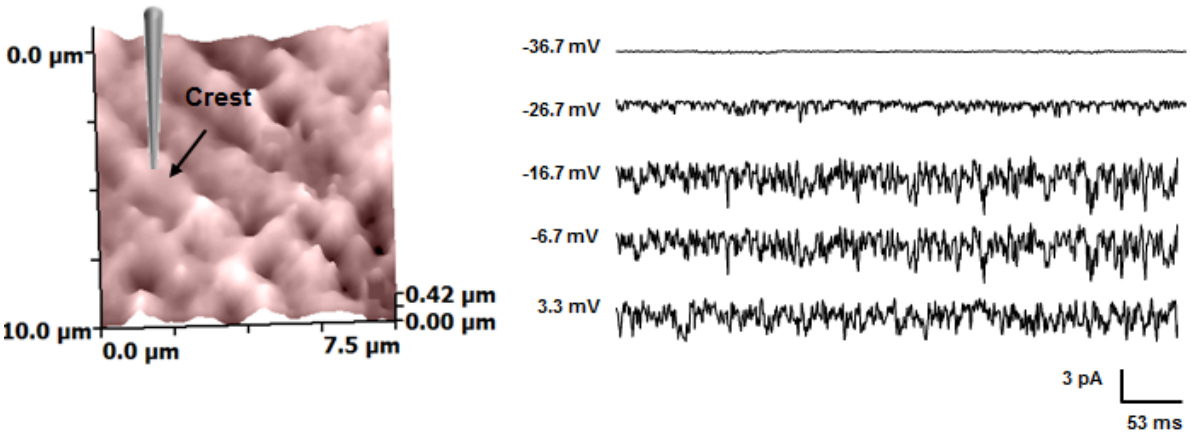

Figure 4.3. Single LTCC activity recorded from the crest area in rat atrial cardiomyocytes after 2µM ISO+50nM ICI incubation.

Left panel: a typical 10µmx10µm topographic scan of cardiomyocytes showing locations where a pipette was placed after clipping and a giga-seal was obtained over a crest area of the sarcolemma. **Right panel:** corresponding representative current traces of single LTCC activity at the given voltages using a pipette of 25MΩ resistance.

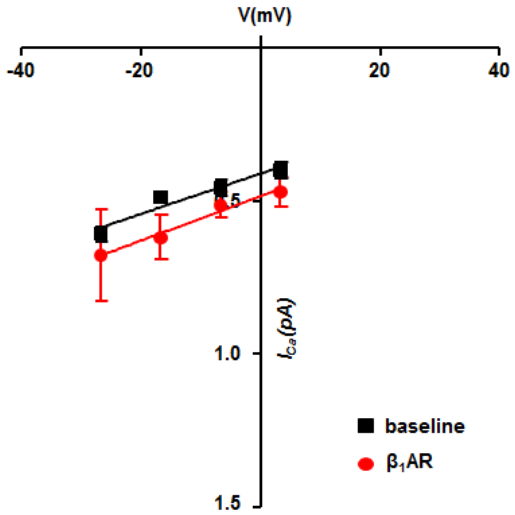

Figure 4.4. Voltage-current characteristic of single LTCCs from the crest in rat atrial cardiomyocytes before and after 2μM ISO+50nM ICI incubation.

I-V of single LTCC activity recorded from the crest before (**baseline**) and after (**β_1AR**) 2uM ISO+50nM ICI incubation. N=7-12 for baseline and n=6-12 for β_1AR.

4.3.2 Antiadrenergic effect of adenosine in regulation of single L-type calcium channels in atrial cardiomyocytes

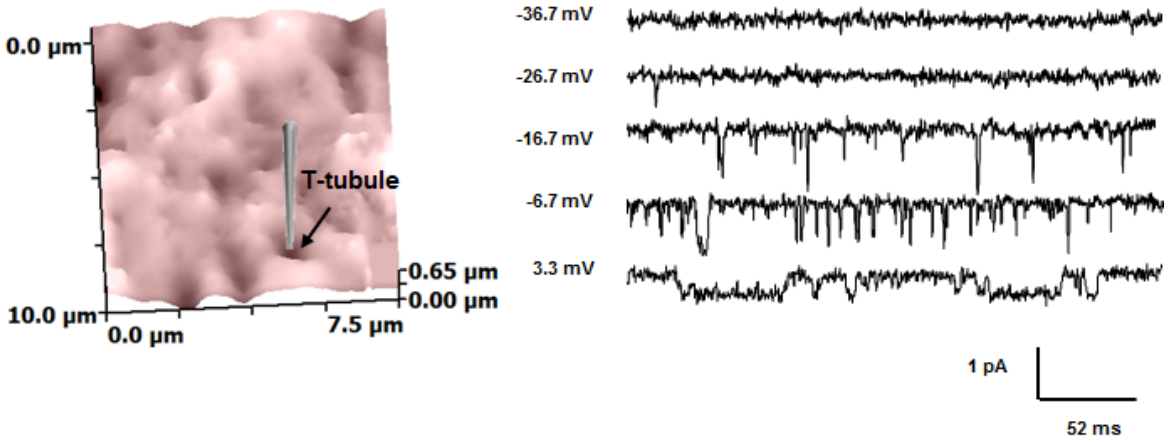

Figure 4.5. Single LTCC activity recorded from the T-tubule area in rat atrial cardiomyocytes after 2µM ISO+50nM ICI incubation with local adenosine application (Ado 20 µM) through the recording pipette.

Left panel: a typical 10µmx10µm topographic scan of cardiomyocytes showing locations where a pipette was placed after clipping and a giga-seal was obtained over a T-tubule area of the sarcolemma. **Right panel:** corresponding representative current traces of single LTCC activity at the given voltages using a pipette of 25MΩ resistance.

Interestingly, local adenosine stimulation by application of 20µM of Ado through the recording pipette completely reversed the enhancement in amplitude of LTCCs located in the T-tubule microdomains (**Figure 4.7**) [at -6.7mV: Amp=0.63±0.04 pA], but not in the crest (**Figure 4.8**).

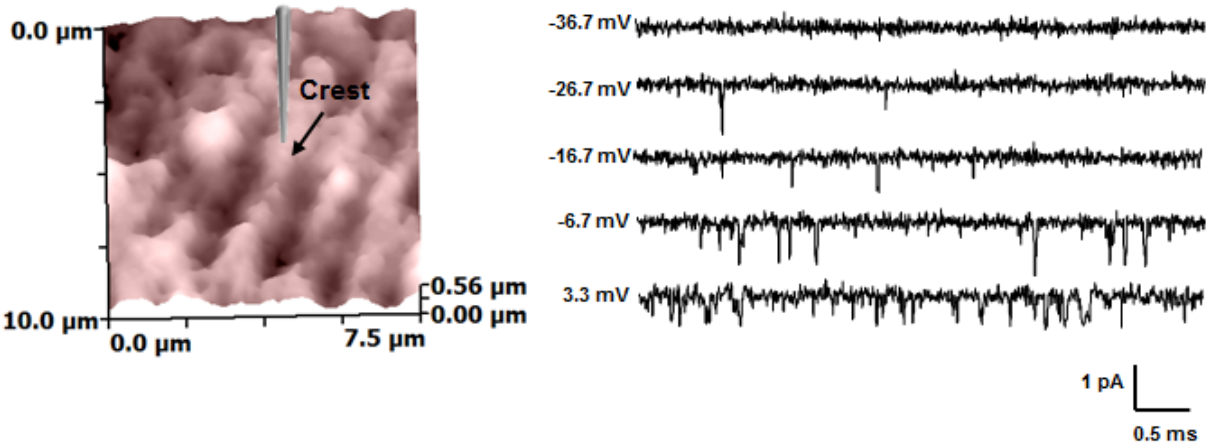

Figure 4.6. Single LTCC activity recorded from the crest area in rat atrial cardiomyocytes after 2µM ISO+50nM ICI incubation with local adenosine application (Ado 20 µM) through the recording pipette.

Left panel: a typical 10µmx10µm topographic scan of cardiomyocytes showing locations where a pipette was placed after clipping and a giga-seal was obtained over a crest area of the sarcolemma. **Right panel:** corresponding representative current traces of single LTCC activity at the given voltages using a pipette of 25MΩ resistance.

At the same time β_1-adrenergic stimulation affected on open probability of single LTCCs [p(open) at -6.7mV: 0.06±0.006, N=36 before vs 0.11 ± 0.02, N=9 after β_1-AR stimulation in the T-tubule, *P<0.01*; and 0.067±0.013, N=25 before vs. 0.18 ± 0.02 N=13 after β_1-AR stimulation in the crest, *P<0.001;* where N is a number of LTCC] with more prominent effect in the crest microdomain (**Figure 4.9**).

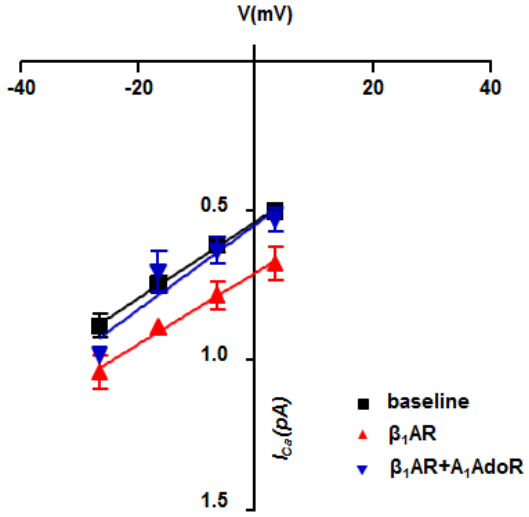

Figure 4.7. Voltage-current characteristic of single LTCCs from the T-tubule in rat atrial cardiomyocytes before and after 2μM ISO+50nM ICI incubation alone, and after 2μM ISO+50nM ICI incubation with local adenosine application (Ado 20 μM) through the recording pipette.

I-V of single LTCC activity recorded from the T-tubules before [N=11-22] (**baseline**) and after 2μM ISO+50nM ICI incubation (**β_1AR**) [N=8-10], and after 2μM ISO+50nM ICI incubation with local application of Ado 20 μM (**β_1AR+A_1AdoR)** [N=4-10].

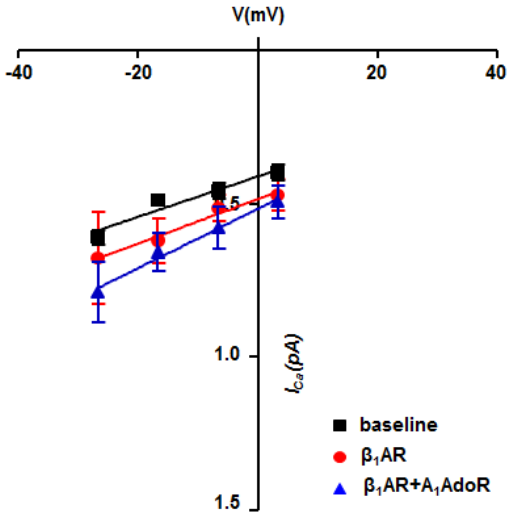

Figure 4.8. Voltage-current characteristic of single LTCCs from the crest in rat atrial cardiomyocytes before and after 2μM ISO+50nM ICI incubation alone, and after 2μM ISO+50nM ICI incubation with local adenosine application (Ado 20 μM) through the recording pipette.

I-V of single LTCC activity recorded from the crest before [N=7-12] (**baseline**) and after 2μM ISO+50nM ICI incubation (**β_1AR**) [N=6-12], and after 2μM ISO+50nM ICI incubation with local application of Ado 20 μM (**β_1AR+A_1AdoR)** [N=6-11].

Local application of Adenosine (20μM) indirectly abolished adrenergic effect of β_1AR stimulation, totally reverting open probability of single LTCCs, localized in both T-tubule and crest microdomains, back to baseline level [p(open) at -6.7mV: 0.035 ± 0.004, N=10 in the T-tubule, 0.06 ± 0.01, N=11 in the crest, *P<0.01*; N is a number of LTCCs] (**Figure 4.9**).

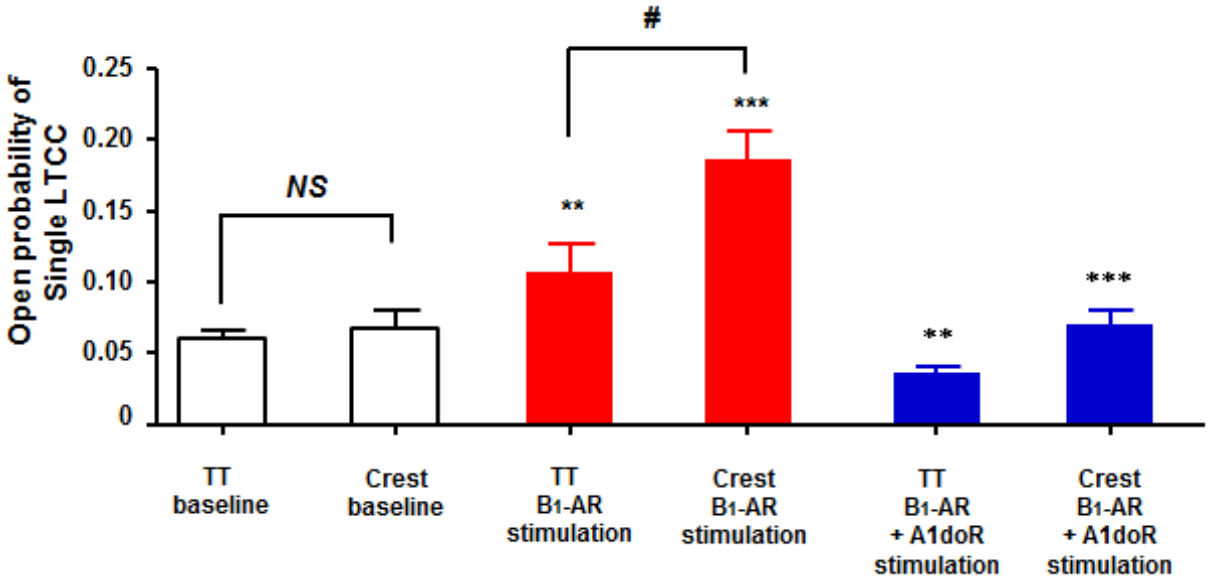

Figure 4.9. Open probability of single LTCC recorded from different areas in rat atrial cardiomyocytes before and after 2μM ISO+50nM ICI incubation and after 2μM ISO+50nM ICI incubation with local adenosine application (Ado 20 μM) through the recording pipette.

P(open) of LTCCs recorded before 2μM ISO+50nM ICI incubation (**baseline**) from T-tubules (TT) [N=43], crest [N=25] and after 2μM ISO+50nM ICI incubation (**B1-AR stimulation**) from T-tubules [N=9], crest [N=13]. P(open) of LTCCs recorded from T-tubules [N=9], crest [N=14] after 2μM ISO+50nM ICI incubation with local application of Ado 20 μM. N is number of channels. (** *P<0.01*; *** *P<0.001*; # *P<0.0001* T-tubule vs. crest).

4.4 CONCLUSION

The main new finding of the present study was the following: A_1-adenosine receptor stimulation in the presence of β_1-adrenergic activation completely abolishes β-adrenergic enhancement of single L-type Ca^{2+} current in atrial cardiomyocytes in both T-tubule and crest microdomains. This investigation may indicate possible co-localisation and, or interaction of A1-adenosine receptors with functional LTCCs.

The Adenosine-induced depression of single Ca^{2+} currents in the presence of β_1-adrenergic stimulants was associated mainly with a decrease in the open probability, previously increased by isoproterenol.

4.5 LIMITATIONS

Based on obtained results the question about co-localisation of β_1-AR with functional LTCCs in different membrane compartments remains unclear. As demonstrated here, general β_1-adrenergic stimulation affects upon the whole cell and, as it has been shown previously, β_1-adrenergic signaling stimulates calcium channels throughout the cell via a general increase in cAMP (Chen-Izu, Xiao et al. 2000; Davare, Avdonin et al. 2001; Xiao 2001). To reveal co-localization of β_1-AR with functional LTCCs local application of isoproterenol with ICI-11855 must be used.

4.6 CLINICAL PROSPECTIVES

Cardiovascular adenosine receptor-based therapies are already in place, and trials of new treatments underway. Although the complex interplay between adenosine receptors and other receptors, and their distribution and effects to calcium inward current makes it difficult to implement site or target specific cardiovascular therapy. However, as our understanding of the role of adenosine receptors under

physiological and pathological conditions deepens, the potential of adenosinergic pharmacological therapy may be fully implemented.

4.7 SUMMARY

This chapter addresses some of the major known and proposed actions of adenosine and adenosine receptors with adrenergic receptor and calcium channels in different compartments in atrial cardiomyocytes, focusing on the ability of the adenosine receptor to regulate calcium current, revenge against stressors, and mediate longer-term adaptive responses.

5 CHAPTER. HEART FAILURE AFFECTS L-TYPE CALCIUM CURRENT LOCALISED IN T-TUBULES AND DESTROYS COUPLING BETWEEN CALCIUM CHANNELS AND β-ADRENERGIC RECEPTORS OUTSIDE OF T-TUBULES

5.1 INTRODUCTION

Heart failure (HF) occurs when the heart is unable to pump sufficiently blood flow to the body. This condition can remain in an acute form or, develop into a further chronic state.

General causes of HF include coronary artery disease including a previous myocardial infarction (heart attack), arterial hypertension, atrial fibrillation, valve disease, such as aortic or mitral regurgitation, and cardiomyopathy. Depending on ethology, HF causes by changing either the structure or the functioning of the heart. There are two types of heart failure depending on the ability of the left ventricle to contract: a HF due to left ventricular (LV) dysfunction and a HF with preserved LV function. Left ventricular function is normally detected by echocardiography test including parameters such as ejection fraction (EF), left ventricular end-diastolic and end-systolic volume (LVEDV) and pressure (LVEDP).

5.1.1 Ejection Fraction, left ventricular end-diastolic volume and pressure

The ejection fraction is calculated by dividing the stroke volume by the end-diastolic volume. It is literally the fraction of the ventricular volume that is ejected with each beat. EF can be measured by a variety of methods in the human heart. These now include ultrasound, nuclear medicine methods, and x-ray angiography. Although the ejection fraction is strongly influenced by contractility, the ejection loop analysis reveals that it is also influenced by filling pressure and aortic pressure. Nevertheless, the ejection fraction is the most important index of contractility in the clinic today, primarily because of its ease of measurement. Normally, the ejection fraction should be about 0.6 for a healthy heart. EF below 0.4 suggest disease and those below 0.3 are associated with high mortality.

Left ventricular end-diastolic volume/pressure is the volume of blood or pressure in the left ventricle at end load or filling in (diastole) just before systole.

Accompanied with left ventricular mass, which is calculated by left ventricular end-diastolic diameter, diastolic posterior wall thickness and diastolic septal wall thickness, EF, LVEDV and LVEDP heart can be diagnosed as dilated or hypertrophic. The dilated heart has a normal mass of muscle and should not be confused with a hypertrophied heart in which the muscle mass has been increased (Suga and Sagawa 1974; Suga, Hisano et al. 1983).

Interestingly, that HF is a relatively common condition, in which left atrial pressure is abnormally high and may contribute to atrial fibrillation promotion and perpetuation.
High left atrial pressure is often caused by a depressed contractility. If this continues for more than a day, the heart can dilate such that the chamber diameter may double or even triple. Dilation is caused by a slippage of the points at which one fiber attaches to its neighbor, in response to sustained high wall tension. With a large chamber radius and a thin wall, the geometry may become so unfavorable that the heart can no longer generate an adequate stroke volume. This is a grave complication for the already failing heart.

The condition is often difficult to treat and the prognosis is poor for advanced cases. Cardiac transplantation has emerged as an effective treatment.

5.1.2 Cellular remodeling during HF

In cellular level, significant decrease of t-tubule density was shown in canine ventricular cardiomyocytes with pacing induced HF (He, Conklin et al. 2001). The same results but in human studies were obtained in ventricular cardiomyocytes from patients with heart disease (Lyon, MacLeod et al. 2009). As it was mentioned

in Chapter 1 loss of T-tubular structure corresponds to changes in Z-grooves in failing ventricular cardiomyocytes (**Figure 1.5**).

Reduction of the T-tubule system in ventricular cells leads to changes in Ca^{2+} transient (Lipp, Huser et al. 1996) and correspondingly to changes in dyads formation.

However, the question how this loss of dyad organization can affect the spatial location and regulation of functional LTCCs, had remained unknown until recently.

In 2012, using the super-resolution scanning patch-clamp method Bhargava et al. for the first time showed in ventricular cardiomyocytes nanoscale changes in the spatial location of functional LTCCs occur during heart failure (Bhargava at al. Nanoscale Movement of L-Type Calcium Channels in the Cardiomyocyte Membrane Can Contribute to Arrhythmia During Heart Failure Circulation 2012 126: A11953-A11953). Re-located channels demonstrated increased open probability in crest microdomains and were supposed to contribute to arrhythmia risk by introducing a source of focal ectopic activity.
Therefore, relocation of channels could be explained due to loss of sarcolemma organization, but increased activity of functional LTCCs needs to be investigated in conjunction of signaling system and cAMP pathways in different membrane compartments.

cAMP causes activation of several kinases PKA, PKC and PKG which phosphorylate and hence activate calcium channels (van der Heyden, Wijnhoven et al. 2005). All these events can happen as part of β-adrenergic signaling.

It is common knowledge that heart failure is characterized by a disruption in the cardiac β-AR system (Grandy, Denovan-Wright et al. 2004).

The β-AR responsiveness of the myocardium is reduced in patients with dilated cardiomyopathy. This disturbed β-AR function may be based on an elevated

sympathetic tone observed in patients with heart failure. In these patients the tissue concentration of norepinephrine is decreased and the plasma concentration elevated, providing evidence of sympathetic stimulation (Thomas and Marks 1978; Leimbach, Wallin et al. 1986). Such an increase in plasma catecholamines may result in downregulation of the β-AR and in the depression of the β-AR-mediated signal transduction axis (Bristow, Ginsburg et al. 1986; Brodde 1991).

Moreover, prolonged adrenergic stimulation may induce metabolic and electrophysiological disturbances in the myocardium, resulting in tachyarrhythmia and sudden death (Haft 1974). Such chronic adrenergic stimulation causes alterations of the expression and activity of the components of the β-AR-mediated signal transduction cascade. These human studies investigated impairment of targets of the β_1-AR signal cascade and reduced expression of the β_1-AR on the mRNA and protein level (Bristow, Minobe et al. 1988; Ungerer, Bohm et al. 1993) accompanied with adrenergic responsiveness of the cardiomyocytes, while the β_2-receptor levels remained unchanged in most studies. It has been also found that in heart failure the potentiation of LTCC current by beta-adrenergic regulation is lost, indicating phosphorylation defects (Zhang, Moore et al. 1995; Aimond, Alvarez et al. 1999).

5.1.3 Antiadrenergic effect of adenosine in heart failure

Antiadrenergic effect of adenosine, its production and degradation, and the modulation of adenosine receptors during heart failure is not fully studied.

Since adenosine was investigated as cardioprotective agent in HF as well as ischemic heart disease, it became important to analyze the adenosine receptor.

Evidence of changes in adrenergic control of inotropic and function were investigated in several disease models. For example, Dobson and colleagues found that A_1AR-mediated antiadrenergic responses in rats are impaired with

pressure-overload hypertrophy (Meyer, Chung et al. 2001). Abolished effect of A_1 adenosine receptor on cardiomyocyte adrenergic responsiveness was also found in hypertensive animals (Tang, Wang et al. 1998).

There is experimental evidence of alterations in adenosine levels, handling and receptor signalling in post-ischemic, hypertensive, hypertrophied and failing myocardium in animal models. Whether these changes reflect mechanistic involvement, compensatory or adaptive changes, or non-specific targets of disease, has to be studied. The adenosine receptor system may be beneficially modulated in response to hypertrophy (Pang, Gan et al. 2010), with upregulating of A_1. In a model of compensated pressure-overload hypertrophy, increased interstitial adenosine is accompanied by increased protective A_1AR expression. However, overexpression is no longer evident after transition to cardiac failure (Perlini, Arosio et al. 2007), suggesting secondary rather than primary involvement. Shifts in A_1AR expression may still be relevant to disease progression, as excess A_1AR expression can induce cardiomyopathy, cardiac dilatation, hypertrophy and dysfunction (dependent upon the timing of expression changes) (Funakoshi, Chan et al. 2006). Possibly alterations in adenosine receptor expression and function may play a role in the contractile dysfunction that occurs in failing hearts.

This chapter presents new results that clarify the function of single L-type calcium channels under stimulation of β_1-adrenoceptors and A1-adenosine receptors and their co-localization in different compartments during heart failure.

5.2 MATERIALS AND METHODS

5.2.1 Animals

Both male and female Sprague Dawley Rats (8-10 weeks old, weight ~250 g) were used in these experiments (number of animals is 28).

5.2.2 Rat Post-Infarction HF Model (Lyon, MacLeod et al. 2009)

Coronary ligation produced transmural infarcts constituting more than 30% of left ventricular circumference (**Figure 5.1A**). Sixteen weeks after infarction, animals had significantly increased heart weight/body weight ratios (g/kg) compared with sham-ligated controls (HF vs. Sham: 4.7 ± 0.2 vs. 3.8 ± 0.1, $P < 0.01$, $n = 6$ in each group), reflecting hypertrophy of the viable left ventricular myocardium. Serum brain natriuretic peptide (BNP) levels were undetectable in sham controls and elevated in HF rats [205 ± 43 pg/mL vs. undetectable (<80 pg/mL), $P < 0.01$]. Pressure–volume (PV) analysis (Fig. 2 *B*–*D*) demonstrated ventricular dilatation [left ventricular end-diastolic volume (LVEDV): 258 ± 27 μL vs. 173 ± 8 μL, $P < 0.01$], with reduced ejection fraction and elevated end-diastolic pressure: [left ventricular ejection fraction (LVEF): 32% ± 4% vs. 76% ± 2%, $P < 0.001$; left ventricular end-diastolic pressure (LVEDP): 24.0 ± 3.3 mm Hg vs. 8.5 ± 0.5 mm Hg, $P < 0.001$]. Dynamic measures of contractile function [end-diastolic PV relationship (EDPVR); 0.60 ± 0.12 mm Hg/mL vs. 1.89 ± 0.24 mm Hg/mL, $P < 0.01$; time-varying maximal elastance (Emax): 1.4 ± 0.2 mm Hg/mL vs. 3.1 ± 0.5 mm Hg/mL, $P < 0.05$; preload recruitable stroke work (PRSW): 61 ± 21 mm Hg vs. 110 ± 11 mm Hg, $P < 0.05$] and ventricular compliance [end-diastolic PV relationship (EDPVR): 0.11 ± 0.01 mm Hg/mL vs. 0.03 ± 0.01 mm Hg/mL, $P < 0.01$] were also significantly impaired in these animals, consistent with the HF phenotype.

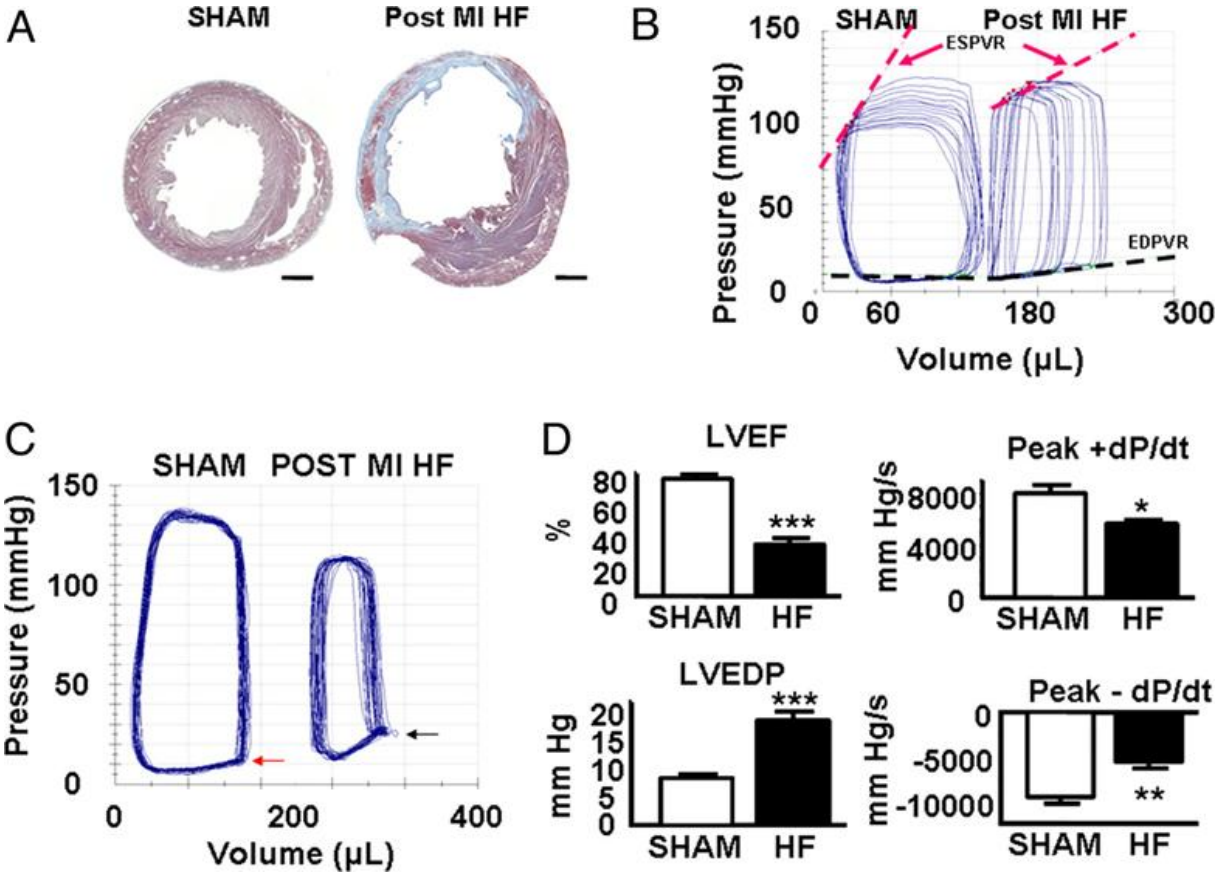

Figure 5.1. The rat chronic post–myocardial infarction (MI) HF model.

(A) Midventricular 10-µm section from a sham control rat heart (Left) and a chronically infarcted rat heart (Right) after staining with Masson's trichrome. (Scale bar, 2 mm.) (B) Representative in vivo PV loops during transient inferior vena caval occlusion from an HF rat and a Sham control. ESPVR (red broken lines) and EDPVR (black broken lines) relationships are presented. (C) Representative in vivo steady-state PV loops demonstrating increased ventricular volumes and elevated end-diastolic pressure in HF rats (black arrow) compared with Sham controls (red arrow). (D) Steady-state PV data demonstrating decreased LVEF, increased LVEDP, and reduced peak velocities of pressure change (dPdt) during isovolumic contraction (Peak + dPdt) and isovolumic relaxation (Peak − dPdt) in rats with HF. *, $P < 0.05$; **, $P < 0.01$; ***, $P < 0.001$ (Lyon, MacLeod et al. 2009)

5.2.3 Atrial cardiomyocytes isolation

Cells were isolated from rats as described in Chapter 2 (General materials and methods). Both left and right atrial appendages were placed all together in isolation tube with enzymes (number of cells is 310).

5.2.4 Super-resolution scanning patch-clamp with pipette clipping modification

All calcium channels were recorded in cell-attached mode using super-resolution scanning patch-clamp technique as described in Chapter 2. In experiment with β_1-adrenergic stimulation specific β-ARs agonist isoproterenol with β_2-AR antagonist ICI-11855 were added in basic external recording solution. Adenosine as an agonist to A1-adenosine receptor were added in pipette recording solution to get local stimulation of A1-adenosine receptor.

5.2.5 Protocol of the whole cell β_1-adrenergic receptor agonist application

Whole-cell β_1-adrenergic stimulation was reached by applied synthetic nonselective βAR agonist isoproterenol (2μM) and β_2AR antagonist ICI 11855 (50 nM) in bath solution. 10-15 minutes were required to achieve full effect of adrenergic receptors stimulation (**Figure 5.2**). As β_1-adrenergic stimulation enhances EC coupling within the heart chronic stimulation and acute overstimulation can provide toxic effect on myocardium and cause damage to cardiac cells. Thus, single L-type calcium channels recording was performed not longer than 90-120 minutes.

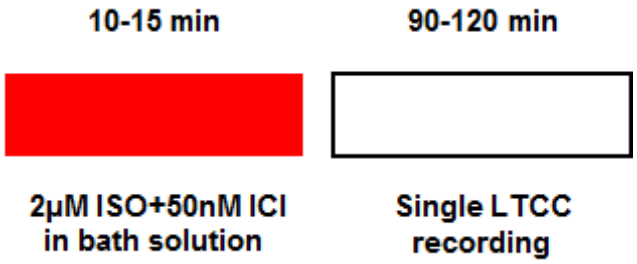

Figure 5.2. Protocol of whole-cell β_1-adrenergic stimulation of rat atrial cardiomyocytes during heart failure.

5.2.6 Protocol of the local A1-adenosine receptor agonist application

As it was mentioned before, activation of A1-adenosine receptor modulates catecholamine-enhanced L-type Ca^{2+} current indirectly. Thus, to reveal compartmentalization of A1-adenosine receptors and co-localization of those with LTCCs whole cell β_1-adrenergic stimulation and local application of adenosine (20μM) through the recording pipette were used. All channels affected with adenosine were recorded in cell-attached mode only 5-7 minutes after giga-seal was obtained.

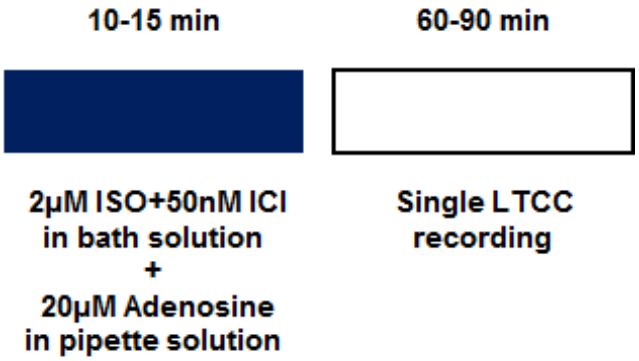

Figure 5.3. Protocol of whole-cell β_1-adrenergic stimulation with local A1- adenosine receptor stimulation of rat atrial cardiomyocytes during heart failure.

5.2.7 Statistical analysis

Quantitative data are shown as mean ± SEM for the given number of experiments. Statistical analysis was carried out using an unpaired student t-test. A value of $P<0.05$ was considered statistically significant.

The analysis was performed using Prism4 software (GraphPad software Inc., San Diego, CA, USA).

5.3 RESULTS

5.3.1 Surface structures in atrial cardiomyocytes in heart failure

SICM imaging of rat control atrial cardiomyocytes clearly showed the heterogeneity of surface topography with evident location of the T-tubule openings, the domed crest between the Z-grooves and non-structural areas (see Chapter 3). It was also demonstrated that surface structure of control atrial cells is correlated with cellular width. In this chapter, the same analysis was applied to characterize topography of atrial cardiomyocytes during heart failure. Moreover, it was found, thicker atrial cells underwent degradation of surface structure in comparison to thiner cardiomyocytes, which showed no changes in Z-groove index (**Figure 5.4C**).

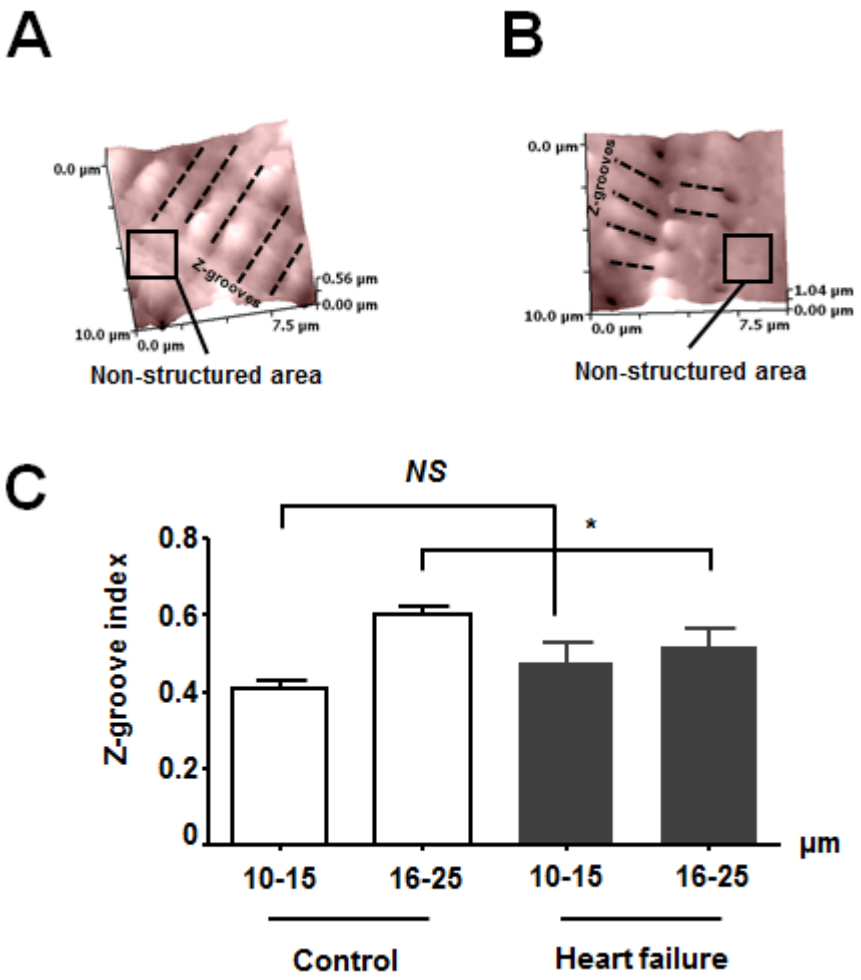

Figure 5.4. Surface structure in rat atrial control cardiomyocytes and during heart failure. Surface topography structure of rat control (A) and atrial cardiomyocyte during heart failure (B), Arrows indicate non-structured areas. (C) Average Z-groove index measured for thin (<15µm) and thick (>16µm) atrial cells in control (n=29 of thin cells and n=53 of thick cells) and heart failure (n=21 of thin cells and n=45 of thick cells) (* P<0.1).

5.3.2 Subcellular T-tubule system in atrial cardiomyocytes in heart failure

Half of the studied atrial cardiomyocytes demonstrate T-tubule structure having been isolated following heart failure. As in control, maturity of the T-tubular network was revealed to be dependent on cell size in heart failure: cells showing

developed T-tubular network had a larger mean diameter (25.1±7.1µm) than cells without a T-tubular network (14.6±4.1µm). HF remodeling caused a significant decrease in T-tubule density from 32±8% in control to 22±5% in failing atrial cells.

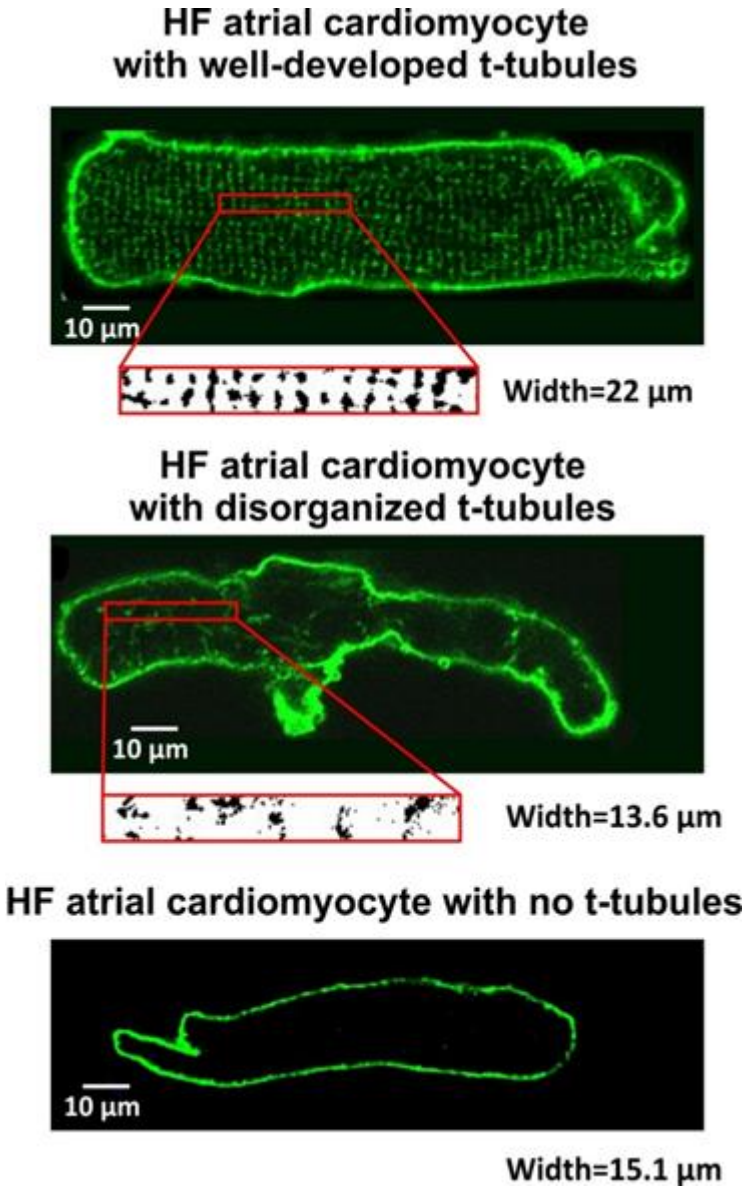

Figure 5.5. Spatial heterogeneity of the atrial T-tubular system in heart failure.
Di-8-ANEPPS membrane staining showing a T-tubule network in atrial cardiomyocytes with well-developed, disorganized, and absent T-tubular systems. Below the confocal images, enlarged areas of 40µmx5µm are shown that were binarized and used in T-tubule density and regularity measurements.

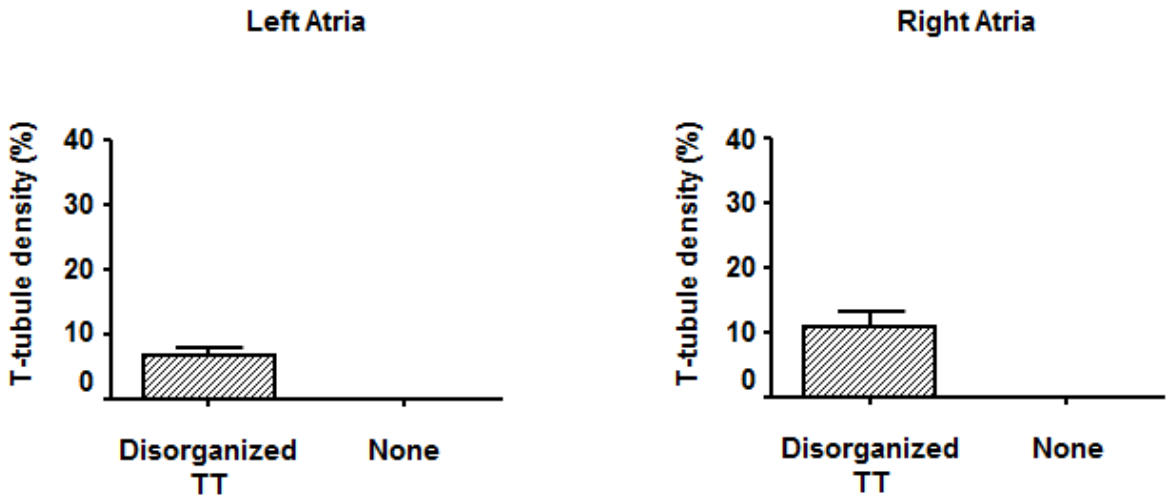

Figure 5.6. Degradation of atrial T-tubular system in heart failure: T-tubular system density in left and right atria.

T-tubular system density measured in left and right atrial cardiomyocytes with disorganized and absent T-tubule systems.

5.3.3 Spatial localization of functional LTCCs in atrial cells during heart failure

Nanoscale changes were found in spatial location of functional LTCCs which occur during heart failure in ventricular cardiomyocytes (Bhargava at al. Nanoscale Movement of L-Type Calcium Channels in the Cardiomyocyte Membrane Can Contribute to Arrhythmia During Heart Failure Circulation 2012 126: A11953-A11953). To answer the question how LTCCs behave in different subcellular compartments in failing atrial cells super-resolution scanning patch-clamp technique was applied.

As in control, LTCC current in atrial cardiomyocytes was recorded with similar frequency from T-tubules and crests (34.3% of 36 successful patches in T-tubules, 30.5% of 36 successful patches in the crest) in heart failure (**Figure 5.9**) vs.

control (28% of 78 successful patches in T-tubules, 30.1% of 63 successful patches in the crest) (**Figure 3.13**).

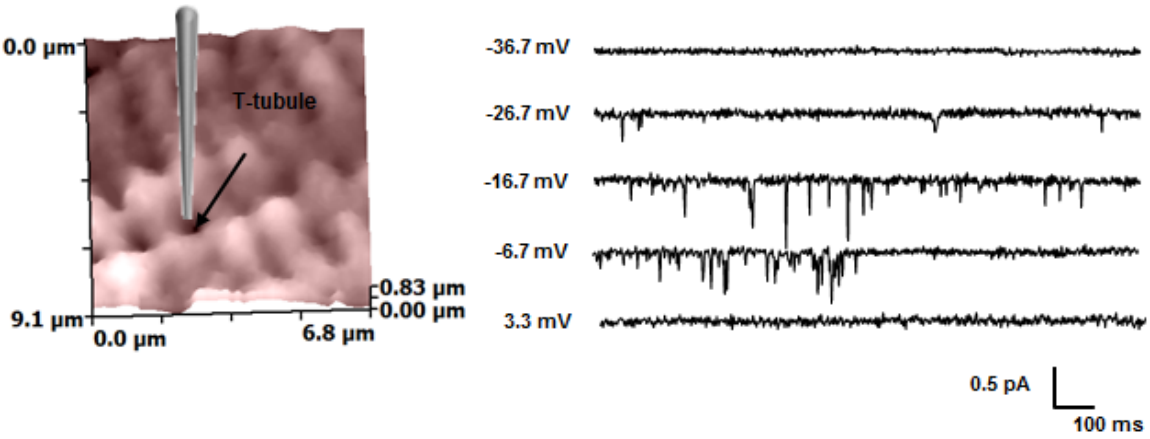

Figure 5.7. Single LTCC activity recorded from the T-tubule area in rat atrial cardiomyocytes during heart failure.

Left panel: a typical 10µmx10µm topographic scan of cardiomyocytes showing locations where a pipette was placed after clipping and a giga-seal was obtained over a T-tubule area of the sarcolemma. **Right panel:** corresponding representative current traces of single LTCC activity at the given voltages using a pipette of 25MΩ resistance.

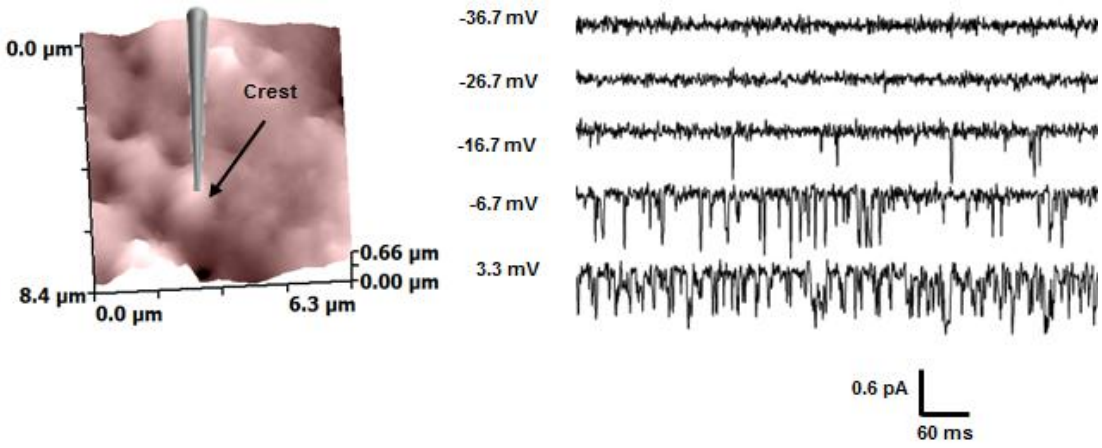

Figure 5.8. Single LTCC activity recorded from the crest area in rat atrial cardiomyocytes during heart failure.

Left panel: a typical 10µmx10µm topographic scan of cardiomyocytes showing locations where a pipette was placed after clipping and a giga-seal was obtained over a crest area of the sarcolemma. **Right panel:** corresponding representative current traces of single LTCC activity at the given voltages using a pipette of 25MΩ resistance.

There was no significant difference in open probability between the channels recorded in control and failing atrial cardiomyocytes [p(open) at -6.7mV: in control, 0.06±0.006, N=36 in the T-tubule, 0.067±0.013 N=25 in the crest; and vs. in heart failure, 0.08± 0.01, N=21 in the T-tubule, in the crest 0.06± 0.005, N=12; NS] (**Figure 5.10**).

At the same time, failing LTCCs located in T-tubules showed ~25% decrease amplitude as compared to the control calcium channels (**Figure 5.11**). No difference in amplitude of LTTCs located in the crest was observed in rat atrial cardiomyocytes between the control and the heart failure groups (**Figure 5.11**).

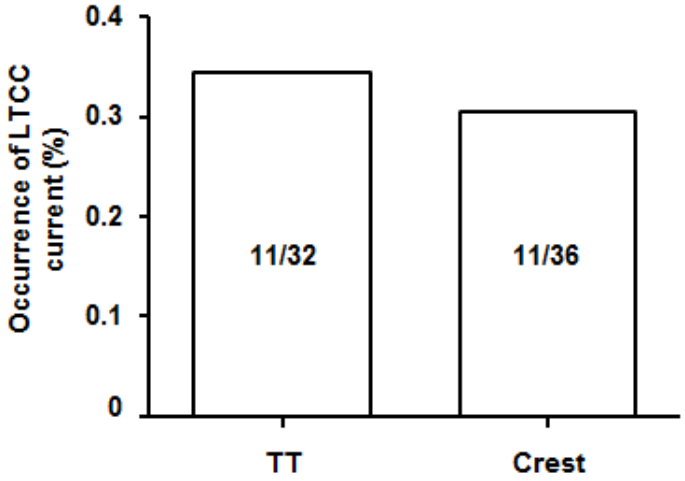

Figure 5.9. Occurrence of L-type calcium current recorded from different areas in rat atrial cardiomyocytes during heart failure.

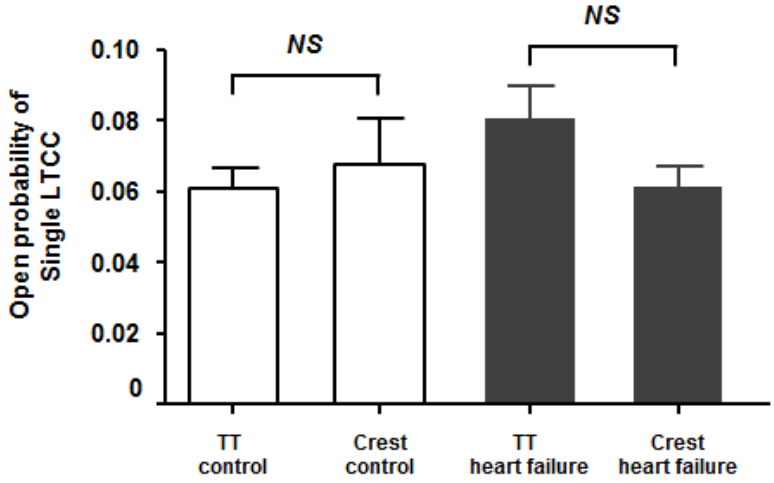

Figure 5.10. Open probability of single LTCC recorded from different areas in control rat atrial cardiomyocytes and during heart failure.

P(open) of LTCCs recorded from control T-tubules (TT) (N=43), crest (N=25) and during heart failure TT (N=21), crest (N=12), where N is number of channels.

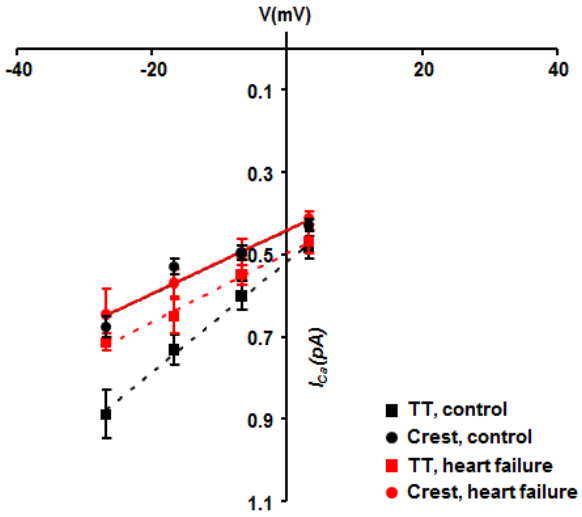

Figure 5.11. Voltage-current characteristic of single LTCCs in rat atrial cardiomyocytes in control and during heart failure.

I-V of single LTCC activity recorded from the T-tubules (TT) and crest in control (black color) and during heart failure (red color). N=6-16 for control T-tubules, n=8-12 for control crests, and n=5-6 for T-tubule in heart failure and n=4-9 for crest in heart failure.

To explain that difference in amplitude of LTCCs located in T-tubule microdomain analysis of sub-conductance levels was used (see results part in Chapter 3).

LTCCs recorded in atrial cardiomyocytes in heart failure demonstrated clear openings to three-four distinct conductance levels at -26.7mV. The LTCCs substates appear to be true openings to smaller conductance states and did not arise from filtering artefacts. Openings to the substates were well resolved, greatly exceeding the filter rise time (average open time of the small substate = 3.01±0.20ms (n=109), shorted open time = 1.1ms; filter rise time = 100μs), so they were not produced by unresolved transitions of relatively slow interconversions between open and closed conformations.

Indeed, the amplitude of all conduction states was voltage-dependent. As summarized in **Figure 5.12**, channels located in the T-tubules had a more accessible occupancy of low-amplitude sub-conductance states in heart failure than in control.

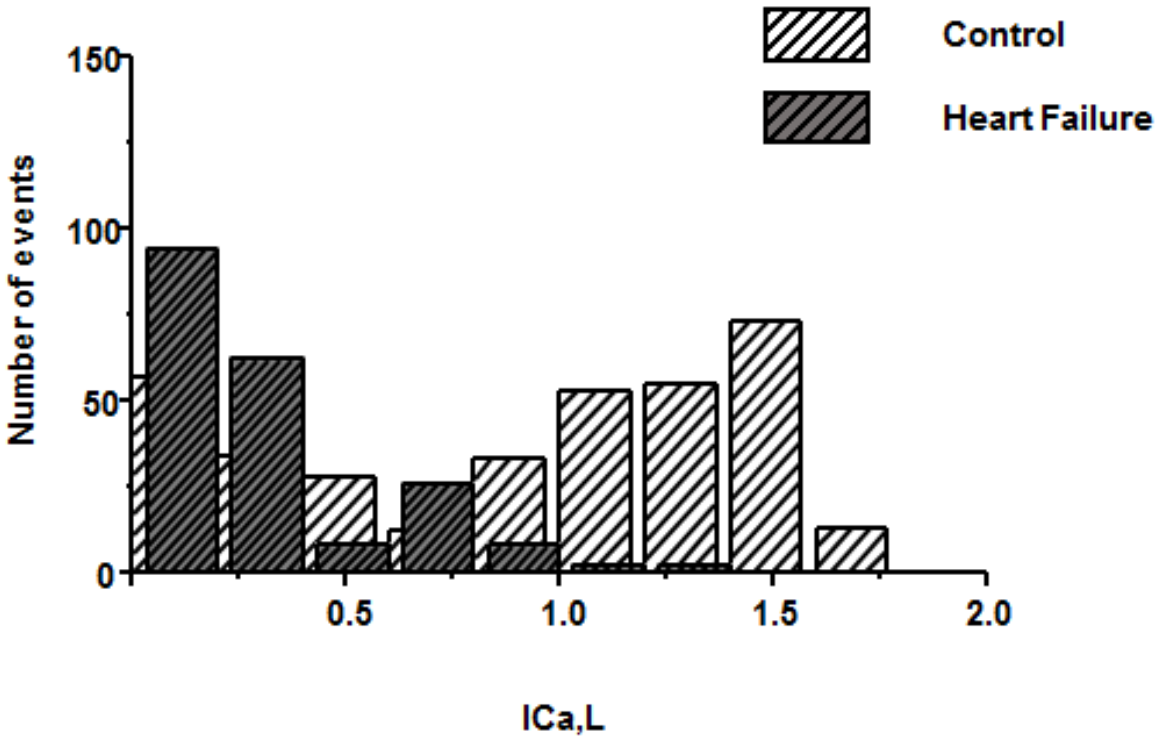

Figure 5.12. The LTCC amplitude histogram of single channel openings to different substate levels of channels recorded from the T-tubule opening in control rat atrial cardiomyocytes and during heart failure, at -26.7 mV measured as shown on the panel above.

5.3.4 Antiadrenergic effect of adenosine in regulation of single L-type calcium channels recorded from different compartments in atrial cardiomyocytes during heart failure

In order to address this question directly, the super-resolution scanning patch-clamp method (Bhargava, Lin et al. 2013) was applied to record single LTCC activity in atrial cardiomyocytes before and after β_1-adrenergic stimulation alone and with local adenosine simulation applied through the recording pipette.

In failing atrial cardiomyocytes, single LTCC current was recorded with similar frequency from T-tubules and crests. But in comparison to control, the occurrence of single LTCCs was not significantly increased (38.2% of 34 successful patches in T-tubules and 40% of 34 successful patches in the crest with β_1-adrenergic stimulation vs. 34.3% of 36 successful patches in T-tubules and 30.5% of 36 successful patches in the crest without β_1-adrenergic stimulation) in presence of 2μM ISO+50nM ICI in bath solution.
Abolished adrenergic signaling and regulation of LTCCs during heart failure might explain this finding.

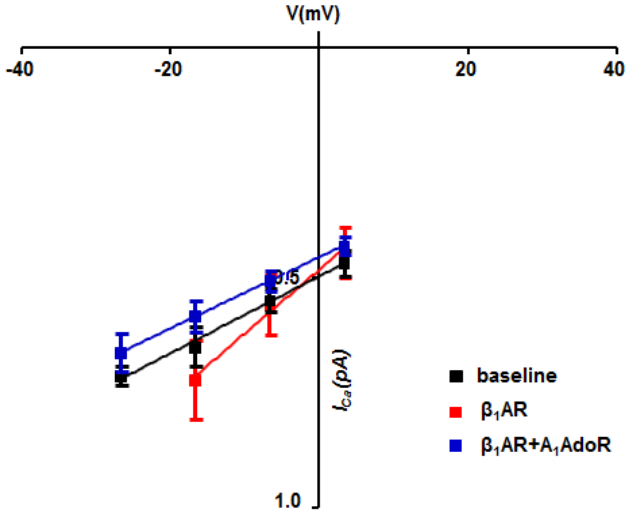

Figure 5.13. Voltage-current characteristic of single LTCCs from the T-tubule in rat atrial cardiomyocytes during heart failure before and after 2μM ISO+50nM ICI incubation alone, and after 2μM ISO+50nM ICI incubation with local adenosine application (Ado 20 μM) through the recording pipette.

I-V of single LTCC activity recorded from the T-tubules before [N=5-6] (**baseline**) and after 2μM ISO+50nM ICI incubation (**β_1AR**) [N=4-6], and after 2μM ISO+50nM ICI incubation with local application of Ado 20 μM (**β_1AR+A_1AdoR)** [N=3-8].

Moreover, in failing atrial cells, amplitude of single LTCCs recorded in the T-tubule and crest microdomains did not undergo significant changes as it was observed in control. Thus, it was complicated to estimate local antiadrenergic effect of adenosine on single LTCC voltage-current characteristics, as baseline, adrenergic and adenosine stimulated channels demonstrated almost the same no effect in both T-tubule and crest domains (**Figures 5.13 and 5.14**).

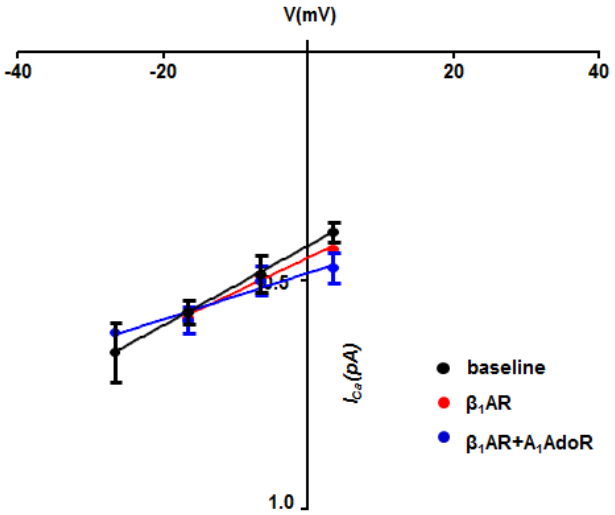

Figure 5.14. Voltage-current characteristic of single LTCCs from the crest in rat atrial cardiomyocytes during heart failure before and after 2μM ISO+50nM ICI incubation alone, and after 2μM ISO+50nM ICI incubation with local adenosine application (Ado 20 μM) through the recording pipette.

I-V of single LTCC activity recorded from the T-tubules before [N=4-9] (**baseline**) and after 2μM ISO+50nM ICI incubation (**β_1AR**) [N=4-6], and after 2μM ISO+50nM ICI incubation with local application of Ado 20 μM (**β_1AR+A_1AdoR)** [N=3-6].

Interestingly, β_1-adrenergic stimulation slightly affected on open probability of single LTCCs in failing cells but only in the T-tubule microdomain [p(open) at -6.7mV: 0.08±0.01, N=21 before vs 0.11 ± 0.01, N=10 after β_1-AR stimulation, *P<0.1,* where N is a number of LTCC]; and not in the crest microdomain [p(open) at -6.7mV: 0.06±0.005, N=12 before vs. 0.06 ± 0.0002 N=11 after β_1-AR stimulation, *NS*, where N is a number of LTCC] (**Figure 5.15**).

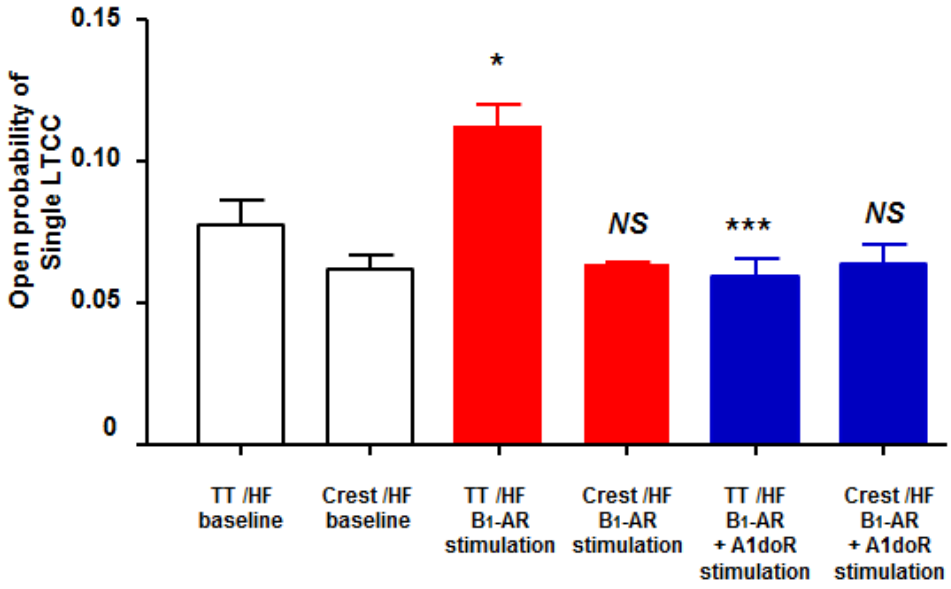

Figure 5.15. Open probability of single LTCC recorded from different areas in rat failing atrial cardiomyocytes before and after 2μM ISO+50nM ICI incubation and after 2μM ISO+50nM ICI incubation with local adenosine application (Ado 20 μM) through the recording pipette.

P(open) of LTCCs recorded before 2μM ISO+50nM ICI incubation (**baseline**) from T-tubules (TT) [N=21], crest [N=12] and after 2μM ISO+50nM ICI incubation (**B1-AR stimulation**) from T-tubules [N=10], crest [N=11]. P(open) of LTCCs recorded from T-tubules [N=17], crest [N=19] after 2μM ISO+50nM ICI incubation with local application of Ado 20 μM. HF – heart failure; N is number of channels. (* *P<0.1*; *** *P<0.001*).

Local application of Adenosine (20μM) abolished adrenergic effect of β_1AR stimulation, totally reverting open probability of single LTCCs, localized in both T-tubule back to baseline level [p(open) at -6.7mV: 0.06 ± 0.006, N=17 in the T-tubule, *P<0.0001*, where N is a number of LTCC] (**Figure 5.15**). The same effect in crest microdomain could not be estimated as adrenergic stimulation was not previously observed on single LTCCs recorded outside of T-tubules.

5.4 CONCLUSION

As in ventricular cardiomyocytes, heart failure causes profound remodeling of the atrial T-tubular system, what can potentially lead to exaggeration of Ca2+-handling abnormalities and arrhythmogenic triggered activity.

L-type calcium channels located in T-tubule compartment showed decrease in single channel amplitude which was associated with increased occupancy of lower amplitude subconductance levels; and can be linked with changes in subunit components of the channel molecule.
In contrast to ventricular cells, atrial cardiomyocytes did not show re-distribution of LTCCs, which is not surprising, as normally this type of cells (atrial) demonstrate quite a homogeneous subcellular localisation of calcium channels.
Absence of β_1-adrenergic stimulation was found in the crest domains. This finding can be related to previously reported low expression of β_1-adrenergic receptors in failing hearts, which is accompanied with low adrenergic responsiveness of the cardiomyocytes (Bristow, Minobe et al. 1988; Ungerer, Bohm et al. 1993).

Antiadrenergic effect of adenosine is not as apparent in heart failure as in control. That is quite complicated to conclude adenosine effect is lost in crest domain while adrenergic stimulation of LTCCs was not observed here. LTCCs located in the crest domains represented nonchanged activity during adrenergic stimulation. Hence, antoadrenergic effect of adenosine was not investigated in the crest region in failing cardiomyocytes.

In T-tubule compartment, LTCCs demonstrated the only slight increase in open probability, which was totally abolished by adenosine application back to base line. Thus, coupling between A_1 and β_1-adrenergic receptors are preserved in the T-tubules even while β_1-adrenergic stimulation is not so marked.

Research also unveils an increasingly complex interplay between members of the adenosine receptor family, and with other receptor groups. Given generally favorable effects of adenosine receptor activity (*e.g.* improving the balance between myocardial energy utilization and supply, limiting injury and adverse remodeling, suppressing inflammation), the adenosine receptor system is an attractive target for therapeutic manipulation.

Cardiovascular adenosine receptor-based therapies are already in place, and trials of new treatments underway. Although the complex interplay between adenosine receptors and other receptors, and their wide distribution and functions, pose challenges to implementation of site/target specific cardiovascular therapy, the potential of adenosinergic pharmacotherapy can be more fully realized with greater understanding of the roles of adenosine receptors under physiological and pathological conditions.

For example, isolated atrial tissues obtained from patients with chronic atrial fibrillation (cAF) shows reduced contractility attributed to a marked decrease in L-type Ca^{2+} current. (Schotten, Ausma et al. 2001). The inotropic responses to isoproterenol are also decreased in cAF along with preserved density of βARs and G proteins (Schotten, Ausma et al. 2001). However, mechanism the function of βARs is perturbed is unknown. That is well known that activation of human atrial βARs produces arrhythmias (Kaumann and Sanders 1993) in atrial preparations obtained from patients with sinus rhythm. Thus, catecholamines have been proposed to initiate AF (Kaumann and Sanders 1993).

The relevance of these in vitro arrhythmias is corroborated by the clinical finding that high sympathetic nervous system activity during and after cardiac surgery causes premature beats and transient postoperative AF in approximately one-third of patients (Kalman, Munawar et al. 1995). The maximum response of $I_{Ca,L}$ to the catecholamines was similarly reduced by one-third in the patients with AF. Similar inotropic response to catecholamines in patients with sinus rhythm along with preserved density of βARs gives a suggestion uncoupling between the L-type Ca^{2+} current and βARs happens. That uncoupling could exist due to loss of structural

components of signaling compartment during pathology, what is examined next chapter.

6 Increased open probability of L-type calcium channels localized in t-tubules in patients with chronic atrial fibrillation: role of channel subunits?

6.1 INTRODUCTION

Atrial fibrillation (AF) is the most common and hard arrhythmia in clinical practice which is associated with increased morbidity and mortality due to increased risk for congestive heart failure and cerebral infarction (stroke) (Khairy and Nattel 2002; van den Berg, van Gelder et al. 2002).
Although AF can clearly occur in patients without evident heart disease (so-called lone AF), organic heart diseases, such as congestive heart failure (CHF), mitral valve disease, and coronary artery disease, are major co-existing conditions that contribute to the occurrence and persistence of AF.

AF is characterized by an irregular, often rapid heart rate. Atria contract with reduced force, thereby favoring thrombus formation. AF occurs in several cardiac diseases, and its incidence is higher in woman than in men, particularly in those with valvular heart disease. Chronic AF (cAF) causes structural and electrical remodeling, as well as enlarged atria, maintaining AF.

AF may be classified based on aetiology, depending on whether it occurs without identifiable aetiology in patients with a structurally normal heart (lone AF what assemble 15% of all cases), or whether it complicates hypertensive, valvar, or other structural heart disease. Recently a classification system based on the temporal pattern of the arrhythmia has been recommended (Fuster, Ryden et al. 2001).

Clinically patients have detected episodes of AF or, if previous episodes have been documented, recurrent arrhythmia. Episodes themselves may be paroxysmal, if they terminate spontaneously, usually within seven days, or persistent if the arrhythmia continues requiring electrical or pharmacological cardioversion to be terminated. AF that cannot be successfully terminated by

cardioversion, and longstanding (> 0.5 year) AF, where cardioversion is not indicated or has not been attempted, is termed permanent or chronic atrial fibrillation (cAF).

Despite the fact that the pathophysiology of AF has been investigated extensively for almost a century, the underlying mechanisms remain incompletely understood (Nattel 2002).

First classical mechanisms of AF were described in the early 20th century (Nattel 2002). However, despite even numerous studies performed over the past 20 years, which afforded more detailed insights into the pathogenesis of clinically relevant AF, mechanism of AF remains still not fully understood.

The pathogenesis of AF is now thought to involve an interaction between initiating triggers, often in ectopic foci located inside one or more pulmonary veins, and abnormal atrial tissue substrate capable of maintaining the arrhythmia. Foci of rapid ectopic activity, which might extend from the left atrium into the proximal parts of pulmonary veins, play a basic role in the initiation of AF in humans (Haissaguerre, Jais et al. 1998). Less frequently, focal initiation of AF may be result from ectopic activity that arises from muscular sleeves in the proximal superior vena cava, or from parts of the right.

Foci into pulmonary veins may play a dominant role in younger patients with relatively normal hearts and short paroxysms of AF, whereas an abnormal atrial tissue substrate may play a more important role in patients with structural heart disease and persistent or permanent AF.

In this chapter, chronic atrial fibrillation is correlated with structural and electrophysiological changes observed in patient groups. Moreover, structural changed are considered as a substrate for possible electrical remodeling.

Both experimental and human mapping studies have previously demonstrated that AF is generally characterised by the presence of ectopic activity producing multiple waves of excitation that propagate around the atrial tissue (Allessie, Bonke et al. 1977; Schilling, Kadish et al. 2000). Multiplicity of electrical wave in atrial tissue is facilitated by conduction slowing and shortening of the refractory period and might be produced by structural changes such as size of chambers, thickness of wall, fibrosis etc.

At macroscopic level, structural remodeling during AF is generally associated with enlargement of the atria. It was shown that atrial enlargement might increase refractoriness to electrical conversion of AF (Eckstein, Verheule et al. 2008).
Atrial dilatation is also believed to lead to the thinning and fibrosis of tissue. Fibrosis results in disordered electrical activation, conductivity (decreasing conduction) and contractility. It does not, however, explain the occurrence of fibrillation in patients with structurally normal hearts, which have been shown to constitute between 3% and 11% of the atrial fibrillation population in large epidemiological studies (Sanfilippo, Abascal et al. 1990).
Interestingly, the role of individual atrium in AF pathogenesis and relationship between two atria explore considerable variability. There are several controversial data suggesting equal involvement of both atria in pathological process triggered primarily by AF or, opposite, enlargement of left atrium alone leading to AF progressive (Sanfilippo, Abascal et al. 1990).
Confirming a primary role for arrhythmia in the genesis of chamber enlargement study showed atrial size decreases after successful electrical conversion but not if atrial fibrillation recurs after conversion (Sanfilippo, Abascal et al. 1990).
Strong evidence suggests that the presence of left atrial (LA) enlargement indicates a clinically significant risk of adverse cardiovascular outcomes for the patient. Several large population-based prospective studies have shown a strong association between anteroposterior LA diameter and the risk of new episode of AF (Vaziri, Larson et al. 1994; Psaty, Manolio et al. 1997). In the Framingham Heart Study, every 5-mm increase in LA diameter increased the development of AF by 39% (Vaziri, Larson et al. 1994), while the Cardiovascular Health Study

showed a four-fold increase in the risk of new AF with LA diameter 0.5 mm (Psaty, Manolio et al. 1997).

Thus, LA size has been established as a prognostic marker for adverse atrial fibrillation (Psaty, Manolio et al. 1997; Tsang, Barnes et al. 2001; Abhayaratna, Fatema et al. 2008; Fatema, Barnes et al. 2009). However, patients who develop atrial fibrillation in the absence of any identifiable structural cardiac abnormalities and also carry an adverse prognosis can be met in clinical practice. Most of them are not surgical patients and are suffered with lone AF.

Recent study showed the equal role of right atrium in AF. Surprisingly, in contrast to previously shown predominant role of LA, RA dilatation had the greatest influence on the development of cAF over LA dilatation in patients with isolated right-sided pathologies (Bouchardy, Marelli et al. 2013). Thus, it is possible to suggest dominant effect of atrial dilatation accordingly sided pathology.

It is interesting to speculate on the mechanism of atrial enlargement consequently or initiators of atrial fibrillation, especially in case of patients undergoing cardiosurgical procedures due to valvular of coronary diseases, what is observed in the following.

Electrophysiological remodeling which can occurs due to structural remodeling involves shortening of action potential duration (APD). APD decrease is believed to be associated with Ca^{2+} current density what was observed in cAF vs sinus rhythm (Bosch, Zeng et al. 1999; Van Wagoner, Pond et al. 1999; Christ, Boknik et al. 2004; Grandi, Pandit et al. 2011) with corresponding reductions in mRNA and protein levels of the pore-forming α_{1c} subunit (Yue, Feng et al. 1997; Bosch, Zeng et al. 1999; Van Gelder, Brundel et al. 1999; Brundel, Van Gelder et al. 2001; Klein, Schroder et al. 2003). However the hypothesis of transcriptional downregulation of $I_{Ca,L}$ was challenged in humans by recent studies that detected no changes in mRNA and protein levels of α_{1c} and the regulatory β_{2a} subunits (Grammer, Zeng et al. 2001; Schotten, Haase et al. 2003).

Although reduced amplitude of $I_{Ca,L}$ is a consistent finding in AF, the molecular mechanisms are not fully understood.

In addition, anomalous increased activity of single LTCCs observed in human atrial cardiomyocytes during cAF (Klein, Schroder et al. 2003) remains not fully understood whether appearing because of enhanced activity of protein kinases increases phosphorylation or reduced activity of phosphatases.

The mechanism involving perturbations of calcium current regulation, excitation-contraction coupling with slower Ca^{2+} transient propagation, may be because of structural disruption of signaling system, for example as a result of lack of T-tubules (Koivumaki, Korhonen et al. 2011).

Healthy human atrial cardiomyocytes exhibit an extensive T-tubular network (Richards et al. 2011), as atrial cardiomyocytes from large mammals (Dibb et al. 2009, Lenaerts et al. 2009). The role of Ca^{2+} in cAF, in which indeed remodeling of the T-tubular network may occur, was not investigated. Significant decreasing of T-tubule density was shown in atrial cardiomycytes but only in animal model of AF (Lenaerts, Bito et al. 2009), whereas no evidence of T-tubule system structure in humans during cAF was demonstrated.

Understanding cAF requires an integrated quantitative investigation of different microdomains and intercellular transport of Ca^{2+} in healthy and remodeled human atria. The present study examines the hypothesis that reduced $I_{Ca,L}$ in patients with cAF is associated with macroscopic (atrial dilatation) and microstructural alterations in intercellular microdomains which can affect compartmentalisation and activity of functional calcium channels.

6.2 MATERIALS AND METHODS

6.2.1 Patients groups

Human cardiomyocytes were isolated from the right atrial appendage left-over samples (n=7, average age 71.4±2.2 years, 5 males and 2 female) obtained during coronary artery bypass surgery (n=5) and mitral valve replacement (n=2) procedure at Hammersmith Hospital, Imperial College London, UK. All the patients had a normal left ventricle function (ejection fraction >60%) and no evidence of atrial arrhythmias. The collected samples were cardioplegically arrested and cooled to 4-7^{o}C in the operating room following cross-clamping of the aorta. The samples were maintained at 4-7^{o}C to preserve tissue during 10 minutes delivery from the operating room to the research laboratory.

6.2.2 Human atrial cardiomyocyte isolation

Human cardiomyocytes were isolated by enzymatic digestion as previously described(Lyon, MacLeod et al. 2009). Briefly, individual specimens were transferred to ice-cold calcium free Krebs-Ringer saline solution consisting of (in g/L): 7.012 NaCl, 0.402 KCl, 1.332 $MgSO_4$, 0.55 Pyruvate, 3.603 Glucose, 2.502 Taurine, 2.383 HEPES, 1.286 Nitrillotriacetic Acid; pH = 6.96. Connective and adipose tissue were removed and approximately 500mg of myocardial tissue was minced with razor blades in small cubes (approx. 1-2 mm^3). Then, the tissue pieces were washed with fresh Ca^{2+}-free Krebs-Ringer solution 3 times for 3 min each at 37^{o}C. After wash, cardiac tissue was incubated for 25 min in 10ml of Krebs-Ringer solution containing (in g/L): NaCl 7.012, KCl 0.402, $MgSO_4$ 1.332, Pyruvate 0.55, Glucose 3.603, Taurine 2.502, HEPES 2.383; pH = 7.4, supplemented with 200 nM $CaCl_2$ and Proteinase type XXIV (0.36mg/ml; Sigma-Aldrich) under gentle agitation. The partially digested tissue was transferred to 10ml of Krebs-Ringer saline supplemented with collagenase type IV (1mg/ml Sigma-Aldrich).

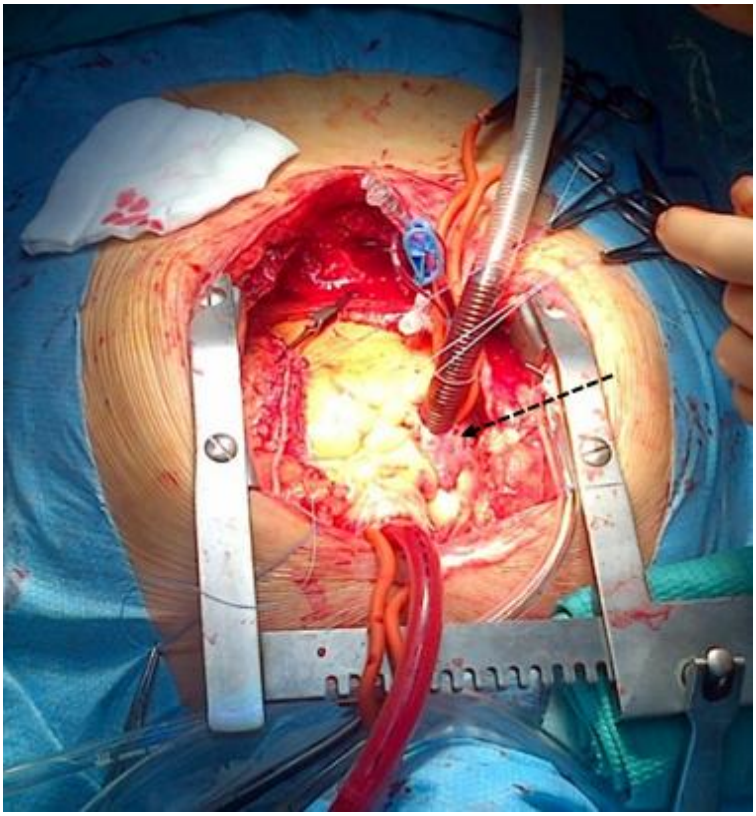

Figure 6.1. Right atrial appendage (showed by arrow) cannulated during open chest cardiac procedure.

The tissue was incubated thrice with this solution for 10 min each at 37^{o}C with gentle agitation. Usually, cardiomyocytes were visible by phase contrast light microscopy after the first incubation step, with the biggest amount of cells after the second incubation step. After each incubation step, the supernatants were transferred to a tube and centrifuged at 600 rpm for 3 min. The pellets were re-suspended in 2-3 mL of Krebs-Ringer solution. After isolation, human cardiomyocytes were plated following the same protocol as rat cardiomyocytes.

6.2.3 T-tubule Labeling

T-tubule density was measured after sarcolemmal membrane labeling with Di-8-ANEPPS as described previously (Kawai, Hussain et al. 1999). Cardiomyocytes were incubated with 10mM Di-8-ANEPPS (Molecular Probes, Eugene, OR, USA) for 1 min and then washed for 3 min before being observed under the confocal microscope. After Di-8-ANEPPS labeling, the density of T-tubules was quantified by the ratio of T-tubule fluorescence (T-tubule membrane) to total plasma membrane fluorescence (total membrane) in the same confocal slice, with excitation at 488 nm and emission detected at 520nm (Louch, Bito et al. 2004). The T-tubule density was calculated by converting the Di-8-ANEPPS signal to a binary signal, using the autothreshold function of ImageJ. After exclusion of the surface sarcolemma, the whole z-series was analysed to provide the percentage stained. This was represented as T-tubule density.

6.2.4 Scanning ion conductance microscopy (SICM) and confocal microscopy

SICM is a scanning probe microscopy technique in which a nano-pipette is used for non-contact visualization of the surface topography of living cells18. The subcellular T-tubule system was visualized by confocal imaging of atrial cells stained with the lipophilic membrane indicator Di-8-ANEPPS.

6.2.5 Super-resolution scanning patch-clamp with pipette clipping modification

After generating a topographical image of the cell surface by SICM, the tip diameter of the pipette was widened by clipping (Novak, Gorelik et al. 2013) to increase the area of attachment. The pipette was then lowered to a specific location (T-tubule or crest) until it touched the membrane and a high resistance

seal was established. Recordings were then performed in a cell-attached mode (Bhargava, Lin et al. 2013). Controlled widening of the scanning nano-pipette tip is described in details in the Chapter 2. Macroscopic calcium currents were recorded using the whole-cell patch-clamp technique as described previously (Wright, Nikolaev et al. 2013).

6.2.6 Whole-cell electrophysiological recordings

Macroscopic Ca^{2+} currents were recorded using the whole-cell patch-clamp configuration with the external recording solution of the following composition (in mmol/L): 120 Tetraethylammonium-chloride, 10 CsCl, 10 Glucose, 10 HEPES, 1.5 $MgCl_2$, 5 $CaCl_2$, pH 7.4 with CsOH. An internal pipette solution contained (in mmol/L): 100 Cs-methanesulfonate, 40 CsCl, 10 HEPES 5 EGTA, 2 $MgCl_2$, 5 Mg-ATP, 0.75 $MgCl_2$, pH 7.2 with CsOH. Patch pipettes had mean resistances of 3.5–5 MΩ. Currents were recorded using an Axopatch-1D amplifier connected to a Digidata1322A acquisition system (Axon Instruments, Foster City, CA, USA). The bath was connected to the ground via an Ag–AgCl pellet. Data were low-pass filtered at 2 kHz using the built-in Bessel filter of the amplifier and sampled at 10 kHz. All recordings were performed at room temperature (22-24°C). $I_{Ca,L}$ channel activity was recorded during 200 ms from a holding potential of -40 mV to test potentials ranging from -40 to +60 mV, with pulses applied every 2s in 5 mV increments. Results were analyzed offline using pCLAMP10 (Axon Instruments) and OriginPro8.6 (OriginLab) software packages. Series resistance and whole cell capacitance were electronically compensated between 70 and 80% for each cell. Current amplitude at 10 mV was taken as a peak current for each cell. This value was divided by cells capacitance and was termed Ca^{2+} current density. Mean current values ± SEM were plotted as current-voltage (I-V) relationship. *I–V*'s were fitted with the modified Boltzmann equation, $I = [G_{max} \times (V_m - E_{rev})]/\{1 + \exp[(V_m - V_{0.5a})/K_a]$, where V_m is the test potential, $V_{0.5a}$ is the half-activation potential, E_{rev} is the extrapolated reversal potential, G_{max} is the maximum slope conductance and K_a reflects the slope of the activation curve.

6.2.7 RNA isolation and cDNA synthesis

Total RNA was isolated from right atria appendage using the method of tissue homogenizing and guanidine-isothiocyanate–containing Buffer RLT Plus (Qiagen) which immediately inactivates RNases to ensure isolation of intact RNA. The lysate is then passed through a gDNA Eliminator spin column. This column, in combination with the high-salt buffer, selectively and efficiently removes genomic DNA. Ethanol is added to provide appropriate binding conditions for RNA, and the sample is applied to an RNeasy MinElute spin column (RNeasy kit for RNA minipreps from tissues by Qiagen). These specialized columns contain a silica membrane that specifically binds RNA from lysed cells extraction (Brundel, Van Gelder et al. 2001)

The reverse transcription 5× buffer and 200 ng of random hexamers with 200 Units of Moloney Murine Leukemia Virus Reverse Transcriptase (Life Technologies), 10 mM of dNTP (Life Technologies), and 40 Unit of RNase inhibitor (Life Technologies) in 20 µl. The synthesis reaction lasted 5 min at 65°C, 5 min at 25°C, 50 min at 50°C, and 15 min at 70°C, respectively (Brundel, Van Gelder et al. 2001).

6.2.8 Real-time PCR analyses

The cDNA of interest and the cDNA of the ubiquitously expressed housekeeping gene glyceraldehyde-3-phosphate dehydrogenase (GAPDH) were co-amplified in a real-time PCR performed using an Realplex^2 Real-Time PCR system (Mastercycler, Eppendorf), Software for Miniopticon (Bio-rad) and homemade designed primers from Sigma (see Table.2). PCR was performed for 40 cycles with automated detection of crossing threshold. Real-time PCR reactions were performed with duplicate lanes with GAPDH as a control reaction and no-template lanes for negative controls (Yang, Katchman et al. 2011) also using spleen RNA as internal control for rat samples and Raji lymphoma as internal control for human samples.

Complementary DNA was added to a 20 µl well containing 10 µl 2× SYBR Green master mix, 0.5 µl gene-specific primers designed by Sigma, see Table 2). The conditions for Real-time PCR was preheating at 94°C for 2 min, followed by 40 cycles of shuttle heating at 94°C for 15 s and at 60°C for 1 min. The cycle threshold Ct value for each sample that was proportional to the log of the initial amount of input cDNA was calculated and plotted (Qu, Karnabi et al. 2011).

name	gene		primer	Tm	Product length
Cav1.2	Cacna1c	Forward	GCTCATTGCCTTCAAACCCA	59.03	72
		Reverse	CCCACAACAATCAAGGCGTC	59.76	
	Cacna1c	Forward	ATCACCGAGGTAAACCCAGC	59.75	96
		Reverse	GAACAGGCGGAAGAAGGTGA	59.97	
	Cacnb1	Forward	ACCTCCAGGGACCCTACCTT	61.46	88
		Reverse	TCCCCTGGGTACTCGTGCAT	62.82	
	Cacnb2	Forward	CAAACCACCGCTCCCCTAAA	60.25	100
		Reverse	GGAGGAGTGTGCTCTGTCTT	59.03	
	Cacnb3	Forward	TACTGGATGAGGAGTGCCCA	59.96	100
		Reverse	CCGATCCACCAGTCATTGCT	60.11	
	Cacnb4	Forward	GGTCCAGCTTAGCGGAAGTA	59.18	100
		Reverse	GGGTGATTGATGGTGTCTGC	58.90	

Table 2. Primers sequences.

6.2.9 Statistical analysis

All graphs and statistical analysis were performed using either GraphPad prism 5 or Origin version 6.1. Quantitative data are shown as mean ± SEM for the given number of experiments. Hypothesis testing was carried out using an unpaired student t-test. A value of $P<0.05$ was considered statistically significant.

6.3 RESULTS

6.3.1 Characteristics of patients

The baseline characteristics of patients with SR (N=31) and AF (N=42) are compiled in Table 1. All patients in cAF group had atrial fibrillation longer than 6 months in anamnesis. Both groups of patients with SR and cAF were the same underwent mitral valve replacement (MVR) and coronary artery bypass grafting (CABG). Patients with cAF underwent MVR significantly more frequently.

	SR	cAF
N	31	42
Gender	M=21; F=10	M=25; F=17
Age	61-78	61-83
CABG, %	33%	10%
MVR	67%	90%
EF, %	> 60%	>55%
LA diameter, mm	34-54	44-72 mm
RA short axis diameter, mm	40-54	44-58
EF, %	> 60	>55
CABG, %	33%	10%
MVR	67%	90%
LA, mm	34-44 mm	43-72 mm
L-type blocker	27%	15%
β-blocker	47%	87%

Table 6.1. Basic patient's characteristics.

Mitral valve pathology more often consists of left-sided atrial remodelling, what additionally confirms correlation between enlargement and dilatation of left atrial chamber with downwarding atrial fibrillation to chronic stage. Most of patients with cAF represented marked LA dilatation along with increased RA short axis diameter.

All patients in this study had normal left ventricular function with EF higher than 60%. According with cardiac pathology regulations most of patients take beta-blockers, what noticed in this study (**Table 6.1**). All patients with cAF had anticoagulant therapy to protect against the stroke.

6.3.2 LA dilatation and RA/LA ratio during cAF

Dilatation of LA was observed in all patients with cAF and in SR patients underwent MVR.

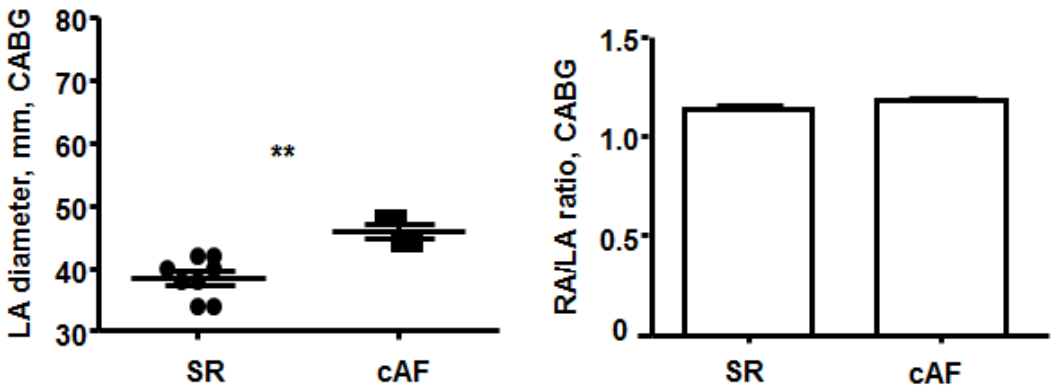

Figure 6.2. cAF affects on left atrium (LA) diameter and RA/LA ratio in patients underwent CABG.

(Left panel) cAF patients had increased LA diameter in contrast to control patients with SR. Right panel shows no changes in RA/LA ration between SR and cAF patients.

In contrast to normal LA size of 30-40 mm, cAF patients demonstrated LA diameter of 56.8±2.8 mm, N=20 in MVR group and 46±1.1 mm, N=5 in CABG, SR patients underwent MVR showed LA diameter of 46.2±0.9 mm, N=16; where N is a number of patients.

Analysis of RA/LA ratio detected no difference between SR and cAF in CABG group, which accordingly to LA dilatation during cAF suggests equal role of both atrial chambers in structural remodeling in presence of cAF accompanying with coronary disease. Controversial results were observed in MVR group. cAF caused significant decreasing of RA/LA ration. Based on these results, LA plays more dominant role in cAF accompanying mitral valve pathology, while LA dilatation.

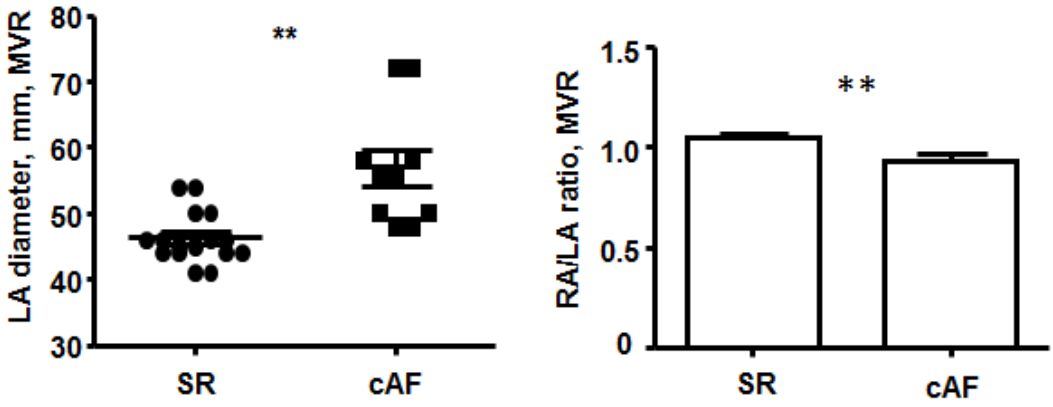

Figure 6.3. cAF affects on left atrium (LA) diameter and RA/LA ratio in patients underwent MVR.

Left panel shows increased (higher than normal) LA diameter in patients with SR and cAF with marked dilatation in cAF patients. Right panel shows significantly smaller RA/LA ration in cAF patients ($P<0.01$).

These results clearly demonstrated that involvement of left atrium in remodeling caused by chronic atrial fibrillation is more prominent independently on type of associated pathology.

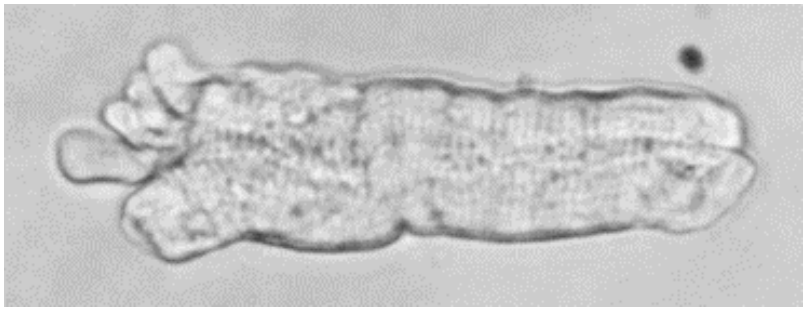

Figure 6.4. Human atrial cardiomyocyte isolated from right atrial appendage

6.3.3 Subcellular T-tubule system in atrial cardiomyocytes in cAF

Half of the studied human atrial cardiomyocytes demonstrate T-tubule structure in both left and right atria. In contrast to rat atrial cells, in human cardiomyocytes correlation between the T-tubular network and cell size was not revealed (**Figure 6.5 A and B**). cAF remodelling caused a dramatical decrease in percentage of all atrial cardiomyocytes with T-tubule structure (**Figure 6.5 C**); and affected on T-tubule density in cells showed T-tubule structures from 13±4% in control (SR) to 7±2.5% in cAF right atrial cells. Cardiomyocytes isolated from left atrium demonstrated lowest T-tubules density 5±2% in cAF.

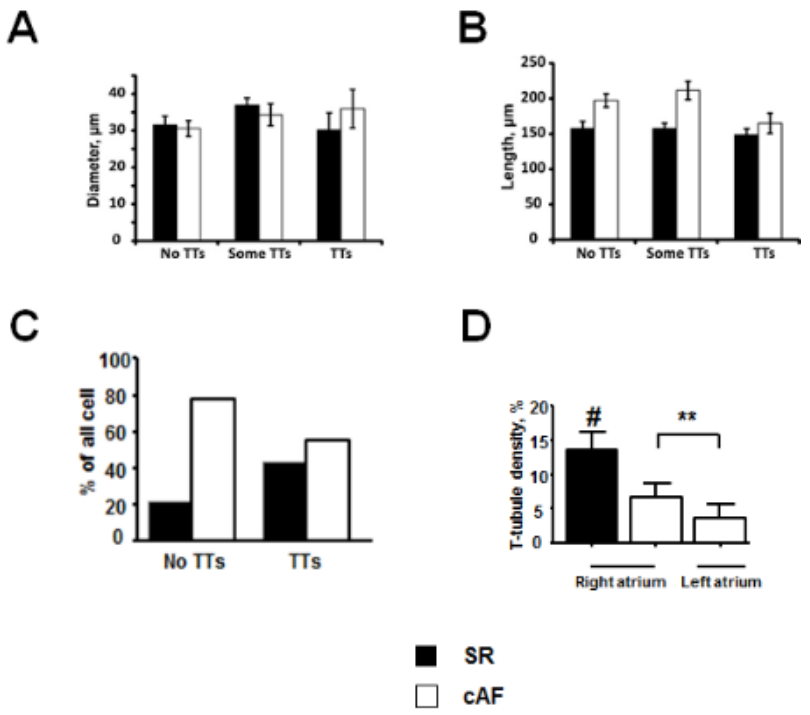

Figure 6.5. T-tubule network in human right and left atrial cardiomyocytes of pts with SR and cAF.

Di-8-ANEPPS membrane staining showing a T-tubular network in human atrial cardiomyocytes isolated from right and left atrial samples. Cell diameter (**A**), length (**B**) and distribution in % (**C**) of right atrial SR (black columns) and cAF (white columns) cardiomyocytes with non-organized and absent T-tubular structures. **(D)** T-tubular system density measured in right atrial cardiomyocytes from SR patients and right and left atrial cardiomyocytes from cAF patients

6.3.4 Surface structures in atrial cardiomyocytes in cAF

SICM imaging of human control (SR) atrial cardiomyocytes clearly showed the heterogeneity of surface topography with evident location of the T-tubule openings, the domed crest between the Z-grooves (**Figure 6.6 A**), as it was observed in rat control cells (see Chapter 3). In contrast to rat cells, human atrial cardiomyocytes did not demonstrate correlation between surface structure and cell width.

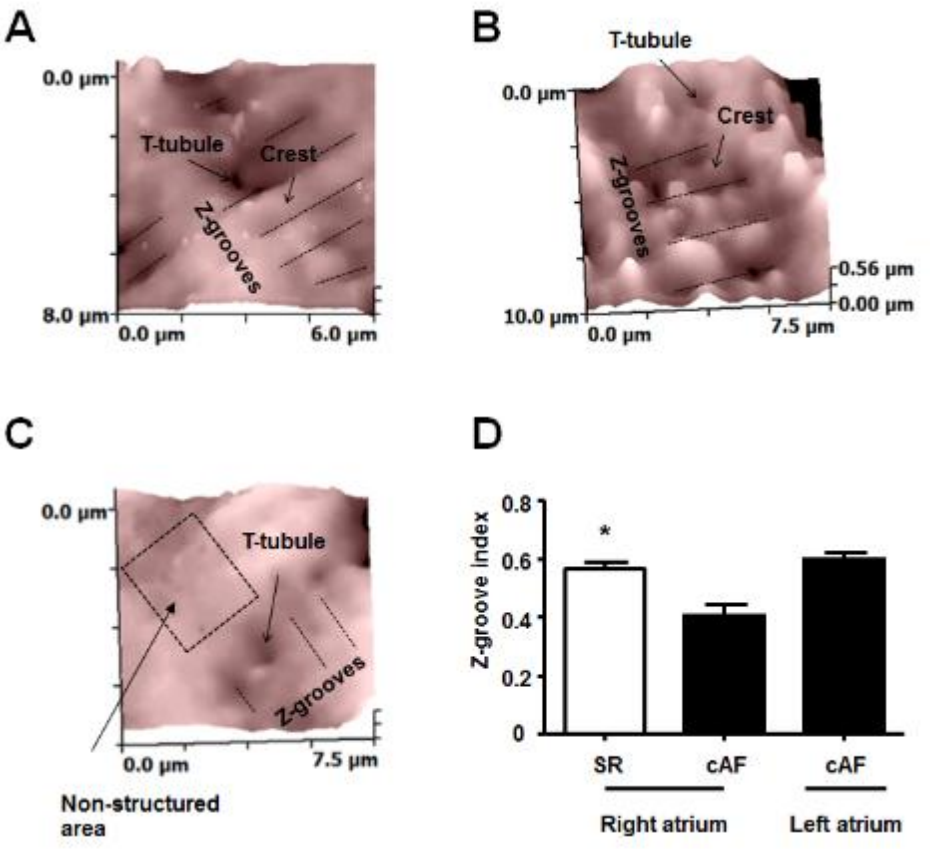

Figure 6.6. Surface structure of living human atrial cardiomyocytes .

Topography scans of a single right atrial cardiomyocytes isolated from patients with SR (**A**) and cAF (**C**), and left atrial cardiomyocytes isolated from patients with cAF (**B**) represent differently organized surface structure. A pipette with tip diameter 100 nm was used to obtain topography scans. T-tubules, crests, and non-structured areas are indicated by arrows. (**D**) Z-groove index was used to quantify cell topography. Average Z-groove index measured for atrial cells isolated from right atrium (n=34) and both right (n=40) and left (n=22) atria from patients with SR and cAF, respectively

In this chapter, the same analysis was applied to characterize topography of atrial cardiomyocytes during cAF. It was found; cardiomyocytes isolated from right atrial appendage in patients with cAF in anamnesis can be characterized by significant destruction in surface topography (**Figure 6.6 C**) in comparison to cells obtained from patients with sinus rhythm. Surprisingly, left atrial cardiomyocytes demonstrated well-organised surface topography (**Figure 6.6 B**). Unfortunately,

due to limitation of human research this study are confined to explore control cells obtained from left atrial appendages. Based on data obtained from rat control cells, it is possible to suggest that control left atrial cardiomyoytes have more developed surface structure than cell obtained from right atrial appendages. The Z-groove index was calculated for human cells as it was previously described (**Figure 6.6 D**).

6.3.5 Spatial localization of functional LTCCs in atrial cells during cAF

As it was expected, human right atrial cardiomyocytes obtained from patients with sinus rhythm demonstrated functional LTCCs localized in both T-tubules and crest microdomains (**Figure 6.7**) with almost equal occurrence (29% of 31 successful patches in T-tubules vs. 21.4% of 14 successful patches in the crest) (**Figure 6.10**).

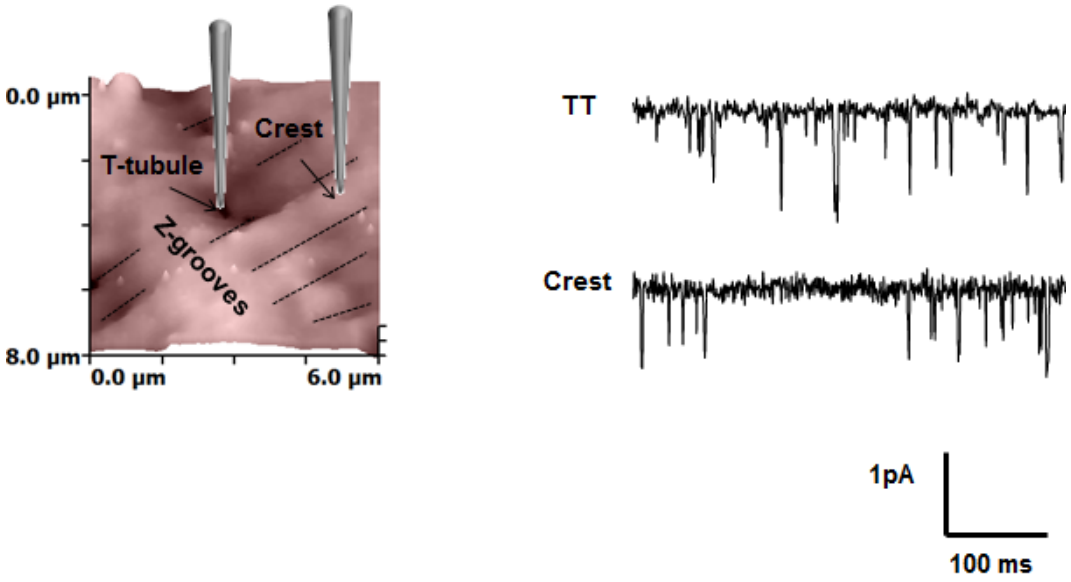

Figure 6.7. Single LTCC activity recorded from the T-tubule and crest areas in cardiomyocytes isolated from right atrial appendages of patients with SR .

Left panel: a typical 10µmx10µm topographic scan of cardiomyocytes showing locations where pipette was placed after clipping and a giga-seal was obtained over a T-tubule/crest area of the sarcolemma. **Right panel:** corresponding representative current traces of single LTCC activity at -6.7 mV recorded from different domains using a pipette of 25MΩ resistance.

However, experiments with right atrial cardiomyocytes isolated from cAF patients showed that the percentage of LTCCs recoded in the crest decreases (21.4% of 28 successful patches in T-tubules vs. 6.25% of 34 successful patches in the crest. Functional LTCCs faded away (6.7% of 29 successful patches in T-tubules and 0% of 22 successful patches in the crest) in cardiomyocytes isolated from left atrial appendages in cAF patients (**Figure 6.10**).

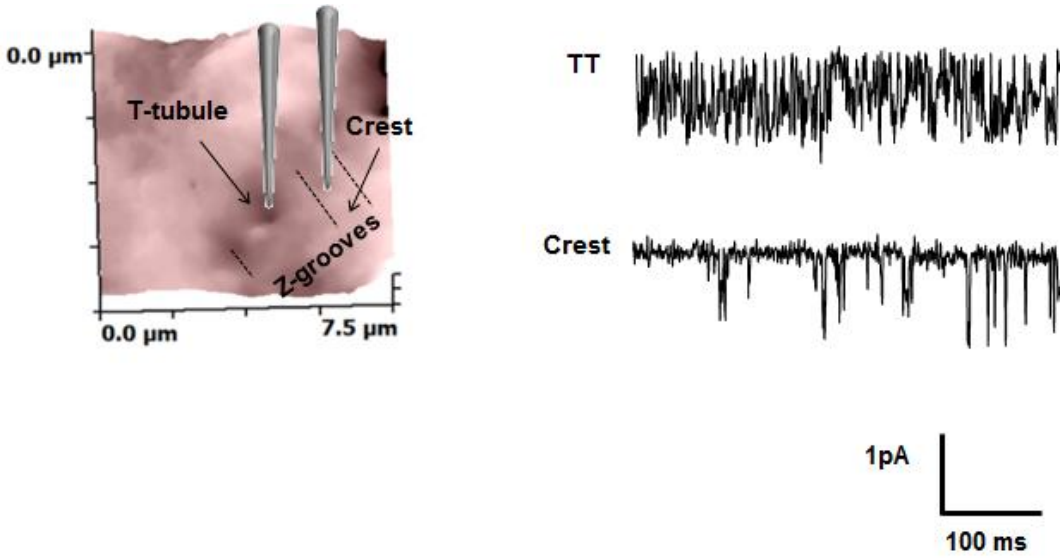

Figure 6.8. Single LTCC activity recorded from the T-tubule and crest areas in cardiomyocytes isolated from right atrial appendages of patients with cAF .
Left panel: a typical 10µmx10µm topographic scan of cardiomyocytes showing locations where pipette were placed after clipping and a giga-seal was obtained over a T-tubule/crest area of the sarcolemma. **Right panel:** corresponding representative current traces of single LTCC activity at -6.7 mV recorded from different domains using a pipette of 25MΩ resistance.

Thus, cAF causes abolishment of single LTCCs in atrial cells and predominantly in the crest microdomains. In case of this study, which involves cardiomyocytes obtained from patients with apparent left atrial remodelling, hence marked intercellular remodelling of cells obtained from left atrium might expect. These

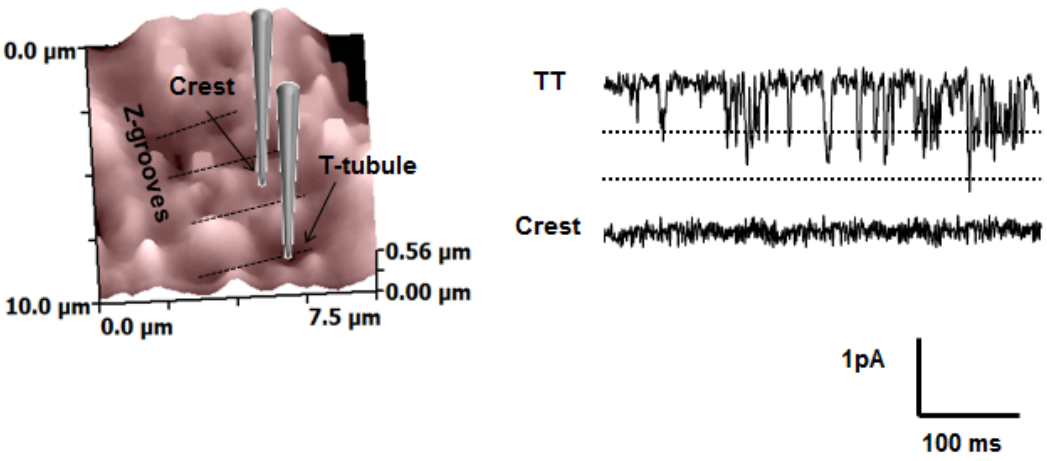

Figure 6.9. Single LTCC activity recorded from the T-tubule and crest areas in cardiomyocytes isolated from left atrial appendages of patients with cAF .

Left panel: a typical 10µmx10µm topographic scan of cardiomyocytes showing locations where pipette were placed after clipping and a giga-seal was obtained over a T-tubule/crest area of the sarcolemma. **Right panel:** corresponding representative current traces of single LTCC activity at -6.7 mV recorded from different domains using a pipette of 25MΩ resistance.

results are absolutely contrary to data obtained from ventricular cells during cardiac failure, where migration of channels from tubular to crest domain was observed.

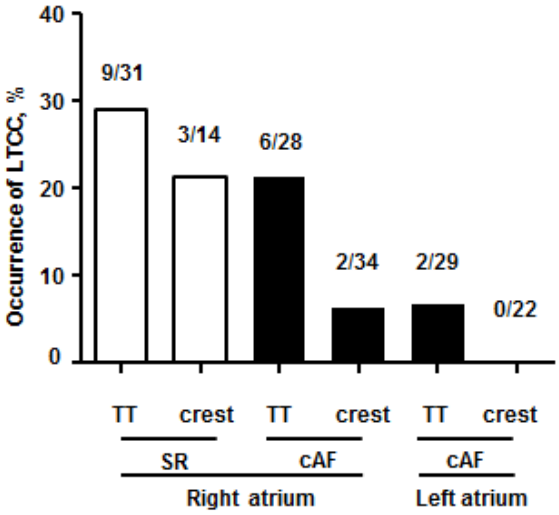

Figure 6.10. Occurrence of single L-type calcium current recorded from different areas in atrial cardiomyocytes isolated from right and left atrial appendages of patients with SR and cAF.

Klein et al. showed increased open probability of LTCCs in patients with cAF (Klein, Schroder et al. 2003). Using standard patch-clamp technique with cell-attached configuration and wide low-resistance pipette limited spatial distribution of recorded single channels. Thus, the question whether all functional LTCCs change their biophysical characteristics or microdomain environment can affect to single channel remains unknown. To answer this question super-resolution scanning patch-clamp method was used (Bhargava, Lin et al. 2013)

And huge difference in open probability between the T-tubular channels recorded in SR and cAF right atrial cells was found [p(open) at -6.7mV: 0.03±0.002 in SR patients, N=12; vs. 0.18±0.02 in cAF patients, N=18, P<0.0001, where N is a number of channels] (**Figure 6.11**). Both right atrial cells from SR and cAF patients showed functional LTCCs in the crest microdomains with open probability lower than in the T-tubules. Moreover, in presence of cAF LTCCs recorded from the crest demonstrated significantly higher single channel activity [p(open) at -6.7mV:

0.02±0.001 in SR patients, N=5; vs. 0.07±0.003 in cAF patients, N=5, P<0.0001, where N is a number of channels]. Thus, both T-tubule and crest microdomains housed functional LTCCs with increased activity; however, T-tubular channels demonstrated 2.5-fold higher open probability than LTCCs in the crest compartment.

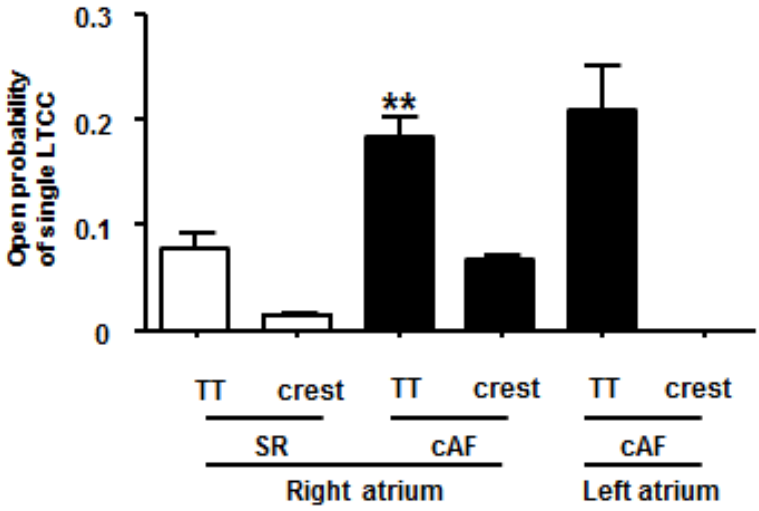

Figure 6.11. Open probability of single LTCC recorded from different areas in atrial cardiomyocytes isolated from right and left atrial appendages of patients with SR and cAF. P(open) of LTCCs recorded from RAA cardiomyocytes from pts with SR from T-tubules (TT) [N=12], crest [N=5] and from pts with cAF from T-tubules [N=6], crest [N=5]. P(open) of LTCCs recorded recorded from LAA cardiomyocytes from pts with cAF from T-tubules [N=8], crest [N=0]. N is number of channels. (** *P<0.01*).

Specific compartmentalization of signaling system might be suggested to explain difference in activity of channels in various microdomains. Another explanation

might include different distribution of auxiliary channel β-subunit isoforms, which can modulate LTCC activity in different way.

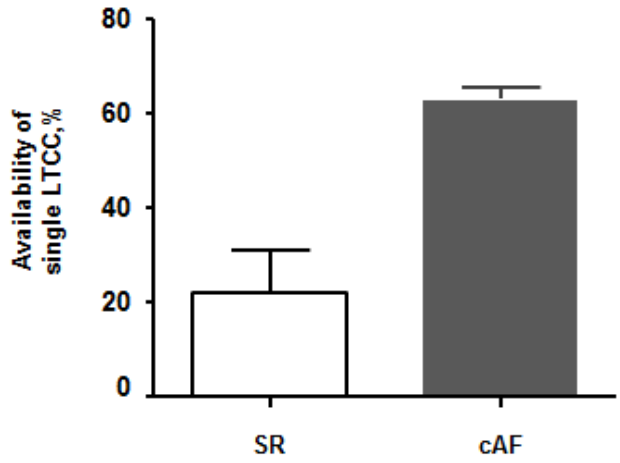

Figure 6.12. Availability of single LTCC recorded from the T-tubule area in atrial cardiomyocytes isolated from right atrial appendages of patients with SR and cAF.
Availability of LTCCs recorded from pts with SR [N=8]; and from pts with cAF [N=5]. N is number of channels.

T-tubular LTCCs recorded in left atrial cardiomyocytes also demonstrated high open probability similar to right atrial cell [p(open) at -6.7mV: 0.17±0.03, N=7, where N is a number of channels].

Additional biophysical analysis of T-tubular LTCCs showed availability significantly increases during cAF [f_{active} at -6.7mV: 22±8%, N=5 in SR vs 63.3±2.4%, N=6 in cAF, where N is a number of channels] (**Figure 6.12**). Availability as a fraction of active sweeps per number of test pulses shows single channel kinetic. Based on Markov analysis phosphorylation-related mechanism was previously shown to be

responsible for changes in single channel availability (Cachelin, de Peyer et al. 1983; Ochi and Kawashima 1990; Yue, Herzig et al. 1990).

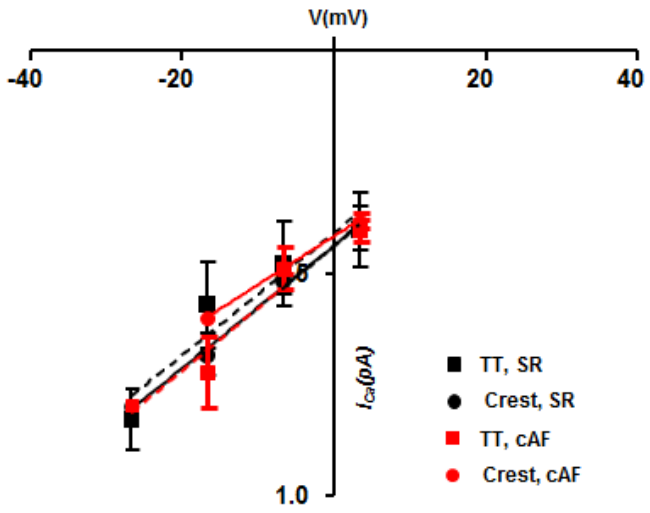

Figure 6.13. Voltage-current characteristic of single LTCCs recorded from the T-tubule and crest areas in right atrial cardiomyocytes of pts with SR and cAF.

I-V of single LTCC activity recorded from the T-tubules [N=5] and from the crest [N=3-5] of pts with SR; and from the T-tubules [N=5] and from the crest [N=3-4] of pts with cAF, where N is a number of channels.

Analysis of current-voltage relationship of functional LTCCs recorded in different microdomains in cardiomyocytes isolated from right atrium did not reveal any difference in amplitude and conductance during cAF. Thus, localization and cAF have no effect to single LTCC amplitude (**Figure 6.13**).

Cardiomyocytes isolated from left atrium in cAF showed only T-tubular LTCCs with slightly increased amplitude at more positive voltage (**Figure 6.14**). This could be related to low number of recordings obtained from left atrial human cells.

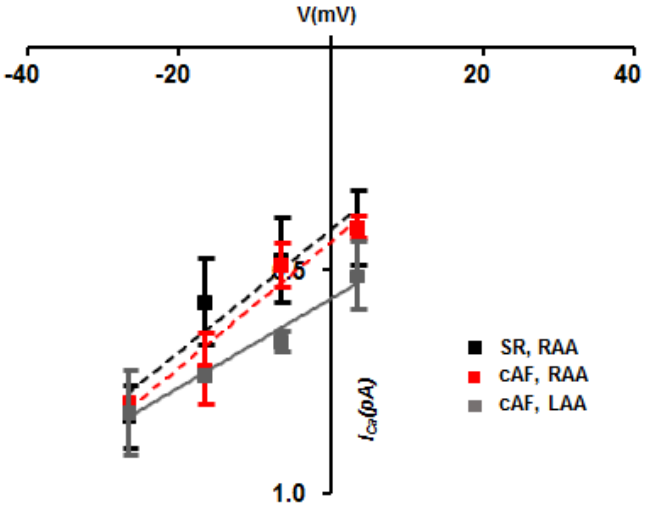

Figure 6.14. Voltage-current characteristic of single LTCCs recorded from the T-tubule area in right atrial cardiomyocytes of pts with SR and cAF and in left atrial cardiomyocytes of pts with cAF.

I-V of single T-tubular LTCC recorded from right atrial cardiomyocytes in SR (SR, RAA) and cAF (SR, cAF) pts; and from left atrial cardiomyocytes in cAF (LAA, cAF) pts.

Based on results about decreased occurrence of functional LTCCs during cAF whole-cell patch-clamp method was used to investigate calcium density.

It was found that cAF affect to calcium current density depressing current predominantly in left atrium (**Figure 6.15**).

Attempting to answer the question what mechanism is responsible for calcium channel remodeling during cAF following equalization should be explored.

$I = N * i * p(open) * f_{active}$,

where *I* is whole-cell calcium current density, N is a number of functional channels, i is a single channel amplitude, p(open) is an open probability of single channel and f_{active} is a single channel availability.

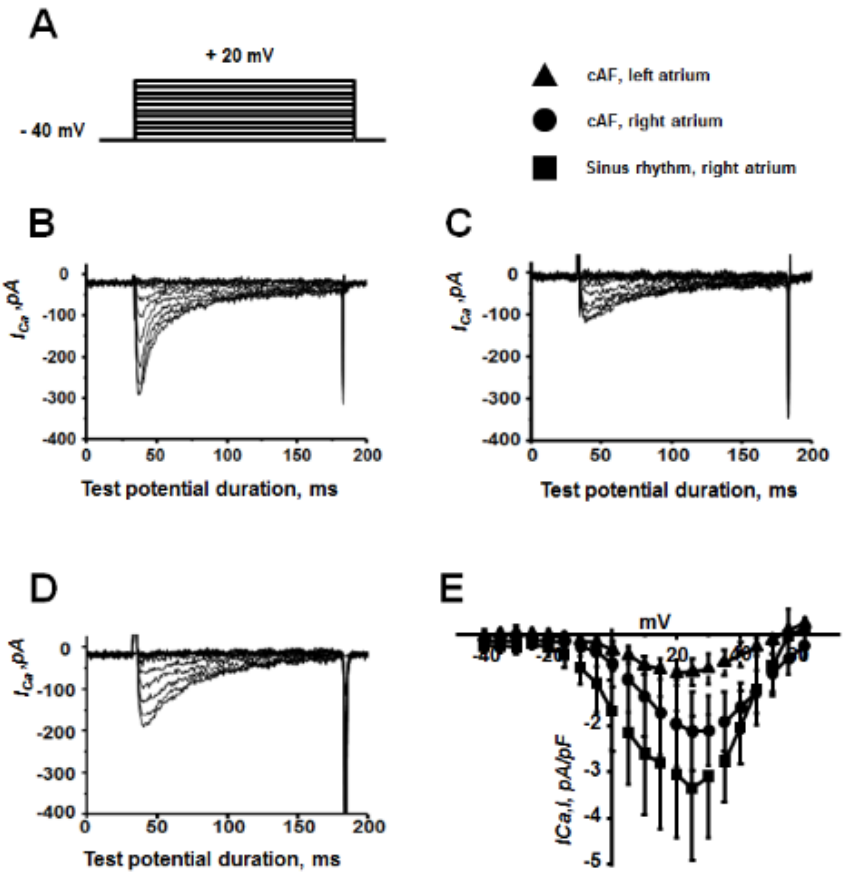

Figure 6.15. Whole-cell Ca^{2+} current in human atrial cardiomyocytes recorded from different atria in pts with SR and cAF.

A - voltage protocol of recordings; **B, C** - representative recordings of whole-cell Ca^{2+} current recorded from right atrial cardiomycytes of pts with SR and cAF, respectively; **D** - representative recordings of whole-cell Ca^{2+} current recorded from left atrial cardiomycytes of pts with cAF; **E** - voltage-current characteristics of whole cell calcium current in right atrial cardiomyocytes of SR [N=4] and cAF [N=6] pts, and in left atrial cardiomyocytes of cAF [N=5] pts. Where N is a number of cells (by Dr. Anita Alvarez-Laviada).

This study demonstrated apparent decreasing of calcium current density while individual parameters of channels such as open probability and availability were markedly enhanced in presence of cAF. As calcium current density is a function of both number of channels and single biophysical characteristics it is logical to

suggest that cAF dramatically abolishes number of functional LTCCs in intercellular microdomains with more apparent effect in the crest compartment.

To confirm decrease of number quantitative analysis of LTTC forming subunits gene expression was applied. The GAPDH levels were used as internal control. The LTCC in humans is composed of several subunits including the pore forming α_1 subunit and the auxiliary β_{1-4} subunits

Using qPCR technique, all subunits showed significant downregulation of mRNA expression in cAF. The effect of cAF is illustrated in Figure 6.16. A significant reduction ~ 20% of the α_1 subunit, 47% of β_1 subunit and ~30% of β_{2-4} subunits mRNA expression were observed in cAF.

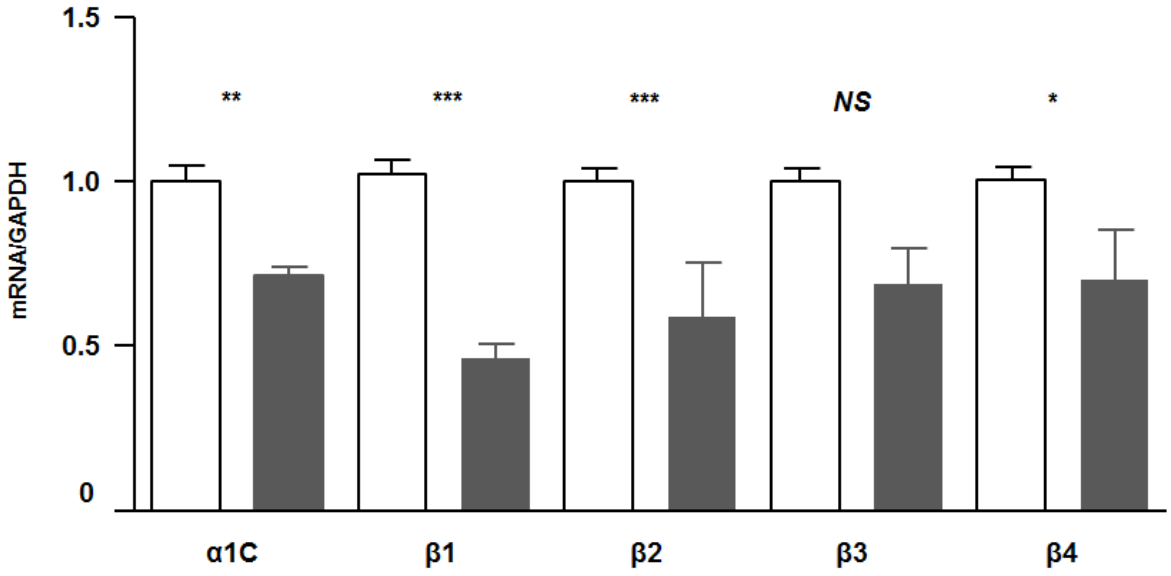

Figure 6.16. Effect of cAF on gene expression in human right atrium.

mRNA gene expression was normalized by GAPDH gene. Empty columns show control SR; N=18, and colored columns show cAF samples; N=16. Where N is a number of patients.

6.4 CONCLUSION

Several studies in patients with chronic AF or in animal model of cAF have addressed changes in ionic currents and channels in electrical remodelling (Bosch, Zeng et al. 1999; Christ, Boknik et al. 2004).

A major mechanism of reduced $I_{Ca,L}$ in chronic AF appears to be transcriptional downregulation of the pore-forming α_{1c} subunit (Brundel, van Gelder et al. 1999; Lai, Su et al. 1999; Yue, Melnyk et al. 1999).

Wei et al. have demonstrated that β subunits are the limiting factor for the expression of L-type Ca^{2+} channels in the heart (Wei, Colecraft et al. 2000). Thus, downregulation of β subunits may affect on general LTCCs expression and integration in membrane. Additionally, β subunits carry phosphorylation sites that might be important in altering channel function (Haase, Karczewski et al. 1993), that was observed in this study during cAF.

Previous human studies demonstrated that gene expression of the Ca^{2+} channel β_1 subunit isoform b (β_{1b}) is significantly reduced in AF compared with sinus rhythm (Grammer, Zeng et al. 2001). From these data, it appears that the reduced expression of β subunits is an important mechanism for the reduction of functional channels in the cell membrane.

Present results in this chapter clearly showed microdomain compartmentalization of functional LTCCs undergoing remodelling variously. Channels localised in the T-tubule compartment are more prominent to demonstrate anomalous increased single channel activity. Klein at al. associated increased open probability with dowregulation of phosphatase, which directly sedatives calcium channel (Klein, Schroder et al. 2003). Perhaps, loss of structure in the T-tubule system results in uncoupling in signalling system regulated LTCCs. This question needs further investigations.

In addition, cAF clearly affects occurrence of functional LTTCs. The loss of channels in the crest microdomain was observed in cAF. The underlying mechanism appears to be a transcriptional downregulation of pore-forming (α) and of auxiliary (β) subunits, which is observed in present study. Other explanation

includes loss in caveolae structures, which were observed as house of extradyadic functional LTCCs (see Chapter 3). Unfortunately, role of caveolae in human atrial cell during cAF was not investigated here.

Interestingly, correlation between macroscopic structural changes and intercellular remodelling was shown here. Thus, marked dilatation of left atrium occurs in cAF along with low T-tubule density, dramatically reduced calcium current density and abolishment of functional single channels in crest microdomain. Potential role of overloading and following overstretching of atrium can be discussed as a trigger for deep intercellular remodelling processes underlying atrial remodelling during cAF.

7 CONCLUSION

In cardiomyocytes, a variety of ion channels and regulatory receptors are spatially compartmentalized to multiple distinct subcellular microdomains (T-tubules, caveolae) and this compartmentalization may influence function and regulation of ion channels. Such organization allows the specificity, reliability and accuracy of the autonomic modulation of excitation–contraction processes by a variety of neurohormonal pathways, either via direct interaction or by second messengers through different G-protein-coupled receptors.

Moreover, structural features of microdomains may be associated with unique macromolecular signaling complexes, which in turn enables spatiotemporal modulation of cellular electrophysiology and contraction. In this respect, disorder of microdomain's structure affect excitation contraction coupling.

The spatial compartmentation of macromolecular signaling complexes is traditionally assessed by a variety of immune- and biochemical techniques. The resulting images are likely to represent mixed populations of both functional and silent channels and receptors, as well as those in the reserve pools, and thus lack information on the functionality of these proteins. The emerging imaging modalities, such as super-resolution scanning patch clamp seems to be promising to explore microdomain-specific functionality of different ion channels and provide direct evidence on protein–protein interaction.

This study shows high structural and electrophysiological inhomogeneity in the atrial appendages and connection into nanoscale definition between structure of microdomains and functionality of L-type calcium channels associated with subcellular compartments in normal and pathological hearts.

7.1 Subcellular T-tubule system in atrial cardiomyocyte

Thus, using *in situ* T-tubule imaging from the intact rat atria preparation, significant anatomical heterogeneity which might correlate with the arrangement of pectinate muscle bundles within the atrial appendages was found. It has been reported in rabbit atria that cardiomyocytes isolated from the crista terminalis were

significantly larger than those from the pectinate muscles, while the shape (the ratio of the length to the width) was found to be similar in the two types of cells (Yamashita, Nakajima et al. 1995). Anatomical variation of T-tubule system throughout the atria has been proposed to underlie heterogeneous calcium current measured within the right atrium, in addition to different expression of LTCCs. In healthy dogs, Ca^{2+} influx through LTCCs was found to be the largest in crista terminalis cells, intermediate in cells from the appendage and pectinate muscles, and smallest in atria-ventricular ring cells (Feng, Yue et al. 1998). In contrast, in rabbit right atrial cardiomyocytes isolated from different areas, whole-cell clamp recordings showed no definite variation in the calcium channels density (Yamashita, Nakajima et al. 1995). On the contrary, Frisk and colleagues used both isolated atrial cells and tissue to demonstrate that in pig and rat atria there was a high variability in the distribution of T-tubules and $I_{Ca,L}$ among cells, with a steep dependence of $I_{Ca,L}$ on atrial cardiomyocyte capacitance and T-tubule density (Frisk, Koivumaki et al. 2014). The authors observed a higher T-tubule density in the epicardium than endocardium, which may promote synchronization of contraction across the atrial wall. Thus, a possible physiological role for, and/or cause of such anatomical heterogeneity of T-tubule network and $I_{Ca,L}$ may relate to the complex activation (Wu, Yashima et al. 1998), action potential duration distribution (Berenfeld, Zaitsev et al. 2002), and contraction/tension pattern throughout the atria.

In mammalian, atrial cardiomyocytes have long been perceived as having no or very few T-tubules (Tidball, Cederdahl et al. 1991; Brette, Komukai et al. 2002; Smyrnias, Mair et al. 2010); however, recent experimental evidence demonstrate that atrial cardiomyocytes from large species, such as sheep (Dibb, Clarke et al. 2009), cows, horses, humans (Richards, Clarke et al. 2011), and even rodents (Kirk, Izu et al. 2003; Smyrnias, Mair et al. 2010; Dibb, Clarke et al. 2013) do possess an organised T-tubule network. At the same time, significant heterogeneity throughout the atria has been noted by many studies of cells with regards to their T-tubule organization. Generally, atrial T-tubules are sparse and less regular when compared with those in ventricular cardiomyocytes assessed

both *in situ* (Wei, Guo et al. 2010) and *in vitro* (Smyrnias, Mair et al. 2010). These observations of T-tubules in rat atrial cardiomyocytes are consistent with those previously observed using electron microscopy (Forssmann and Girardier 1970; Yamasaki, Furuya et al. 1997) and fluorescent membrane labelling (Kirk, Izu et al. 2003; Frisk, Koivumaki et al. 2014). Using the peroxidase labelling method, Forssmann and Girardier revealed that there are two types of muscle cells in the right atrium of the rat (Forssmann and Girardier 1970). They found that in most atrial cardiomyocytes, T-tubule system was either missing or poorly developed; however, some atrial cells exhibited a highly developed network of T-tubules. Similarly, Frisk *et al.* found three groups of atrial cardiomyocytes: untubulated, tubulated (disorganized T-tubules) and organized tubulated atrial cells (Frisk, Koivumaki et al. 2014). Discrepancy between some studies could be due to different isolation protocols and/or anatomical regions of the atria used for cell isolation.

Loss of T-tubules in both heart failure and chronic atrial fibrillation was found in rat and human studies presented here. Despite our understanding of the role of atrial T-tubules in calcium transient abnormality is rather limited, fundamental mechanisms of disruption of atrial excitation contraction coupling might be associated with atrial T-tubules and their degradation during decease (Dibb, Clarke et al. 2009).

7.2 Distinct distribution of functional calcium channels revealed by super-resolution scanning patch-clamp in adult atrial cardiomyocytes

In ventricular cardiomyocytes, functional LTCCs are prominently clustered in the well-developed T-tubule region where they are functionally and spatially coupled to the SR Ca^{2+} release channel (Bhargava, Lin et al. 2013). It has been proposed that due to lack of a regular T-tubular system in atrial cardiomyocytes, differential spatial distribution of LTCCs with regards to their coupling to RyR2s may underlie a unique atrial cardiomyocyte Ca^{2+} signaling process (Dobrev, Teos et al. 2009; Trafford, Clarke et al. 2013). The findings describing spatial compartmentation of Ca^{2+} signaling complexes were obtained by immunofluorescence microscopy

methods, and lacked information on the functional integrity of ion channel proteins within a subcellular domain. Recent methodological advances have made it possible to image the topography of a live cardiomyocyte and to study clustering of functional ion channels from a specific microdomain (Bhargava, Lin et al. 2013). Here, because of applying the novel method of super-resolution scanning patch-clamp (Bhargava, Lin et al. 2013), which allows to probe functional LTCCs in different microdomains (crest or T-tubules) of cardiomyocytes with nanoscale precision. Firstly, the T-tubule opening structures were resolved on the surface of atrial cardiomyocytes with regard to the subcellular T-tubular network. Then, for the first time the distinct distribution of functional atrial LTCCs was uncovered in the sarcolemma where they appear at a similar frequency both in the T-tubules and crest, in contrast to ventricular cardiomyocytes where LTCCs were exclusively clustered in T-tubules (Bhargava, Lin et al. 2013). This unique distribution of LTCCs was preserved in atrial failing cardiomyocytes, but not in chronic AF, where the crest microdomains showed decrease of number of channels, especially in left atrium where functional LTCCs vanished out of the crest microdomain. A major mechanism of reduced whole –cell $I_{Ca,L}$ and decrease occurrence of single LTCCs in the crest microdomain in chronic AF appears to be transcriptional downregulation of the pore-forming α_{1c} subunit (Brundel, van Gelder et al. 1999; Lai, Su et al. 1999; Yue, Melnyk et al. 1999). Downregulated β subunits may be also involved as the limiting factor for the expression of L-type Ca^{2+} channels in the heart (Wei, Colecraft et al. 2000) and carrier of phosphorylation sites that might be important in altering channel function (Haase, Karczewski et al. 1993), that was observed in this study during cAF.

Finally, it was demonstrated in this study, that the extradyadic channels were linked to caveolae structures and demonstrated their importance in the regulation of Ca^{2+} signaling in atrial cardiomyocytes.

7.3 β_1-adrenergic regulation of single L-type calcium channels in atrial cardiomyocytes and antiadrenergic effect of adenosine

Anti-adrenergic effect of adenosine might be associated with a specific interaction between β_1-AR and A1-adenosine receptor, which appears to be linked to caveolae structures. Immunoelectron microscopy techniques showed in smooth muscle cells the involvement of caveolae in the internalization of A1 adenosine receptors (Escriche, Burgueno et al. 2003).

The fact, that A_1-adenosine receptor stimulation increases IP_3 content in the heart while IP_3-associated G_q-protein coupled receptor signaling pathway directly interacts with Cav3 also suggests a link between caveolae and A1-adenosine receptors.
β_1-adrenergic stimulation dramatically increased the appearance and activity of functional L-type calcium channels. That can be explained by the increase in the availability of the channel, related to the number of functional channels.

Surprisingly, the effects of β_1-adrenergic stimulation on the open probability of the channels was significantly stronger (almost two times) localized outside of T-tubule microdomains (2.74 fold increase) as compared to the channels in the T-tubules (1.7626 fold increase).

Rybin et al. proved that the β_1-adrenergic stimulation appears to be most effective in the non-caveolar areas of the plasma membrane. And, based on evidence presented in Chapter 3, that Cav-linked LTCC are localized predominantly in the crest microdomains, a stronger effect of β_1-adrenergic stimulation in T-tubule microdomains, where functional LTCCs are not associated with caveolae, was logically expected.

Moreover, failing atrial cells missed adrenergic effect on functional LTCCs in the crest compartment, and demonstrated only slight increase of single channel activity in the T-tubules.

On the other hand, detailed analysis of LTCC open probability revealed two distinct subpopulations of channels localised in the crest in healthy cells. It was found that some channels have low open probability but other demonstrate relatively high mean open probability (**Figure 7.1**).

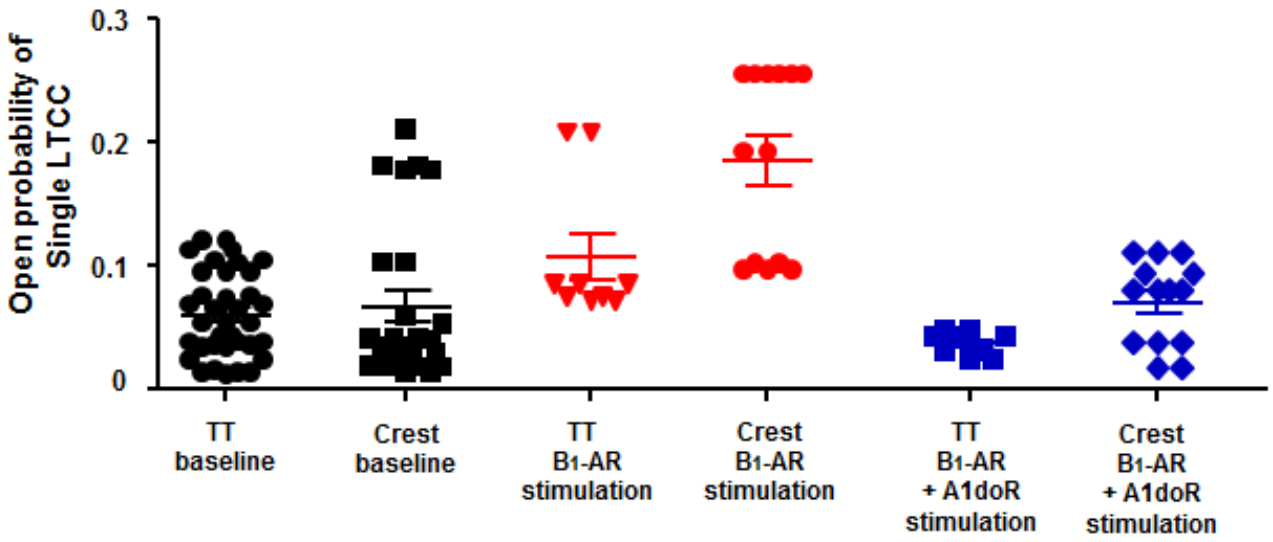

Figure 7.1. Open probability of single LTCC recorded from different areas in rat atrial cardiomyocytes before and after 2μM ISO+50nM ICI incubation and after 2μM ISO+50nM ICI incubation with local adenosine application (Ado 20 μM) through the recording pipette.
P(open) of LTCCs recorded before 2μM ISO+50nM ICI incubation (**baseline**) from T-tubules (TT) [N=43], crest [N=25] and after 2μM ISO+50nM ICI incubation (**B1-AR stimulation**) from T-tubules [N=9], crest [N=13]. P(open) of LTCCs recorded from T-tubules [N=9], crest [N=14] after 2μM ISO+50nM ICI incubation with local application of Ado 20 μM. N is number of channels. (** *P<0.01*; *** *P<0.001*; # *P<0.0001* T-tubule vs. crest).

Moreover, both subpopulations undergo β_1-adrenergic stimulation, showing increased activity, which was abolished back to baseline after A1-adenosine receptor stimulation.

Interestingly, second population of functional LTCCs with high open probability disappeared in heart failure. Moreover, the single preserved subpopulation did not undergo β_1-adrenergic stimulation. Taking it all into account, heart failure might affect cellular compartments, distribution of functional L-type calcium channels in lipid-rich areas of membrane and their coupling with adrenergic and adenosine receptors, which leads to the disruption of signaling system in atrial cardiomyocytes.

7.4 Caveolar structures as a potential source of Ca^{2+} sparks in atrial cardiomyocytes

The function of LTCCs localized in caveolae remains open to question. It has been proposed that some LTCCs housed in Cav3–rich microdomains, could play an important role in modulation of Ca^{2+} signaling. Indeed, calcium sparks are plentiful and seem to be normally present in atrial cardiomyocytes (Huser, Lipsius et al. 1996; Woo, Cleemann et al. 2003). Present results correspond to previous observations that atrial cardiomyocytes exhibit a significantly higher occurrence of spontaneous Ca^{2+} release events than ventricular cardiomyocytes (Woo, Cleemann et al. 2003). Löhn *et al* proposed that caveolae may have a key function in controlling the formation of local SR Ca^{2+} release events in the absence of global cytosolic Ca^{2+} elevations in cells lacking organized T-tubules such as atrial (Schulson, Scriven et al. 2011) and neonatal (Lohn, Furstenau et al. 2000) cardiomyocytes.

Important differences in Ca^{2+} handling mechanism between ventricular and atrial cardiomyocytes has been demonstrated by Walden and colleagues: a more robust and abundant Ca^{2+} uptake mechanism and a higher SR Ca^{2+} content has been revealed in atrial versus ventricular cardiomyocytes (Walden, Dibb et al. 2009). It has been further hypothesized that a higher SR Ca^{2+} content may lead to Ca^{2+} overload and thus increase sensitivity of RyR2s to cytosolic $[Ca^{2+}]_i$ (Dobrev, Teos et al. 2009). This means that one Ca^{2+} spark is more likely to trigger another Ca^{2+} spark in atrial cardiomyocytes but remains a rare event in normal ventricular

cardiomyocytes. Therefore, the benefit of the elevated SR Ca^{2+} content is that it should improve synchrony of the atrial $[Ca^{2+}]_i$ transients when T-tubules are disorganized or absent. The disadvantage of such an elevated SR Ca^{2+} content and enhanced $[Ca^{2+}]_{SR}$ is the increased sensitivity of the Ca^{2+}-induced Ca^{2+} release process. For thin cells or thick cells with organized T-tubules, the Ca^{2+} signal propagation is likely to be relatively stable. Larger cardiomyocytes with disorganized T-tubules, however, will have an increased proclivity towards subcellular Ca^{2+} alternant and thus appear to be prone to induction of Ca^{2+} sparks as demonstrated in present study (**Figure 3.8**).

It is possible that the mechanism behind Ca^{2+} sparks occurrence in atria differs from that in ventricles. In rat ventricular cardiomyocytes, 85% of all Ca^{2+} sparks evoked by electrical stimulation occurred within 0.5μm of a T-tubule (Shacklock, Wier et al. 1995), and formamide induced detubulation significantly reduced Ca^{2+} sparks in rat ventricular cardiomyocytes (Brette, Despa et al. 2005) suggesting an important role for T-tubules in Ca^{2+} spark initiation. Despite the broad distribution of RyRs in atrial cardiomyocytes principally along the Z-lines, most Ca^{2+} sparks occur within 1 μm of the sarcolemma (Mackenzie, Bootman et al. 2001; Kirk, Izu et al. 2003). In contrast to ventricular cardiomyocytes, where the close (≈12 nm) proximity of the RyRs and LTCCs in dyadic junctions of T-tubules (Franzini-Armstrong, Protasi et al. 1999) provides for the crucial Ca^{2+} release from the SR (Sham, Cleemann et al. 1995), atrial cardiomyocytes have an additional, functionally separated non-junctional Ca^{2+} release site in the central SR not associated with T-tubules (Mackenzie, Bootman et al. 2001; Woo, Cleemann et al. 2003). Based on immunochemical experiments, it has been then hypothesized that various atrial sites differ in their probability of initiating a Ca^{2+} spark, with some being designated as “eager” sites while others fail to spark (Mackenzie, Bootman et al. 2001; Schulson, Scriven et al. 2011; Trafford, Clarke et al. 2013). As demonstrated by Woo *et al* in rat atrial cardiomyocytes, although the frequency of spontaneous unitary Ca^{2+} sparks was significantly higher in the dyads, the compound sparks, i.e. localized Ca^{2+} release composed of several five unitary events occurring more or less synchronously and occupying normally more than two sarcomeres, appeared more prevalent in non-junctional sites (Woo, Cleemann

et al. 2003). These findings support the idea that the retarded dissipation of unitary non-junctional focal Ca^{2+} releases may facilitate the activation of neighboring release sites, leading to recruitment of a larger number of unitary events which in turn improves a synchrony of the atrial $[Ca^{2+}]_i$ transients when T-tubules are disorganized or absent (Dobrev, Teos et al. 2009).

Zima and Blatter have shown that non-junctional Ca^{2+} events might be attributed to inositol-1,4,5-trisphosphate (IP_3) dependent activation of non-junctional RyRs (Zima and Blatter 2004). Atrial cardiomyocytes express functional IP_3-receptors at 6-10 times higher levels than ventricular cardiomyocytes (Lipp, Laine et al. 2000). Recently, Horn *et al* have shown that IP_3 can effectively modulate RyR openings and Ca^{2+} spark probability (Horn, Ullrich et al. 2013). Direct interaction between Cav3 and IP_3-associated G_q-protein coupled receptor signaling pathway has been demonstrated by Guo and colleagues in canine ventricular cardiomyocytes (Guo, Golebiewska et al. 2011). It thus may link IP_3-dependent non-junctional Ca^{2+} events to caveolae structures and explain a significant decrease in occurrence of spontaneous Ca^{2+} sparks observed in our experiments in atrial cardiomyocytes treated with MβCD (**Figure 3.32**). Interestingly, a similar reduction in Ca^{2+} sparks via direct inhibition of caveolae housed LTCCs by Rem protein (**Figures 3.33 and 3.34**), highlights an importance of these channels in initiation of Ca^{2+} sparks. Alternatively, it is possible that MβCD- or Rem^{1-265}-Cav-induced reduction in the whole-cell $I_{Ca,L}$ decreased steady state SR Ca^{2+} load and thus suppressed the occurrence of spontaneous Ca^{2+} transients observed in our experiments.

In conclusion, all of the above considerations demonstrate the importance and the complexity of the microdomain specific modulation and remodeling of ion channel biophysical properties. This extends beyond the classical concept of electrical remodeling in cardiac disease according to which dysfunction can be explained by straightforward increases or decreases in protein expression alone. Thus, a better understanding of the various subcellular macromolecular signaling complexes may enable new therapeutic approaches for predicting and ameliorating the risk of sudden cardiac death and malignant arrhythmias in patients with cardiac diseases.

8 REFERENCES

Abhayaratna, W. P., K. Fatema, et al. (2008). "Left atrial reservoir function as a potent marker for first atrial fibrillation or flutter in persons > or = 65 years of age." Am J Cardiol **101**(11): 1626-1629.

Aimond, F., J. L. Alvarez, et al. (1999). "Ionic basis of ventricular arrhythmias in remodeled rat heart during long-term myocardial infarction." Cardiovasc Res **42**(2): 402-415.

Allessie, M. A., F. I. Bonke, et al. (1977). "Circus movement in rabbit atrial muscle as a mechanism of tachycardia. III. The "leading circle" concept: a new model of circus movement in cardiac tissue without the involvement of an anatomical obstacle." Circ Res **41**(1): 9-18.

Andersen, J. S., H. Egeblad, et al. (1991). "Atrial fibrillation and left atrial enlargement: cause or effect?" J Intern Med **229**(3): 253-256.

Anumonwo, J. M., Y. N. Tallini, et al. (2001). "Action potential characteristics and arrhythmogenic properties of the cardiac conduction system of the murine heart." Circ Res **89**(4): 329-335.

Ayettey, A. S. and V. Navaratnam (1978). "The T-tubule system in the specialized and general myocardium of the rat." J Anat **127**(Pt 1): 125-140.

Balijepalli, R. C., J. D. Foell, et al. (2006). "Localization of cardiac L-type Ca(2+) channels to a caveolar macromolecular signaling complex is required for beta(2)-adrenergic regulation." Proc Natl Acad Sci U S A **103**(19): 7500-7505.

Balijepalli, R. C. and T. J. Kamp (2008). "Caveolae, ion channels and cardiac arrhythmias." Prog Biophys Mol Biol **98**(2-3): 149-160.

Barouch, L. A., R. W. Harrison, et al. (2002). "Nitric oxide regulates the heart by spatial confinement of nitric oxide synthase isoforms." Nature **416**(6878): 337-339.

Bassani, J. W., R. A. Bassani, et al. (1994). "Relaxation in rabbit and rat cardiac cells: species-dependent differences in cellular mechanisms." J Physiol **476**(2): 279-293.

Bean, B. P., M. C. Nowycky, et al. (1984). "Beta-adrenergic modulation of calcium channels in frog ventricular heart cells." Nature **307**(5949): 371-375.

Benitah, J. P., J. L. Alvarez, et al. (2010). "L-type Ca(2+) current in ventricular cardiomyocytes." J Mol Cell Cardiol **48**(1): 26-36.

Berenfeld, O., A. V. Zaitsev, et al. (2002). "Frequency-dependent breakdown of wave propagation into fibrillatory conduction across the pectinate muscle network in the isolated sheep right atrium." Circ Res **90**(11): 1173-1180.

Berlin, J. R. (1995). "Spatiotemporal changes of Ca2+ during electrically evoked contractions in atrial and ventricular cells." Am J Physiol **269**(3 Pt 2): H1165-1170.

Bers, D. M. (2002). "Cardiac excitation-contraction coupling." Nature **415**(6868): 198-205.

Bers, D. M. (2008). "Calcium cycling and signaling in cardiac myocytes." Annu Rev Physiol **70**: 23-49.

Bers, D. M. and E. Perez-Reyes (1999). "Ca channels in cardiac myocytes: structure and function in Ca influx and intracellular Ca release." Cardiovasc Res **42**(2): 339-360.

Best, J. M. and T. J. Kamp (2012). "Different subcellular populations of L-type Ca2+ channels exhibit unique regulation and functional roles in cardiomyocytes." J Mol Cell Cardiol **52**(2): 376-387.

Bettex, D. A., R. Pretre, et al. (2014). "Is our heart a well-designed pump? The heart along animal evolution." Eur Heart J **35**(34): 2322-2332.

Beuckelmann, D. J., M. Nabauer, et al. (1992). "Intracellular calcium handling in isolated ventricular myocytes from patients with terminal heart failure." Circulation **85**(3): 1046-1055.

Beuckelmann, D. J. and W. G. Wier (1988). "Mechanism of release of calcium from sarcoplasmic reticulum of guinea-pig cardiac cells." J Physiol **405**: 233-255.

Bhargava, A., X. Lin, et al. (2013). "Super-resolution Scanning Patch Clamp Reveals Clustering of Functional Ion Channels in Adult Ventricular Myocyte." Circ Res **112**(8): 1112-1120.

Bhargava, A., T. O'Hara, et al. (2012). "Nanoscale Movement of L-Type Calcium Channels in the Cardiomyocyte Membrane Can Contribute to Arrhythmia During Heart Failure." Circulation **126**: A11953.

Bialecki, R. A. and T. N. Tulenko (1989). "Excess membrane cholesterol alters calcium channels in arterial smooth muscle." Am J Physiol **257**(2 Pt 1): C306-314.

Bichet, D., V. Cornet, et al. (2000). "The I-II loop of the Ca2+ channel alpha1 subunit contains an endoplasmic reticulum retention signal antagonized by the beta subunit." Neuron **25**(1): 177-190.

Birnbaumer, L., N. Qin, et al. (1998). "Structures and functions of calcium channel beta subunits." J Bioenerg Biomembr **30**(4): 357-375.

Bito, V., F. R. Heinzel, et al. (2008). "Crosstalk between L-type Ca2+ channels and the sarcoplasmic reticulum: alterations during cardiac remodelling." Cardiovasc Res **77**(2): 315-324.

Bootman, M. D., I. Smyrnias, et al. (2011). "Atrial cardiomyocyte calcium signalling." Biochim Biophys Acta **1813**(5): 922-934.

Bosch, R. F., X. Zeng, et al. (1999). "Ionic mechanisms of electrical remodeling in human atrial fibrillation." Cardiovasc Res **44**(1): 121-131.

Bouchardy, J., A. J. Marelli, et al. (2013). "Mirror image atrial dilatation in adult patients with atrial fibrillation and congenital heart disease." Int J Cardiol **167**(3): 816-820.

Boulware, M. I., H. Kordasiewicz, et al. (2007). "Caveolin proteins are essential for distinct effects of membrane estrogen receptors in neurons." J Neurosci **27**(37): 9941-9950.

Bovo, E., P. P. de Tombe, et al. (2014). "The role of dyadic organization in regulation of sarcoplasmic reticulum Ca(2+) handling during rest in rabbit ventricular myocytes." Biophys J **106**(9): 1902-1909.

Brette, F., S. Despa, et al. (2005). "Spatiotemporal characteristics of SR Ca(2+) uptake and release in detubulated rat ventricular myocytes." J Mol Cell Cardiol **39**(5): 804-812.

Brette, F., K. Komukai, et al. (2002). "Validation of formamide as a detubulation agent in isolated rat cardiac cells." Am J Physiol Heart Circ Physiol **283**(4): H1720-1728.

Brette, F. and C. Orchard (2003). "T-tubule function in mammalian cardiac myocytes." Circ Res **92**(11): 1182-1192.

Brette, F., L. Salle, et al. (2004). "Differential modulation of L-type Ca2+ current by SR Ca2+ release at the T-tubules and surface membrane of rat ventricular myocytes." Circ Res **95**(1): e1-7.

Brette, F., L. Salle, et al. (2006). "Quantification of calcium entry at the T-tubules and surface membrane in rat ventricular myocytes." Biophys J **90**(1): 381-389.

Bristow, M. R., R. Ginsburg, et al. (1986). "Beta 1- and beta 2-adrenergic-receptor subpopulations in nonfailing and failing human ventricular myocardium: coupling of both receptor subtypes to muscle contraction and selective beta 1-receptor down-regulation in heart failure." Circ Res **59**(3): 297-309.

Bristow, M. R., W. Minobe, et al. (1988). "Alpha-1 adrenergic receptors in the nonfailing and failing human heart." J Pharmacol Exp Ther **247**(3): 1039-1045.

Brodde, O. E. (1991). "Beta 1- and beta 2-adrenoceptors in the human heart: properties, function, and alterations in chronic heart failure." Pharmacol Rev **43**(2): 203-242.

Brodde, O. E. and M. C. Michel (1999). "Adrenergic and muscarinic receptors in the human heart." Pharmacol Rev **51**(4): 651-690.

Brundel, B. J., I. C. Van Gelder, et al. (2001). "Ion channel remodeling is related to intraoperative atrial effective refractory periods in patients with paroxysmal and persistent atrial fibrillation." Circulation **103**(5): 684-690.

Brundel, B. J., I. C. van Gelder, et al. (1999). "Gene expression of proteins influencing the calcium homeostasis in patients with persistent and paroxysmal atrial fibrillation." Cardiovasc Res **42**(2): 443-454.

Bunemann, M., B. L. Gerhardstein, et al. (1999). "Functional regulation of L-type calcium channels via protein kinase A-mediated phosphorylation of the beta(2) subunit." J Biol Chem **274**(48): 33851-33854.

Burgdorf, C., D. Richardt, et al. (2001). "Adenosine inhibits norepinephrine release in the postischemic rat heart: the mechanism of neuronal stunning." Cardiovasc Res **49**(4): 713-720.

Cachelin, A. B., J. E. de Peyer, et al. (1983). "Ca2+ channel modulation by 8-bromocyclic AMP in cultured heart cells." Nature **304**(5925): 462-464.

Calaghan, S. and E. White (2006). "Caveolae modulate excitation-contraction coupling and beta2-adrenergic signalling in adult rat ventricular myocytes." Cardiovasc Res **69**(4): 816-824.

Cannell, M. B., H. Cheng, et al. (1995). "The control of calcium release in heart muscle." Science **268**(5213): 1045-1049.

Cannell, M. B. and C. H. Kong (2012). "Local control in cardiac E-C coupling." J Mol Cell Cardiol **52**(2): 298-303.

Carafoli, E., L. Santella, et al. (2001). "Generation, control, and processing of cellular calcium signals." Crit Rev Biochem Mol Biol **36**(2): 107-260.

Carl, S. L., K. Felix, et al. (1995). "Immunolocalization of sarcolemmal dihydropyridine receptor and sarcoplasmic reticular triadin and ryanodine receptor in rabbit ventricle and atrium." J Cell Biol **129**(3): 673-682.

Catterall, W. A. (2000). "Structure and regulation of voltage-gated Ca2+ channels." Annu Rev Cell Dev Biol **16**: 521-555.

Catterall, W. A., E. Perez-Reyes, et al. (2005). "International Union of Pharmacology. XLVIII. Nomenclature and structure-function relationships of voltage-gated calcium channels." Pharmacol Rev **57**(4): 411-425.

Cavalie, A., D. Pelzer, et al. (1986). "Fast and slow gating behaviour of single calcium channels in cardiac cells. Relation to activation and inactivation of calcium-channel current." Pflugers Arch **406**(3): 241-258.

Cavalli, A., M. Eghbali, et al. (2007). "Localization of sarcolemmal proteins to lipid rafts in the myocardium." Cell Calcium **42**(3): 313-322.

Cerbai, E., U. Klockner, et al. (1988). "Ca-antagonistic effects of adenosine in guinea pig atrial cells." Am J Physiol **255**(4 Pt 2): H872-878.

Cerrone, M. and M. Delmar (2014). "Desmosomes and the sodium channel complex: implications for arrhythmogenic cardiomyopathy and Brugada syndrome." Trends Cardiovasc Med **24**(5): 184-190.

Chase, A. and C. H. Orchard (2011). "Ca efflux via the sarcolemmal Ca ATPase occurs only in the t-tubules of rat ventricular myocytes." J Mol Cell Cardiol **50**(1): 187-193.

Chen-Izu, Y. (2010). "Multiple levels of the single L-type Ca2+ channel conductance in adult mammalian ventricular myocytes." Biochem Biophys Res Commun **391**(1): 604-608.

Chen-Izu, Y., S. L. McCulle, et al. (2006). "Three-dimensional distribution of ryanodine receptor clusters in cardiac myocytes." Biophys J **91**(1): 1-13.

Chen-Izu, Y., R. P. Xiao, et al. (2000). "G(i)-dependent localization of beta(2)-adrenergic receptor signaling to L-type Ca(2+) channels." Biophys J **79**(5): 2547-2556.

Chien, A. J., X. Zhao, et al. (1995). "Roles of a membrane-localized beta subunit in the formation and targeting of functional L-type Ca2+ channels." J Biol Chem **270**(50): 30036-30044.

Christ, T., P. Boknik, et al. (2004). "L-type Ca2+ current downregulation in chronic human atrial fibrillation is associated with increased activity of protein phosphatases." Circulation **110**(17): 2651-2657.

Chu, P. J., J. K. Larsen, et al. (2004). "Distribution and relative expression levels of calcium channel beta subunits within the chambers of the rat heart." J Mol Cell Cardiol **36**(3): 423-434.

Church, P. J. and E. F. Stanley (1996). "Single L-type calcium channel conductance with physiological levels of calcium in chick ciliary ganglion neurons." J Physiol **496 (Pt 1)**: 59-68.

Cioffi, G., G. de Simone, et al. (2007). "Right atrial size and function in patients with pulmonary hypertension associated with disorders of respiratory system or hypoxemia." Eur J Echocardiogr **8**(5): 322-331.

Clancy, C. E., M. Tateyama, et al. (2002). "Insights into the molecular mechanisms of bradycardia-triggered arrhythmias in long QT-3 syndrome." J Clin Invest **110**(9): 1251-1262.

Cloues, R. K. and W. A. Sather (2000). "Permeant ion binding affinity in subconductance states of an L-type Ca2+ channel expressed in Xenopus laevis oocytes." J Physiol **524 Pt 1**: 19-36.

Cohen, A. W., R. Hnasko, et al. (2004). "Role of caveolae and caveolins in health and disease." Physiol Rev **84**(4): 1341-1379.

Cohen, R. M., J. D. Foell, et al. (2005). "Unique modulation of L-type Ca2+ channels by short auxiliary beta1d subunit present in cardiac muscle." Am J Physiol Heart Circ Physiol **288**(5): H2363-2374.

Collin, T., J. J. Wang, et al. (1993). "Molecular cloning of three isoforms of the L-type voltage-dependent calcium channel beta subunit from normal human heart." Circ Res **72**(6): 1337-1344.

Conrath, C. E. and T. Opthof (2002). "beta3-Adrenoceptors in the heart." Cardiovasc Res **56**(3): 353-356.

Cooper, D. M. (2005). "Compartmentalization of adenylate cyclase and cAMP signalling." Biochem Soc Trans **33**(Pt 6): 1319-1322.

Cordeiro, J. M., K. W. Spitzer, et al. (2001). "Location of the initiation site of calcium transients and sparks in rabbit heart Purkinje cells." J Physiol **531**(Pt 2): 301-314.

Correll, R. N., C. Pang, et al. (2007). "Plasma membrane targeting is essential for Rem-mediated Ca2+ channel inhibition." J Biol Chem **282**(39): 28431-28440.

Davare, M. A., V. Avdonin, et al. (2001). "A beta2 adrenergic receptor signaling complex assembled with the Ca2+ channel Cav1.2." Science **293**(5527): 98-101.

Davare, M. A., M. C. Horne, et al. (2000). "Protein phosphatase 2A is associated with class C L-type calcium channels (Cav1.2) and antagonizes channel phosphorylation by cAMP-dependent protein kinase." J Biol Chem **275**(50): 39710-39717.

De Jongh, K. S., B. J. Murphy, et al. (1996). "Specific phosphorylation of a site in the full-length form of the alpha 1 subunit of the cardiac L-type calcium channel by adenosine 3',5'-cyclic monophosphate-dependent protein kinase." Biochemistry **35**(32): 10392-10402.

Dibb, K. M., J. D. Clarke, et al. (2013). "A functional role for transverse (t-) tubules in the atria." J Mol Cell Cardiol **58**: 84-91.

Dibb, K. M., J. D. Clarke, et al. (2009). "Characterization of an extensive transverse tubular network in sheep atrial myocytes and its depletion in heart failure." Circ Heart Fail **2**(5): 482-489.

Dobrev, D., L. Y. Teos, et al. (2009). "Unique atrial myocyte Ca2+ signaling." J Mol Cell Cardiol **46**(4): 448-451.

Dobson, J. G., Jr. (1978). "Reduction by adenosine of the isoproterenol-induced increase in cyclic adenosine 3',5'-monophosphate formation and glycogen phosphorylase activity in rat heart muscle." Circ Res **43**(5): 785-792.

Dobson, J. G., Jr. (1983). "Mechanism of adenosine inhibition of catecholamine-induced responses in heart." Circ Res **52**(2): 151-160.

Dobson, J. G., Jr., L. G. Shea, et al. (2008). "Adenosine A2A and beta-adrenergic calcium transient and contractile responses in rat ventricular myocytes." Am J Physiol Heart Circ Physiol **295**(6): H2364-2372.

Dolphin, A. C. (2003). "Beta subunits of voltage-gated calcium channels." J Bioenerg Biomembr **35**(6): 599-620.

Doyle, J. L. and L. Stubbs (1998). "Ataxia, arrhythmia and ion-channel gene defects." Trends Genet **14**(3): 92-98.

Dukes, I. D. and E. M. Vaughan Williams (1984). "Effects of selective alpha 1-, alpha 2-, beta 1-and beta 2-adrenoceptor stimulation on potentials and contractions in the rabbit heart." J Physiol **355**: 523-546.

Eckstein, J., S. Verheule, et al. (2008). "Mechanisms of perpetuation of atrial fibrillation in chronically dilated atria." Prog Biophys Mol Biol **97**(2-3): 435-451.

El-Armouche, A., P. Boknik, et al. (2006). "Molecular determinants of altered Ca2+ handling in human chronic atrial fibrillation." Circulation **114**(7): 670-680.

Ellinor, P. T., J. Yang, et al. (1995). "Ca2+ channel selectivity at a single locus for high-affinity Ca2+ interactions." Neuron **15**(5): 1121-1132.

Escriche, M., J. Burgueno, et al. (2003). "Ligand-induced caveolae-mediated internalization of A1 adenosine receptors: morphological evidence of endosomal sorting and receptor recycling." Exp Cell Res **285**(1): 72-90.

Fabiato, A. and F. Fabiato (1979). "Calcium and cardiac excitation-contraction coupling." Annu Rev Physiol **41**: 473-484.

Fatema, K., M. E. Barnes, et al. (2009). "Minimum vs. maximum left atrial volume for prediction of first atrial fibrillation or flutter in an elderly cohort: a prospective study." Eur J Echocardiogr **10**(2): 282-286.

Feng, J., L. Yue, et al. (1998). "Ionic mechanisms of regional action potential heterogeneity in the canine right atrium." Circ Res **83**(5): 541-551.

Fenton, R. A. and J. G. Dobson, Jr. (2007). "Adenosine A1 and A2A receptor effects on G-protein cycling in beta-adrenergic stimulated ventricular membranes." J Cell Physiol **213**(3): 785-792.

Fenton, R. A., L. G. Shea, et al. (2010). "Myocardial adenosine A(1)-receptor-mediated adenoprotection involves phospholipase C, PKC-epsilon, and p38 MAPK, but not HSP27." Am J Physiol Heart Circ Physiol **298**(6): H1671-1678.

Feron, O. and J. L. Balligand (2006). "Caveolins and the regulation of endothelial nitric oxide synthase in the heart." Cardiovasc Res **69**(4): 788-797.

Finlin, B. S., S. M. Crump, et al. (2003). "Regulation of voltage-gated calcium channel activity by the Rem and Rad GTPases." Proc Natl Acad Sci U S A **100**(24): 14469-14474.

Foell, J. D., R. C. Balijepalli, et al. (2004). "Molecular heterogeneity of calcium channel beta-subunits in canine and human heart: evidence for differential subcellular localization." Physiol Genomics **17**(2): 183-200.

Forbes, M. S. and E. E. van Neil (1988). "Membrane systems of guinea pig myocardium: ultrastructure and morphometric studies." Anat Rec **222**(4): 362-379.

Forssmann, W. G. and L. Girardier (1970). "A study of the T system in rat heart." J Cell Biol **44**(1): 1-19.

Fozzard, H. A. (2002). "Cardiac sodium and calcium channels: a history of excitatory currents." Cardiovasc Res **55**(1): 1-8.

Franzini-Armstrong, C., F. Protasi, et al. (1999). "Shape, size, and distribution of Ca(2+) release units and couplons in skeletal and cardiac muscles." Biophys J **77**(3): 1528-1539.

Frisk, M., J. T. Koivumaki, et al. (2014). "Variable t-tubule organization and Ca2+ homeostasis across the atria." Am J Physiol Heart Circ Physiol **307**(4): H609-620.

Funakoshi, H., T. O. Chan, et al. (2006). "Regulated overexpression of the A1-adenosine receptor in mice results in adverse but reversible changes in cardiac morphology and function." Circulation **114**(21): 2240-2250.

Fuster, V., L. E. Ryden, et al. (2001). "ACC/AHA/ESC Guidelines for the Management of Patients With Atrial Fibrillation: Executive Summary A Report of the American College of Cardiology/American Heart Association Task Force on Practice Guidelines and the European Society of Cardiology Committee for Practice Guidelines and Policy Conferences (Committee to Develop Guidelines for the Management of Patients With Atrial Fibrillation) Developed in Collaboration With the North American Society of Pacing and Electrophysiology." Circulation **104**(17): 2118-2150.

Galbiati, F., J. A. Engelman, et al. (2001). "Caveolin-3 null mice show a loss of caveolae, changes in the microdomain distribution of the dystrophin-glycoprotein complex, and t-tubule abnormalities." J Biol Chem **276**(24): 21425-21433.

Gao, T., T. S. Puri, et al. (1997). "Identification and subcellular localization of the subunits of L-type calcium channels and adenylyl cyclase in cardiac myocytes." J Biol Chem **272**(31): 19401-19407.

Gerhardstein, B. L., T. Gao, et al. (2000). "Proteolytic processing of the C terminus of the alpha(1C) subunit of L-type calcium channels and the role of a proline-rich

domain in membrane tethering of proteolytic fragments." J Biol Chem **275**(12): 8556-8563.

Gerhardstein, B. L., T. S. Puri, et al. (1999). "Identification of the sites phosphorylated by cyclic AMP-dependent protein kinase on the beta 2 subunit of L-type voltage-dependent calcium channels." Biochemistry **38**(32): 10361-10370.

Glukhov, A. V., A. Kalyanasundaram, et al. (2013). "Calsequestrin 2 deletion causes sinoatrial node dysfunction and atrial arrhythmias associated with altered sarcoplasmic reticulum calcium cycling and degenerative fibrosis within the mouse atrial pacemaker complex." Eur Heart J.

Goebel, J., B. Logan, et al. (2005). "Atorvastatin affects interleukin-2 signaling by altering the lipid raft enrichment of the interleukin-2 receptor beta chain." J Investig Med **53**(6): 322-328.

Gomez, A. M., H. H. Valdivia, et al. (1997). "Defective excitation-contraction coupling in experimental cardiac hypertrophy and heart failure." Science **276**(5313): 800-806.

Gondo, N., K. Ono, et al. (1998). "Four conductance levels of cloned cardiac L-type Ca2+ channel alpha1 and alpha1/beta subunits." FEBS Lett **423**(1): 86-92.

Gorelik, J., L. Q. Yang, et al. (2006). "A novel Z-groove index characterizing myocardial surface structure." Cardiovasc Res **72**(3): 422-429.

Gossop, M. R. and P. H. Connell (1975). "Attitudes of oral and intravenous multiple drug users toward drugs of abuse." Int J Addict **10**(3): 453-466.

Grabner, M., R. T. Dirksen, et al. (1998). "Tagging with green fluorescent protein reveals a distinct subcellular distribution of L-type and non-L-type Ca2+ channels expressed in dysgenic myotubes." Proc Natl Acad Sci U S A **95**(4): 1903-1908.

Grammer, J. B., X. Zeng, et al. (2001). "Atrial L-type Ca2+-channel, beta-adrenorecptor, and 5-hydroxytryptamine type 4 receptor mRNAs in human atrial fibrillation." Basic Res Cardiol **96**(1): 82-90.

Grandi, E., S. V. Pandit, et al. (2011). "Human atrial action potential and Ca2+ model: sinus rhythm and chronic atrial fibrillation." Circ Res **109**(9): 1055-1066.

Grandy, S. A., E. M. Denovan-Wright, et al. (2004). "Overexpression of human beta2-adrenergic receptors increases gain of excitation-contraction coupling in mouse ventricular myocytes." Am J Physiol Heart Circ Physiol **287**(3): H1029-1038.

Gratton, J. P., P. Bernatchez, et al. (2004). "Caveolae and caveolins in the cardiovascular system." Circ Res **94**(11): 1408-1417.

Greif, G. J., Y. J. Lin, et al. (1995). "Role of cyclic AMP in dopamine modulation of potassium channels on rat striatal neurons: regulation of a subconductance state." Synapse **21**(3): 275-277.

Greiser, M., H. R. Neuberger, et al. (2009). "Distinct contractile and molecular differences between two goat models of atrial dysfunction: AV block-induced atrial dilatation and atrial fibrillation." J Mol Cell Cardiol **46**(3): 385-394.

Gu, Y., J. Gorelik, et al. (2002). "High-resolution scanning patch-clamp: new insights into cell function." FASEB J **16**(7): 748-750.

Guatimosim, S., K. Dilly, et al. (2002). "Local Ca(2+) signaling and EC coupling in heart: Ca(2+) sparks and the regulation of the [Ca(2+)](i) transient." J Mol Cell Cardiol **34**(8): 941-950.

Guo, Y., U. Golebiewska, et al. (2011). "Modulation of Ca(2)+ activity in cardiomyocytes through caveolae-Galphaq interactions." Biophys J **100**(7): 1599-1607.

Haase, H., P. Karczewski, et al. (1993). "Phosphorylation of the L-type calcium channel beta subunit is involved in beta-adrenergic signal transduction in canine myocardium." FEBS Lett **335**(2): 217-222.

Haase, H., B. Pfitzmaier, et al. (2000). "Expression of Ca(2+) channel subunits during cardiac ontogeny in mice and rats: identification of fetal alpha(1C) and beta subunit isoforms." J Cell Biochem **76**(4): 695-703.

Haase, H., T. Podzuweit, et al. (1999). "Signaling from beta-adrenoceptor to L-type calcium channel: identification of a novel cardiac protein kinase A target possessing similarities to AHNAK." FASEB J **13**(15): 2161-2172.

Haddock, P. S., W. A. Coetzee, et al. (1999). "Subcellular [Ca2+]i gradients during excitation-contraction coupling in newborn rabbit ventricular myocytes." Circ Res **85**(5): 415-427.

Haft, J. I. (1974). "Cardiovascular injury induced by sympathetic catecholamines." Prog Cardiovasc Dis **17**(1): 73-86.

Haissaguerre, M., P. Jais, et al. (1998). "Spontaneous initiation of atrial fibrillation by ectopic beats originating in the pulmonary veins." N Engl J Med **339**(10): 659-666.

Han, M. K., V. V. McLaughlin, et al. (2007). "Pulmonary diseases and the heart." Circulation **116**(25): 2992-3005.

Hanlon, M. R. and B. A. Wallace (2002). "Structure and function of voltage-dependent ion channel regulatory beta subunits." Biochemistry **41**(9): 2886-2894.

Hansma, P. K., B. Drake, et al. (1989). "The scanning ion-conductance microscope." Science **243**(4891): 641-643.

Harvey, R. D. and S. C. Calaghan (2012). "Caveolae create local signalling domains through their distinct protein content, lipid profile and morphology." J Mol Cell Cardiol **52**(2): 366-375.

Hatem, S. N., A. Benardeau, et al. (1997). "Different compartments of sarcoplasmic reticulum participate in the excitation-contraction coupling process in human atrial myocytes." Circ Res **80**(3): 345-353.

He, J., M. W. Conklin, et al. (2001). "Reduction in density of transverse tubules and L-type Ca(2+) channels in canine tachycardia-induced heart failure." Cardiovasc Res **49**(2): 298-307.

Head, B. P., H. H. Patel, et al. (2005). "G-protein-coupled receptor signaling components localize in both sarcolemmal and intracellular caveolin-3-associated microdomains in adult cardiac myocytes." J Biol Chem **280**(35): 31036-31044.

Headrick, J. and R. J. Willis (1989). "Endogenous adenosine improves work rate to oxygen consumption ratio in catecholamine stimulated isovolumic rat heart." Pflugers Arch **413**(4): 354-358.

Heinzel, F. R., V. Bito, et al. (2008). "Remodeling of T-tubules and reduced synchrony of Ca2+ release in myocytes from chronically ischemic myocardium." Circ Res **102**(3): 338-346.

Hell, J. W., C. T. Yokoyama, et al. (1995). "Phosphorylation of presynaptic and postsynaptic calcium channels by cAMP-dependent protein kinase in hippocampal neurons." EMBO J **14**(13): 3036-3044.

Hell, J. W., C. T. Yokoyama, et al. (1993). "Differential phosphorylation of two size forms of the neuronal class C L-type calcium channel alpha 1 subunit." J Biol Chem **268**(26): 19451-19457.

Henderson, S. A., J. I. Goldhaber, et al. (2004). "Functional adult myocardium in the absence of Na+-Ca2+ exchange: cardiac-specific knockout of NCX1." Circ Res **95**(6): 604-611.

Heo, W. D., T. Inoue, et al. (2006). "PI(3,4,5)P3 and PI(4,5)P2 lipids target proteins with polybasic clusters to the plasma membrane." Science **314**(5804): 1458-1461.

Hermosilla, T., C. Moreno, et al. (2011). "L-type calcium channel beta subunit modulates angiotensin II responses in cardiomyocytes." Channels (Austin) **5**(3): 280-286.

Hess, P., J. B. Lansman, et al. (1984). "Different modes of Ca channel gating behaviour favoured by dihydropyridine Ca agonists and antagonists." Nature **311**(5986): 538-544.

Hobai, I. A. and B. O'Rourke (2001). "Decreased sarcoplasmic reticulum calcium content is responsible for defective excitation-contraction coupling in canine heart failure." Circulation **103**(11): 1577-1584.

Hoffman BF, C. P. (1960). "Electrophysiology of the Heart." New York: McGraw-Hill Book Company

1-323: 323.

Hohendanner, F., S. Walther, et al. (2014). "Inositol-1,4,5-trisphosphate induced Ca2+ release and excitation-contraction coupling in atrial myocytes from normal and failing hearts." J Physiol.

Horn, T., N. D. Ullrich, et al. (2013). "'Eventless' InsP3-dependent SR-Ca2+ release affecting atrial Ca2+ sparks." J Physiol **591**(Pt 8): 2103-2111.

Houslay, M. D., G. S. Baillie, et al. (2007). "cAMP-Specific phosphodiesterase-4 enzymes in the cardiovascular system: a molecular toolbox for generating compartmentalized cAMP signaling." Circ Res **100**(7): 950-966.

Hullin, R., F. Asmus, et al. (1999). "Subunit expression of the cardiac L-type calcium channel is differentially regulated in diastolic heart failure of the cardiac allograft." Circulation **100**(2): 155-163.

Hullin, R., I. F. Khan, et al. (2003). "Cardiac L-type calcium channel beta-subunits expressed in human heart have differential effects on single channel characteristics." J Biol Chem **278**(24): 21623-21630.

Hullin, R., J. Matthes, et al. (2007). "Increased expression of the auxiliary beta(2)-subunit of ventricular L-type Ca(2)+ channels leads to single-channel activity characteristic of heart failure." PLoS One **2**(3): e292.

Hullin, R., D. Singer-Lahat, et al. (1992). "Calcium channel beta subunit heterogeneity: functional expression of cloned cDNA from heart, aorta and brain." EMBO J **11**(3): 885-890.

Hulme, J. T., T. W. Lin, et al. (2003). "Beta-adrenergic regulation requires direct anchoring of PKA to cardiac CaV1.2 channels via a leucine zipper interaction with A kinase-anchoring protein 15." Proc Natl Acad Sci U S A **100**(22): 13093-13098.

Huser, J., S. L. Lipsius, et al. (1996). "Calcium gradients during excitation-contraction coupling in cat atrial myocytes." J Physiol **494 (Pt 3)**: 641-651.

Ibrahim, M., J. Gorelik, et al. (2011). "The structure and function of cardiac t-tubules in health and disease." Proc Biol Sci **278**(1719): 2714-2723.

Judge, T. P., J. W. Kennedy, et al. (1971). "Quantitative hemodynamic effects of heart rate in aortic regurgitation." Circulation **44**(3): 355-367.

Jurevicius, J., V. A. Skeberdis, et al. (2003). "Role of cyclic nucleotide phosphodiesterase isoforms in cAMP compartmentation following beta2-adrenergic stimulation of ICa,L in frog ventricular myocytes." J Physiol **551**(Pt 1): 239-252.

Kaftan, E., A. R. Marks, et al. (1996). "Effects of rapamycin on ryanodine receptor/Ca(2+)-release channels from cardiac muscle." Circ Res **78**(6): 990-997.

Kalman, J. M., M. Munawar, et al. (1995). "Atrial fibrillation after coronary artery bypass grafting is associated with sympathetic activation." Ann Thorac Surg **60**(6): 1709-1715.

Kamada, Y., Y. Yamada, et al. (2004). "Single-channel activity of L-type Ca2+ channels reconstituted with the beta2c subunit cloned from the rat heart." Eur J Pharmacol **487**(1-3): 37-45.

Kamp, T. J. and J. W. Hell (2000). "Regulation of cardiac L-type calcium channels by protein kinase A and protein kinase C." Circ Res **87**(12): 1095-1102.

Kamp, T. J., M. T. Perez-Garcia, et al. (1996). "Enhancement of ionic current and charge movement by coexpression of calcium channel beta 1A subunit with alpha 1C subunit in a human embryonic kidney cell line." J Physiol **492 (Pt 1)**: 89-96.

Kass, D. A., J. G. Bronzwaer, et al. (2004). "What mechanisms underlie diastolic dysfunction in heart failure?" Circ Res **94**(12): 1533-1542.

Kaumann, A. J. and L. Sanders (1993). "Both beta 1- and beta 2-adrenoceptors mediate catecholamine-evoked arrhythmias in isolated human right atrium." Naunyn Schmiedebergs Arch Pharmacol **348**(5): 536-540.

Kawai, M., M. Hussain, et al. (1999). "Excitation-contraction coupling in rat ventricular myocytes after formamide-induced detubulation." Am J Physiol **277**(2 Pt 2): H603-609.

Keef, K. D., J. R. Hume, et al. (2001). "Regulation of cardiac and smooth muscle Ca(2+) channels (Ca(V)1.2a,b) by protein kinases." Am J Physiol Cell Physiol **281**(6): C1743-1756.

Khairy, P. and S. Nattel (2002). "New insights into the mechanisms and management of atrial fibrillation." CMAJ **167**(9): 1012-1020.

Kirk, M. M., L. T. Izu, et al. (2003). "Role of the transverse-axial tubule system in generating calcium sparks and calcium transients in rat atrial myocytes." J Physiol **547**(Pt 2): 441-451.

Klein, G., H. Drexler, et al. (2000). "Protein kinase G reverses all isoproterenol induced changes of cardiac single L-type calcium channel gating." Cardiovasc Res **48**(3): 367-374.

Klein, G., F. Schroder, et al. (2003). "Increased open probability of single cardiac L-type calcium channels in patients with chronic atrial fibrillation. role of phosphatase 2A." Cardiovasc Res **59**(1): 37-45.

Klockner, U. and G. Isenberg (1994). "Intracellular pH modulates the availability of vascular L-type Ca2+ channels." J Gen Physiol **103**(4): 647-663.

Kockskamper, J., K. A. Sheehan, et al. (2001). "Activation and propagation of Ca(2+) release during excitation-contraction coupling in atrial myocytes." Biophys J **81**(5): 2590-2605.

Koivumaki, J. T., T. Korhonen, et al. (2011). "Impact of sarcoplasmic reticulum calcium release on calcium dynamics and action potential morphology in human atrial myocytes: a computational study." PLoS Comput Biol **7**(1): e1001067.

Korchev, Y. E., C. L. Bashford, et al. (1997). "Scanning ion conductance microscopy of living cells." Biophys J **73**(2): 653-658.

Korchev, Y. E., M. Milovanovic, et al. (1997). "Specialized scanning ion-conductance microscope for imaging of living cells." J Microsc **188**(Pt 1): 17-23.

Kroll, K., U. K. Decking, et al. (1993). "Rapid turnover of the AMP-adenosine metabolic cycle in the guinea pig heart." Circ Res **73**(5): 846-856.

Kunze, D. L. and A. K. Ritchie (1990). "Multiple conductance levels of the dihydropyridine-sensitive calcium channel in GH3 cells." J Membr Biol **118**(2): 171-178.

Kuo, C. C. and B. P. Bean (1993). "G-protein modulation of ion permeation through N-type calcium channels." Nature **365**(6443): 258-262.

Kurzchalia, T. V. and R. G. Parton (1999). "Membrane microdomains and caveolae." Curr Opin Cell Biol **11**(4): 424-431.

Kuznetsov, V., E. Pak, et al. (1995). "Beta 2-adrenergic receptor actions in neonatal and adult rat ventricular myocytes." Circ Res **76**(1): 40-52.

Lacerda, A. E., H. S. Kim, et al. (1991). "Normalization of current kinetics by interaction between the alpha 1 and beta subunits of the skeletal muscle dihydropyridine-sensitive Ca2+ channel." Nature **352**(6335): 527-530.

Lacinova, L., A. Ludwig, et al. (1995). "The block of the expressed L-type calcium channel is modulated by the beta 3 subunit." FEBS Lett **373**(2): 103-107.

Lai, L. P., M. J. Su, et al. (1999). "Down-regulation of L-type calcium channel and sarcoplasmic reticular Ca(2+)-ATPase mRNA in human atrial fibrillation without significant change in the mRNA of ryanodine receptor, calsequestrin and phospholamban: an insight into the mechanism of atrial electrical remodeling." J Am Coll Cardiol **33**(5): 1231-1237.

Lefkowitz, R. J., H. A. Rockman, et al. (2000). "Catecholamines, cardiac beta-adrenergic receptors, and heart failure." Circulation **101**(14): 1634-1637.

Leimbach, W. N., Jr., B. G. Wallin, et al. (1986). "Direct evidence from intraneural recordings for increased central sympathetic outflow in patients with heart failure." Circulation **73**(5): 913-919.

Lenaerts, I., V. Bito, et al. (2009). "Ultrastructural and functional remodeling of the coupling between Ca2+ influx and sarcoplasmic reticulum Ca2+ release in right atrial myocytes from experimental persistent atrial fibrillation." Circ Res **105**(9): 876-885.

Levin, K. R. and E. Page (1980). "Quantitative studies on plasmalemmal folds and caveolae of rabbit ventricular myocardial cells." Circ Res **46**(2): 244-255.

Lindner, M., M. C. Brandt, et al. (2002). "Calcium sparks in human ventricular cardiomyocytes from patients with terminal heart failure." Cell Calcium **31**(4): 175-182.

Lindner, M., E. Erdmann, et al. (1998). "Calcium content of the sarcoplasmic reticulum in isolated ventricular myocytes from patients with terminal heart failure." J Mol Cell Cardiol **30**(4): 743-749.

Lipp, P., J. Huser, et al. (1996). "Spatially non-uniform Ca2+ signals induced by the reduction of transverse tubules in citrate-loaded guinea-pig ventricular myocytes in culture." J Physiol **497 (Pt 3)**: 589-597.

Lipp, P., M. Laine, et al. (2000). "Functional InsP3 receptors that may modulate excitation-contraction coupling in the heart." Curr Biol **10**(15): 939-942.

Lipp, P., L. Pott, et al. (1990). "Simultaneous recording of Indo-1 fluorescence and Na+/Ca2+ exchange current reveals two components of Ca2(+)-release from sarcoplasmic reticulum of cardiac atrial myocytes." FEBS Lett **275**(1-2): 181-184.

Lisanti, M. P., P. E. Scherer, et al. (1994). "Characterization of caveolin-rich membrane domains isolated from an endothelial-rich source: implications for human disease." J Cell Biol **126**(1): 111-126.

Liu, W., K. Yasui, et al. (1999). "beta-adrenergic modulation of L-type Ca2+-channel currents in early-stage embryonic mouse heart." Am J Physiol **276**(2 Pt 2): H608-613.

Lohn, M., M. Furstenau, et al. (2000). "Ignition of calcium sparks in arterial and cardiac muscle through caveolae." Circ Res **87**(11): 1034-1039.

Lorbar, M., E. S. Chung, et al. (2004). "Receptors subtypes involved in adenosine-mediated modulation of norepinephrine release from cardiac nerve terminals." Can J Physiol Pharmacol **82**(11): 1026-1031.

Lou, Q., V. V. Fedorov, et al. (2011). "Transmural heterogeneity and remodeling of ventricular excitation-contraction coupling in human heart failure." Circulation **123**(17): 1881-1890.

Louch, W. E., V. Bito, et al. (2004). "Reduced synchrony of Ca2+ release with loss of T-tubules-a comparison to Ca2+ release in human failing cardiomyocytes." Cardiovasc Res **62**(1): 63-73.

Louch, W. E., H. K. Mork, et al. (2006). "T-tubule disorganization and reduced synchrony of Ca2+ release in murine cardiomyocytes following myocardial infarction." J Physiol **574**(Pt 2): 519-533.

Luo, C. H. and Y. Rudy (1994). "A dynamic model of the cardiac ventricular action potential. I. Simulations of ionic currents and concentration changes." Circ Res **74**(6): 1071-1096.

Luss, I., P. Boknik, et al. (1999). "Expression of cardiac calcium regulatory proteins in atrium v ventricle in different species." J Mol Cell Cardiol **31**(6): 1299-1314.

Lyon, A. R., M. L. Bannister, et al. (2011). "SERCA2a gene transfer decreases sarcoplasmic reticulum calcium leak and reduces ventricular arrhythmias in a model of chronic heart failure." Circ Arrhythm Electrophysiol **4**(3): 362-372.

Lyon, A. R., K. T. MacLeod, et al. (2009). "Loss of T-tubules and other changes to surface topography in ventricular myocytes from failing human and rat heart." Proc Natl Acad Sci U S A **106**(16): 6854-6859.

Ma, J. and R. Coronado (1988). "Heterogeneity of conductance states in calcium channels of skeletal muscle." Biophys J **53**(3): 387-395.

Mackenzie, L., M. D. Bootman, et al. (2001). "Predetermined recruitment of calcium release sites underlies excitation-contraction coupling in rat atrial myocytes." J Physiol **530**(Pt 3): 417-429.

Mackenzie, L., H. L. Roderick, et al. (2004). "The spatial pattern of atrial cardiomyocyte calcium signalling modulates contraction." J Cell Sci **117**(Pt 26): 6327-6337.

Maguy, A., T. E. Hebert, et al. (2006). "Involvement of lipid rafts and caveolae in cardiac ion channel function." Cardiovasc Res **69**(4): 798-807.

Maisel, W. H. and L. W. Stevenson (2003). "Atrial fibrillation in heart failure: epidemiology, pathophysiology, and rationale for therapy." Am J Cardiol **91**(6A): 2D-8D.

Makarewich, C. A., R. N. Correll, et al. (2012). "A caveolae-targeted L-type Ca(2)+ channel antagonist inhibits hypertrophic signaling without reducing cardiac contractility." Circ Res **110**(5): 669-674.

Mallet, R. T., S. C. Lee, et al. (1996). "Endogenous adenosine increases O2 utilisation efficiency in isoprenaline-stimulated canine myocardium." Cardiovasc Res **31**(1): 102-116.

Mangoni, M. E., B. Couette, et al. (2003). "Functional role of L-type Cav1.3 Ca2+ channels in cardiac pacemaker activity." Proc Natl Acad Sci U S A **100**(9): 5543-5548.

Marban, E. (2002). "Cardiac channelopathies." Nature **415**(6868): 213-218.

Markandeya, Y. S., L. Feng, et al. (2013). "Caveolin-3 Regulates Cardiac Repolarization by Integrated Regulation of Multiple Ionic Currents." Circulation **128**: A15009.

Marx, S. O., S. Reiken, et al. (2000). "PKA phosphorylation dissociates FKBP12.6 from the calcium release channel (ryanodine receptor): defective regulation in failing hearts." Cell **101**(4): 365-376.

Matsuda, Y., Y. Toma, et al. (1983). "Importance of left atrial function in patients with myocardial infarction." Circulation **67**(3): 566-571.

Matsumura, T., E. Ohtaki, et al. (2003). "Echocardiographic prediction of left ventricular dysfunction after mitral valve repair for mitral regurgitation as an indicator to decide the optimal timing of repair." J Am Coll Cardiol **42**(3): 458-463.

McDonald, T. F., S. Pelzer, et al. (1994). "Regulation and modulation of calcium channels in cardiac, skeletal, and smooth muscle cells." Physiol Rev **74**(2): 365-507.

Meyer, T. E., E. S. Chung, et al. (2001). "Antiadrenergic effects of adenosine in pressure overload hypertrophy." Hypertension **37**(3): 862-868.

Mikami, A., K. Imoto, et al. (1989). "Primary structure and functional expression of the cardiac dihydropyridine-sensitive calcium channel." Nature **340**(6230): 230-233.

Mitterdorfer, J., M. Froschmayr, et al. (1994). "Calcium channels: the beta-subunit increases the affinity of dihydropyridine and Ca2+ binding sites of the alpha 1-subunit." FEBS Lett **352**(2): 141-145.

Nattel, S. (2002). "New ideas about atrial fibrillation 50 years on." Nature **415**(6868): 219-226.

Nattel, S., J. Andrade, et al. (2014). "New directions in cardiac arrhythmia management: present challenges and future solutions." Can J Cardiol **30**(12 Suppl): S420-430.

Nattel, S. and R. A. Khan (2007). "Protein kinase C, connexin43, and ischemic preconditioning: complex interactions of potential importance for controlling arrhythmias." Heart Rhythm **4**(9): 1194-1195.

Neef, S., N. Dybkova, et al. (2010). "CaMKII-dependent diastolic SR Ca2+ leak and elevated diastolic Ca2+ levels in right atrial myocardium of patients with atrial fibrillation." Circ Res **106**(6): 1134-1144.

Nerbonne, J. M. and R. S. Kass (2005). "Molecular physiology of cardiac repolarization." Physiol Rev **85**(4): 1205-1253.

Newby, A. C., Y. Worku, et al. (1985). "Adenosine formation. Evidence for a direct biochemical link with energy metabolism." Adv Myocardiol **6**: 273-284.

Nikolaev, V. O., A. Moshkov, et al. (2010). "Beta2-adrenergic receptor redistribution in heart failure changes cAMP compartmentation." Science **327**(5973): 1653-1657.

Norman, R. I. and R. N. Leach (1994). "Subunit structure and phosphorylation of the cardiac L-type calcium channel." Biochem Soc Trans **22**(2): 492-496.

Novak, P., J. Gorelik, et al. (2013). "Nanoscale-targeted patch-clamp recordings of functional presynaptic ion channels." Neuron **79**(6): 1067-1077.

Novak, P., C. Li, et al. (2009). "Nanoscale live-cell imaging using hopping probe ion conductance microscopy." Nat Methods **6**(4): 279-281.

Ochi, R. and Y. Kawashima (1990). "Modulation of slow gating process of calcium channels by isoprenaline in guinea-pig ventricular cells." J Physiol **424**: 187-204.

Pang, T., X. T. Gan, et al. (2010). "Compensatory upregulation of the adenosine system following phenylephrine-induced hypertrophy in cultured rat ventricular myocytes." Am J Physiol Heart Circ Physiol **298**(2): H545-553.

Parton, R. G., M. Way, et al. (1997). "Caveolin-3 associates with developing T-tubules during muscle differentiation." J Cell Biol **136**(1): 137-154.

Peivandi, A. A., A. Huhn, et al. (2005). "Upregulation of phospholipase d expression and activation in ventricular pressure-overload hypertrophy." J Pharmacol Sci **98**(3): 244-254.

Perets, T., Y. Blumenstein, et al. (1996). "A potential site of functional modulation by protein kinase A in the cardiac Ca2+ channel alpha 1C subunit." FEBS Lett **384**(2): 189-192.

Perez-Reyes, E. (2003). "Molecular physiology of low-voltage-activated t-type calcium channels." Physiol Rev **83**(1): 117-161.

Perez-Reyes, E., A. Castellano, et al. (1992). "Cloning and expression of a cardiac/brain beta subunit of the L-type calcium channel." J Biol Chem **267**(3): 1792-1797.

Perez-Reyes, E. and T. Schneider (1995). "Molecular biology of calcium channels." Kidney Int **48**(4): 1111-1124.

Perlini, S., B. Arosio, et al. (2007). "Adenosine A1 receptor expression during the transition from compensated pressure overload hypertrophy to heart failure." J Hypertens **25**(2): 449-454.

Perlini, S., E. P. Khoury, et al. (1998). "Adenosine mediates sustained adrenergic desensitization in the rat heart via activation of protein kinase C." Circ Res **83**(7): 761-771.

Phillip, B., D. Pastor, et al. (2003). "The prevalence of preoperative diastolic filling abnormalities in geriatric surgical patients." Anesth Analg **97**(5): 1214-1221.

Pierard, L. A. and B. A. Carabello (2010). "Ischaemic mitral regurgitation: pathophysiology, outcomes and the conundrum of treatment." Eur Heart J **31**(24): 2996-3005.

Platzer, J., J. Engel, et al. (2000). "Congenital deafness and sinoatrial node dysfunction in mice lacking class D L-type Ca2+ channels." Cell **102**(1): 89-97.

Pogwizd, S. M., K. Schlotthauer, et al. (2001). "Arrhythmogenesis and contractile dysfunction in heart failure: Roles of sodium-calcium exchange, inward rectifier potassium current, and residual beta-adrenergic responsiveness." Circ Res **88**(11): 1159-1167.

Post, S. R., H. K. Hammond, et al. (1999). "Beta-adrenergic receptors and receptor signaling in heart failure." Annu Rev Pharmacol Toxicol **39**: 343-360.

Psaty, B. M., T. A. Manolio, et al. (1997). "Incidence of and risk factors for atrial fibrillation in older adults." Circulation **96**(7): 2455-2461.

Qu, Y., E. Karnabi, et al. (2011). "Perinatal and postnatal expression of Cav1.3 alpha1D Ca(2)(+) channel in the rat heart." Pediatr Res **69**(6): 479-484.

Rasmussen, H. H., G. A. Figtree, et al. (2009). "The use of beta3-adrenergic receptor agonists in the treatment of heart failure." Curr Opin Investig Drugs **10**(9): 955-962.

Ratajczak, P., T. Damy, et al. (2003). "Caveolin-1 and -3 dissociations from caveolae to cytosol in the heart during aging and after myocardial infarction in rat." Cardiovasc Res **57**(2): 358-369.

Razani, B., S. E. Woodman, et al. (2002). "Caveolae: from cell biology to animal physiology." Pharmacol Rev **54**(3): 431-467.

Reuter, H. (1983). "Calcium channel modulation by neurotransmitters, enzymes and drugs." Nature **301**(5901): 569-574.

Rheinlaender, J. S., Tilman E. (2009). "Image formation, resolution, and height measurement in scanning ion conductance microscopy." Journal of Applied Physics **105**(9).

Richards, M. A., J. D. Clarke, et al. (2011). "Transverse tubules are a common feature in large mammalian atrial myocytes including human." Am J Physiol Heart Circ Physiol **301**(5): H1996-2005.

Richardt, G., W. Waas, et al. (1987). "Adenosine inhibits exocytotic release of endogenous noradrenaline in rat heart: a protective mechanism in early myocardial ischemia." Circ Res **61**(1): 117-123.

Rickert, D. E. and L. J. Fischer (1975). "Cyproheptadine and beta cell function in the rat: insulin secretion from pancreas segments in vitro." Proc Soc Exp Biol Med **150**(1): 1-6.

Romano, F. D. and J. G. Dobson, Jr. (1990). "Adenosine modulates beta-adrenergic signal transduction in guinea-pig heart ventricular membranes." J Mol Cell Cardiol **22**(12): 1359-1370.

Rosca, M., P. Lancellotti, et al. (2011). "Left atrial function: pathophysiology, echocardiographic assessment, and clinical applications." Heart **97**(23): 1982-1989.

Rosenberg, M. A. and W. J. Manning (2012). "Diastolic dysfunction and risk of atrial fibrillation: a mechanistic appraisal." Circulation **126**(19): 2353-2362.

Rosenberg, R. L., P. Hess, et al. (1988). "Cardiac calcium channels in planar lipid bilayers. L-type channels and calcium-permeable channels open at negative membrane potentials." J Gen Physiol **92**(1): 27-54.

Rudy, Y., M. J. Ackerman, et al. (2008). "Systems approach to understanding electromechanical activity in the human heart: a national heart, lung, and blood institute workshop summary." Circulation **118**(11): 1202-1211.

Rybin, V. O., X. Xu, et al. (2000). "Differential targeting of beta -adrenergic receptor subtypes and adenylyl cyclase to cardiomyocyte caveolae. A mechanism to functionally regulate the cAMP signaling pathway." J Biol Chem **275**(52): 41447-41457.

Saks, V., P. Dzeja, et al. (2006). "Cardiac system bioenergetics: metabolic basis of the Frank-Starling law." J Physiol **571**(Pt 2): 253-273.

Sanchez-Alonso, J. L., N. Bhogal, et al. (2014). "Microdomain specific modulation of single L-type calcium channels revealed by super-resolution scanning patch-clamp in human failing cardiomyocytes." Heart Rhythm.

Sanfilippo, A. J., V. M. Abascal, et al. (1990). "Atrial enlargement as a consequence of atrial fibrillation. A prospective echocardiographic study." Circulation **82**(3): 792-797.

Santos, P. E., L. C. Barcellos, et al. (1995). "Ventricular action potential and L-type calcium channel in infarct-induced hypertrophy in rats." J Cardiovasc Electrophysiol **6**(11): 1004-1014.

Saraiva, R. M., Y. Matsumura, et al. (2010). "Relation of left atrial dysfunction to pulmonary artery hypertension in patients with aortic stenosis and left ventricular systolic dysfunction." Am J Cardiol **106**(3): 409-416.

Schaper, J., S. Kostin, et al. (2002). "Structural remodelling in heart failure." Exp Clin Cardiol **7**(2-3): 64-68.

Schilling, R. J., A. H. Kadish, et al. (2000). "Endocardial mapping of atrial fibrillation in the human right atrium using a non-contact catheter." Eur Heart J **21**(7): 550-564.

Schindelin, J., I. Arganda-Carreras, et al. (2012). "Fiji: an open-source platform for biological-image analysis." Nat Methods **9**(7): 676-682.

Schotten, U., J. Ausma, et al. (2001). "Cellular mechanisms of depressed atrial contractility in patients with chronic atrial fibrillation." Circulation **103**(5): 691-698.

Schotten, U., M. Greiser, et al. (2002). "Atrial fibrillation-induced atrial contractile dysfunction: a tachycardiomyopathy of a different sort." Cardiovasc Res **53**(1): 192-201.

Schotten, U., H. Haase, et al. (2003). "The L-type Ca2+-channel subunits alpha1C and beta2 are not downregulated in atrial myocardium of patients with chronic atrial fibrillation." J Mol Cell Cardiol **35**(5): 437-443.

Schulson, M. N., D. R. Scriven, et al. (2011). "Couplons in rat atria form distinct subgroups defined by their molecular partners." J Cell Sci **124**(Pt 7): 1167-1174.

Schwencke, C., M. Yamamoto, et al. (1999). "Compartmentation of cyclic adenosine 3',5'-monophosphate signaling in caveolae." Mol Endocrinol **13**(7): 1061-1070.

Schwinger, R. H., G. Munch, et al. (1999). "Reduced Ca(2+)-sensitivity of SERCA 2a in failing human myocardium due to reduced serin-16 phospholamban phosphorylation." J Mol Cell Cardiol **31**(3): 479-491.

Scriven, D. R., P. Asghari, et al. (2013). "Microarchitecture of the dyad." Cardiovasc Res **98**(2): 169-176.

Scriven, D. R., P. Dan, et al. (2000). "Distribution of proteins implicated in excitation-contraction coupling in rat ventricular myocytes." Biophys J **79**(5): 2682-2691.

Scriven, D. R., A. Klimek, et al. (2002). "The molecular architecture of calcium microdomains in rat cardiomyocytes." Ann N Y Acad Sci **976**: 488-499.

Shacklock, P. S., W. G. Wier, et al. (1995). "Local Ca2+ transients (Ca2+ sparks) originate at transverse tubules in rat heart cells." J Physiol **487 (Pt 3)**: 601-608.

Sham, J. S., L. Cleemann, et al. (1995). "Functional coupling of Ca2+ channels and ryanodine receptors in cardiac myocytes." Proc Natl Acad Sci U S A **92**(1): 121-125.

Sheehan, K. A. and L. A. Blatter (2003). "Regulation of junctional and non-junctional sarcoplasmic reticulum calcium release in excitation-contraction coupling in cat atrial myocytes." J Physiol **546**(Pt 1): 119-135.

Shibata, E. F., T. L. Brown, et al. (2006). "Autonomic regulation of voltage-gated cardiac ion channels." J Cardiovasc Electrophysiol **17 Suppl 1**: S34-S42.

Shorofsky, S. R., R. Aggarwal, et al. (1999). "Cellular mechanisms of altered contractility in the hypertrophied heart: big hearts, big sparks." Circ Res **84**(4): 424-434.

Shryock, J. C. and L. Belardinelli (1997). "Adenosine and adenosine receptors in the cardiovascular system: biochemistry, physiology, and pharmacology." Am J Cardiol **79**(12A): 2-10.

Singer, D., M. Biel, et al. (1991). "The roles of the subunits in the function of the calcium channel." Science **253**(5027): 1553-1557.

Sipido, K. R., K. Acsai, et al. (2013). "T-tubule remodelling and ryanodine receptor organization modulate sodium-calcium exchange." Adv Exp Med Biol **961**: 375-383.

Sipido, K. R. and H. Cheng (2013). "T-tubules and ryanodine receptor microdomains: on the road to translation." Cardiovasc Res **98**(2): 159-161.

Sjaastad, I., J. A. Wasserstrom, et al. (2003). "Heart failure -- a challenge to our current concepts of excitation-contraction coupling." J Physiol **546**(Pt 1): 33-47.

Smyrnias, I., W. Mair, et al. (2010). "Comparison of the T-tubule system in adult rat ventricular and atrial myocytes, and its role in excitation-contraction coupling and inotropic stimulation." Cell Calcium **47**(3): 210-223.

Soeller, C. and M. B. Cannell (1999). "Examination of the transverse tubular system in living cardiac rat myocytes by 2-photon microscopy and digital image-processing techniques." Circ Res **84**(3): 266-275.

Song, K. S., P. E. Scherer, et al. (1996). "Expression of caveolin-3 in skeletal, cardiac, and smooth muscle cells. Caveolin-3 is a component of the sarcolemma and co-fractionates with dystrophin and dystrophin-associated glycoproteins." J Biol Chem **271**(25): 15160-15165.

Song, L. S., Y. Pi, et al. (2005). "Paradoxical cellular Ca2+ signaling in severe but compensated canine left ventricular hypertrophy." Circ Res **97**(5): 457-464.

Song, L. S., E. A. Sobie, et al. (2006). "Orphaned ryanodine receptors in the failing heart." Proc Natl Acad Sci U S A **103**(11): 4305-4310.

Stagg, M. A., E. Carter, et al. (2008). "Cytoskeletal protein 4.1R affects repolarization and regulates calcium handling in the heart." Circ Res **103**(8): 855-863.

Steinberg, S. F. (2004). "beta(2)-Adrenergic receptor signaling complexes in cardiomyocyte caveolae/lipid rafts." J Mol Cell Cardiol **37**(2): 407-415.

Steinberg, S. F. and L. L. Brunton (2001). "Compartmentation of G protein-coupled signaling pathways in cardiac myocytes." Annu Rev Pharmacol Toxicol **41**: 751-773.

Striessnig, J. (1999). "Pharmacology, structure and function of cardiac L-type Ca(2+) channels." Cell Physiol Biochem **9**(4-5): 242-269.

Suga, H., R. Hisano, et al. (1983). "Effect of positive inotropic agents on the relation between oxygen consumption and systolic pressure volume area in canine left ventricle." Circ Res **53**(3): 306-318.

Suga, H. and K. Sagawa (1974). "Instantaneous pressure-volume relationships and their ratio in the excised, supported canine left ventricle." Circ Res **35**(1): 117-126.

Swift, F., J. A. Birkeland, et al. (2008). "Altered Na+/Ca2+-exchanger activity due to downregulation of Na+/K+-ATPase alpha2-isoform in heart failure." Cardiovasc Res **78**(1): 71-78.

Takimoto, K., D. Li, et al. (1997). "Distribution, splicing and glucocorticoid-induced expression of cardiac alpha 1C and alpha 1D voltage-gated Ca2+ channel mRNAs." J Mol Cell Cardiol **29**(11): 3035-3042.

Talvenheimo, J. A., J. F. Worley, 3rd, et al. (1987). "Heterogeneity of calcium channels from a purified dihydropyridine receptor preparation." Biophys J **52**(5): 891-899.

Tang, X. L., H. X. Wang, et al. (1998). "Reduced responsiveness of [Ca2+]i to adenosine A1- and A2-receptor stimulation in the isoproterenol-stimulated ventricular myocytes of spontaneously hypertensive rats." J Cardiovasc Pharmacol **31**(4): 493-498.

Thomas, J. A. and B. H. Marks (1978). "Plasma norepinephrine in congestive heart failure." Am J Cardiol **41**(2): 233-243.

Thomas, M. J., I. Sjaastad, et al. (2003). "Localization and function of the Na+/Ca2+-exchanger in normal and detubulated rat cardiomyocytes." J Mol Cell Cardiol **35**(11): 1325-1337.

Tidball, J. G., J. E. Cederdahl, et al. (1991). "Quantitative analysis of regional variability in the distribution of transverse tubules in rabbit myocardium." Cell Tissue Res **264**(2): 293-298.

Trafford, A. W., J. D. Clarke, et al. (2013). "Calcium signalling microdomains and the t-tubular system in atrial mycoytes: potential roles in cardiac disease and arrhythmias." Cardiovasc Res **98**(2): 192-203.

Trautwein, W. and J. Hescheler (1990). "Regulation of cardiac L-type calcium current by phosphorylation and G proteins." Annu Rev Physiol **52**: 257-274.

Tribouilloy, C., F. Grigioni, et al. (2009). "Survival implication of left ventricular end-systolic diameter in mitral regurgitation due to flail leaflets a long-term follow-up multicenter study." J Am Coll Cardiol **54**(21): 1961-1968.

Tsang, T. S., M. E. Barnes, et al. (2001). "Left atrial volume: important risk marker of incident atrial fibrillation in 1655 older men and women." Mayo Clin Proc **76**(5): 467-475.

Tsien, R. W. (1983). "Calcium channels in excitable cell membranes." Annu Rev Physiol **45**: 341-358.

Ungerer, M., M. Bohm, et al. (1993). "Altered expression of beta-adrenergic receptor kinase and beta 1-adrenergic receptors in the failing human heart." Circulation **87**(2): 454-463.

Vaidyanathan, R., A. L. Vega, et al. (2013). "The interaction of caveolin 3 protein with the potassium inward rectifier channel Kir2.1: physiology and pathology related to long qt syndrome 9 (LQT9)." J Biol Chem **288**(24): 17472-17480.

van den Berg, M. P., I. C. van Gelder, et al. (2002). "Impact of atrial fibrillation on mortality in patients with chronic heart failure." Eur J Heart Fail **4**(5): 571-575.

van der Heyden, M. A., T. J. Wijnhoven, et al. (2005). "Molecular aspects of adrenergic modulation of cardiac L-type Ca2+ channels." Cardiovasc Res **65**(1): 28-39.

Van Gelder, I. C., B. J. Brundel, et al. (1999). "Alterations in gene expression of proteins involved in the calcium handling in patients with atrial fibrillation." J Cardiovasc Electrophysiol **10**(4): 552-560.

Van Wagoner, D. R., A. L. Pond, et al. (1999). "Atrial L-type Ca2+ currents and human atrial fibrillation." Circ Res **85**(5): 428-436.

Vatta, M., M. J. Ackerman, et al. (2006). "Mutant caveolin-3 induces persistent late sodium current and is associated with long-QT syndrome." Circulation **114**(20): 2104-2112.

Vaziri, S. M., M. G. Larson, et al. (1994). "Echocardiographic predictors of nonrheumatic atrial fibrillation. The Framingham Heart Study." Circulation **89**(2): 724-730.

Vescovo, G., S. M. Jones, et al. (1989). "Isoproterenol sensitivity of isolated cardiac myocytes from rats with monocrotaline-induced right-sided hypertrophy and heart failure." J Mol Cell Cardiol **21**(10): 1047-1061.

Voigt, N., N. Li, et al. (2012). "Enhanced sarcoplasmic reticulum Ca2+ leak and increased Na+-Ca2+ exchanger function underlie delayed afterdepolarizations in patients with chronic atrial fibrillation." Circulation **125**(17): 2059-2070.

Walden, A. P., K. M. Dibb, et al. (2009). "Differences in intracellular calcium homeostasis between atrial and ventricular myocytes." J Mol Cell Cardiol **46**(4): 463-473.

Walker, D. and M. De Waard (1998). "Subunit interaction sites in voltage-dependent Ca2+ channels: role in channel function." Trends Neurosci **21**(4): 148-154.

Wang, Y. G., E. N. Dedkova, et al. (2005). "Phenylephrine acts via IP3-dependent intracellular NO release to stimulate L-type Ca2+ current in cat atrial myocytes." J Physiol **567**(Pt 1): 143-157.

Wang, Z., L. Yue, et al. (1998). "Differential distribution of inward rectifier potassium channel transcripts in human atrium versus ventricle." Circulation **98**(22): 2422-2428.

Wei, S., A. Guo, et al. (2010). "T-tubule remodeling during transition from hypertrophy to heart failure." Circ Res **107**(4): 520-531.

Wei, S. K., H. M. Colecraft, et al. (2000). "Ca(2+) channel modulation by recombinant auxiliary beta subunits expressed in young adult heart cells." Circ Res **86**(2): 175-184.

Weiss, S., S. Oz, et al. (2013). "Regulation of cardiac L-type Ca(2)(+) channel CaV1.2 via the beta-adrenergic-cAMP-protein kinase A pathway: old dogmas, advances, and new uncertainties." Circ Res **113**(5): 617-631.

Wier, W. G., T. M. Egan, et al. (1994). "Local control of excitation-contraction coupling in rat heart cells." J Physiol **474**(3): 463-471.

Willoughby, D. and D. M. Cooper (2007). "Organization and Ca2+ regulation of adenylyl cyclases in cAMP microdomains." Physiol Rev **87**(3): 965-1010.

Winslow, R. L. and J. L. Greenstein (2011). "Cardiac myocytes and local signaling in nano-domains." Prog Biophys Mol Biol **107**(1): 48-59.

Wong, J., D. Baddeley, et al. (2013). "Nanoscale distribution of ryanodine receptors and caveolin-3 in mouse ventricular myocytes: dilation of t-tubules near junctions." Biophys J **104**(11): L22-24.

Wong, P. C. and A. F. Smith (1975). "Comparison of 3 methods of analysis of the MB isoenzyme of creatine kinase in serum." Clin Chim Acta **65**(1): 99-107.

Woo, S. H., L. Cleemann, et al. (2002). "Ca2+ current-gated focal and local Ca2+ release in rat atrial myocytes: evidence from rapid 2-D confocal imaging." J Physiol **543**(Pt 2): 439-453.

Woo, S. H., L. Cleemann, et al. (2003). "Spatiotemporal characteristics of junctional and nonjunctional focal Ca2+ release in rat atrial myocytes." Circ Res **92**(1): e1-11.

Workman, A. J., K. A. Kane, et al. (2001). "The contribution of ionic currents to changes in refractoriness of human atrial myocytes associated with chronic atrial fibrillation." Cardiovasc Res **52**(2): 226-235.

Wright, P. T., V. O. Nikolaev, et al. (2013). "Caveolin-3 regulates compartmentation of cardiomyocyte beta2-adrenergic receptor-mediated cAMP signaling." J Mol Cell Cardiol.

Wu, T. J., M. Yashima, et al. (1998). "Role of pectinate muscle bundles in the generation and maintenance of intra-atrial reentry: potential implications for the mechanism of conversion between atrial fibrillation and atrial flutter." Circ Res **83**(4): 448-462.

Xiang, Y. and B. K. Kobilka (2003). "Myocyte adrenoceptor signaling pathways." Science **300**(5625): 1530-1532.

Xiao, R. P. (2000). "Cell logic for dual coupling of a single class of receptors to G(s) and G(i) proteins." Circ Res **87**(8): 635-637.

Xiao, R. P. (2001). "Beta-adrenergic signaling in the heart: dual coupling of the beta2-adrenergic receptor to G(s) and G(i) proteins." Sci STKE **2001**(104): re15.

Xiao, R. P., H. Cheng, et al. (1999). "Recent advances in cardiac beta(2)-adrenergic signal transduction." Circ Res **85**(11): 1092-1100.

Xiao, R. P. and E. G. Lakatta (1993). "Beta 1-adrenoceptor stimulation and beta 2-adrenoceptor stimulation differ in their effects on contraction, cytosolic Ca2+, and Ca2+ current in single rat ventricular cells." Circ Res **73**(2): 286-300.

Xiao, R. P., S. J. Zhang, et al. (2003). "Enhanced G(i) signaling selectively negates beta2-adrenergic receptor (AR)--but not beta1-AR-mediated positive inotropic effect in myocytes from failing rat hearts." Circulation **108**(13): 1633-1639.

Xiao, R. P., W. Zhu, et al. (2006). "Subtype-specific alpha1- and beta-adrenoceptor signaling in the heart." Trends Pharmacol Sci **27**(6): 330-337.

Xiao, R. P., W. Zhu, et al. (2004). "Subtype-specific beta-adrenoceptor signaling pathways in the heart and their potential clinical implications." Trends Pharmacol Sci **25**(7): 358-365.

Xu, L., D. Lai, et al. (2010). "Alterations of L-type calcium current and cardiac function in CaMKII{delta} knockout mice." Circ Res **107**(3): 398-407.

Yamada, Y., M. Nagashima, et al. (2001). "Cloning of a functional splice variant of L-type calcium channel beta 2 subunit from rat heart." J Biol Chem **276**(50): 47163-47170.

Yamasaki, Y., Y. Furuya, et al. (1997). "Ultra-high-resolution scanning electron microscopy of the sarcoplasmic reticulum of the rat atrial myocardial cells." Anat Rec **248**(1): 70-75.

Yamashita, T., T. Nakajima, et al. (1995). "Regional differences in transient outward current density and inhomogeneities of repolarization in rabbit right atrium." Circulation **92**(10): 3061-3069.

Yang, L., A. Katchman, et al. (2011). "Cardiac L-type calcium channel (Cav1.2) associates with gamma subunits." FASEB J **25**(3): 928-936.

Yeh, Y. H., R. Wakili, et al. (2008). "Calcium-handling abnormalities underlying atrial arrhythmogenesis and contractile dysfunction in dogs with congestive heart failure." Circ Arrhythm Electrophysiol **1**(2): 93-102.

Yue, D. T., S. Herzig, et al. (1990). "Beta-adrenergic stimulation of calcium channels occurs by potentiation of high-activity gating modes." Proc Natl Acad Sci U S A **87**(2): 753-757.

Yue, L., J. Feng, et al. (1997). "Ionic remodeling underlying action potential changes in a canine model of atrial fibrillation." Circ Res **81**(4): 512-525.

Yue, L., P. Melnyk, et al. (1999). "Molecular mechanisms underlying ionic remodeling in a dog model of atrial fibrillation." Circ Res **84**(7): 776-784.

Zaccolo, M. (2009). "cAMP signal transduction in the heart: understanding spatial control for the development of novel therapeutic strategies." Br J Pharmacol **158**(1): 50-60.

Zaccolo, M. and M. A. Movsesian (2007). "cAMP and cGMP signaling cross-talk: role of phosphodiesterases and implications for cardiac pathophysiology." Circ Res **100**(11): 1569-1578.

Zhang, Q., V. Timofeyev, et al. (2011). "Expression and roles of Cav1.3 (alpha1D) L-type Ca(2)+ channel in atrioventricular node automaticity." J Mol Cell Cardiol **50**(1): 194-202.

Zhang, X. Q., R. L. Moore, et al. (1995). "Calcium currents in postinfarction rat cardiac myocytes." Am J Physiol **269**(6 Pt 1): C1464-1473.

Zima, A. V. and L. A. Blatter (2004). "Inositol-1,4,5-trisphosphate-dependent Ca(2+) signalling in cat atrial excitation-contraction coupling and arrhythmias." J Physiol **555**(Pt 3): 607-615.